



MONASH University

NANOCELLULOSE GELS: CONCEPTS AND APPLICATIONS

*Thesis in fulfilment of the requirement for the degree of Doctor of
Philosophy in Chemical Engineering*

by

Llyza Ellena Mendoza

BE/ME Chemical and Materials Engineering

Department of Chemical Engineering

Faculty of Engineering

Monash University

February 2019

THIS PAGE HAS BEEN INTENTIONALLY LEFT BLANK

So we fix our eyes not on what is seen, but on what is unseen, since what is seen is temporary, but what is unseen is eternal.

2 Cor 4:18 (NIV)

THIS PAGE HAS BEEN INTENTIONALLY LEFT BLANK

COPYRIGHT NOTICE

© Llyza Ellena Mendoza, 2018. Except as provided in the Copyright Act 1968, this thesis may not be reproduced in any form without written permission of the author.

I certify that I have made all reasonable efforts to secure copyright permissions for third-party content included in this thesis and have not knowingly added copyright content to my work without the owner's permission.

.....

Llyza Ellena Mendoza

GENERAL DECLARATION

This thesis contains no material which has been accepted for the award of any other degree or diploma at any university or equivalent institution and that, to the best of my knowledge and belief, this thesis contains no material previously published or written by another person, except where due reference is made in the text of the thesis.

Signature:.....

Print Name:.....

Date:.....

TABLE OF CONTENTS

<u>TITLE PAGE</u>	<u>i</u>
<u>COPYRIGHT NOTICE</u>	<u>v</u>
<u>GENERAL DECLARATION</u>	<u>vi</u>
<u>TABLE OF CONTENTS</u>	<u>vii</u>
<u>DECLARATION OF PUBLICATION AND AUTHORSHIP</u>	<u>ix</u>
<u>ACKNOWLEDGEMENTS</u>	<u>xii</u>
<u>ABSTRACT</u>	<u>xiii</u>
<u>LIST OF PUBLICATIONS</u>	<u>xv</u>
<u>LIST OF FIGURES</u>	<u>xvi</u>
<u>LIST OF TABLES</u>	<u>xxii</u>
<u>CHAPTER 1 INTRODUCTION AND LITERATURE REVIEW</u>	<u>1</u>
<u>CHAPTER 2 GELATION MECHANISM OF CELLULOSE NANOFIBRE GELS: A COLLOIDS AND INTERFACIAL PERSPECTIVE</u>	<u>50</u>
<u>CHAPTER 3 EFFECTS OF FIBRE DIMENSION AND CHARGE DENSITY ON NANOCELLULOSE GELS</u>	<u>77</u>
<u>CHAPTER 4 CARBOXYLATED NANOCELLULOSE FOAMS AS SUPERABSORBENTS</u>	<u>103</u>
<u>CHAPTER 5 NANOCELLULOSE FOR GEL ELECTROPHORESIS</u>	<u>129</u>
<u>CHAPTER 6 CONCLUSIONS AND PERSPECTIVES</u>	<u>151</u>

APPENDIX

APPENDIX I PUBLICATIONS INCLUDED IN THESIS IN THEIR PUBLISHED FORMAT I

**GELATION MECHANISM OF CELLULOSE NANOFIBRE GELS: A COLLOIDS AND
INTERFACIAL PERSPECTIVE III**

**EFFECTS OF FIBRE DIMENSION AND CHARGE DENSITY ON NANOCELLULOSE
GELS XI**

CARBOXYLATED NANOCELLULOSE FOAMS AS SUPERABSORBENTS XX

NANOCELLULOSE FOR GEL ELECTROPHORESIS XXVIII

APPENDIX II CO-AUTHORED PUBLICATIONS NOT INCLUDED IN THESIS XXXVII

**PICKERING EMULSIONS ELECTROSTATICALLY STABILIZED BY CELLULOSE
NANOCRYSTALS XXXIX**

Monash University

Thesis including published works Declaration

I hereby declare that this thesis contains no material which has been accepted for the award of any other degree or diploma at any university or equivalent institution and that, to the best of my knowledge and belief, this thesis contains no material previously published or written by another person, except where due reference is made in the text of the thesis.

This thesis includes 4 original papers published in peer reviewed journals (Chapters 2 - 5). The core theme of the thesis is the characterisation and applications development of nanocellulose gels. The ideas, development and writing up of all the papers in the thesis were the principal responsibility of myself, the student, working within the Department of Chemical Engineering, Monash University under the supervision of Prof. Gil Garnier and Assoc. Prof. Warren Batchelor.

The inclusion of co-authors reflects the fact that the work came from active collaboration between researchers and acknowledges input into team-based research.

In the case of Chapters 2 to 5 my contribution to the work involved the following:

Thesis Chapter	Publication Title	Status	Nature and % of student contribution	Co-author name(s) Nature and % of Co-author's contribution	Co-author(s), Monash student
2	<i>Gelation mechanism of cellulose nanofibre gels: A colloids and interfacial perspective</i>	<i>Published</i>	<i>85%. Initiation, key ideas, experimental work, analysis of results, writing up</i>	1) <i>Warren Batchelor, Manuscript feedback, 5%</i> 2) <i>Rico Tabor, Key ideas, paper reviewing and editing, 5%</i> 3) <i>Gil Garnier, Key ideas, paper reviewing and editing, 5%</i>	<i>No</i> <i>No</i> <i>No</i>
3	Effects of fibre dimension and charge density on nanocellulose gels	Published	80%. Initiation, key ideas, experimental work, analysis of results, writing up	1) <i>Thilina Gunawardhana, Key ideas, experimental work, 10%</i> 2) <i>Warren Batchelor, Manuscript feedback, 5%</i>	<i>Yes</i> <i>Yes</i>

PREFACE

				3) <i>Gil Garnier, Key ideas, paper reviewing and editing, 5%</i>	Yes
4	Carboxylated nanocellulose foams as superabsorbents	Published	70%. <i>Initiation, key ideas, experimental work, analysis of results, writing up</i>	1) <i>Laila Hossain, Experimental work, analysis of results, 10%</i> 2) <i>Emma Downey, Experimental work, 5%</i> 3) <i>Camilla Scales, Experimental work, 5%</i> 4) <i>Warren Batchelor, Manuscript feedback, 5%</i> 5) <i>Gil Garnier, Key ideas, paper reviewing and editing, 5%</i>	Yes Yes Yes No No
5	Nanocellulose for gel electrophoresis	Published	85%. <i>Initiation, key ideas, experimental work, analysis of results, writing up</i>	1) <i>Thilina Gunawardhana, Key ideas, 5%</i> 2) <i>Warren Batchelor, Manuscript feedback, 5%</i> 3) <i>Gil Garnier, Key ideas, paper reviewing and editing, 5%</i>	Yes No No

I have renumbered sections of submitted or published papers in order to generate a consistent presentation within the thesis.

Student signature:

Date:

The undersigned hereby certify that the above declaration correctly reflects the nature and extent of the student's and co-authors' contributions to this work. In instances where I am not the responsible author I have consulted with the responsible author to agree on the respective contributions of the authors.

Main Supervisor Signature:

Date:

THIS PAGE HAS BEEN INTENTIONALLY LEFT BLANK

ACKNOWLEDGEMENTS

Firstly, I would like to express my gratitude to my supervisors Prof. Gil Garnier and A/Prof. Warren Batchelor for the opportunity to work on a challenging topic. I never have seen myself as an academic researcher, but your steady guidance and enthusiasm has moulded myself and this thesis journey into what it is today. Thank you also for the opportunity to present my work at different conferences and be able to meet other student researchers and industry leaders.

I also would like to acknowledge the staff at BioPRIA and the Monash Department of Chemical Engineering for their support every day. I have learnt a lot from all of you: from purchasing equipment, to filing my reimbursements, and reading my MSDS and doing my experiments safely.

To my friends in this journey, who have also have/had their own PhD journeys too: Aysu Onur (coffee buddy/ best housemate), Thilina Gunawardhana (a loyal and uber smart friend), Whui Lyn Then and Uthpala Garusinghe (my advisors), Laila Hossain and Maisha Maliha (my Bangladeshi gang), Ragesh Prathapan (the academic and dancing extraordinaire), Michael Hertaeg and Shaun Ang (for their daily musings in life). You all enriched my PhD journey and know that I couldn't have made it without you all. Here's to all the coffees and laughs!

I also would like to acknowledge my parents, Yolly and Zaldy Mendoza, and Alyson and Peter Moore for their endless support. I definitely have the best parents in the world! Thank you, Ma and Dad, for all emotional support and for always being available to listen and to give pep talks. Thank you for always believing in me, both of you are my coaches, when you tell me that I can do it, I really feel it in my bones that I can achieve it. Also, thank you, Uncle and Auntie, for all the trips to Beaudesert. I know I always look like I'm freaked out with my PhD but I always appreciate the change of scenery and being around you all.

I also would like to thank my spiritual family: my connect group, Victory Christian Fellowship and Hillsong Church. There's so many of you who poured in your time and encouragement in my life. Thank you for covering this season of my life in prayers.

To my forever beb, Jackson Moore, thank you for everything. You are the best co-pilot and the better cook. We have finished this PhD marathon together!

And lastly, to my Lord and Saviour Jesus Christ, through all things work out together for good. You promised springs and rivers from wastelands and here we are. Praises and all honour to You! Thank You for walking with me every day even when I falter. You are always gentle and steady. Great is Thy Faithfulness!

ABSTRACT

Cellulose, the most abundant polymer occurring in nature, can be processed into carboxylated cellulose nanofibres which form biodegradable and biocompatible hydrogels. These nanocellulose hydrogels present interesting potential for high value products, from strength additives to food and biomedical applications. However, characterisation and fundamental understanding of their gelation mechanism are required to efficiently engineer their properties.

This thesis focuses on demonstrating a step-wise understanding of the fundamentals of self-assembly and characterisation of nanocellulose gels and employing this knowledge to develop applications. Through extensive characterisation, the achievable rheological properties of neat nanocellulose gels were mapped. It is determined that the gelation and the strong viscoelastic response of the hydrogel predominantly arises from the entanglement of high aspect ratio fibres and electrostatic stabilisation from the high surface density of carboxylate groups on the nanocellulose fibres. Pulp source, whether softwood or hardwood kraft pulp, influences the average length of nanocellulose fibres which results to changes in the viscosity behaviour at a given fibre concentration. Varying the surface charge density has minimal effects at the exception of the percolation threshold wherein the critical strain and viscosity are influenced.

In the second part of this work, the applicability of nanocellulose gels as a superabsorbent agent and an electrophoresis media is demonstrated. Nanocellulose gels were converted into foams through a freeze-lyophilisation process. It was shown that nanocellulose foams are capable of absorbing 110-120 g/g (deionised water) and 60 g/g (0.9 wt.% NaCl). Gel properties such as fibre content and surface charge influence the absorption by dictating the foam density, pore size distribution and carboxylate groups, respectively. The freezing rate affects foam morphology whether ice formation is dominated by nucleation or crystallisation. The rate of absorption follows a pseudo second-order kinetics. Another application is a proof-of-concept validating that nanocellulose gels can be utilised as a separating media for gel electrophoresis. Nanocellulose dispersions were chemically cross-linked by boric acid - catalysed amide linkages and casted to form horizontal gel slabs. Gel electrophoresis is performed and monitored via the migration of tracking dyes, bromophenol blue and orange G.

Migration rate and behaviour were related to gel pore size and stability as influenced by the carbon-chain length of the cross-linker. Separation of the tracking dyes can be tuned in nanocellulose gels by varying the electrophoretic voltage. This thesis demonstrates the potential for these nanocellulose gels to be a commercialised sustainable and renewable nanomaterial.

LIST OF PUBLICATIONS

Peer-Reviewed Journal Papers

The following published and submitted papers are included in the body of this thesis as individual chapters. The sections of these published papers have been renumbered in order to generate a consistent presentation within the thesis. Papers in the published format are included as Appendix I.

1. **Mendoza, L.**, Batchelor, W., Tabor, R. F. & Garnier, G. 2018. Gelation mechanism of cellulose nanofibre gels: A colloids and interfacial perspective. *Journal of Colloid and Interface Science*, 509, 39-46.
2. **Mendoza, L.**, Gunawardhana, T., Batchelor, W., Garnier, G. 2018. Effects of fibre dimension and charge density on nanocellulose gels. *Journal of Colloid and Interface Science*, 525, 119-125.
3. **Mendoza, L.**, Hossain, L., Downey, E., Scales, C., Batchelor, W., Garnier, G. 2019. Carboxylated nanocellulose foams as superabsorbents. *Journal of Colloid and Interface Science*, 538, 433-439.
4. **Mendoza, L.**, Gunawardhana, T., Batchelor, W., Garnier, G. 2019. Nanocellulose for gel electrophoresis. *Journal of Colloid and Interface Science*. 540,148-154

The following published papers are not included in the main body of this thesis and can be found in their published format in Appendix II.

1. Varanasi, S., Henzel, L., **Mendoza, L.**, Prathapan, R., Batchelor, W., Tabor, R., and Garnier G. 2018. Pickering emulsions electrostatically stabilized by cellulose nanocrystals. *Frontiers in Chemistry*, 6(409).

LIST OF FIGURES

Chapter 1

- Figure 1:** Hierarchical structure of cellulose in wood biomass
- Figure 2:** Various microscopy images showing (A) unrefined bamboo kraft pulp, (B) cellulose nanocrystals from cotton pulp, (C) bacterial cellulose, and (D) TEMPO-oxidised cellulose nanofibres.
- Figure 3:** Mechanism Diagram for TEMPO/NaBr/NaClO Reaction for producing nanocellulose fibres.
- Figure 4:** (A) Schematic Diagram illustrating the electrical double layer consisting of the Stern and diffuse layers. The Debye length indicated represents the decrease in the surface electrical potential by e^{-1} . (B) Diagram representing the attractive van der Waals and repulsive electrical double layer potentials as a function of the distance between interacting colloidal particles.
- Figure 5:** The effect of pH on the dispersion and aggregation behaviour of surface-modified nanocellulose.
- Figure 6:** The production of nanocellulose aerogels and foams via various methodologies
- Figure 7:** Different geometry systems for rheological characterisation in rotational rheometers
- Figure 8:** The rheological behaviour of fluids over a range of time-scales
- Figure 9:** Deformation of a fluid under constant shear force by two plates and the equation of viscosity
- Figure 10:** Characteristic shear stress-shear rate relationship for Newtonian and non-Newtonian time-independent fluids
- Figure 11:** Viscosity behaviour of time-dependent rheopectic and thixotropic materials.
- Figure 12:** Oscillatory strain input and output stress wave-forms with the loss angle indicated
- Figure 11:** Oscillatory strain sweep with the key parameters indicated.

- Figure 12:** Typical rheological spectra of a: (A) dispersion, (B) entangled polymer solution, (C) weak gel, and (D) strong gel. G' is represented by a bold line whereas G'' is represented by a dashed line.
- Figure 15:** Schematic Diagram of an atomic force microscope.
- Figure 16:** Schematic Diagram illustrating the operating modes of the AFM: (a) contact mode, (b) tapping mode, and (c) non-contact mode.
- Figure 17** (A) Horizontal and (B) vertical gel electrophoresis systems.
- Figure 18** Electrophoretic separation in 1wt.% agarose gel of digested plasmid (lane 1), undigested plasmid (lane 2), and synthesised Cas9 mRNA (lane 3) contrasted against a molecular marker (lane M).

Chapter 2

- Figure 1:** AFM images of TOCNF spin coated onto a glass slide. (a, b) AFM height images of the fibres at different image sizes. c) A cross-sectional profile of the surface topology at the point indicated by the white dotted line in a) showing that the height (diameter) of individual fibres in the dry state is 2–3 nm.
- Figure 2:** The effect of (A) pH and (B) salt on the stability of 1 wt. % TEMPO-oxidised cellulose nanofibre gels. Fibre ratio is calculated as the ratio between the final height of gel after centrifugation and the total gel height. Insets show water released from gels at different conditions with pure water as reference.
- Figure 3:** Complex viscosity profile of shear-thinning TEMPO-oxidised cellulose nanofibre gels at various concentrations derived from dynamic strain sweep measurements (25°C). A yield point is clearly evident for fibre concentrations of 0.29% and above.
- Figure 4:** Viscoelastic properties of TEMPO-oxidised cellulose nanofibre gels at different fibre concentrations: dynamic strain sweep (25°C) at a frequency of 1 Hz. Filled symbols indicate elastic moduli whereas unfilled symbols indicate loss moduli.

- Figure 5:** Viscoelastic properties of TEMPO-oxidised cellulose nanofibre gels as at different fibre concentrations: dynamic frequency sweep (25°C) at 0.1% strain.
- Figure 3:** Rheological properties of 1 wt. % TEMPO-oxidised cellulose nanofibre gel in a step strain test: strain has been varied between 0.1% and 10% at constant 1Hz and 25°C for 5 cycles.
- Figure 4:** Effect of ionic strength on the electrical double layer of TOCNF fibres estimated from the Gouy-Chapman equation (reference pH of original gel: 7.4). Dashed line indicates 63% decrease in surface charge corresponding to decreased double layer thickness at increased ionic strength.

Chapter 3

- Figure 1:** Population Length and width distributions for hardwood and softwood bleached kraft pulp fibres.
- Figure 2:** Nanocellulose fibres produced from softwood and hardwood bleached kraft pulp. Width (A) and length (B) distributions for nanocellulose produced from softwood (1mmol COO⁻ .g⁻¹) and hardwood (0.65, 1, and 1.4 mmol .g⁻¹) at various surface charges. (C) and (D) AFM image of a single HW-TOCN fibre with surface topology shown.
- Figure 3:** Oscillatory strain measurement for nanocellulose gels made from bleached softwood fibres (1 mmol .g⁻¹) as a function of solids concentration. Important spectral rheological data including the G' and G'' at the linear viscoelastic region (LVR), and the critical strain γ_c are identified for the 0.5 wt.% gel used as example. Measurements were done at 25°C, 1Hz.
- Figure 4:** (A) Dynamic Moduli (G' and G'') of nanocellulose gels produced from unrefined softwood and hardwood as a function of solids concentration at constant charge density (1 mmol .g⁻¹). (B) Critical

Strain of SW-TOCN and HW-TOCN as a function of solids concentration.

Figure 5: Viscosity Profile of TOCNs from hardwood (solid symbol) and softwood (open symbol) as a function of concentration for constant charge density (1 mmol. g^{-1}). Measurements were done at 25°C.

Figure 6: The effect of charge density on the (A) dynamic moduli at LVR and (B) critical strain of HW-TOCN nanocellulose gels at different solids concentrations. Yellow symbols for 0.65mmol. g^{-1} , green symbols for 1mmol. g^{-1} and red symbols for 1.4 mmol. g^{-1} . Measurements were done at 25°C, 1Hz.

Figure 7: Viscosity Profile for HW-TOCNs at three levels of charge density (0.65, 1, and 1.4 mmol. g^{-1}) and different solids content. Measurements were done at 25°C.

Chapter 4

Figure 1: Free Swell Capacity (FSC) in deionised water of Nanocellulose Foams (-80°C) at different solids concentrations as a function of swelling time.

Figure 2: (A) Pore Size Distribution of Nanocellulose Foams (-80°C) at different solids concentrations. Foam properties such as (B) porosity (1 atma and totalb), (C) bulk density and pore area derived from mercury porosimetry. Further details on porosimetry data and related calculations are provided in the Supplementary Information.

Figure 3: Effect of cellulose fibre surface charge of Nanocellulose Foams (-80°C) at different solids concentration on FSC in deionised water

Figure 4: (A) The Effect of Freezing Rate (initial freezing at -20°C, -80°C, and 196°C) on the FSC in deionised water. Optical microscopy illustrating the effect of freezing at (B) -20°C (C) -80°C, and (D) -196°C on the morphology of nanocellulose foams.

Figure 5: FSC of nanocellulose (-80°C) in 0.9 wt.% saline as a function of swelling time compared against the equilibrium absorption capacity

of a commercial SAP polymer. Images showing a (A) NC foam and (B) commercial SAP polymer.

Figure 6: Effect of the initial gel solids content on the superabsorbent nanocellulose foam FSC (-80°C) in deionised water (2 hours) and available pore volume at 1atm and total pore volume from mercury porosimetry

Figure 7: Calculated Swelling Kinetic Parameters of Nanocellulose Foams (-80°C): (A) Linearisation of FSC by Schott's Equation (B) Equilibrium Absorption Capacity W_{∞} and (C) Swelling Rate Constant

Chapter 5

Figure 1: FTIR spectra evolution of cross-linking of nanocellulose gel slabs with 8:1 (A) HMDA and (B) EDA. Room temperature and 80°C reactions catalysed by boric acid.

Figure 2: A casted 8:1 EDA-NC gel placed on a horizontal electrophoresis system.

Figure 3: Migration of Bromophenol Blue (BB) and Orange G (OG) dyes in HMDA- (8:1) and EDA- (8:1) cross-linked nanocellulose gel slabs. Bold lines indicate trend lines and faint lines indicate the actual migration behaviour of tracking dyes. Chemical structures of EDA and HMDA. Electrophoresis voltage constant at 100V.

Figure 4: Migration of Tracking Dyes at 30 min intervals in 8:1 EDA-NC gel. Electrophoresis voltage constant at 100V.

Figure 5: Migration of Bromophenol Blue (BB) and Orange G (OG) in a (A) HMDA cross-linked and (B) EDA cross-linked nanocellulose gel at various NH_2 : COO^- concentrations. Electrophoresis voltage constant at 100V.

Figure 6: Migration of (A) Orange G (OG) and (B) Bromophenol Blue (BB) in an 8:1 HMDA cross-linked nanocellulose gel at different electrophoresis voltages. The linear trendlines were added with a y-

intercept set at zero. The slope represents the average migration rate under various voltages.

LIST OF TABLES

Chapter 3

Table I: Fibre length statistics of hardwood and softwood kraft pulp and the nanocellulose fibres produced from those.

Table II: Fibre width statistics of hardwood and softwood bleached kraft pulp and the nanocellulose fibres produced from those.

Chapter 5

Table I: Cross-linker type and ratios for the different casted nanocellulose gel slabs

Chapter 6

Table I: The effect of key process variables to the rheological behaviour of nanocellulose gels

THIS PAGE HAS BEEN INTENTIONALLY LEFT BLANK

THIS PAGE HAS BEEN INTENTIONALLY LEFT BLANK

CHAPTER 1

INTRODUCTION AND LITERATURE REVIEW

THIS PAGE HAS BEEN INTENTIONALLY LEFT BLANK

CHAPTER 1	INTRODUCTION AND LITERATURE REVIEW
1.1	INTRODUCTION4
1.2	LITERATURE REVIEW6
1.2.1	CELLULOSE AND NANOCELLULOSE6
1.2.1.1	<i>Nanocellulose Production</i>8
1.2.1.2	<i>Colloidal Nanocelluloses</i>11
1.2.1.3	<i>Characterisation Techniques of Nanocellulose Hydrogels and Foams</i>14
1.2.1.4	<i>Applications of Nanocellulose Hydrogels and Foams</i>17
1.2.2	RHEOLOGY.....20
1.2.2.1	<i>Steady-state Shear</i>22
1.2.2.2	<i>Dynamic Oscillatory Shear</i>24
1.2.3	ATOMIC FORCE MICROSCOPY.....27
1.2.4	ELECTROPHORESIS.....29
1.2.5	PERSPECTIVES.....32
1.3	GAPS IN KNOWLEDGE33
1.4	RESEARCH OBJECTIVES34
1.5	THESIS OUTLINE35
1.6	REFERENCES39

1.1 INTRODUCTION

Trees have been utilised over thousands of years for different purposes, initially as a combustible resource for heat and light, and now as a versatile material for tools, structures, paper, and textiles. There is an increasing demand for the production of products from renewable and sustainable resources using wood as a carbon source. Wood-based materials are an un-tapped resource to be developed. Wood is composed of three main polymers: cellulose, hemicellulose, and lignin- which can be harnessed to produce the next generation of value-added products. Commercialization of products from plants will empower a more sustainable society of decreased reliance on fossil-based resources.

The hierarchical structure of cellulose allows the extraction of cellulosic nanoparticles which possesses excellent mechanical and reinforcing properties, while being sustainable and biodegradable. A number of different techniques have been developed such that different classes of nanocellulose are formed – some are stiff rod-like particles which self-assemble in ordered structures, another is formed through bacterial synthesis, and the last type are semi-flexible fibrils capable of forming nano-based composites of increased strength and toughness. Nanocellulose possesses nano-scale dimensions producing high surface area in combination with a modifiable surface chemistry. This provides some types of nanocellulose the ability to form colloids such as stable dispersions and hydrogels.

Research on nanocellulose has expanded greatly over the last decade. Studies encompass the characterisation of the individual fibre to bulk behaviour as well as the effect of different processing conditions to nanocellulose quality. Nanocellulose has gained substantial interest due to its applicability not just in the existing pulp and paper industry as a strength additive but also for its potential in many other fields such as agriculture, waste water treatment, and biomedical applications. However, there is still a need for a sequential understanding of the structure-property relationship of nanocellulose.

To address this, this dissertation aims to quantify the physico-chemical fibre properties and their effect on the bulk material properties, which will allow the selection and development of applications. Herein, a hydrogel-forming nanocellulose type is selected and characterised in order to uncover the mechanism of its formation, material properties and assessing its stability as a function of variables. This was achieved by comprehensive rheological characterisation of the gels. From this, the feasibility of nanocellulose gels is tested in two different applications: superabsorbents and gel electrophoresis. Moreover, areas for further development are then highlighted.

To begin this thesis, a review of recent literature is laid out in the following section of this chapter to provide an overview of the progress in the field of nanocellulose. The review of related literature is divided into two parts: nanocellulose, and the outline of critical experimental techniques. An overview of the fundamentals of nanocellulose is firstly presented followed by an analysis on the recent advances in applications development (Sec 1.2.1). On the latter part, the working principle of several characterisation methods applicable to nanocellulose are presented (Sec 1.2.2 - 1.2.4). Identification of the research gap and justification of the research aims is proposed by the end of the chapter (Sec 1.3 – 1.5).

1.2 LITERATURE REVIEW

1.2.1 CELLULOSE AND NANOCELLULOSE

Cellulose, one of the most abundant biopolymers, naturally exists in plants, bacteria, fungi, and certain animals [1]. It is a linear homopolymer composed of *D*-glucose monomers connected by β -1,4-glycosidic linkages. Every *D*-glucose monomer contains three hydroxyl groups: the primary alcohol at the C6 position and two secondary alcohols at the C2 and C3 positions. The degree of polymerisation of cellulose can vary between 2,000 to 27,000 units depending on the source and can be present in shorter chains in industrial pulp [2, 3]. In plants, cellulose is arranged in a highly organised hierarchical structure, as shown in Figure 1, intertwined with other biopolymers such as lignin and hemicellulose. Individual cellulose polymer chains are ordered in a 2x2 matrix to form elementary fibrils [4]. Bundles of elementary fibrils consequently form a microfibril which are organised into crystalline and amorphous regions. Within an individual microfibril, chains of cellulose are tightly contained and bonded together through an extensive network of intra- and inter- chain hydrogen bonding [5]. This ordered assembly from *nano*- to *macro*- scale confers strength in the cell wall of plants.

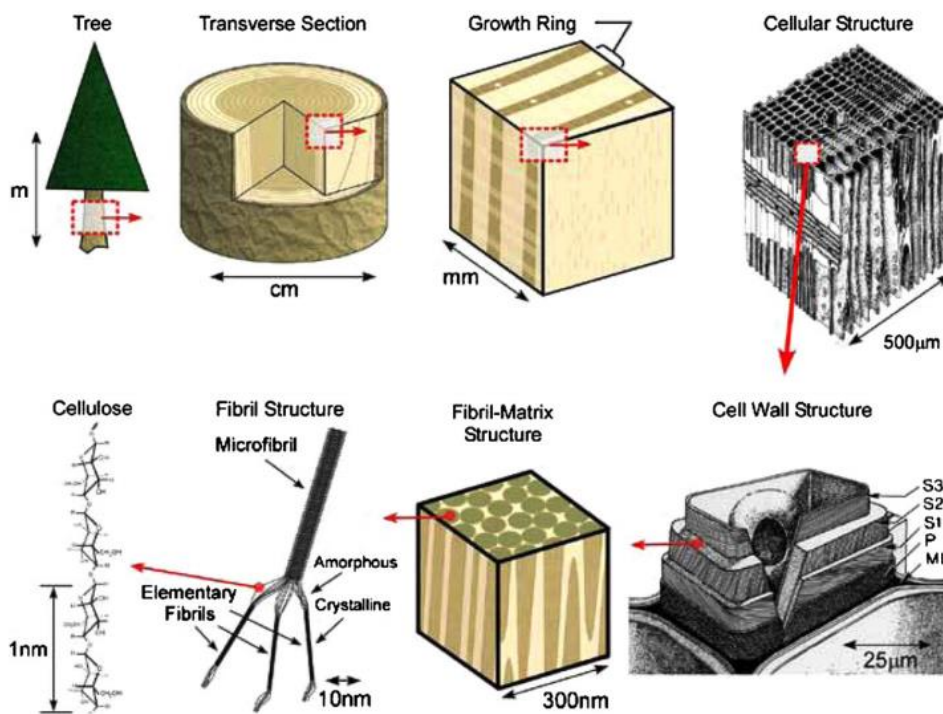
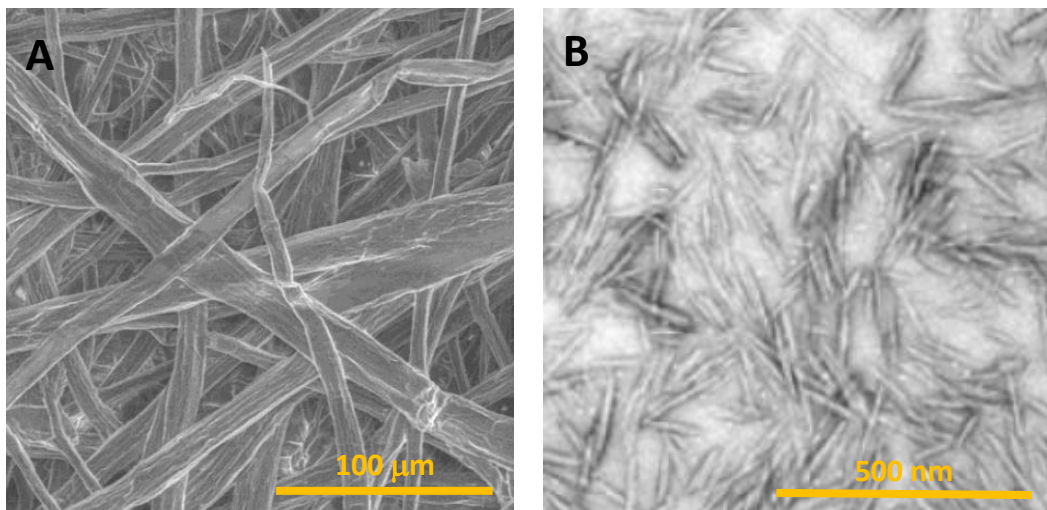


Figure 1. Hierarchical structure of cellulose in wood biomass. Reproduced from [6] with permission from IOP Publishing.

The initial study by Turbak, Snyder [7] revealed that wood pulp can be repetitively fibrillated and delaminated to liberate cellulose at the micro-fibril level. Nanocellulose is a coined term referring to cellulose fibres which possess dimensions within the nanometer scale [8]. Dimensions of nanocelluloses can vary widely depending on the cellulose source and extraction method. There are three main classes of nanocelluloses, namely: cellulose nanocrystals (CNC), cellulose nanofibrils (CNF) and bacterial nanocellulose (BNC) [9] as shown in Figure 2. Other forms of nanocellulose can also be extracted from tunicates and algae [1]. Cellulose nanocrystals (CNCs) appear as stiff cylindrical rods which possess diameters of 5 -70 nm and length of 100 nm to several microns which arise from acid hydrolysis [10, 11]. CNCs are also known as nanocrystalline cellulose, cellulose whiskers or nanowhiskers due to the tapering present at the ends of the nanoparticle. Bacterial nanocellulose is produced through oxidative fermentation of acetic acid bacteria such as *Acetobacter xylinum*. BNC is characterised by its high purity and formation of ribbon-like cellulose microfibril structure [12, 13]. Lastly, cellulose nanofibrils (CNFs) are long semi-flexible fibrils which possess far higher aspect ratios (diameter = 5-60nm, length of several microns) and contain both crystalline and amorphous domains [10].



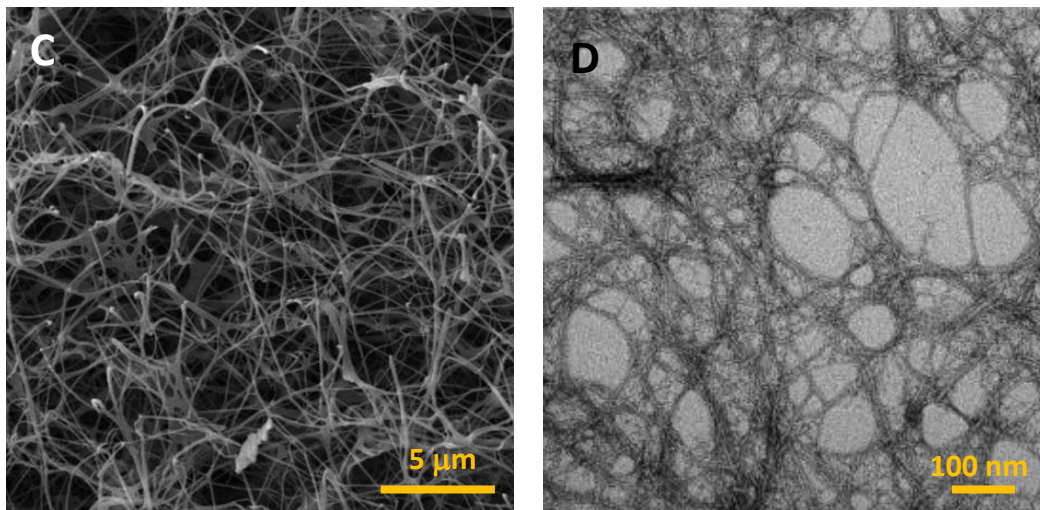


Figure 2. Various microscopy images showing (A) unrefined bamboo kraft pulp, (B) cellulose nanocrystals from cotton pulp, (C) bacterial cellulose, and (D) TEMPO-oxidised cellulose nanofibres. (A) Reproduced with permission from [14] under creative commons policy. (B) Reprinted with permission from [15]. Copyright 2018 American Chemical Society. (C) Reproduced from [16] with permission from The Royal Society of Chemistry. (D) Reproduced from [17] with permission from The Royal Society of Chemistry.

1.2.1.1 Nanocellulose Production

There are numerous methodologies which produce nanocellulose from various cellulosic sources. Production methods can either have a top-down approach which includes plant cell wall delamination or a bottom-up approach through bacterial synthesis of individual glucose units to form nanofibres [10]. Mechanical methods such as refining and homogenising, microfluidisation, grinding, cryocrushing, and high intensity ultrasonication can be utilised to defibrillate macro-fibres [18]. These processes utilise high shear to induce cleavage along the longitudinal axis resulting into extraction of higher aspect ratio cellulose fibrils [1]. In fact, the first studies in nanocellulose production of Turbak *et al.* relied on high pressure homogenisation of sulphite softwood pulp [7]. However, processes relying on mechanical treatments solely are energy intensive and inefficient [19]. Thus, pre-treatment before mechanical fibrillation is necessary. Enzymes can selectively hydrolyse the bonding of cellulose to other lignocellulosic components and also within itself to produce nanofibres [20]. Cellulases (endoglucanase, exoglucanase, and β -glucosidase) can cleave the hydrogen bonding at different locations between the cellulose fibres [20]. Acid hydrolysis with

either sulphuric acid, phosphoric or hydrochloric acid produces nanocellulose through cleaving of the amorphous regions within the cellulose fibrils and producing nanocellulose crystals [21, 22].

Another method is via chemical oxidation which can modify the cellulose surface. There are non-selective oxidative systems such as nitrogen oxides [23], alkali metal nitrite and nitrates [24], ozone [25], and sodium monochloroacetate (carboxymethylation) [26] which increase the carboxyl content of cellulose. Another group of chemical oxidants is regioselective which utilises periodate (periodate oxidation) and nitroxyl radical (TEMPO-mediated oxidation). The use of carboxymethylation and nitrogen oxides are limited industrially due to low reaction efficiency and regioselectivity, chemical safety and other environmental issues [27]. These methods insert anionic groups within the cellulose chain which introduces electrostatic repulsion between the fibres. The repulsive forces present allow the ease of separation consequently liberating cellulose nanofibres. In TEMPO-mediated oxidation, a hypohalite oxidant regioselectively oxidises the primary alcohols of native cellulose fibres in the presence of a nitroxyl catalyst [28-30]. TEMPO (2,2,6,6-tetramethylpiperidine-1-oxyl), is a water-soluble and commercially available nitroxyl radical [30]. In a basic environment, the primary alcohol groups along the cellulose backbone are converted to carboxylic groups. In this process, the conversion of the C6 groups does not affect the crystallinity of the cellulose source [31]. The electrostatic repulsion gained through the introduction of carboxylic groups causes the separation and liberation of individual nanofibers whilst also increasing the hydrophilicity. The mild mechanical disintegration of the carboxylated cellulose fibres in water consequently produces TEMPO-oxidised cellulose nanofibers (TOCN). The resulting functionalised nanocellulose has an average diameter of 3-4nm and several microns in length [32]. Figure 3 represents a schematic diagram of the oxidation process utilising NaClO as the primary oxidant.

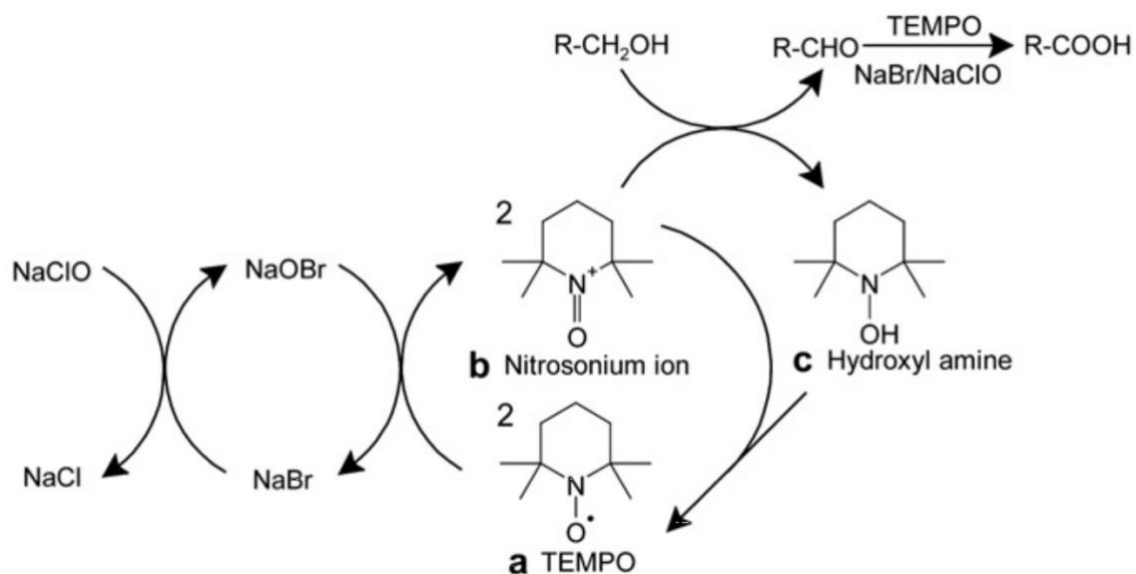


Figure 3. Mechanism Diagram for TEMPO /NaBr/NaClO Reaction for producing nanocellulose fibres. Reprinted from [33], Copyright (2018), with permission from Elsevier.

Different oxidant and catalyst systems can be used for primary alcohol oxidation via TEMPO-mediated oxidation. Analogues of TEMPO which arise from modifying the 4th ring carbon, such as 4-acetamide-TEMPO, 4-carboxyl-TEMPO and 4-phosphonoxy-TEMPO can be utilised as a catalyst in a NaBr/NaClO system [34]. Primary oxidants can also be varied in TEMPO-mediated oxidation. Oxidants serve two primary functions: (a) aiding the regeneration of the reactive group of the TEMPO catalyst and, (b) transforming the intermediate aldehyde to the carboxylate group [33]. The most utilised TEMPO-mediated systems either utilise the NaBr/NaClO at pH 10 or NaClO/NaClO₂ at pH 4-7. Enzymes such as laccase have also been studied as an oxidant in conjunction with a TEMPO derivative [35, 36]. Electrochemically - mediated TEMPO oxidation can produce carboxylate groups without the need of chlorine-based reagents [27, 37, 38]. Ultrasonication-assisted TEMPO-oxidation has also been studied showing improvements to the extent of oxidation of cellulose [39]. A critical review by Pierre, Punta [40] provides an excellent summary of the various TEMPO systems which have been studied including the oxidation conditions and yields.

Other aspects of TEMPO-mediated oxidation process were also studied. Various polysaccharide substrates from agarose, carageenan, chitosan, and curdlan amongst others can be oxidised at various yields and carboxylate content [40]. Oxidising different cellulosic sources such as hardwood and softwood kraft pulp, cotton, bacterial cellulose, tunicate cellulose and algal cellulose result in differing carboxylate content due to their differences in crystal structure and size but overall display similar electrokinetic potential (zeta potential) [32, 35]. Increasing the amount of primary oxidant results in an increased carboxylate content in bleached softwood kraft pulp however at the expense of reduced polymer length [29, 35]. Reaction time influences the relative amounts of aldehyde groups which have not been converted to carboxylate group in the TEMPO/NaBr/NaClO system [32] and the total carboxylate content in TEMPO/NaClO/NaClO₂ [41]. Reaction pH affects the reaction kinetics of the C6 oxidation. The optimal reaction pH for the TEMPO/NaBr/NaClO is at pH 10. Under less basic conditions (pH 8.5), the formation of the TEMPO-alcohol complex limits the reaction rate. Conversely, if the pH is increased to 11.5, the reaction between NaBr and NaClO becomes the rate limiting step. Lastly, the amounts of catalyst and other reactants (i.e. NaBr, NaClO etc.) influence the rate of formation of the carboxylate groups [28].

1.2.1.2 Colloidal Nanocelluloses

Typically, unmodified cellulose macro-fibres or mechanically fibrillated cellulose nanofibres dispersed in an aqueous solvent form a cloudy suspension wherein the fibres settle over time. Stable cellulosic colloids such as dispersions and hydrogels can be formed via multiple methods. Cellulose can be dissolved in solvents such as lithium chloride/dimethyl acetamide (LiCl/DmAc), *N*-methylmorpholine-*N*-oxide (NMMO), ionic liquids, and alkali-urea to produce modified cellulose which are capable of forming gels [42, 43]. Cellulose derivatives such as methyl cellulose (MC), hydroxypropyl cellulose (HPC) and hydroxypropylmethyl cellulose (HPMC) are water-soluble and commonly used as a emulsion stabiliser and rheology modifier [42]. Composites of cellulose blended with other biopolymers can form interpenetrating networks and

polyelectrolyte complexes [44-47]. Lastly, another method is through the production of surface-modified nanocellulose such as TEMPO-oxidised cellulose nanofibres [29].

Colloids are defined as materials which comprise stable constituents (dispersed phase) possessing dimensions between 1 nm to 1 μm , dispersed in a medium (continuous phase) [48]. In the case of nanocellulose, nano-scale fibres are dispersed in an aqueous or organic solvent [49]. The properties of a colloid such as its stability is influenced by the interaction of the dispersed particles [50]. The Derjaguin-Landau-Verwey-Overbeek (DLVO) theory describes colloidal stability from the balance of forces between charged surfaces interacting in a medium [51, 52]. The total interaction energy within a colloid is the sum of the attractive van der Waals forces (Hamaker attraction) and the repulsive electrostatic forces (estimated from Coulomb's law equation) [53, 54]. The attraction arises from long-range dispersion forces whereas the repulsive forces arise from the particle surface charge [54, 55]. Fundamentally, a colloid remains stable when the energy barrier from the repulsive forces dominates the attraction between particles [56]. Conversely, the dispersed phase coagulates when the attractive forces are larger than the electrostatic repulsive force. The main parameters which dictate the interaction energy are the Hamaker constant (H_A), surface potential (ψ_s) and the electrolyte concentration which influences the Debye length and zeta (ζ) potential [57]. For rod-like colloids, which is the case for nanocellulose, factors such as interparticle forces (charge, dispersion, depletion forces, and frictional interactions), aspect ratio, number density, and fibre flexibility must be taken into account [58].

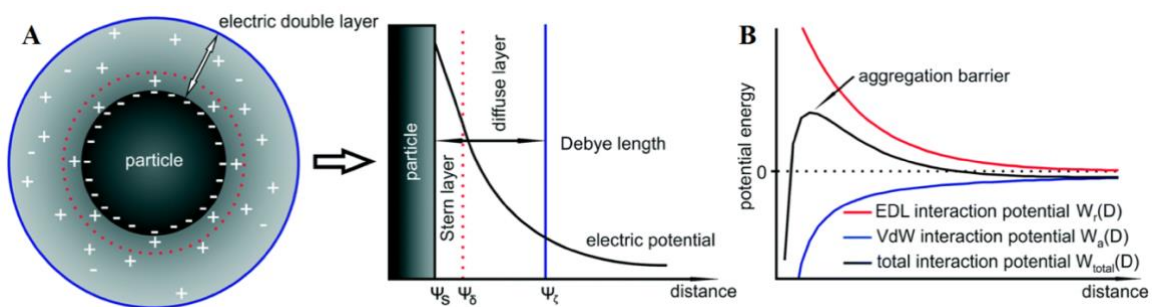


Figure 4. (A) Schematic Diagram illustrating the electrical double layer consisting of the Stern and diffuse layers. The Debye length indicated represents the decrease in the surface electrical potential

by e^{-1} . (B) Diagram representing the attractive van der Waals and repulsive electrical double layer potentials as a function of the distance between interacting colloidal particles. Adapted from [59] with permission from the Royal Society of Chemistry under Creative Commons License 3.

The colloidal stability of surface-modified nanocellulose is primarily determined by fibre properties (surface charge), chemical environment (pH, ionic strength), and the presence of other constituents promoting steric hindrance. pH ($\text{pH} < \text{pK}_a$) can encourage fibril aggregation by promoting the protonation of pendant groups leading to reduced surface charge and electrostatic repulsion between fibrils [53] as shown in Figure 5. Increasing the ionic strength of the continuous phase leads to a shielding of the electrical double layer causing to a dominating attractive interaction [53, 57, 60]. In a dilute TOCN dispersion (0.1 wt.%), the critical concentration is at 100 mM NaCl wherein gel aggregates have been observed. Moreover, this critical concentration is affected by the electrolyte ion valency (Na^+ , Ca^{2+} , Mg^{2+}) as predicted satisfactorily by the Schultz-Hardy rule [57]. The addition of metal cations promotes screening of the electrostatic repulsion between TOCNs by providing metal-carboxylate bonding [61]. In CNCs, it has been reported that larger monovalent cations ($\text{Li}^+ \rightarrow \text{Na}^+ \rightarrow \text{K}^+ \rightarrow \text{Cs}^+$) cause a higher CAC due to enhanced affinity between the cation and the pendant group [62]. Other non-adsorbing macromolecules and polyelectrolytes can control the attractive interactions among particles providing steric hindrance and further affecting colloidal stability [50, 62, 63]. Lastly, modelling of the aggregation and colloidal stability based on the DLVO theory has been performed on various nanocelluloses [53, 57, 64].

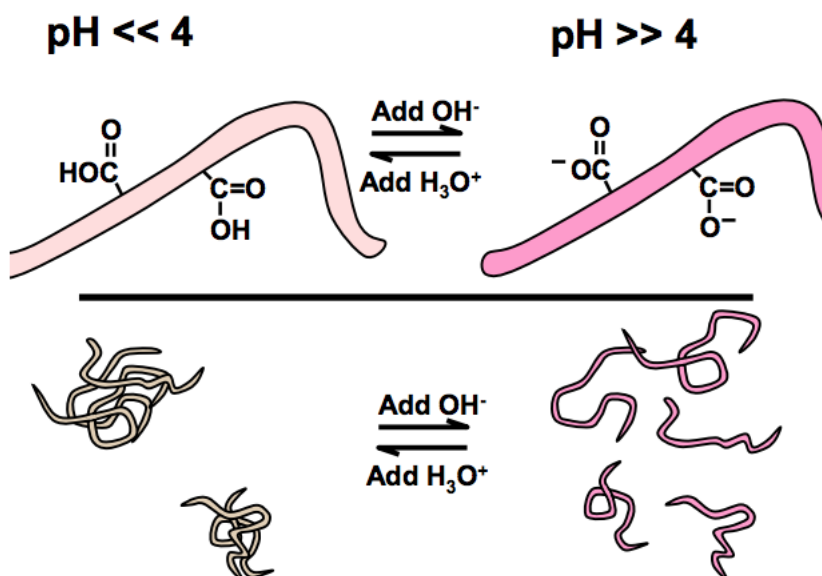


Figure 5. The effect of pH on the dispersion and aggregation behaviour of surface-modified nanocellulose. Reproduced with permission from [65] under creative commons policy.

1.2.1.3 Characterisation Techniques of Nanocellulose Hydrogels and Foams

Characterisation of nanocellulose span different levels – from its individual fibril properties to the bulk behaviour of self-assembled structures. The physico-chemical properties of individual nanocellulose fibres can be characterised by their length and diameter dimensions, surface charge, and crystallinity. The diameter distribution of nanocellulose can be determined via electron microscopy (scanning or transmission electron microscopy) or by contact and force scanning microscopy techniques such as atomic force microscopy (discussed in Sec 1.2.3). Length determination, however, is complex due to the entangled nature of nanocellulose and the difficulty in differentiating the ends of a nanofibre [66]. Hence, semi-empirical methods based on fibre sedimentation or rheology of dilute nanocellulose dispersions have been developed to determine fibre aspect ratio (length / diameter) which can be used to ascertain length [66-68]. TOCNs, in particular have been reported to possess length in the micron-scale and diameter in the nano-scale [68-70]. The degree of polymerisation, defined as the number of repeating monomeric units in a polymer can be determined in nanocellulose by chromatographic methods or by viscosity measurements by dissolution in copper ethylenediamine [71-73]. However, it has been reported that the

dissolution of TOCNs in copper ethylenediamine can yield inaccurate results due to the instability of beta linkages between monomeric units in the alkaline solution [71]. Changes in the crystallinity of cellulose post-treatment can be monitored by X-ray diffraction [74]. TOCNs were investigated and showed the retainment of the primary crystal structure of various celluloses after chemical treatment (TEMPO-mediated oxidation) [32]. Lastly, fibril structural assembly such as the right-handed chirality and 2x2 chain-packing arrangement in nanocellulose has been determined [4].

The fundamental chemical characterisation of surface-modified nanocellulose deals with the extent or degree of substitution (DS). Qualitatively, changes in the FTIR spectra of the key bonding sites can be monitored to demonstrate substitution/oxidation of the cellulose polymer. Conductometric titration and methylene blue absorption can quantitatively determine the extent of primary alcohol oxidation [75]. In the case of TEMPO-mediated oxidation, complete oxidation of the primary alcohol (1.7 mmol.g^{-1} in softwood kraft pulp) can be achieved whereas in carboxymethylation, a lower DS of 0.087 ($0.515 \text{ } \mu\text{equiv.g}^{-1}$) is attained [26, 32]. With periodate – oxidation, a similar carboxylate content ($0.38 - 1.75 \text{ mmol.g}^{-1}$) is reported however this also includes the oxidation of C2 and C3 alcohols [76]. Lastly, the electrokinetic potential of surface-modified nanocellulose fibres can be measured through its zeta potential. TEMPO-oxidised cellulose nanofibres have been reported to have -75 mV even at various cellulosic sources [32].

The bulk behaviour of nanocellulose gels is centred on understanding the different aspects which influence its rheological phenomena. The fundamental principles of rheological characterization are discussed in further detail in Sec 1.2.2. A combination of factors including processing conditions, physical, and chemical characteristics affect the rheological behaviour of TOCNs. For instance, cation (Al^{3+}) - crosslinked TOCN gels showed higher G' and G'' values at longer sonication intervals [77]. In another study, increasing the acid hydrolysis severity (time) has influenced the aspect ratio of CNCs (shortening) leading to a higher critical gelation concentration as shown by the rheological spectra [78]. Moreover, the evolution behaviour of nanocellulose has been

investigated from dilute to semi-dilute regimes. In the dilute regime, primary electroviscous effects dominate the intrinsic viscosity with the viscosity also responding to a change in pH [70]. Furthermore, the intrinsic viscosity of dilute TOCN suspensions can be related to the classical theory of rod-like particles [70]. In the semi-dilute regime, the hydrogel behaves as a shear-thinning material with viscosity largely depending on the concentration [79-83]. Nanocellulose gels have demonstrated to have history-dependent behaviour such as hysteresis, thixotropy, and creep-recovery [82, 84, 85]. Fibre flexibility affects suspension rigidity and has been demonstrated by simulation to increase specific viscosities in a suspension containing semi-flexible fibrils in contrast to straight ones [86, 87]. Local flow phenomena such as wall slip, and shear banding have also been reported in nanocellulose flow behaviour [65, 88-90].

The effect of surface and environmental chemistry on nanocellulose gel behaviour is also studied through rheology. In CNCs, the type and concentration of the pendant group dictates concentration- and time- dependent viscosity behaviour by the ability of fibres to aggregate depending on the surface charges [91]. Introduction of cations in TOCNs promoted carboxylate-cation coordination leading to an increase in the gel dynamic moduli (G' and G'') according to the cation valency [61]. pH, on the other hand, promoted the aggregation of 0.1 wt.% TOCN fibres leading to a stiff gel as confirmed by the rheological spectra [92]. Varying the ionic strength in nanocellulose suspensions have a varied effect on its rheology. Some literature suggests a lowering of viscosity due to compression of the electrical double layer [70, 93, 94] whereas other literature suggest increased viscosity due to aggregation [88, 95]. The presence of amphiphilic molecules, such as surfactants, can adsorb on the nanocellulose inducing both gelation and destabilisation effects depending on the headgroup of the surfactant [96-98].

Nanocellulose cryogels and aerogels can be produced from the hydrogels through either supercritical drying of hydrogels or freezing and ice templating methods [99]. Characterization of the foam structure includes determining porosity, density, and specific surface area via intrusion methods (mercury porosimetry) and visualisation methods (tomography) [100, 101]. A wide range of densities spanning from 1 to 200 kg.

m⁻³ were produced using various methodologies [99]. Volume changes due to shrinkage were also reported depending on the type and concentration of nanocellulose as well as the processing conditions [99, 101, 102]. Aerogels (pore size distribution < 50nm) can be obtained by supercritical drying whereas ice templating methods often produce larger pores which is controlled by solvent behaviour [101, 103]. Other foam analysis includes mechanical testing, thermal, electric and acoustic testing depending on the intended applications [104-107].

1.2.1.4 Applications of Nanocellulose Hydrogels and Foams

Nanocellulose hydrogels and foams can be utilised for a variety of applications spanning from pulp and paper to biomedical industries. In this section, a particular emphasis on the applications on TOCNs are reviewed. The incorporation of TOCNs in paper to produce cellulosic composites have produced improvements in key paper characteristics. TOCNs have been studied for use as reinforcing filler to improve the wet tensile strength of paper. The interaction of TOCNs together with cationic polymers such as cationic poly(acrylamide) (C-PAM) and poly(vinylamine) (PVAm) have improved the wet strength of the sheets [108]. TOCNs have also been introduced to toughen plastics such as poly(lactic acid) (PLA). PLA modified with 1 wt% TOCN exhibited a 25x increase in strain-to-failure and an order of magnitude increase in work of fracture [109]. In the field of nanocomposites, TOCN has been studied as a reinforcing and dispersing agent for single walled carbon nanotubes (CNTs). It was found that the surface-anionic TOCN (with abundant sodium carboxyl groups) was effective at nanodispersing CNTs in water and also as a dried composite film. The nanocomposite film was found to be flexible and highly conductive even with a small amount of CNTs, and therefore it provides a promising candidate as a green matrix for electrical materials, as opposed to conventional polymers [110].

In the biomedical field, TOCN hydrogels have been studied for a variety of applications. TOCN hydrogels are often converted into films or membranes which are then utilised as a nucleation platform for biominerals, anti-bacterial membranes, or muscular actuators [67, 111, 112]. TOCN hydrogels have been studied for potential use as tissue engineering

scaffolds which provide a three-dimensional foundation for cellular attachment, proliferation, and differentiation, ultimately leading to tissue formation. Cellulosic materials have a lot of potential in this area due to their innate biocompatibility, inertness, and biodegradability. Fibrillation of cellulose into nanofibres has drastically improved mechanical strength and its similarity to the natural collagen fibrils found in the extracellular matrix in the human body [113]. However, cellulose lacks bio-recognitions required for cell growth. To solve this issue, various proteins have been inserted into the nanocellulose network.

In [114], fibronectin protein was attached to TOCN hydrogels. The addition of proteins, regardless whether physically or covalently bonded, improved the adhesion of fibroblasts in comparison to unmodified TOCN hydrogels. However, most of the cell growth occurred on top of the hydrogel surface. Cell penetration was minimal and was attributed to the nano-scale pore size of the hydrogels. In [115], elastin-like polypeptide (ELP) was utilised as a cross-linking agent in TEMPO-oxidised bacterial cellulose (TEMPO-BC). ELP is a positively charged artificial protein which is able to bridge between negatively charged nanocellulose fibres. ELP produces a thermo-responsiveness and thermo-reversibility in this hydrogel due to its folding and coacervation when heated to 37°C. It was determined that the resulting hybrid hydrogel is non-cytotoxic and suitable for cell encapsulation.

Accordingly, there are studies which investigate cell cytotoxicity and behaviour in nanocellulose regardless of its form (i.e. gel, membrane, film). Most studies report little to no significant cytotoxicity effects of nanocellulose fibres on cells [9]. A few studies have been encountered which dealt specifically with TOCN fibres. A study reported a low level of cytotoxicity for TOCN fibres even with the addition of polyethyleneimine and cetyl trimethylammonium bromide [116]. TOCNs seem to promote fibroblast adhesion and cell viability comparable to a commercially available tissue culture material [117]. Only one study has been encountered which correlated cell adhesion to the carboxylate content, specifically for TOCN films. It was determined that increased

carboxylate content increases the cell adhesion and cytocompatibility of the TOCN film [118].

Nanocellulose have also been investigated as a potential stabilising agent for emulsions. Solid particles can act as stabilisers to form Pickering emulsions as they can irreversibly adsorb at the liquid-liquid interface. Pickering emulsions tend to form a more stable emulsion than surfactants due to their high energy of adsorption [119]. In a study by Gestranius *et al.* [120]., TOCNs have been studied as a stabiliser for an emulsion consisting of dodecane in water. The creaming phase formation is dependent on the TOCN concentration and is seen to be more stable than in contrast with CNC. Underneath the creaming phase, emulsions form a dilute and stable dispersion of oil droplets. In another study [121], a nano-composite film containing polystyrene and TOCNs is produced through the formation of an aqueous Pickering emulsion. It has been reported that the emulsion has a monomodal size distribution and has remained unchanged for a week. It is attributed in this study that the stability can be attributed to the stronger repulsive forces and increased viscosity arising from the TOCNs.

Cryogels and aerogels were produced from hydrogels using various methodologies (Figure 6) and utilised for multiple applications [99]. The high porosity of TOCN foams arising from their nano-scale fibrils makes them feasible for thermal, acoustic, and electric insulation [103]. TOCN foams were produced via dilute acid addition to promote gelation followed by solvent exchange and supercritical drying [122]. In the study of Gordeyeva, Fall [123], non-ionic surfactant templating coupled with Ca^{2+} -induced gelation has resulted in TOCN foams which possess higher specific elastic modulus than conventional polyurethane foams which can be used for thermal insulation. Complex shapes are also possible to be made with a new methodology of oven-drying to produce TOCN foams which are capable of absorbing and release 34 times its own weight in water [124]. A polyethyleneimine (PEI)-TOCN composite foam was produced and is capable to perform fast and reversible CO_2 capture ($2.22 \text{ mmol CO}_2 \cdot \text{g}^{-1} \text{ foam}$) [125].

TOCNs have also been processed into superabsorbent foams and aerogels. The effect of process variables such as pulp types, composition and oxidation severity on the absorption capacity of TOCN foams were quantified in saline (0.9 wt.% NaCl) [126-129]. Functionalisation of TOCN aerogel via vapour deposition of triethoxy(octyl) silane produced an oleophilic aerogel capable of absorbing at least 200 g.g⁻¹ of hexane and up to approximately 300 g.g⁻¹ of chloroform [130]. However, the relationship between foam properties to the changes in the fibre density and composite structure have not been established. Swelling kinetics have also not been studied in TOCN foams.

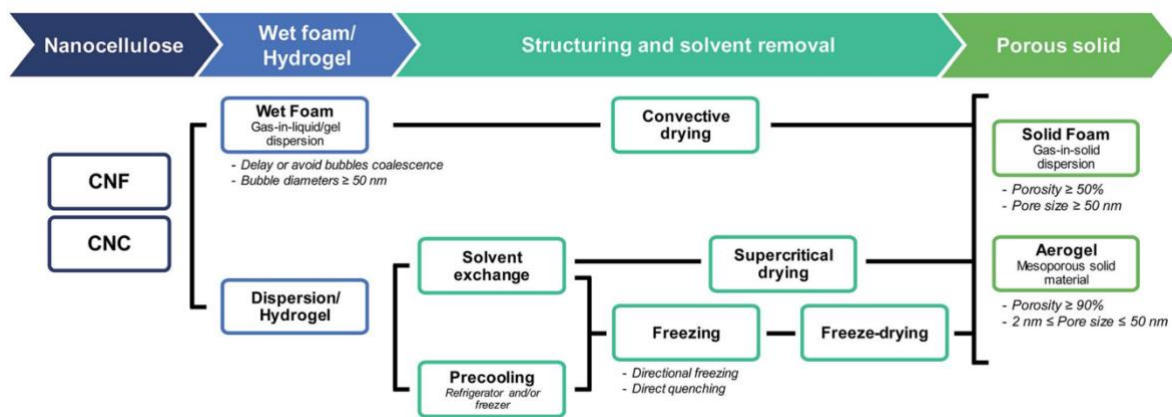


Figure 6. The production of nanocellulose aerogels and foams via various methodologies. Reproduced with permission from [99] under creative commons policy.

1.2.2 RHEOLOGY

Rheology is the study of the flow of matter. It is a heavily utilised characterisation technique necessary for understanding complex ‘soft’ material systems such as hydrogels. Rheological properties can be measured by applying controlled mechanical deformation via shear or extension (elongation) and measuring its response. The mechanical deformation applied on a material can be varied – from small to large perturbations which may or may not cause fluid flow. This can provide insight to the complex microstructure present in hydrogels – its formation, understanding the effect of different chemical and environmental parameters as well as its compatibility in different applications [131].

Rheological behaviour can be determined using a great variety of instruments such as single-result viscometers (Ubbelohde Viscometer, Falling Ball Viscometer) to the more complex rheometers. For soft materials such as hydrogels, stress- or strain- controlled rotational rheometers can be utilised [132]. Different measurement geometries (*cone and plate, parallel plate, cup and bob*) must be employed according to the sample tested. The selection of the correct geometry depends on the individual particle size, sample form (self-standing or liquid) and volume, desired testing range (shear rate or shear stress), temperature range, and potential evaporation problems. The selection of the correct geometry affects the accuracy of the rheological testing [133].

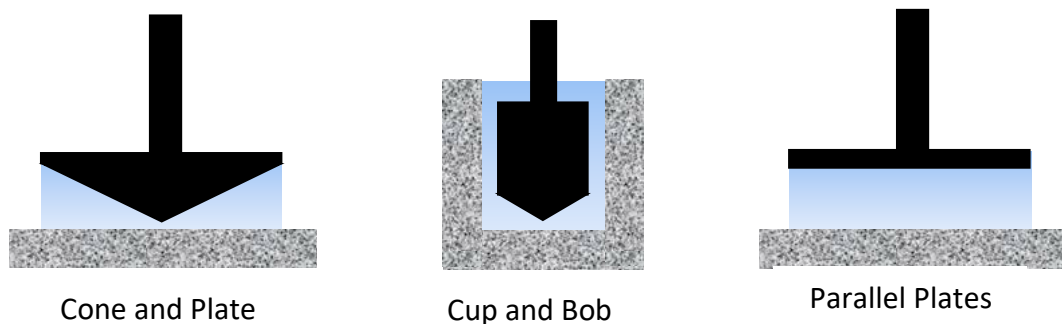


Figure 7. Different geometry systems for rheological characterisation in rotational rheometers

Materials behave differently depending upon the time scale of rheological testing. This is characterised by the Deborah Number (De), which is the ratio between the characteristic sample relaxation time λ and the observation time t . An ideal Newtonian viscous fluid which changes rapidly upon applying stress or deformation will have an infinitesimally short relaxation time ($\lambda \approx 0$) and hence, De approaches 0. Conversely, a purely elastic material (*Hookean solid*) possesses an infinitely long relaxation time resulting in an equally large De value. A material may also appear solid-like when the observation time-scale t is very small. For instance, water ($\lambda \approx 10^{-12}$) is typically considered to be liquid-like in ambient conditions but can behave more solid-like when tested at extremely short time scales (10^{-8} s) or very high frequencies. There are also materials which behave in between these two extremes – they are commonly referred to as *viscoelastic fluids*. Hydrogels display this behaviour because the time required for its microstructure to rearrange is within the experimental timescale (De approaches 1).

Figure 8 illustrates the types of rheological behaviour which occurs at various Deborah number ranges [134, 135].

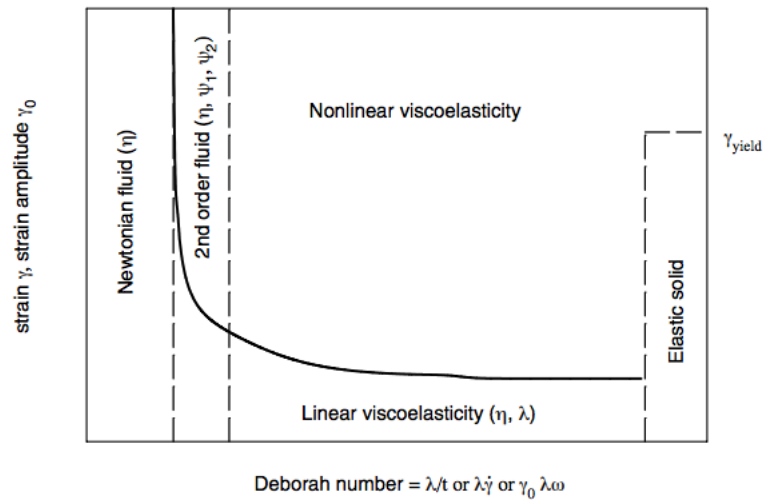


Figure 8. The rheological behaviour of fluids over a range of time-scales. Reproduced with permission from [134].

1.2.2.1 Steady-state Shear

The deformation of a fluid in between plates under shear in ideal Couette flow is illustrated in Figure 9. When the top plate is sheared while the bottom plate remained stationary, this generates a shear stress on the fluid. Upon flow, fluid velocity increases from 0 at the bottom plate to velocity U at the top plate. The velocity therefore increases at a rate of $\frac{\partial u}{\partial y}$. When steady flow is reached, the viscosity η can be defined as [136]:

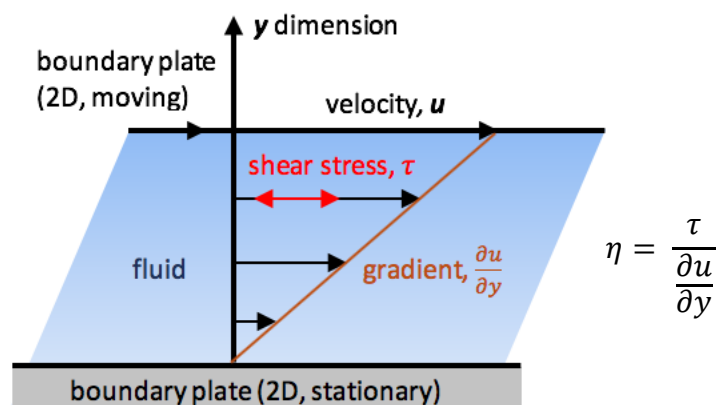


Figure 9. Deformation of a fluid under constant shear force by two plates and the equation of viscosity.

Continuous deformation of a material allows the identification of its flow behaviour. *Newtonian fluids* are characterised by the constitutive relations between stress and strain rate as dictated by Newton's law of viscosity. As a result, they possess viscosity independent of the shear rate and only varies due to temperature. However, there are materials wherein their viscosity varies as a function of shear rate (*Non-Newtonian*), as shown in Figure 10. Colloidal suspensions and polymer solutions possess viscosities which decrease on increasing shear rate which are referred to as *shear-thinning*. On the other hand, substances which possess microstructures that agglomerate together causing an increase in viscosity are called *shear-thickening*. Non-newtonian fluids that require a minimum stress in order to flow are called *Bingham fluids*. There are also materials which possess a combination of rheological properties such as ketchup which is classified as a *Bingham pseudo-plastic fluid* [134, 137].

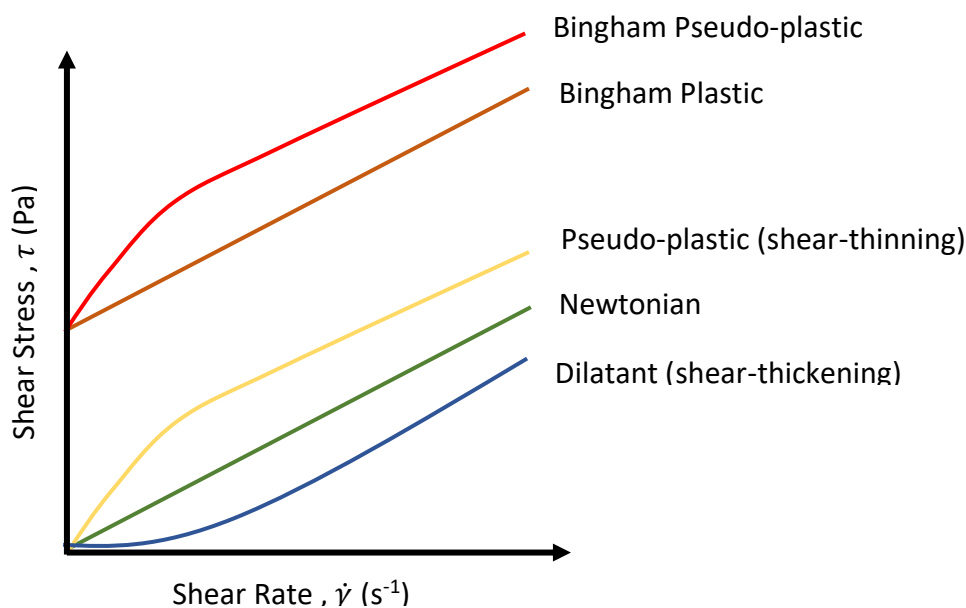


Figure 10. Characteristic shear stress-shear rate relationship for Newtonian and non-Newtonian time-independent fluids.

The steady-shear behaviour of materials can also be time-dependent as shown in Figure 11. Materials which exhibit viscosity reduction upon applying shear and is reversible on removal of shear force are classified as *thixotropic* materials. On the other hand, *rheopectic* behaviour occurs when the viscosity increases with the duration of applied shear stress but is also reversible when shear is removed. The extent of recovery between the initial and final state can be quantified by the degree of hysteresis [138].

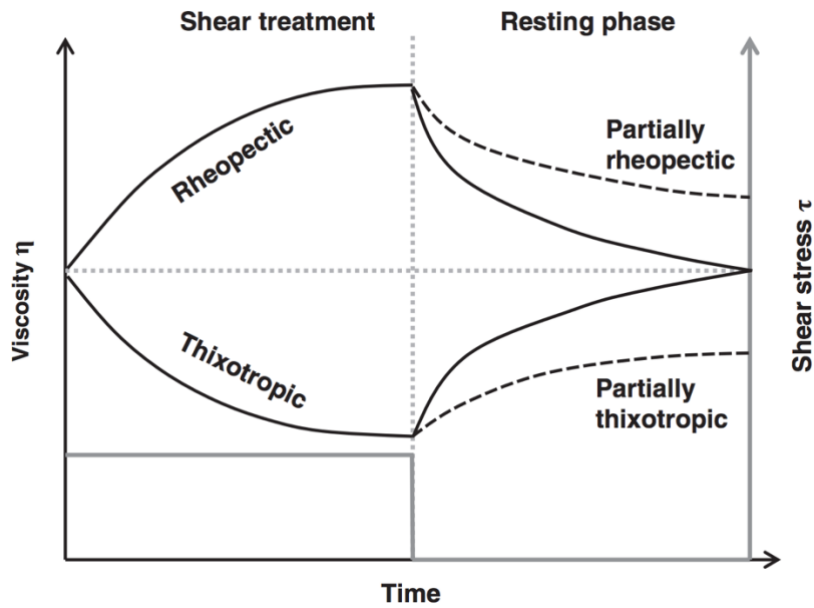


Figure 11. Viscosity behaviour of time-dependent rheopectic and thixotropic materials. Reproduced with permission from [138].

There are several ways to define the viscosity of material. Dynamic viscosity is expressed in the SI Pa. s units or in cP (1 Pa.s = 1000 cP). Normalised (kinematic) viscosity, which is defined as the resistance to flow under gravity, can be reported by dividing the dynamic viscosity by the sample density (m^2/s) [139].

1.2.2.2 Dynamic Oscillatory Shear

Dynamic deformation is conducted at sufficiently low strains such that the hydrogel maintains equilibrium structural states (close to 'at-rest' conditions), revealing information about the network structure. An oscillatory shear test, as the name suggests, involves oscillatory perturbations of a material while continuously measuring its response to increasing amplitude over a specified range. The oscillatory strain γ and the associated stress σ applied to the material can be represented by the following equations [134]:

$$\gamma = \gamma_0 \sin \omega t$$

$$\sigma = \sigma_0 (\sin \omega t + \delta)$$

Where γ_0 and σ_0 pertain to the oscillation amplitude, ω is the angular frequency (rad/s), t is time (s), and $\delta(\omega)$ is the loss angle which is the phase difference between the stress and strain (Figure 12).

The dynamic or complex modulus is given by the following [134]:

$$G^* = \frac{\sigma_0}{\gamma_0} e^{i\delta}$$

$$G^* = G' + iG''$$

$$|G^*| = \sqrt{G'^2 + G''^2}$$

$$\tan \delta = \frac{G''}{G'}$$

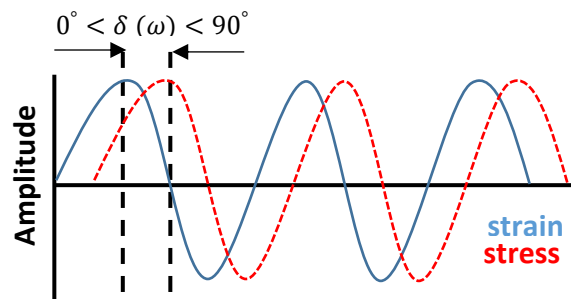


Figure 12. Oscillatory strain input and output stress wave-forms with the loss angle indicated.

For instance, in a cone and plate geometry, the sample is loaded into the gap between a stationary plate and rotating cone. For most studies, an increasing strain amplitude at constant frequency is applied. Viscoelastic materials such as hydrogels exhibit both elastic and viscous properties which are captured by the storage modulus (G') and loss modulus (G'') respectively. The ratio of the loss modulus to the storage modulus can be expressed as $\tan \delta$. Figure 13 illustrates typical oscillatory strain test spectra. At sufficiently low shear, the hydrogel network structure remains stable, indicated by constant G' and G'' (i.e. material properties are independent of shear). This is defined as the *linear viscoelastic region* (LVR). Generally speaking, the longer the LVR, the stronger the existing polymeric network structure. Once the critical strain is reached, the network cannot maintain its original shape as seen in the drop in the moduli. The cross-over point wherein $G' = G''$ dictates the onset of material yield. When $G'' > G'$, the material will start flowing [140].

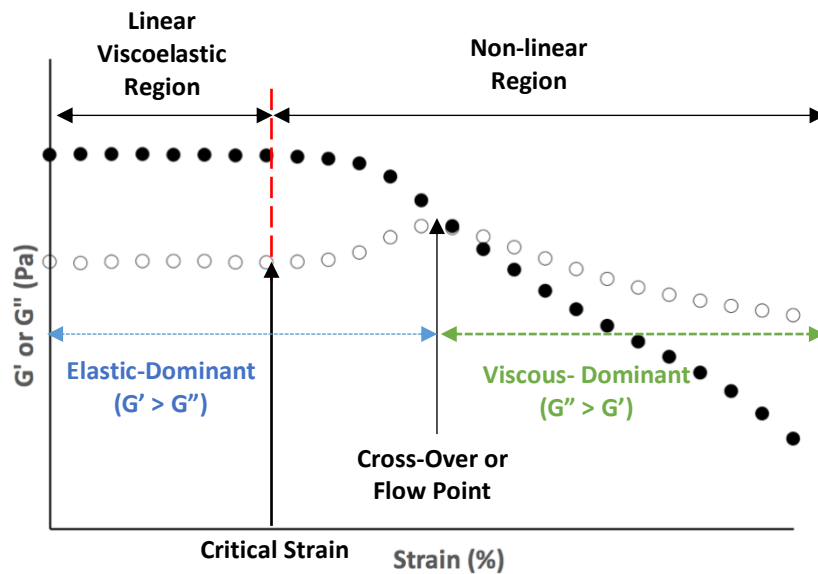


Figure 13. Oscillatory strain sweep with the key parameters indicated

The viscoelastic behaviour of hydrogels can be further characterised if the dependence of its dynamic moduli (G' , G'' , $\tan \delta$) can be understood not only as a function of shear but also as a function of frequency ω (i.e. time-scale). A frequency sweep (at a constant amplitude) can be utilised to understand the time-dependent behaviour of the gel at various time-scales. At lower frequencies, the long-term behaviour of the gel is probed (how it responds to deformation over a long time-scale) whereas the short-term behaviour is probed at higher frequencies (under rapid oscillation) [140]. How the material responds at various time-scales gives an indication of the structural conditions of the system, allowing to categorise and differentiate dispersions and entangled polymer solutions from gels as shown in Figure 14.

Dispersions can be identified when viscous behaviour dominates ($G'' > G'$) over a wide frequency range (Figure 14A). However, when ω increases, G' increases more rapidly than G'' indicating the increasing short-term elastic behaviour. At high enough concentrations, entangled polymer solutions can behave as pseudo gels (Figure 14B) because the oscillation frequency (i.e. measurement time-scale) is more rapid than the 'relaxation' time of the entangled polymer network, resulting in the material appearing more elastic ($G' > G''$) with a characteristic G'' curve. Weak gels, on the other hand,

clearly show elastic dominant behaviour ($G' > G''$) over a large range of frequencies (Figure 14C), with the moduli 'ramping' showing the cooperation of secondary interactions (i.e. H-bonding, van der Waals forces, hydrophobic interactions, etc.). These weak gels represent a behaviour intermediate of a polymer solution and a strong gel. Strong gels, which consist of a continuous 3D network, show an elastic dominant behaviour that is completely independent of frequency (Figure 14D) [131].

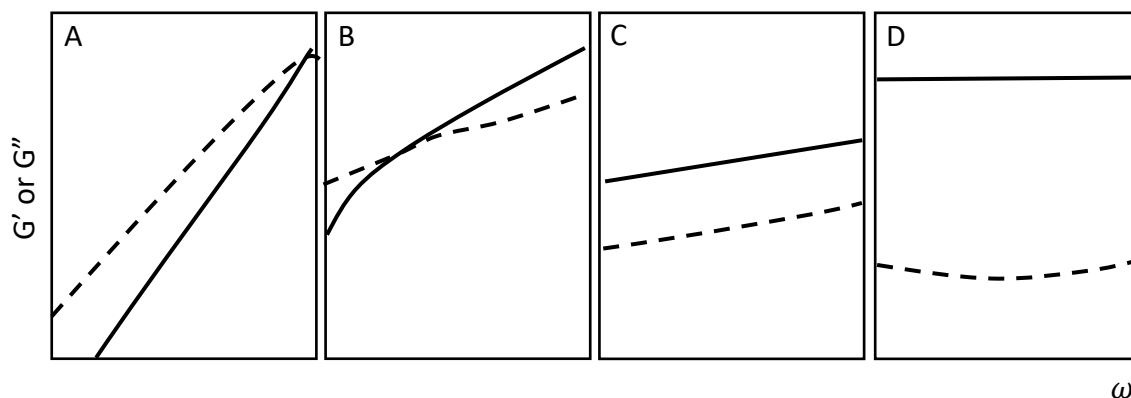


Figure 14. Typical rheological spectra of a: (A) dispersion, (B) entangled polymer solution, (C) weak gel, and (D) strong gel. G' is represented by a bold line whereas G'' is represented by a dashed line.

1.2.3 ATOMIC FORCE MICROSCOPY

Atomic force microscopy (AFM) is a technique which allows the visualisation and measurement of surface structure with high resolution and accuracy. AFM is capable of visualising down to the atom-scale without the need for intensive sample preparation or specific microscopy environment (i.e. cryogenic conditions, vacuum). It is capable of testing different types of materials easily: from hard ceramics, dispersions, to biological specimens. An AFM acquires an image by raster-scanning an area of a small sample whilst measuring the local properties. It is a type of scanning probe microscope, different from other forms of microscopy as it *physically interacts* with the sample surface by using a probe. Aside from imaging, atomic force microscopy can measure local properties such as height, friction, and magnetism.

The AFM is essentially composed of a probe attached to a mechanism which controls and records its movement to measure physical information (Figure 15). The probe, which has a sharp pyramidal tip, is attached to one end of a spring-like cantilever. A piezoelectric element is often attached to the cantilever for controlled oscillation. The movement of the probe in the vertical and lateral directions is measured by an optical lever which sends a laser at the cantilever. The laser beam is reflected towards a position-sensitive four-segment photodetector which translates to the angular deflections of the cantilever [141].

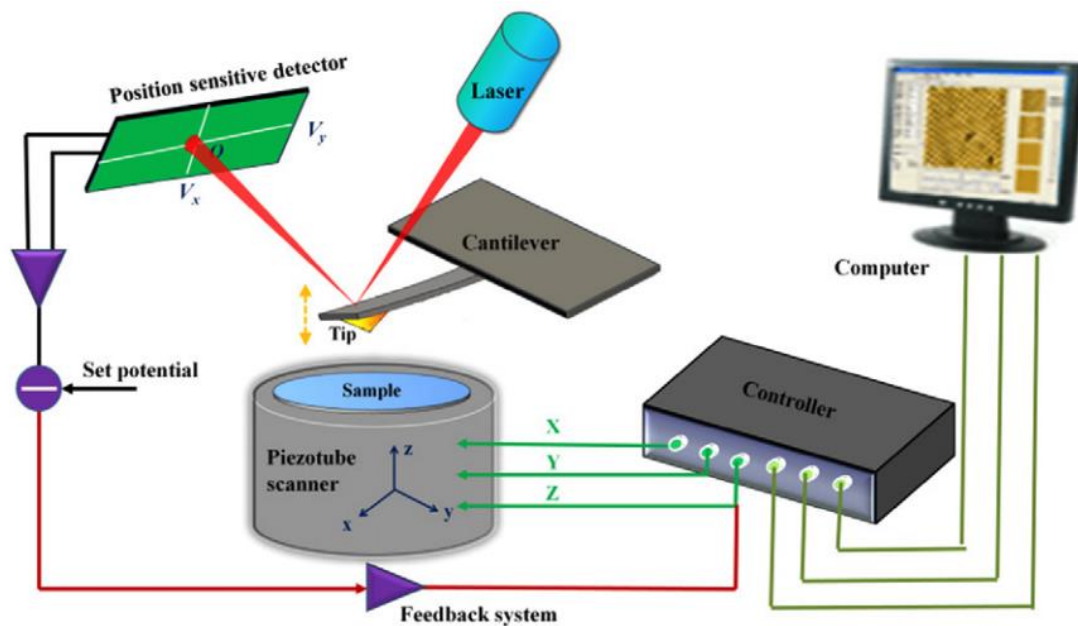


Figure 15. Schematic Diagram of an atomic force microscope. Reproduced with permission from [142] under creative commons policy.

There are three imaging modes that are available with the AFM: (1) Contact mode, (2) Non-contact mode, and (3) Tapping mode. In contact mode, also known as static mode, the probe is consistently in contact with the surface. Any deflections in the cantilever due to changes in the height in the z-direction is recorded at a particular x,y point to generate a topographical image. In tapping mode, a type of dynamic operating mode, the cantilever is closer to the surface and vibrating at a higher frequency close to its resonance frequency. At the lowest trajectory, the tip is briefly touching the surface. In non-contact mode, the tip is vibrating at a constant frequency above the surface without any contact with the sample. In this mode, long range forces such as magnetic,

electrostatic and van der Waals forces can be measured [143]. Figure 16 shows a diagram illustrating the various imaging modes of the AFM.

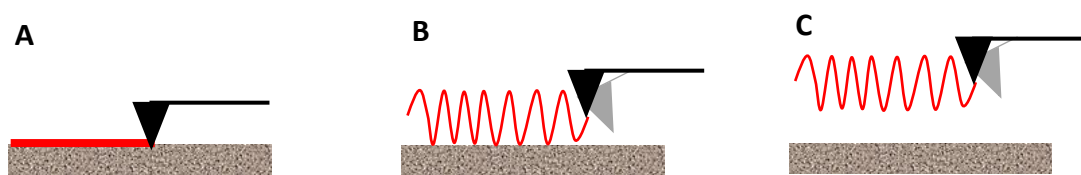


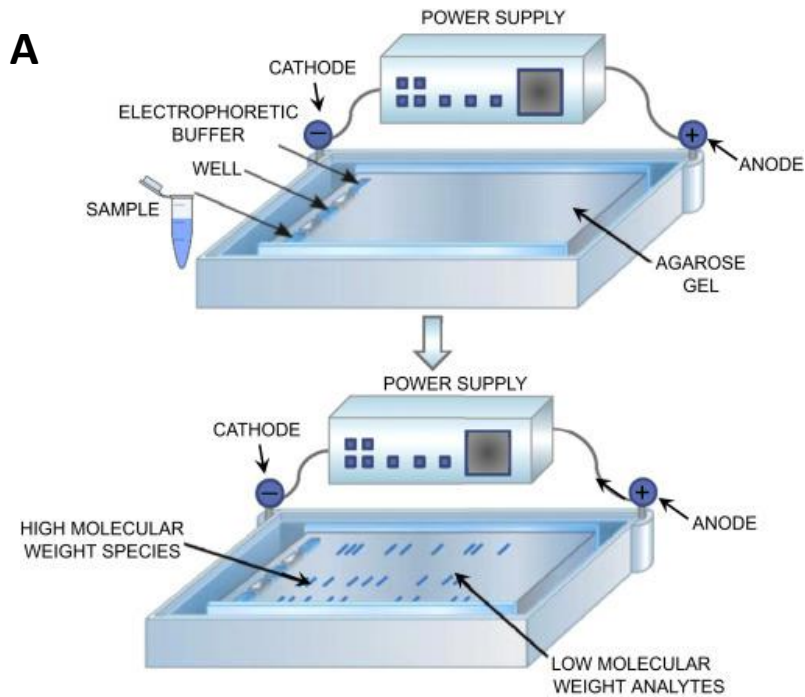
Figure 16. Schematic Diagram illustrating the operating modes of the AFM: (a) contact mode, (b) tapping mode, and (c) non-contact mode.

1.2.4 ELECTROPHORESIS

Electrophoresis refers to the technique for separating protein and nucleic acids by different mobilities under an electric field. This technique is heavily utilised for life science research particularly in DNA and protein purification, characterisation (size, structure, and amount) and determining DNA mutations or gene expression in the mRNA or protein amongst others. There are many variations of electrophoresis methods (isoelectric focusing, pulsed field gel electrophoresis); however, the most commonly used is the gel electrophoresis. Gel electrophoresis, specifically, utilises gels for separation. Conventional materials include agarose (DNA separation) and polyacrylamide (Protein separation) [144].

In a typical configuration, the sample (protein or DNA mixture) is loaded near the negatively charged electrode of the gel tank. When power is applied, the negatively charged molecules (DNA or RNA) will migrate to the positively charged electrode. Current travels through the gel and within the tank through electrophoresis buffers. The most common electrophoresis buffers for nucleic acids are Tris/Acetate/EDTA (TAE) or Tris/Borate/EDTA (TBE) whereas Tris-glycine (Laemmli buffer) is usually utilised for protein separation. Electrophoresis buffers also maintain the constant pH throughout the testing. DNA or RNA separation are often performed through an agarose gel. Agarose is a polysaccharide gel which is thermoresponsive - when agarose is melted in a buffer and cooled, it will form a solid gel. The agarose acts like a sieve by varying the solids concentration (different pore size): large molecules are not able to pass through the gel as easy as small molecules. Moreover, differently size molecules will migrate at

different rates [145, 146]. Figure 17 illustrates the horizontal and vertical gel electrophoresis systems. Once the electrophoresis is finished, the separated molecules can be visualised by the addition of a stain such as ethidium bromide for DNA and Coomassie blue for proteins [145, 146]. Figure 18 shows an example of protein separation through agarose gel electrophoresis.



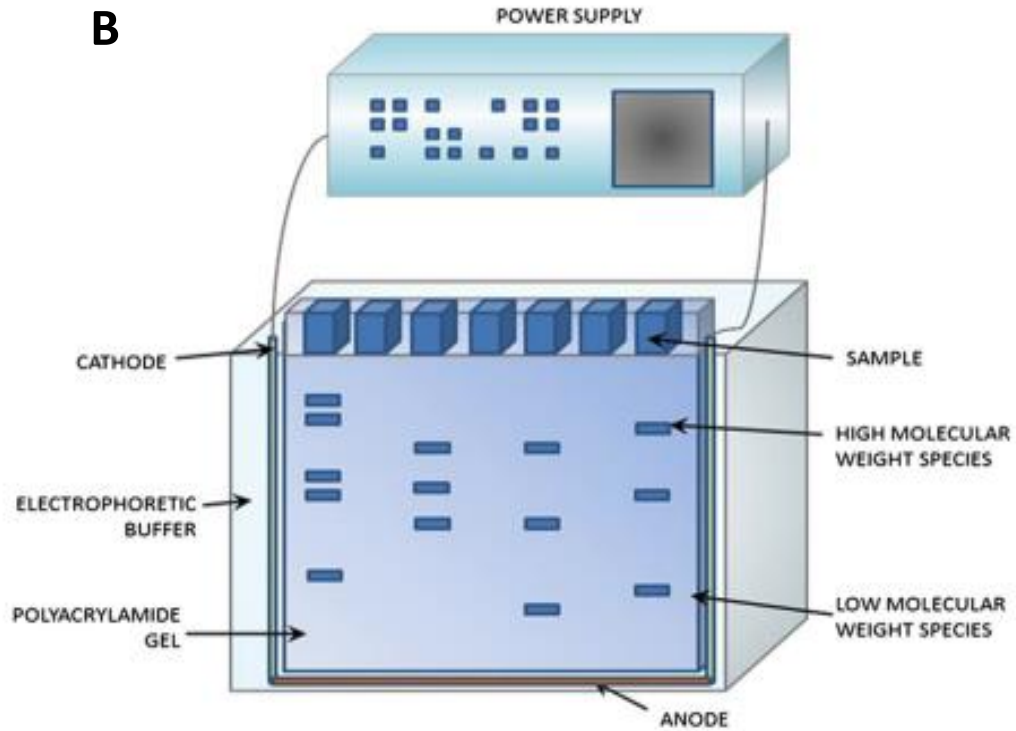


Figure 17. (A) Horizontal and (B) vertical gel electrophoresis systems. Reprinted from [147] Copyright (2019), with permission from Elsevier.

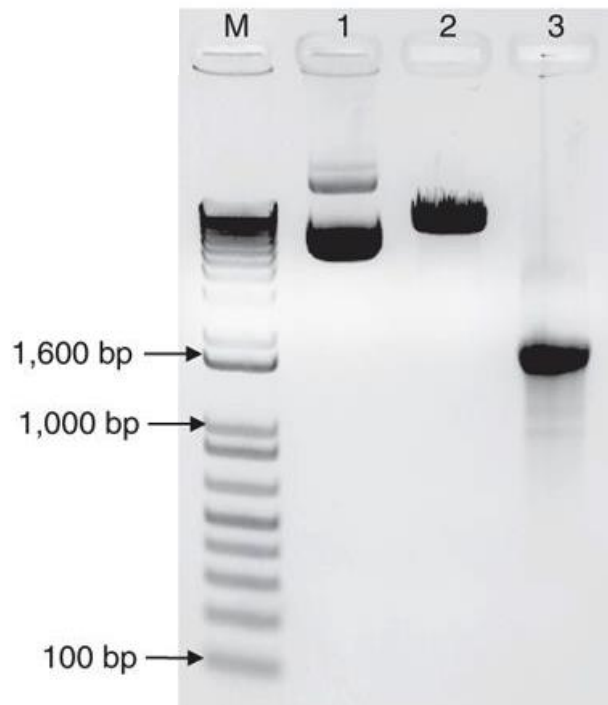


Figure 18. Electrophoretic separation in 1wt.% agarose gel of digested plasmid (lane 1), undigested plasmid (lane 2), and synthesised Cas9 mRNA (lane 3) contrasted against a molecular marker (lane

M). Smaller proteins (ie. lower base pairs or bp) travel further down the agarose gel. Reprinted by permission from Nature, Nature Protocols, [148], 2016.

1.2.5 PERSPECTIVES

Nanocellulose is an emerging nanomaterial that is highly appealing due to its sustainable and renewable origins. The performance and behaviour of nanocellulose are highly dependent on processing and production methods. Moreover, the usage of chemical pre-treatment methods allows more energy efficient extraction of nanocellulose. These methods introduce new moieties on the cellulose polymer surface leading to differences in physico-chemical behaviour in contrast to the original macro-fibres.

TEMPO-mediated oxidation is a commonly utilised pre-treatment to produce nano-scale fibres containing carboxylate groups. This surface modification of cellulose fibre leads to a different material state (gels) than the typically observed suspension of cellulose fibres in water. There is a need for fundamental understanding of the phenomena involved. Chain length and surface charge have been shown to be influenced by oxidation conditions and cellulosic origins. However, there are fundamental structure-property relationships which must be established. Comprehensive rheological characterisation of this material will form this understanding. Characterisation of nanocellulose gels is critical in order to define the property range available and design specific applications.

Applications of TEMPO-oxidised nanocellulose are clearly increasing in literature. Initial studies of this type of nanocellulose began as an additive for pulp and paper and then progressed in other fields such as in biomedicine. The formation of bio-based gels can be mainly exploited as a potential tissue engineering scaffold or cell culture media. Formation of foams from gels have also been steadily explored. There is an avenue for development from both gels and foams. The development of high value products can drive the commercialisation of nanocellulose.

1.3 GAPS IN KNOWLEDGE

From the literature review, gaps in scientific knowledge were identified leading to hindrances in developing the potential of nanocellulose to be utilised for novel applications. Hence, the following gaps needs to be addressed:

1. The formation of nanofibrillated cellulose into colloidally stable hydrogels in contrast to quasi- stable suspensions
2. The range of achievable physical properties of neat nanofibrillated cellulose gels
3. The effect of fibre properties (surface charge, pulp source, concentration) and environmental variables (pH and ionic strength) on the physical properties and stability of gels
4. Step-wise development of appropriate novel applications for nanocellulose gels

1.4 RESEARCH OBJECTIVES

This thesis endeavours to increase the knowledge in this field of research by exploring the fundamental science of nanocellulose colloidal systems and the step-wise development of novel applications. The following are the objectives of this thesis:

- 1) To understand the mechanism of self-assembly and gel formation of TEMPO-oxidised nanocellulose fibres in water
- 2) To understand the effect of the following process variables on the stability and rheological properties of TEMPO-oxidised nanocellulose gels:
 - i) fibre concentration
 - ii) pH
 - iii) ionic strength
 - iv) fibre surface charge
 - v) pulp source
- 3) To develop and test the feasibility of novel applications for nanocellulose
 - i) Produce carboxylated nanocellulose foams and test its capability as a superabsorbent agent.
 - ii) Cast nanocellulose gel slabs and test its feasibility as an electrophoresis media.

1.5 THESIS OUTLINE

This dissertation is presented in the format of “*Thesis including published works*” based on the Monash University guidelines for Doctoral and MPhil Degrees 2016 and the Thesis including Published works guidelines. It contains four experimental chapters wherein all of them are published. The published papers are reformatted for a consistent presentation whilst the content remains unchanged. The original publications are provided in Appendix I.

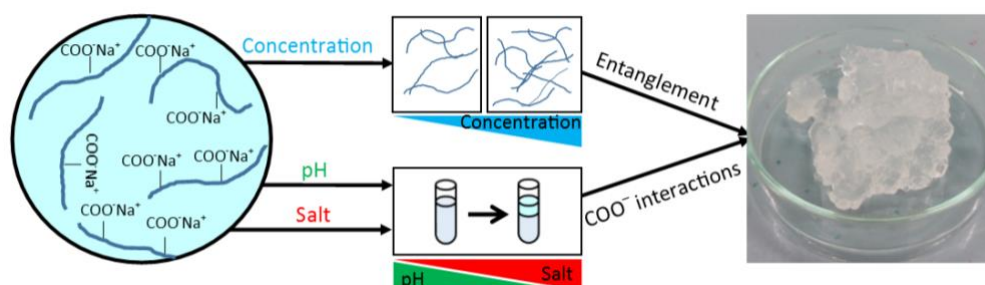
The following is the thesis structure outlining the aims, conducted research and outcomes:

- **Chapter 1 – Literature Review.**

This chapter aims to provide a summary of the recent studies on various aspects of nanocellulose. It includes an overview of nanocellulose production methods, discussion of colloidal nanocelluloses, and characterisation at different scales. Furthermore, the principles of critical techniques utilised for characterisation and testing are presented. A perspective on the reviewed literature is provided followed by the identified gaps in knowledge and subsequently, the overall research objectives.

- **Chapter 2 – Gelation Mechanism of Cellulose Nanofibre Gels: A colloids and interfacial perspective.**

Llyza Mendoza, Warren Batchelor, Rico F. Tabor, Gil Garnier (2018). Gelation mechanism of cellulose nanofibre gels: A colloids and interfacial perspective. Journal of Colloid and Interface Science. 509: 39-46.

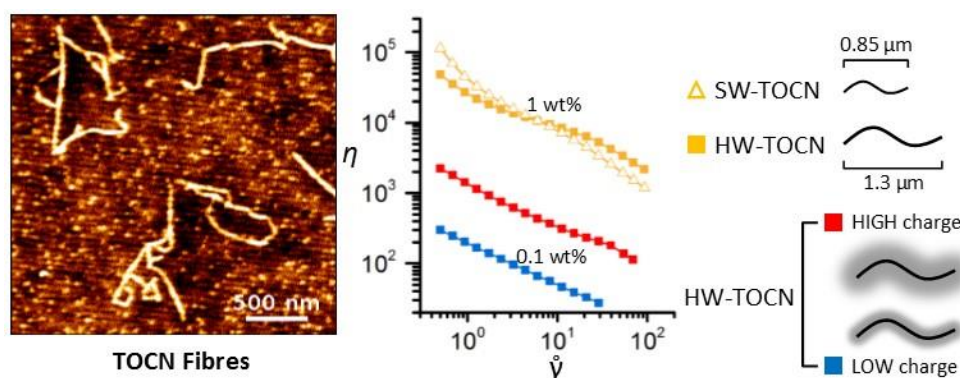


This second chapter focuses on the rheological studies of TEMPO-oxidised nanocellulose to understand gel formation and assembly. Gels with different concentrations of cellulose nanofibres were produced and rheological tests were performed. It was

determined that gel rheological properties are sensitive to fibre concentration. Moreover, gel colloidal stability is influenced by changes in pH and salt content. It is explained that the formation of gels by surface-modified nanocellulose is through the combination of electrostatic stabilising interactions and physical entanglement.

- **Chapter 3 – Effects of fibre dimension and surface charge on nanocellulose gels.**

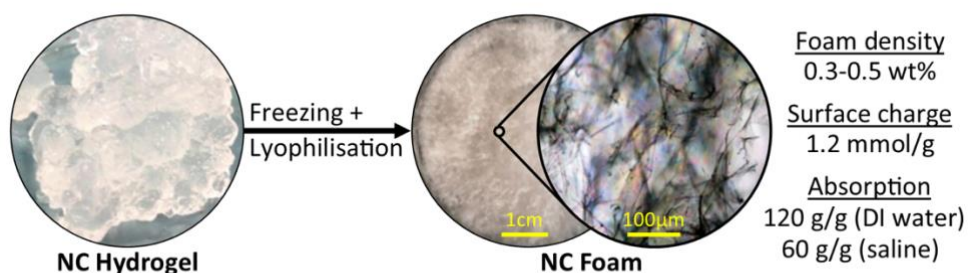
Llyza Mendoza, Thilina Gunawardhana, Warren Batchelor, Gil Garnier (2018). Effects of fibre dimension and charge density on nanocellulose gels. Journal of Colloid and Interface Science 525: 119-125.



In this chapter, the effects of different types of pulp – softwood and hardwood, and charge density to the resulting nanocellulose gel properties are reported. Nanocellulose fibres extracted from both pulp types exhibit similar widths but different length dimensions as revealed by AFM analysis. Rheological measurements show that the dynamic moduli (G' and G'') of nanocellulose gels are independent of pulp source and are mostly influenced by fibre concentration. Differences in the steady-state behaviour at constant surface charge can be attributed to differences in fibre length. Increasing the surface charge density influences the critical strain and the viscosity at the percolation concentration due to higher electrostatic interactions.

- **Chapter 4 – Carboxylated nanocellulose foams as superabsorbents.**

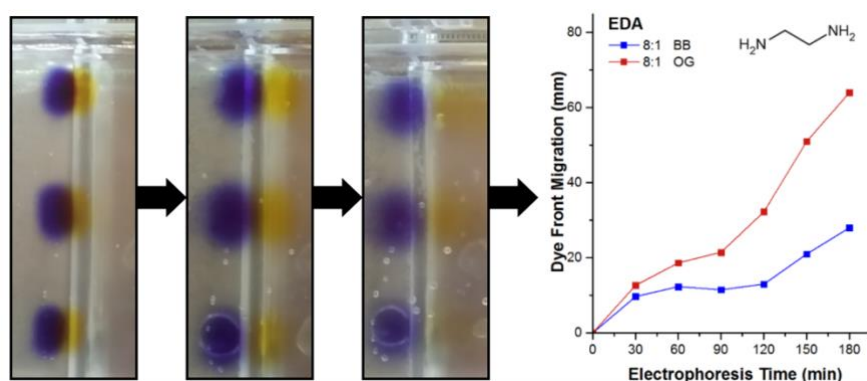
Llyza Mendoza, Laila Hossain, Emma Downey, Camilla Scales, Warren Batchelor, Gil Garnier (2019). Carboxylated nanocellulose foams as superabsorbents. Journal of Colloid and Interface Science 538: 433-439.



The hydrophilic nature of TEMPO-oxidised cellulose nanofibres can be exploited to produce a superabsorbent agent. In this chapter, the feasibility of nanocellulose gels as a superabsorbent media is demonstrated. Nanocellulose superabsorbents are made via a freezing- lyophilisation process and its capacity can be fine-tuned from initial gel properties. The effect of variables such as fibre concentration, charge density, and freezing rate were related to the resulting pore structure and distribution as well as its capacity. It was determined that an optimal foam consisting 0.3 wt.% to 0.5 wt.% nanocellulose, containing 1.2 mmol COO^-/g fibre is capable of absorbing 110-120 g/g (deionised water) and 60 g/g (0.9 wt.% NaCl).

- **Chapter 5 – Nanocellulose for gel electrophoresis.**

Llyza Mendoza, Thilina Gunawardhana, Warren Batchelor, Gil Garnier (2019).
Nanocellulose for gel electrophoresis. Journal of Colloid and Interface Science. 540:148-154



TEMPO-oxidised cellulose nanofibres are chemically cross-linked by boric acid catalysed amide linkages for gel electrophoresis separation. Nanocellulose gel slabs containing different cross-linker types and ratios were produced. Changing the cross-linker chain

length and concentration resulted in the variation in the gel network pore size and stability. The effect is assessed via the changes in the migration behaviour of conventional tracking dyes (bromophenol blue and orange G) and gel stability during electrophoresis. Moreover, varying the electrophoresis voltage and observing its effect on the separation of the tracking dyes has been studied.

- **Chapter 6 – Conclusions and Perspectives**

The final chapter of this thesis summarises the key outcomes and perspectives for each of the studies.

1.6 REFERENCES

1. Moon, R.J., et al., *Cellulose nanomaterials review: structure, properties and nanocomposites*. Chemical Society Reviews, 2011. **40**(7): p. 3941-3994.
2. Dufresne, A., *Nanocellulose, From Nature to High Performance Tailored Materials*. 2012.
3. Funahashi, R., et al., *Changes in the degree of polymerization of wood celluloses during dilute acid hydrolysis and TEMPO-mediated oxidation: Formation mechanism of disordered regions along each cellulose microfibril*. International Journal of Biological Macromolecules, 2018. **109**: p. 914-920.
4. Usov, I., et al., *Understanding nanocellulose chirality and structure-properties relationship at the single fibril level*. Nature Communications, 2015. **6**: p. 7564.
5. Khan, A., et al., *Nanocellulose-Based Composites and Bioactive Agents for Food Packaging*. Critical Reviews in Food Science and Nutrition, 2014. **54**(2): p. 163-174.
6. Michael, T.P., et al., *Development of the metrology and imaging of cellulose nanocrystals*. Measurement Science and Technology, 2011. **22**(2): p. 024005.
7. Turbak, A.F., F.W. Snyder, and K.R. Sandberg, *Microfibrillated cellulose, a new cellulose product: properties, uses, and commercial potential*. Journal Name: J. Appl. Polym. Sci.: Appl. Polym. Symp.; (United States); Journal Volume: 37; Conference: 9. cellulose conference, Syracuse, NY, USA, 24 May 1982. 1983: ; ITT Rayonier Inc., Shelton, WA. Medium: X; Size: Pages: 815-827.
8. Klemm, D., et al., *Cellulose: Fascinating Biopolymer and Sustainable Raw Material*. Angewandte Chemie International Edition, 2005. **44**(22): p. 3358-3393.
9. Lin, N. and A. Dufresne, *Nanocellulose in biomedicine: Current status and future prospect*. European Polymer Journal, 2014. **59**: p. 302-325.
10. Klemm, D., et al., *Nanocelluloses: A New Family of Nature-Based Materials*. Angewandte Chemie International Edition, 2011. **50**(24): p. 5438-5466.
11. George, J., S.N. Sabapathi, and Siddaramaiah, *Water Soluble Polymer-Based Nanocomposites Containing Cellulose Nanocrystals*, in *Eco-friendly Polymer Nanocomposites: Processing and Properties*, V.K. Thakur and M.K. Thakur, Editors. 2015, Springer India: New Delhi. p. 259-293.
12. Zhang, K., *Illustration of the development of bacterial cellulose bundles/ribbons by *Gluconacetobacter xylinus* via atomic force microscopy*. Applied Microbiology and Biotechnology, 2013. **97**(10): p. 4353-4359.
13. Esa, F., S.M. Tasirin, and N.A. Rahman, *Overview of Bacterial Cellulose Production and Application*. Agriculture and Agricultural Science Procedia, 2014. **2**: p. 113-119.
14. Heijnesson-Hultén, A., et al., *Impact of Drying on the Quality of Bamboo Kraft Pulps*. 2013. Vol. 8. 2013.
15. Azizi Samir, M.A.S., F. Alloin, and A. Dufresne, *Review of Recent Research into Cellulosic Whiskers, Their Properties and Their Application in Nanocomposite Field*. Biomacromolecules, 2005. **6**(2): p. 612-626.
16. Torres, F.G., et al., *Reversible stress softening and stress recovery of cellulose networks*. Soft Matter, 2009. **5**(21): p. 4185-4190.
17. Song, J., et al., *Fast and continuous preparation of high polymerization degree cellulose nanofibrils and their three-dimensional macroporous scaffold fabrication*. Nanoscale, 2013. **5**(6): p. 2482-2490.

18. Abdul Khalil, H.P.S., et al., *Production and modification of nanofibrillated cellulose using various mechanical processes: A review*. Carbohydrate Polymers, 2014. **99**: p. 649-665.
19. Chinga-Carrasco, G., *Cellulose fibres, nanofibrils and microfibrils: The morphological sequence of MFC components from a plant physiology and fibre technology point of view*. Nanoscale Research Letters, 2011. **6**(1): p. 417.
20. Pääkkö, M., et al., *Enzymatic Hydrolysis Combined with Mechanical Shearing and High-Pressure Homogenization for Nanoscale Cellulose Fibrils and Strong Gels*. Biomacromolecules, 2007. **8**(6): p. 1934-1941.
21. George, J. and S.N. Sabapathi, *Cellulose nanocrystals: synthesis, functional properties, and applications*. Nanotechnology, science and applications, 2015. **8**: p. 45-54.
22. Camarero Espinosa, S., et al., *Isolation of Thermally Stable Cellulose Nanocrystals by Phosphoric Acid Hydrolysis*. Biomacromolecules, 2013. **14**(4): p. 1223-1230.
23. Yackel, E.C. and W.O. Kenyon, *The Oxidation of Cellulose by Nitrogen Dioxide**. Journal of the American Chemical Society, 1942. **64**(1): p. 121-127.
24. Kumar, V. and T. Yang, *HNO₃/H₃PO₄-NANO₂ mediated oxidation of cellulose — preparation and characterization of bioabsorbable oxidized celluloses in high yields and with different levels of oxidation*. Carbohydrate Polymers, 2002. **48**(4): p. 403-412.
25. Gashti, M.P., et al., *Surface oxidation of cellulose by ozone-gas in a vacuum cylinder to improve the functionality of fluoromonomer*. Vacuum, 2013. **91**: p. 7-13.
26. Wågberg, L., et al., *The Build-Up of Polyelectrolyte Multilayers of Microfibrillated Cellulose and Cationic Polyelectrolytes*. Langmuir, 2008. **24**(3): p. 784-795.
27. Isogai, A., et al., *Review: Catalytic oxidation of cellulose with nitroxyl radicals under aqueous conditions*. Progress in Polymer Science, 2018. **86**: p. 122-148.
28. de Nooy, A.E.J., A.C. Besemer, and H. van Bekkum, *Highly selective tempo mediated oxidation of primary alcohol groups in polysaccharides*. Recueil des Travaux Chimiques des Pays-Bas, 1994. **113**(3): p. 165-166.
29. Isogai, A., T. Saito, and H. Fukuzumi, *TEMPO-oxidized cellulose nanofibers*. Nanoscale, 2011. **3**(1): p. 71-85.
30. Saito, T., et al., *Cellulose Nanofibers Prepared by TEMPO-Mediated Oxidation of Native Cellulose*. Biomacromolecules, 2007. **8**(8): p. 2485-2491.
31. Saito, T. and A. Isogai, *TEMPO-Mediated Oxidation of Native Cellulose. The Effect of Oxidation Conditions on Chemical and Crystal Structures of the Water-Insoluble Fractions*. Biomacromolecules, 2004. **5**(5): p. 1983-1989.
32. Okita, Y., T. Saito, and A. Isogai, *Entire Surface Oxidation of Various Cellulose Microfibrils by TEMPO-Mediated Oxidation*. Biomacromolecules, 2010. **11**(6): p. 1696-1700.
33. Iwamoto, S., et al., *Comparison study of TEMPO-analogous compounds on oxidation efficiency of wood cellulose for preparation of cellulose nanofibrils*. Polymer Degradation and Stability, 2010. **95**(8): p. 1394-1398.
34. Shibata, I. and A. Isogai, *Nitroxide-mediated oxidation of cellulose using TEMPO derivatives: HPSEC and NMR analyses of the oxidized products*. Cellulose, 2003. **10**(4): p. 335-341.

35. Jaušovec, D., R. Vogrinčič, and V. Kokol, *Introduction of aldehyde vs. carboxylic groups to cellulose nanofibers using laccase/TEMPO mediated oxidation*. Carbohydrate Polymers, 2015. **116**: p. 74-85.
36. Kulys, J. and R. Vidziunaite, *Kinetics of laccase-catalysed TEMPO oxidation*. Journal of Molecular Catalysis B: Enzymatic, 2005. **37**(1): p. 79-83.
37. Parpot, P., et al., *TEMPO mediated oxidation of carbohydrates using electrochemical methods*. Cellulose, 2010. **17**(4): p. 815-824.
38. Carlsson, D.O., et al., *Cooxidant-free TEMPO-mediated oxidation of highly crystalline nanocellulose in water*. RSC Advances, 2014. **4**(94): p. 52289-52298.
39. Rohaizu, R. and W.D. Wanrosli, *Sono-assisted TEMPO oxidation of oil palm lignocellulosic biomass for isolation of nanocrystalline cellulose*. Ultrason Sonochem, 2017. **34**: p. 631-639.
40. Pierre, G., et al., *TEMPO-mediated oxidation of polysaccharides: An ongoing story*. Carbohydrate Polymers, 2017. **165**: p. 71-85.
41. Saito, T., et al., *Oxidation of bleached wood pulp by TEMPO/NaClO/NaClO₂ system: effect of the oxidation conditions on carboxylate content and degree of polymerization*. Journal of Wood Science, 2010. **56**(3): p. 227-232.
42. Chang, C. and L. Zhang, *Cellulose-based hydrogels: Present status and application prospects*. Carbohydrate Polymers, 2011. **84**(1): p. 40-53.
43. Isobe, N., et al., *Mechanism of cellulose gelation from aqueous alkali-urea solution*. Carbohydrate Polymers, 2012. **89**(4): p. 1298-1300.
44. Li, N. and R. Bai, *Copper adsorption on chitosan–cellulose hydrogel beads: behaviors and mechanisms*. Separation and Purification Technology, 2005. **42**(3): p. 237-247.
45. Baumann, M.D., et al., *An injectable drug delivery platform for sustained combination therapy*. Journal of Controlled Release, 2009. **138**(3): p. 205-213.
46. Shang, J., Z. Shao, and X. Chen, *Electrical Behavior of a Natural Polyelectrolyte Hydrogel: Chitosan/Carboxymethylcellulose Hydrogel*. Biomacromolecules, 2008. **9**(4): p. 1208-1213.
47. Nakayama, A., et al., *High Mechanical Strength Double-Network Hydrogel with Bacterial Cellulose*. Advanced Functional Materials, 2004. **14**(11): p. 1124-1128.
48. Dukhin, A.S. and P.J. Goetz, *Chapter 2 - Fundamentals of Interface and Colloid Science*, in *Characterization of Liquids, Dispersions, Emulsions, and Porous Materials Using Ultrasound (Third Edition)*, A.S. Dukhin and P.J. Goetz, Editors. 2017, Elsevier. p. 19-83.
49. Okita, Y., et al., *TEMPO-Oxidized Cellulose Nanofibrils Dispersed in Organic Solvents*. Biomacromolecules, 2011. **12**(2): p. 518-522.
50. Kaldéus, T., et al., *Insights into the EDC-mediated PEGylation of cellulose nanofibrils and their colloidal stability*. Carbohydrate Polymers, 2018. **181**: p. 871-878.
51. Derjaguin, B. and L.D. Landau, *Theory of the Stability of Strongly Charged Lyophobic Sols and of the Adhesion of Strongly Charged Particles in Solutions of Electrolytes*. Acta Physicochimica U.R.S.S., 1941. **14**: p. 633-662.
52. Verwey, E.J.W., *Theory of the Stability of Lyophobic Colloids*. The Journal of Physical and Colloid Chemistry, 1947. **51**(3): p. 631-636.
53. Fall, A.B., et al., *Colloidal Stability of Aqueous Nanofibrillated Cellulose Dispersions*. Langmuir, 2011. **27**(18): p. 11332-11338.
54. Israelachvili, J.N., *Intermolecular and Surface Forces (3rd Edition)*. Elsevier.
55. Hamaker, H.C., *The London—van der Waals attraction between spherical particles*. Physica, 1937. **4**(10): p. 1058-1072.

56. Araki, J., *Electrostatic or steric? – preparations and characterizations of well-dispersed systems containing rod-like nanowhiskers of crystalline polysaccharides*. *Soft Matter*, 2013. **9**(16): p. 4125-4141.
57. Fukuzumi, H., et al., *Dispersion stability and aggregation behavior of TEMPO-oxidized cellulose nanofibrils in water as a function of salt addition*. *Cellulose*, 2014. **21**(3): p. 1553-1559.
58. Solomon, M.J. and P.T. Spicer, *Microstructural regimes of colloidal rod suspensions, gels, and glasses*. *Soft Matter*, 2010. **6**(7): p. 1391-1400.
59. Polte, J., *Fundamental growth principles of colloidal metal nanoparticles – a new perspective*. *CrystEngComm*, 2015. **17**(36): p. 6809-6830.
60. Schmitt, J., et al., *TEMPO-oxidised cellulose nanofibrils; probing the mechanisms of gelation via small angle X-ray scattering*. *Physical Chemistry Chemical Physics*, 2018. **20**(23): p. 16012-16020.
61. Dong, H., et al., *Cation-Induced Hydrogels of Cellulose Nanofibrils with Tunable Moduli*. *Biomacromolecules*, 2013. **14**(9): p. 3338-3345.
62. Oguzlu, H., C. Danumah, and Y. Boluk, *Colloidal behavior of aqueous cellulose nanocrystal suspensions*. *Current Opinion in Colloid & Interface Science*, 2017. **29**: p. 46-56.
63. Prathapan, R., et al., *Modulating the zeta potential of cellulose nanocrystals using salts and surfactants*. *Colloids and Surfaces A: Physicochemical and Engineering Aspects*, 2016. **509**: p. 11-18.
64. Notley, S.M., *Effect of introduced charge in cellulose gels on surface interactions and the adsorption of highly charged cationic polyelectrolytes*. *Physical Chemistry Chemical Physics*, 2008. **10**(13): p. 1819-1825.
65. Hubbe, M.A., et al., *Rheology of Nanocellulose-rich Aqueous Suspensions: A Review*. 2017. Vol. 12. 2017.
66. Varanasi, S., R. He, and W. Batchelor, *Estimation of cellulose nanofibre aspect ratio from measurements of fibre suspension gel point*. *Cellulose*, 2013. **20**(4): p. 1885-1896.
67. Feng, J., et al., *Antimicrobial activity of silver nanoparticles in situ growth on TEMPO-mediated oxidized bacterial cellulose*. *Cellulose*, 2014. **21**(6): p. 4557-4567.
68. Ishii, D., T. Saito, and A. Isogai, *Viscoelastic Evaluation of Average Length of Cellulose Nanofibers Prepared by TEMPO-Mediated Oxidation*. *Biomacromolecules*, 2011. **12**(3): p. 548-550.
69. Onyianta, A.J. and R. Williams. *The Use of Sedimentation for the Estimation of Aspect Ratios of Charged Cellulose Nanofibrils*. 2018. Cham: Springer International Publishing.
70. Jowkarderis, L. and T.G.M. van de Ven, *Intrinsic viscosity of aqueous suspensions of cellulose nanofibrils*. *Cellulose*, 2014. **21**(4): p. 2511-2517.
71. Hiraoki, R., et al., *Molecular Mass and Molecular-Mass Distribution of TEMPO-Oxidized Celluloses and TEMPO-Oxidized Cellulose Nanofibrils*. *Biomacromolecules*, 2015. **16**(2): p. 675-681.
72. Shinoda, R., et al., *Relationship between Length and Degree of Polymerization of TEMPO-Oxidized Cellulose Nanofibrils*. *Biomacromolecules*, 2012. **13**(3): p. 842-849.
73. Mishra, S.P., et al., *The Use of Sodium Chlorite in Post-Oxidation of TEMPO-Oxidized Pulp: Effect on Pulp Characteristics and Nanocellulose Yield*. *Journal of Wood Chemistry and Technology*, 2012. **32**(2): p. 137-148.

74. Abraham, E., et al., *X-ray diffraction and biodegradation analysis of green composites of natural rubber/nanocellulose*. *Polymer Degradation and Stability*, 2012. **97**(11): p. 2378-2387.
75. da Silva Perez, D., S. Montanari, and M.R. Vignon, *TEMPO-Mediated Oxidation of Cellulose III*. *Biomacromolecules*, 2003. **4**(5): p. 1417-1425.
76. Liimatainen, H., et al., *Enhancement of the Nanofibrillation of Wood Cellulose through Sequential Periodate–Chlorite Oxidation*. *Biomacromolecules*, 2012. **13**(5): p. 1592-1597.
77. Masruchin, N., B.-D. Park, and V. Causin, *Influence of sonication treatment on supramolecular cellulose microfibril-based hydrogels induced by ionic interaction*. *Journal of Industrial and Engineering Chemistry*, 2015. **29**: p. 265-272.
78. Li, M.-C., et al., *Cellulose Nanoparticles: Structure–Morphology–Rheology Relationships*. *ACS Sustainable Chemistry & Engineering*, 2015. **3**(5): p. 821-832.
79. Lasseguette, E., D. Roux, and Y. Nishiyama, *Rheological properties of microfibrillar suspension of TEMPO-oxidized pulp*. *Cellulose*, 2008. **15**(3): p. 425-433.
80. Besbes, I., M.R. Vilar, and S. Boufi, *Nanofibrillated cellulose from Alfa, Eucalyptus and Pine fibres: Preparation, characteristics and reinforcing potential*. *Carbohydrate Polymers*, 2011. **86**(3): p. 1198-1206.
81. Naderi, A., T. Lindström, and J. Sundström, *Carboxymethylated nanofibrillated cellulose: rheological studies*. *Cellulose*, 2014. **21**(3): p. 1561-1571.
82. Iotti, M., et al., *Rheological Studies of Microfibrillar Cellulose Water Dispersions*. *Journal of Polymers and the Environment*, 2011. **19**(1): p. 137-145.
83. Hill, R.J., *Elastic Modulus of Microfibrillar Cellulose Gels*. *Biomacromolecules*, 2008. **9**(10): p. 2963-2966.
84. Jowkarderis, L. and T.G.M. van de Ven, *Rheology of semi-dilute suspensions of carboxylated cellulose nanofibrils*. *Carbohydrate Polymers*, 2015. **123**: p. 416-423.
85. Nechyporchuk, O., M.N. Belgacem, and F. Pignon, *Rheological properties of micro-/nanofibrillated cellulose suspensions: Wall-slip and shear banding phenomena*. *Carbohydrate Polymers*, 2014. **112**: p. 432-439.
86. Switzer III, L.H. and D.J. Klingenberg, *Rheology of sheared flexible fiber suspensions via fiber-level simulations*. *Journal of Rheology*, 2003. **47**(3): p. 759-778.
87. Férec, J. and G. Ausias, *4 - Rheological Modeling of Non-dilute Rod Suspensions*, in *Rheology of Non-Spherical Particle Suspensions*, F. Chinesta and G. Ausias, Editors. 2015, Elsevier. p. 77-117.
88. Saarikoski, E., et al., *Flocculated flow of microfibrillated cellulose water suspensions: an imaging approach for characterisation of rheological behaviour*. *Cellulose*, 2012. **19**(3): p. 647-659.
89. Mohtaschemi, M., et al., *Rheological characterization of fibrillated cellulose suspensions via bucket vane viscometer*. *Cellulose*, 2014. **21**(3): p. 1305-1312.
90. Karppinen, A., et al., *Flocculation of microfibrillated cellulose in shear flow*. *Cellulose*, 2012. **19**(6): p. 1807-1819.
91. Araki, J., et al., - *Influence of surface charge on viscosity anomaly of microcrystalline cellulose suspensions*, in *Hydrocolloids*, K. Nishinari, Editor. 2000, Elsevier Science: Amsterdam. p. 283-288.

92. Saito, T., et al., *Self-aligned integration of native cellulose nanofibrils towards producing diverse bulk materials*. *Soft Matter*, 2011. **7**(19): p. 8804-8809.
93. Tanaka, R., et al., *Determination of nanocellulose fibril length by shear viscosity measurement*. *Cellulose*, 2014. **21**(3): p. 1581-1589.
94. Naderi, A., T. Lindström, and T. Pettersson, *The state of carboxymethylated nanofibrils after homogenization-aided dilution from concentrated suspensions: a rheological perspective*. *Cellulose*, 2014. **21**(4): p. 2357-2368.
95. Lowys, M.P., J. Desbrières, and M. Rinaudo, *Rheological characterization of cellulosic microfibril suspensions. Role of polymeric additives*. *Food Hydrocolloids*, 2001. **15**(1): p. 25-32.
96. Hu, Z., et al., *Tuning Cellulose Nanocrystal Gelation with Polysaccharides and Surfactants*. *Langmuir*, 2014. **30**(10): p. 2684-2692.
97. Quennouz, N., et al., *Rheology of cellulose nanofibrils in the presence of surfactants*. *Soft Matter*, 2016. **12**(1): p. 157-164.
98. Tardy, B.L., et al., *Nanocellulose–surfactant interactions*. *Current Opinion in Colloid & Interface Science*, 2017. **29**: p. 57-67.
99. Lavoine, N. and L. Bergström, *Nanocellulose-based foams and aerogels: processing, properties, and applications*. *Journal of Materials Chemistry A*, 2017. **5**(31): p. 16105-16117.
100. Mariano, M., et al., *Microstructural characterization of nanocellulose foams prepared in the presence of cationic surfactants*. *Carbohydrate Polymers*, 2018. **195**: p. 153-162.
101. Martoia, F., et al., *Cellulose nanofibril foams: Links between ice-templating conditions, microstructures and mechanical properties*. *Materials & Design*, 2016. **104**: p. 376-391.
102. Li, Y., et al., *Nanocellulose Aerogels Inspired by Frozen Tofu*. *ACS Sustainable Chemistry & Engineering*, 2017. **5**(8): p. 6387-6391.
103. Sakai, K., et al., *Partitioned pores at microscale and nanoscale: thermal diffusivity in ultrahigh porosity solids of nanocellulose*. *Scientific Reports*, 2016. **6**: p. 20434.
104. Duong, H.M. and S.T. Nguyen, *Nanocellulose Aerogels as Thermal Insulation Materials*, in *Nano and Biotech Based Materials for Energy Building Efficiency*, F. Pacheco Torgal, et al., Editors. 2016, Springer International Publishing: Cham. p. 411-427.
105. Voisin, H.P., et al., *3D Printing of Strong Lightweight Cellular Structures Using Polysaccharide-Based Composite Foams*. *ACS Sustainable Chemistry & Engineering*, 2018. **6**(12): p. 17160-17167.
106. Nechita, P. and S. Năstac, *Foam-formed cellulose composite materials with potential applications in sound insulation*. *Journal of Composite Materials*, 2017. **52**(6): p. 747-754.
107. Zhou, S., et al., *Facile Template Synthesis of Microfibrillated Cellulose/Polypyrrole/Silver Nanoparticles Hybrid Aerogels with Electrical Conductive and Pressure Responsive Properties*. *ACS Sustainable Chemistry & Engineering*, 2015. **3**(12): p. 3346-3354.
108. Saito, T. and A. Isogai, *Wet Strength Improvement of TEMPO-Oxidized Cellulose Sheets Prepared with Cationic Polymers*. *Industrial & Engineering Chemistry Research*, 2007. **46**(3): p. 773-780.
109. Bulota, M. and M. Hughes, *Toughening mechanisms in poly(lactic) acid reinforced with TEMPO-oxidized cellulose*. *Journal of Materials Science*, 2012. **47**(14): p. 5517-5523.

110. Koga, H., et al., *Transparent, Conductive, and Printable Composites Consisting of TEMPO-Oxidized Nanocellulose and Carbon Nanotube*. *Biomacromolecules*, 2013. **14**(4): p. 1160-1165.
111. Morimune-Moriya, S., et al., *Hydroxyapatite formation on oxidized cellulose nanofibers in a solution mimicking body fluid*. *Polym J*, 2015. **47**(2): p. 158-163.
112. Kim, S.-S., et al., *High-Fidelity Bioelectronic Muscular Actuator Based on Graphene-Mediated and TEMPO-Oxidized Bacterial Cellulose*. *Advanced Functional Materials*, 2015. **25**(23): p. 3560-3570.
113. Venugopal, J., et al., *Interaction of cells and nanofiber scaffolds in tissue engineering*. *Journal of Biomedical Materials Research Part B: Applied Biomaterials*, 2008. **84B**(1): p. 34-48.
114. Zander, N.E., et al., *Metal Cation Cross-Linked Nanocellulose Hydrogels as Tissue Engineering Substrates*. *ACS Applied Materials & Interfaces*, 2014. **6**(21): p. 18502-18510.
115. Cheng, J., M. Park, and J. Hyun, *Thermoresponsive hybrid hydrogel of oxidized nanocellulose using a polypeptide crosslinker*. *Cellulose*, 2014. **21**(3): p. 1699-1708.
116. Alexandrescu, L., et al., *Cytotoxicity tests of cellulose nanofibril-based structures*. *Cellulose*, 2013. **20**(4): p. 1765-1775.
117. Hua, K., et al., *Translational study between structure and biological response of nanocellulose from wood and green algae*. *RSC Advances*, 2014. **4**(6): p. 2892-2903.
118. Hua, K., et al., *Transition from Bioinert to Bioactive Material by Tailoring the Biological Cell Response to Carboxylated Nanocellulose*. *Biomacromolecules*, 2016. **17**(3): p. 1224-1233.
119. Fujisawa, S., E. Togawa, and K. Kuroda, *Nanocellulose-stabilized Pickering emulsions and their applications*. *Science and Technology of Advanced Materials*, 2017. **18**(1): p. 959-971.
120. Gestranus, M., et al., *Phase behaviour and droplet size of oil-in-water Pickering emulsions stabilised with plant-derived nanocellulosic materials*. *Colloids and Surfaces A: Physicochemical and Engineering Aspects*, 2017. **519**: p. 60-70.
121. Fujisawa, S., E. Togawa, and K. Kuroda, *Facile Route to Transparent, Strong, and Thermally Stable Nanocellulose/Polymer Nanocomposites from an Aqueous Pickering Emulsion*. *Biomacromolecules*, 2017. **18**(1): p. 266-271.
122. Kobayashi, Y., T. Saito, and A. Isogai, *Aerogels with 3D Ordered Nanofiber Skeletons of Liquid-Crystalline Nanocellulose Derivatives as Tough and Transparent Insulators*. *Angewandte Chemie International Edition*, 2014. **53**(39): p. 10394-10397.
123. Gordeyeva, K.S., et al., *Stabilizing nanocellulose-nonionic surfactant composite foams by delayed Ca-induced gelation*. *Journal of Colloid and Interface Science*, 2016. **472**: p. 44-51.
124. Cervin, N.T., et al., *Strong, Water-Durable, and Wet-Resilient Cellulose Nanofibril-Stabilized Foams from Oven Drying*. *ACS Applied Materials & Interfaces*, 2016. **8**(18): p. 11682-11689.
125. Sehaqui, H., et al., *Fast and Reversible Direct CO₂ Capture from Air onto All-Polymer Nanofibrillated Cellulose—Polyethylenimine Foams*. *Environmental Science & Technology*, 2015. **49**(5): p. 3167-3174.
126. Brodin, P.W. and H. Theliander, *Absorbent materials based on kraft pulp: Preparation and material characterization*. *BioResources*, 2012. **7**(2): p. 1666-1686.

127. Brodin, F.W. and H. Theliander, *A comparison of softwood and birch kraft pulp fibers as raw materials for production of TEMPO-oxidized pulp, MFC and superabsorbent foam*. Cellulose, 2013. **20**(6): p. 1-14.
128. Brodin, F.W., Y. Sonavane, and H. Theliander, *Preparation of absorbent foam based on softwood kraft pulp: Advancing from gram to kilogram scale*. BioResources, 2013. **8**(2): p. 2099-2117.
129. Brodin, F.W., et al., *Reinforced absorbent material: A cellulosic composite of TEMPO-oxidized MFC and CTMP fibres*. Cellulose, 2012. **19**(4): p. 1413-1423.
130. Jiang, F. and Y.-L. Hsieh, *Amphiphilic superabsorbent cellulose nanofibril aerogels*. Journal of Materials Chemistry A, 2014. **2**(18): p. 6337-6342.
131. Lapasin, R., *Rheological Characterization of Hydrogels*, in *Polysaccharide Hydrogels: Characterization and Biomedical Applications*, P. Matricardi, F. Alhaique, and T. Coviello, Editors. 2016, Pan Stanford Publishing.
132. Kulkarni, V.S. and C. Shaw, *Chapter 9 - Rheological Studies*, in *Essential Chemistry for Formulators of Semisolid and Liquid Dosages*, V.S. Kulkarni and C. Shaw, Editors. 2016, Academic Press: Boston. p. 145-182.
133. Mewis, J. and N.J. Wagner, *Rheometry of suspensions*, in *Colloidal Suspension Rheology*. 2011, Cambridge University Press: Cambridge. p. 291-324.
134. Pruska-Kedzior, A. and Z. Kedzior, *Rheological Properties of Food Systems*, in *Chemical and Functional Properties of Food Components*, Z.E. Sikorski, Editor. 2006, CRC Press: Boca Raton. p. 211.
135. Barnes, H.A., J.F. Hutton, and K. Walters, *An introduction to rheology*. 1989, Oxford: Elsevier.
136. Phan-Thien, N. and N. Mai-Duy, *Rheological Properties*, in *Understanding Viscoelasticity*, N. Phan-Thien and N. Mai-Duy, Editors. 2017, Springer Nature. p. 29-31,36.
137. Koochehi, A., et al., *The rheological properties of ketchup as a function of different hydrocolloids and temperature*. International Journal of Food Science & Technology, 2009. **44**(3): p. 596-602.
138. Wustenberg, T., *Rheology of Food Hydrocolloids*, in *Cellulose and Cellulose Derivatives in the Food Industry*. 2014, Wiley-VCH Verlag GmbH & Co. KGaA.
139. Harding, S.E., *Dilute solution viscometry of food biopolymers*, in *Functional Properties of Food Macromolecules*, S.E. Hill, D.A. Ledward, and J.R. Mitchell, Editors. 1998, Aspen Publishers, Inc.: Gaithersburg, Maryland.
140. Mezger, T.G., *The Rheology Handbook*. 2nd edition ed. 2006: Vincentz Network.
141. Eaton, P.J., *Atomic force microscopy*, ed. P. West and P. Oxford University. 2010, Oxford: Oxford University Press.
142. Dan, G., X. Guoxin, and L. Jianbin, *Mechanical properties of nanoparticles: basics and applications*. Journal of Physics D: Applied Physics, 2014. **47**(1): p. 013001.
143. Sun, S.-S. and L.R. Dalton, *Introduction to organic electronic and optoelectronic materials and devices*. 2008, Boca Raton: Boca Raton : CRC Press.
144. Gallagher, S.R., *Overview of Electrophoresis*. Current Protocols in Essential Laboratory Techniques, 2008. **00**(1): p. 7.1.1-7.1.6.
145. Armstrong, J.A. and J.R. Schulz, *Agarose Gel Electrophoresis*. Current Protocols in Essential Laboratory Techniques, 2008. **00**(1): p. 7.2.1-7.2.20.
146. Gallagher, S.R., *SDS-Polyacrylamide Gel Electrophoresis (SDS-PAGE)*. Current Protocols in Essential Laboratory Techniques, 2008. **00**(1): p. 7.3.1-7.3.25.

147. Drabik, A., A. Bodzoń-Kułakowska, and J. Silberring, 7 - *Gel Electrophoresis*, in *Proteomic Profiling and Analytical Chemistry (Second Edition)*, P. Ciborowski and J. Silberring, Editors. 2016, Elsevier: Boston. p. 115-143.
148. Varshney, G.K., et al., *A high-throughput functional genomics workflow based on CRISPR/Cas9-mediated targeted mutagenesis in zebrafish*. *Nature Protocols*, 2016. **11**: p. 2357.

THIS PAGE HAS BEEN INTENTIONALLY LEFT BLANK

THIS PAGE HAS BEEN INTENTIONALLY LEFT BLANK

CHAPTER 2

GELATION MECHANISM OF CELLULOSE NANOFIBRE GELS: A COLLOIDS AND INTERFACIAL PERSPECTIVE

THIS PAGE HAS BEEN INTENTIONALLY LEFT BLANK

CHAPTER 2 GELATION MECHANISM OF CELLULOSE NANOFIBRE GELS: A COLLOIDS AND INTERFACIAL PERSPECTIVE

2.1	ABSTRACT.....	54
2.1.1	HYPOTHESIS	54
2.1.2	EXPERIMENTS	54
2.1.3	FINDINGS	54
2.1.4	KEYWORDS	54
2.2	INTRODUCTION	55
2.3	MATERIALS AND METHODS.....	57
2.3.1	MATERIALS.....	57
2.3.2	TEMPO-MEDIATED OXIDATION	57
2.3.3	DETERMINING SOLIDS CONCENTRATION	57
2.3.4	RHEOLOGY	58
2.3.5	VISUALISING THE EFFECT OF PH AND IONIC STRENGTH.....	58
2.3.6	DYNAMIC LIGHT SCATTERING.....	58
2.3.7	ATOMIC FORCE MICROSCOPY (AFM) IMAGING	58
2.4	RESULTS	59
2.4.1	FIBRE DIMENSIONS AND MORPHOLOGY	59
2.4.2	EFFECT OF PH AND IONIC STRENGTH	59
2.4.3	EFFECT OF FIBRE CONCENTRATION.....	62
2.5	DISCUSSION.....	65
2.5.1	FACTORS INFLUENCING GEL STABILITY	65
2.5.1.1	<i>Effect of pH.....</i>	65
2.5.1.2	<i>Effect of Ionic Strength.....</i>	66
2.5.2	FACTORS GOVERNING GEL FORMATION AND BEHAVIOUR	68
2.5.2.1	<i>Effect of Fibre Concentration.....</i>	68
2.6	CONCLUSION	70
2.7	ACKNOWLEDGMENTS	71
2.8	REFERENCES	72

THIS PAGE HAS BEEN INTENTIONALLY LEFT BLANK

Gelation Mechanism of Cellulose Nanofibre Gels: A colloids and interfacial perspective

Llyza Mendoza¹, Warren Batchelor¹, Rico F. Tabor² and Gil Garnier^{1,}*

¹Bioresource Processing Research Institute of Australia (BioPRIA), Department of Chemical Engineering, Monash University, VIC 3800, Australia

²School of Chemistry, Monash University, Clayton, VIC 3800, Australia

*E-mail: gil.garnier@monash.edu

2.1 ABSTRACT

2.1.1 HYPOTHESIS

Nanocellulose gels form a new category of sustainable soft materials of industrial interest for a wide range of applications. There is a need to map the rheological properties and understand the mechanism which provides the colloidal stability and gelation of these nanofibre suspensions.

2.1.2 EXPERIMENTS

TEMPO (2,2,6,6-tetramethylpiperidine-1-oxyl)-oxidised cellulose nanofibre gels were investigated at different fibre concentrations, pH, temperatures and ionic strength. Dynamic and cyclic rheological studies were performed to quantify gel behaviour and properties. Gels were produced at different pH and salt contents to map and understand colloidal stability of the nanocellulose gel.

2.1.3 FINDINGS

Rheology indicates gelation as a transitional state starting at a fibre concentration of 0.1 wt. %. The colloidal stability of the nanocellulose gel network is controlled by pH and salt, whereas fibre concentration mainly dictates the dynamic rheological properties. Decreasing pH and adding salt destabilises the gel network by eluting bound water which is correlated with the decrease in electrostatic repulsion between fibres. The gelation and colloidal stability of these nanocellulose gels is driven by electrostatic forces and the entanglement ability of the fibrous system to overlap.

2.1.4 KEYWORDS

Nanocellulose, TEMPO-mediated oxidation, hydrogels, colloids, rheology, AFM

2.2 INTRODUCTION

Cellulose fibrils of nano-scale width – referred to as nanocellulose – can be extracted from plants and bacterial sources through a variety of mechanical and chemical methods [1, 2]. Nanocellulose exhibits exceptional characteristics such as high tensile strength, ease of functionalisation, combined with its expected biological characteristics: renewability, biocompatibility, biodegradability and low toxicity [3-5]. Isogai et al. developed the TEMPO-mediated oxidation process which utilises a nitroxyl catalyst (TEMPO, 2,2,6,6-tetramethylpiperidine-1-oxyl) to convert the primary alcohol groups of the cellulose anhydro-D-glucose units into carboxylate groups. This provides the necessary electrostatic repulsion which allows the liberation of nanocellulose fibres [6-8]. TEMPO-oxidised cellulose nanofibres (TOCNFs) macroscopically appear as viscous and stable colloidal dispersion even at low solids content (1-2 wt.%) [9]. This surface modification produces nanofibres 3 to 4nm in width and several microns in length [8, 10] and is currently considered among the most effective methods for producing nanocellulose [11]. Recent TOCNF studies have focussed on biomedical applications such as drug delivery [12], wound dressing [13], tissue engineering substrate [14] and cell encapsulation [15, 16], engineering reinforcement materials in plastics and paper [17-20], rheology modifier [21, 22], and the development of novel materials such as aerogels [23]. Previous studies on the properties of TOCNFs investigated the structure at the individual fibril level [24], determining the fibre aspect ratio through rheological measurements [25, 26] and modelling properties at the dilute and semi-dilute concentration regimes [26, 27]. However, there is poor understanding on what drives the gelation and provides the colloidal stability in TOCNFs. Limited studies have analysed the properties of nanofiber cellulose gels from a colloidal and interfacial perspective.

Polysaccharides, owing to their high degrees of polymerisation and hydrogen bonding ability, can form hydrogels through physical interactions. κ -carrageenan undergoes a coil-to-helix structural transformation as a response to temperature changes and forms gels [28]. Thermo-responsive polysaccharides, which contain methyl or other short hydrophobic groups such as methylcellulose and carboxymethylcellulose, gel through the formation of specific hydrogen bonding combined with hydrophobic associations

within the cellulose backbone [29-31]. Alginates, on the other hand, require coordinating cations (i.e. Ca^{2+}) to bridge neighbouring alginate polymer chains which induces gelation [32]. However, none of these gelation mechanisms can describe the gelation of TOCNFs. This type of nanocellulose has been known to form stable gels without the aid of temperature nor cations [27, 33]. Although it is recognized that modification of its rheological properties, resulting in stiff and self-standing gels, can be achieved by manipulating pH and the addition of cations [14, 34, 35].

The objective of this study is to investigate the gelation mechanism of TOCNFs. These fibres, possessing nano-scale diameter and micro-scale length and strong surface charges, can be viewed as flexible colloidal particles of high aspect ratio able to interact, deform and entangle. It is desired to quantify fibre-fibre interactions and determine the factors which affect the stability of the fibres by modifying surface charge and electrical double layer thickness. This is achieved by combining rheology, atomic force microscopy (AFM) and qualitative imaging. Rheology is a well-established method to quantify the viscoelastic characteristics of complex soft materials such as gels. It provides an insight to the state of the gel network by controlled macroscopic deformation [36]. Through rheology, we can monitor the gelation state and properties of TOCNFs as a function of different variables. AFM and light scattering allows the imaging of the cellulose nanofibres enabling us to resolve the fibre dimensions. The combination of these techniques allows us to explore the source of the exceptional colloidal stability and properties of these gels.

To understand the gelation of TOCNFs, we characterised the range of viscoelastic properties in the dilute to semi-dilute range. Their rheological behaviour provides insight into how the fibres organize into a network. The effect of pH and salt on the colloidal stability of the gels was determined and analysed in terms of colloids and interfacial chemistry. We aim at relating the mechanism of cellulose nanofibre gel properties to the well-established colloid and interface science to efficiently engineer applications in food, biomedicine and as rheology modifier.

2.3 MATERIALS AND METHODS

2.3.1 MATERIALS

Bleached Eucalyptus Kraft (BEK) pulp of approximately 10 wt.% solids was supplied by Australian Paper, Maryvale, Australia. 2,2,6,6-Tetramethylpiperidine-1-oxyl (TEMPO) and sodium bromide (NaBr) were purchased from Sigma-Aldrich. Hydrochloric acid (HCl) and sodium hydroxide (NaOH) were diluted for solutions as required and were purchased from ACL Laboratories and Merck, respectively. 12 w/v% sodium hypochlorite (NaClO) was purchased from Thermo Fisher Scientific and used as received.

2.3.2 TEMPO-MEDIATED OXIDATION

The TEMPO-mediated oxidation process employed is based on the method of Saito and Isogai [6]. 100g BEK pulp was suspended in 2500mL water containing 0.4g TEMPO and 2.5g NaBr. The 12 w/v% NaClO solution was initially adjusted to pH 10 via addition of 36% HCl. To initiate the oxidation process, 75mL NaClO was added drop-wise to the suspension whilst stirred. The pH of the reaction was maintained at 10 through the addition of 0.5M NaOH. The oxidation process was maintained for 2 hours. The oxidised fibres were recovered through filtration and stored refrigerated (4°C).

The oxidised pulp was then dispersed in deionised water to a desired concentration. Fibrillation was accomplished through a high-pressure homogeniser (GEA Niro Soavi Homogeniser Panda) at 1000 bar. Suspensions which contain less than 1wt.% TEMPO-oxidised pulp was homogenised for two passes. More concentrated suspensions were homogenised with only one pass. TEMPO-oxidised cellulose nanofibres (TOCNFs) possess an average length of several microns and diameter of 3-4 nm [8, 10].

2.3.3 DETERMINING SOLIDS CONCENTRATION

The solids concentration of all samples (i.e. gel or pulp) were determined through drying. The sample was weighed before (w_i) and after (w_d) drying. Sample moisture was evaporated by drying in an oven at 105° for at least 4 hours. The solids content was calculated with:

$$\text{solids content (\%)} = \frac{w_d}{w_i} \times 100 \% \quad (1)$$

2.3.4 RHEOLOGY

All rheological testing of the gels were performed with an Anton Paar MCR302 rheometer. A cone (0.997°) and plate (49.975 mm) geometry were selected. Testing was done at ambient temperature (25°C). To ensure stable temperature during the testing, a solvent trap was used.

Viscosity was measured at shear rate ranging from 0.5 to 100s⁻¹. Oscillatory strain sweep was performed from 0.01 to 100% at a constant 1Hz frequency. Frequency sweep was measured from 0.1 to 100 rad/s and at 0.1% strain. All measurements were in triplicates. A thixotropic loop test was performed with a 1 wt.% gel by varying the shear stress between the LVR (0.1%, 1Hz) and the yielded region (10%, 1Hz) for 5 cycles.

2.3.5 VISUALISING THE EFFECT OF PH AND IONIC STRENGTH

The effect of pH and salt content on the gel structure was observed qualitatively. The pH of the gels was increased and decreased by adding 0.5M NaOH and 1M HCl, respectively. The salt content of the gel was varied between 8.9mM to 68.5 mM by the addition of 3M NaCl. The gels were then loaded into test tubes and centrifuged at 4000rpm for 20 minutes to separate any released water. The experiment was done in triplicates. Fibre ratio is then calculated as the ratio between the final and initial gel height. The gels were imaged with a black background to enhance visualisation.

2.3.6 DYNAMIC LIGHT SCATTERING

A DLS measurement (Nanobrook Omni Particle Size Analyser) was performed with a dilute (0.03 wt. %) suspension to estimate fibre length.

2.3.7 ATOMIC FORCE MICROSCOPY (AFM) IMAGING

AFM imaging was performed using a JPK Nanowizard 3 to determine fibre diameter and morphology. Samples were prepared by spin coating (Laurell technologies, WS-400BZ-6NPP/LITE) a 0.01 wt% CNF dispersion onto glass microscope slides. Images were obtained in intermittent contact mode using Brüker NCHV model cantilevers. Due to convolution effects from the finite size of the AFM tip, fibre diameters were obtained from the reported height of single fibres on the surface.

2.4 RESULTS

2.4.1 FIBRE DIMENSIONS AND MORPHOLOGY

To characterise the fibre dimensions, atomic force microscopy (AFM) imaging was used, with results shown in Figure 1. From the images of spin-coated and dried fibres, it is clear that the fibres are quite monodisperse in diameter, with reported diameters from AFM height measurements of 2–3 nm. Previous reports have shown a similar diameter distribution [8, 10]. The fibre lengths are, as expected from previous literature protocols [8, 37], more variable and typically the fibres are several microns in length. These fibres have been shown to swell in water depending on their counterion present with the carboxylate pendant group. A Na^+ counterion was shown to have a higher fibre swelling in contrast to H^+ [38].

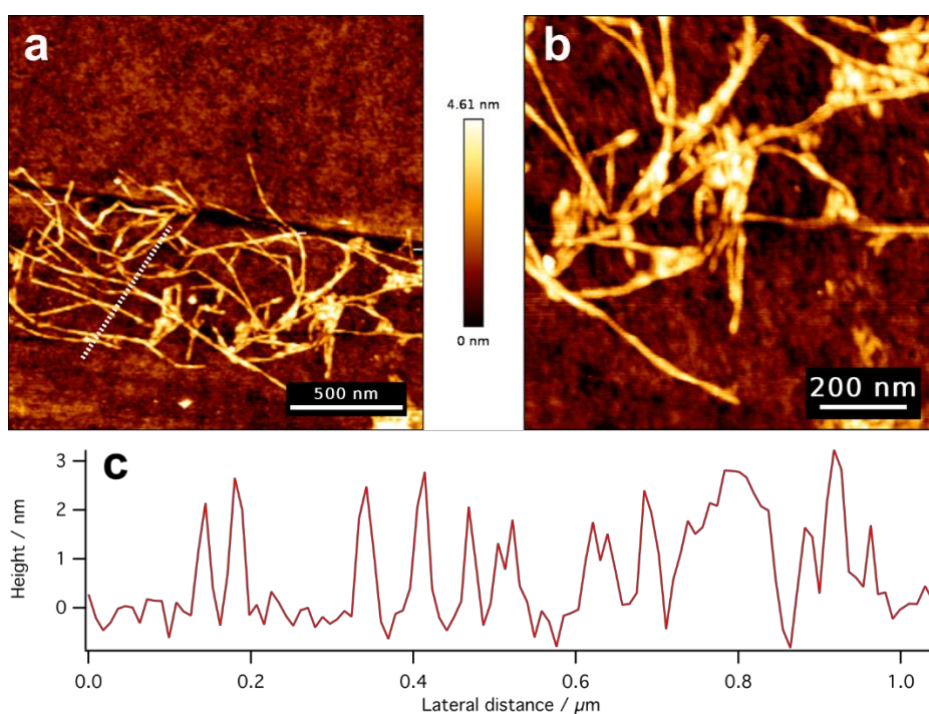


Figure 1. AFM images of TOCNF spin coated onto a glass slide. (a, b) AFM height images of the fibres at different image sizes. c) A cross-sectional profile of the surface topology at the point indicated by the white dotted line in a) showing that the height (diameter) of individual fibres in the dry state is 2–3 nm.

2.4.2 EFFECT OF PH AND IONIC STRENGTH

The effect of pH and ionic strength on gel is shown in Figure 2. Varying both variables resulted in the gel losing its homogeneous structure with the formation of

heterogeneous clumps in a dilute water matrix. Hence, rheological measurements were not completed due to the phase separation (i.e. release of water) resulting in inaccurate measurements. To visualise the effect of both variables, the gels were placed in tubes and centrifuged to observe any eluted water. Figure 2A shows the effect of varying the pH of gels. TOCNF gels have an original pH of 7.4. Adding acid increases the amount of water eluted from the gel. The fibres forming the gel become heterogeneously distributed and compact as pH is decreased- indicated by the whitish appearance. However, increasing the pH does not have any observable effects on gel. Figure 2B shows the effect of salt concentration on gel stability. The addition of up to 17.4mM NaCl did not affect nanocellulose gel stability; water is however released over this concentration. The addition of 34.7mM and 68.5mM NaCl released increasing amounts of water, respectively. The water released by the gel at the highest salt concentration is comparable to the gel at pH 2.

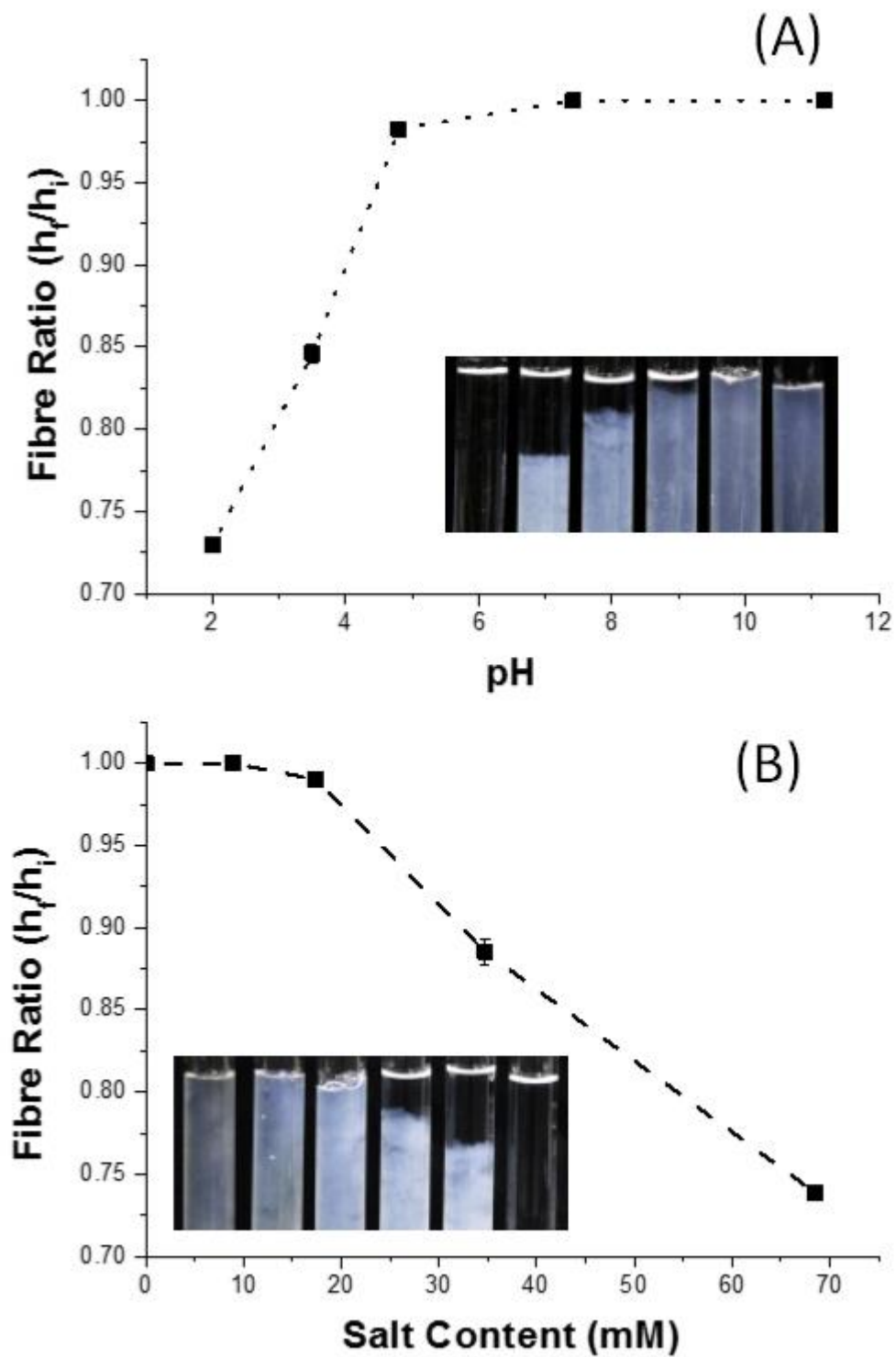


Figure 2. The effect of (A) pH and (B) salt on the stability of 1 wt. % TEMPO-oxidised cellulose nanofibre gels. Fibre ratio is calculated as the ratio between the final height of gel after centrifugation and the total gel height. Insets show water released from gels at different conditions with pure water as reference.

2.4.3 EFFECT OF FIBRE CONCENTRATION

In order to measure the effect of fibre concentration on gel properties, rheology is utilised. Rheology is an effective method to characterise the behaviour of soft matter such as gels. Rheological measurements can be performed in two modes: steady-shear or oscillatory flow. The effect of shear rate and nanofibre concentration on TOCNF dispersion complex viscosity are presented in Figure 3. Gel viscosity decreases with shear, denoting shear-thinning behaviour in line with expectation [9, 39, 40]. Higher zero-shear viscosities are observed with increasing TOCNF concentrations. Gels containing at least 0.29 wt. % TOCNF possess clear yield points, indicating that these are true gels. Indeed, we see some evidence for two yielding zones in the viscosity curves at higher fibre concentrations (discussed later), whereas gels containing less TOCNF (0.09%) have a linearly decreasing viscosity profile.

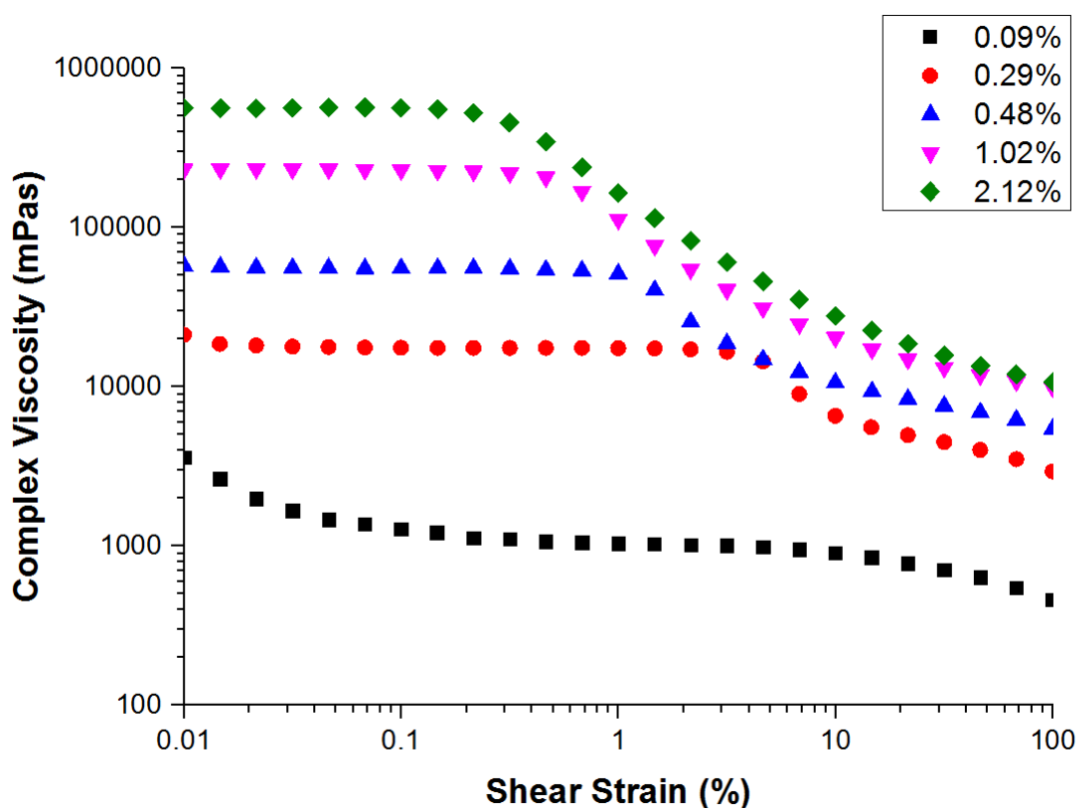


Figure 3. Complex viscosity profile of shear-thinning TEMPO-oxidised cellulose nanofibre gels at various concentrations derived from dynamic strain sweep measurements (25°C). A yield point is clearly evident for fibre concentrations of 0.29% and above.

In oscillatory rheology, the gels are subjected to an increasing oscillating strain (strain sweep) at a constant frequency or vice versa (frequency sweep). In a strain sweep, the range of viscoelastic behaviour can be quantified for gels. The elastic modulus G' describes the solid-like behaviour of TOCNF gel whereas the loss or viscous modulus G'' defines the liquid-like behaviour of the material. Figure 4 shows the rheological spectra of gels as a function of concentration. At low shear stresses, gels possess a linear viscoelastic region (LVR) wherein the elastic modulus G' and viscous modulus G'' are independent of the shear stress. Within this region, G' is dominant over G'' , indicating that the material is acting consistently solid-like; elastic behaviour dominates over viscous behaviour. At a critical shear stress, the gel yields as shown by the decrease in G' , and then reaches a “cross-over point” where G'' becomes dominant and the gel begins to flow. Past this critical stress, the viscous regime dominates ($G'' > G'$) indicating that the network structure has yielded and begins to behave as a non-Newtonian shear thinning fluid. Gels containing a fibre content of at least 0.29 wt.% possess a distinct linear viscoelastic region and a yield point. For 0.09 wt.%, the linear viscoelastic region is significantly lengthened, and the cross-over point is not observed in the selected strain range.

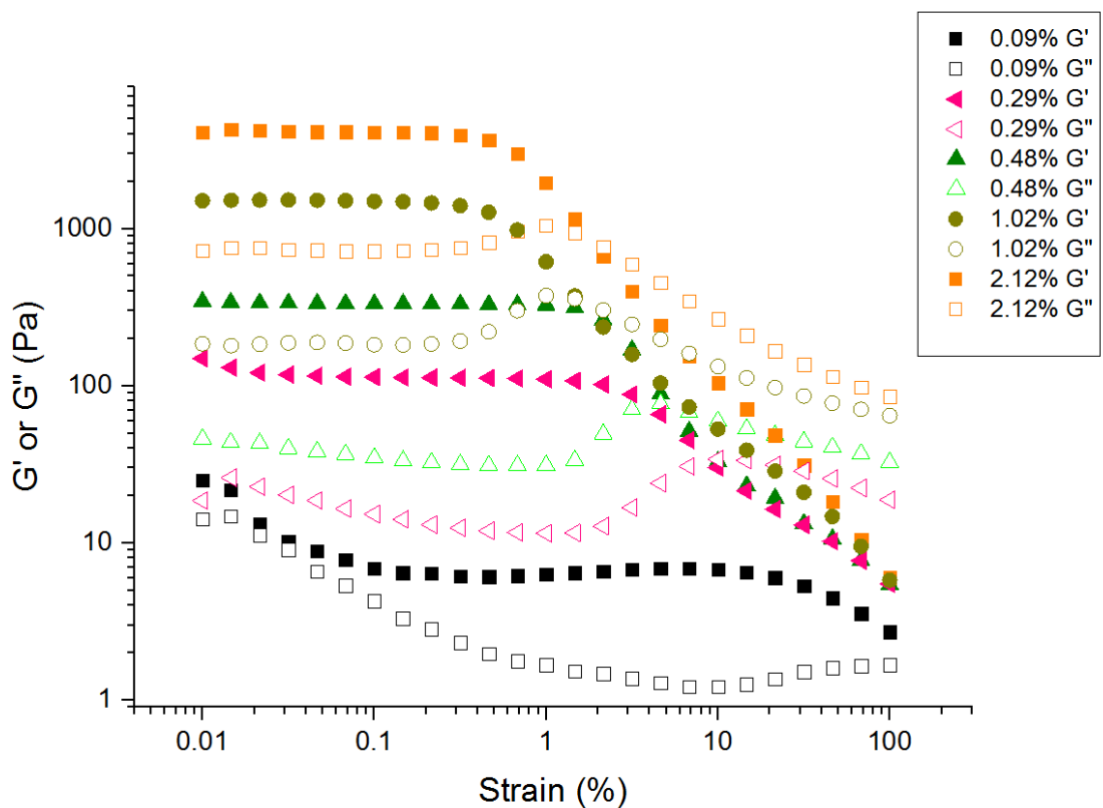


Figure 4. Viscoelastic properties of TEMPO-oxidised cellulose nanofibre gels at different fibre concentrations: dynamic strain sweep (25°C) at a frequency of 1 Hz. Filled symbols indicate elastic moduli whereas unfilled symbols indicate loss moduli.

The frequency sweep shows the time-dependent behaviour of TOCNF gels at increasing concentrations (Figure 5). The G' and G'' values are non-intersecting for concentrations of at least 0.29 wt.% where G' increases gradually with angular frequency. This slight increase in the moduli is common for weak physically cross-linked gels [41]. For the higher concentration samples a minimum in G'' is apparent across the tested frequency range. This minimum has been related to the viscous relaxations which occur between the low and high frequencies: at low frequency, the fibres undergo glasslike rearrangement; at high frequency, the contribution of the solvent viscosity is increasingly important [42].

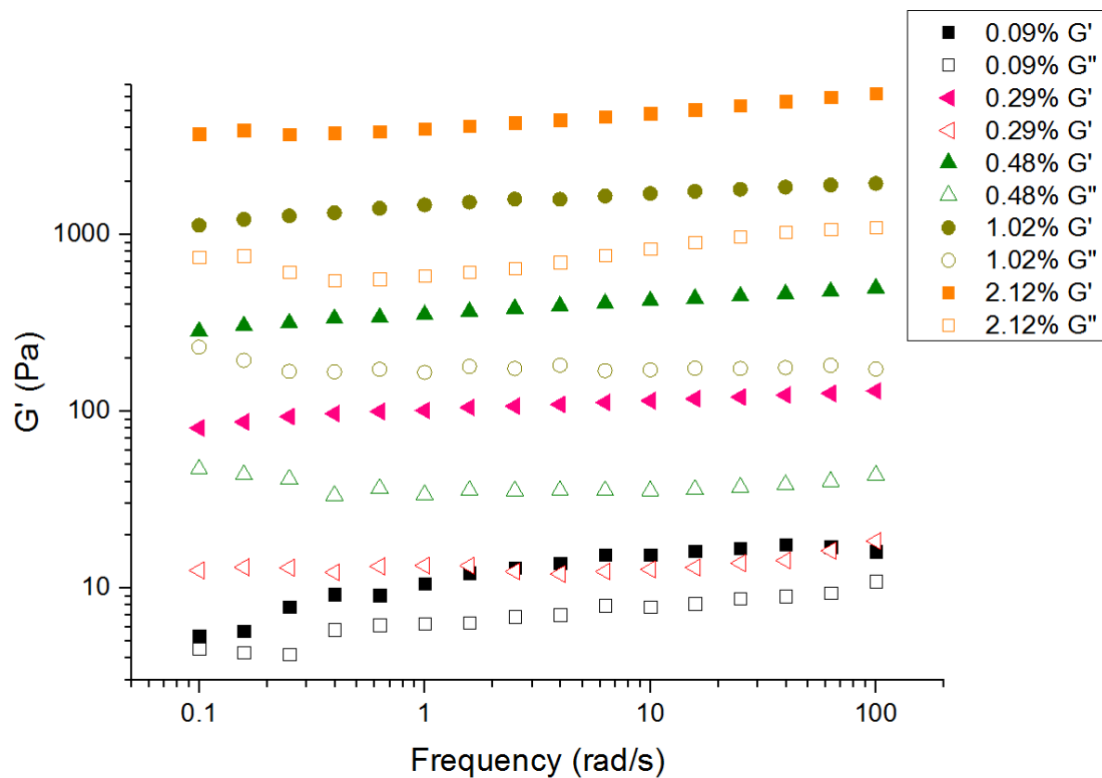


Figure 5. Viscoelastic properties of TEMPO-oxidised cellulose nanofibre gels as at different fibre concentrations: dynamic frequency sweep (25°C) at 0.1% strain.

The thixotropic behaviour of the TOCNF gels was tested through a step strain test. The strain is varied by setting the strain (at constant frequency) either within the LVR region

or outside. Similar to the oscillatory amplitude sweep, when $G' > G''$ the gel is behaving solid-like and vice versa. Figure 6 shows the self-healing behaviour of a 1wt.% nanocellulose gel. At low strain (0.1%), the gel is acting more solid-like. But once the strain (10%) is increased past the yield point, the gel immediately responds and flows in a viscous manner. Gel behaviour is reversible and changes between elastic-dominated and viscous-dominated regimes instantaneously.

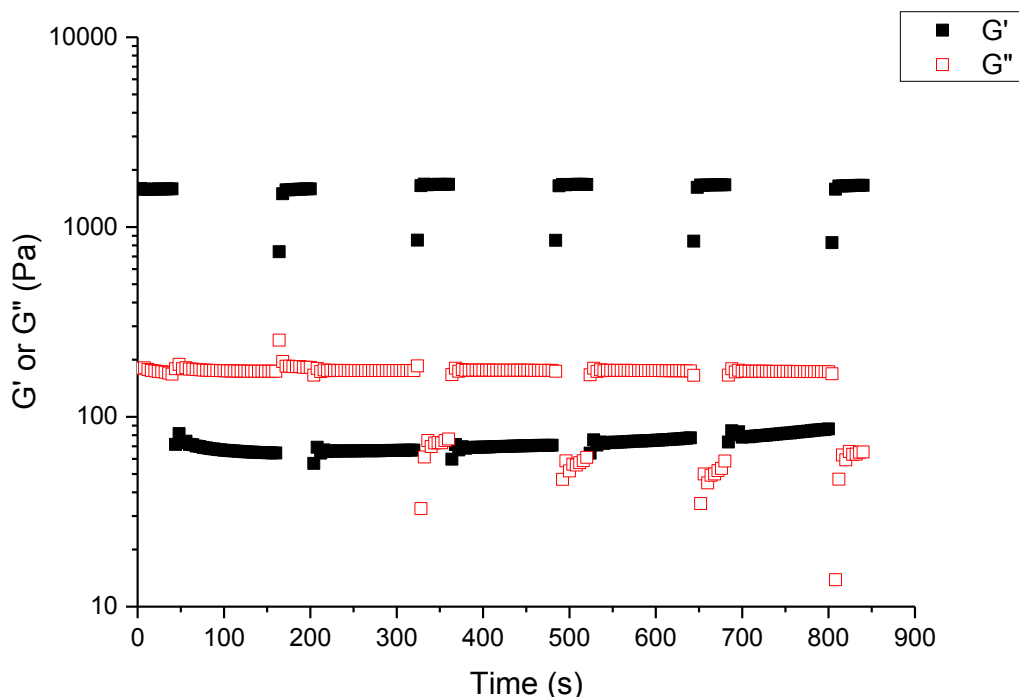


Figure 6. Rheological properties of 1 wt. % TEMPO-oxidised cellulose nanofibre gel in a step strain test: strain has been varied between 0.1% and 10% at constant 1Hz and 25°C for 5 cycles.

2.5 DISCUSSION

The discussion is divided into two sections namely: the effect of pH and ionic strength (explaining electrostatic stabilisation) and the effect of fibre concentration (explaining fibre overlap and entanglement).

2.5.1 FACTORS INFLUENCING GEL STABILITY

2.5.1.1 Effect of pH

pH affects the level of dissociation of the carboxylic groups, thus changing the density and strength of fibre-fibre interactions. The TOCNF gels produced typically have a pH of

7.4, indicating that most of the pendant groups present are in the sodium carboxylate form as the carboxylic acid pKa is much lower at 4.8. Upon lowering pH, the gel destabilises resulting in the agglomeration of fibres, appearing as semi-translucent aggregates accompanied by the release of water. This was previously observed by Besbes et al. [43] wherein the transmittance of the nanocellulose gels decreased drastically at lower pH indicating fibre agglomeration and destabilisation of the gels. The protonation of the carboxylic groups at low pH decreases the surface potential and electrostatic repulsion allowing the fibres to come in closer contact [44], as shown by the increase in fibres compaction (Figure 2A). This is likely a result of Van der Waals forces becoming dominant when insufficient charge repulsion is present between the fibres. Another consequence of low pH is the release of water from the gel (Figure 2A). The change in the counter-ion group from a Na⁺ to H⁺ drastically decreases the individual fibre and network swelling of TEMPO-oxidised nanocellulose [38]. These evidences prove that electrostatic stabilisation of the COO⁻ groups conferred by the TEMPO-oxidised cellulose nanofibres govern gel stability and formation.

2.5.1.2 Effect of Ionic Strength

Salt addition also causes the gel to release water, however not to the same extent as pH (Figure 2B). Increasing the salt concentration reduces the electrical double layer, which causes an imbalance of the attractive and repulsive forces required for a stable colloid. The double layer thickness is estimated as a function of ionic strength with the Gouy-Chapman equation (Figure 7). The double layer thickness (63% decay) ranging from 1.2 to 3.2 nm is similar in magnitude to the diameter of the nanofibers (3-4 nm)[8, 10]. Hence, for TEMPO-oxidised nanocellulose fibres, a charge is required in order to form stable network gels.

There is divergence in opinion regarding the effect of ionic strength on the rheological properties of cellulose suspensions. Some studies claimed that the addition of monovalent salts (e.g. NaCl) to cellulose suspensions can increase both flow (viscosity) and dynamic (G' and G'') rheological properties [45, 46]. These microfibrillated cellulose solutions studied were not carboxylated (bearing only OH- groups), which could potentially be a different regime. Both studies linked the increase in rheological

properties to the enhanced screening of electrostatic repulsion leading to improved H-bonding between cellulose microfibrils. However, in these studies the microfibrillated cellulose suspensions were not surface modified (only containing OH- groups); hence, the increase in ionic strength allows improved H-bonding between the cellulose microfibrils which results in increased rheological properties. Other studies reported the opposite effect – a decreased viscosity with an increase in ionic strength [26, 47, 48], however the main difference is these fibres had polarizable groups (carboxylated or carboxymethylated). Carboxylate (~ -75 mV) and carboxymethyl groups ($\sim 590 \mu\text{eq/g}$) have a higher surface potential than the hydroxyl groups (~ -25 mV) on nanocellulose [8, 48, 49] leading to higher electrostatic repulsive force between fibres and a different form of fibre-fibre interaction. The screening of these forces results in the collapse of the existing fibre network leading to decreased gel strength properties, as reported.

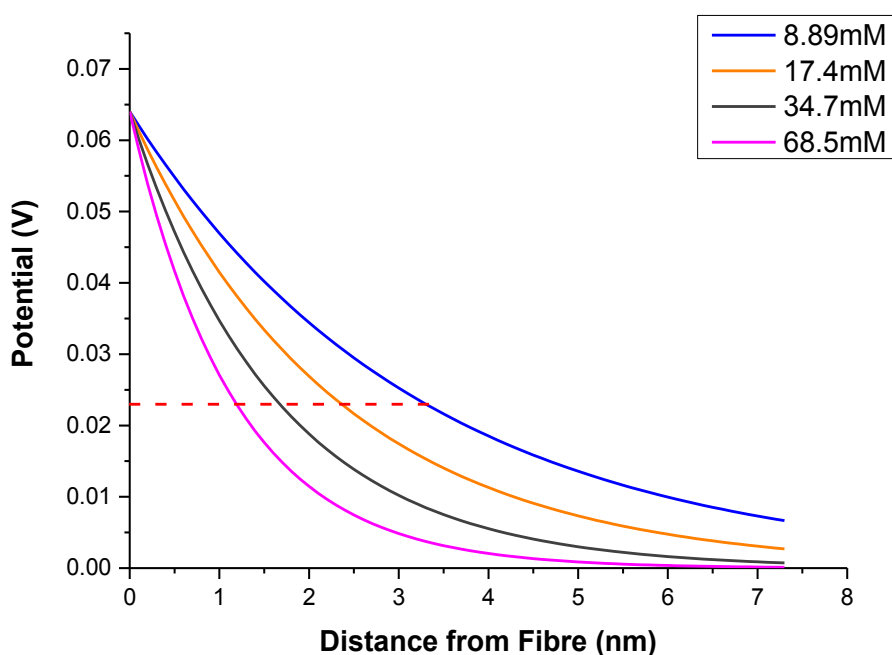


Figure 7. Effect of ionic strength on the electrical double layer of TOCNF fibres estimated from the Gouy-Chapman equation (reference pH of original gel: 7.4). Dashed line indicates 63% decrease in surface charge corresponding to decreased double layer thickness at increased ionic strength.

2.5.2 FACTORS GOVERNING GEL FORMATION AND BEHAVIOUR

2.5.2.1 Effect of Fibre Concentration

We utilised rheology to understand the effect of TEMPO-oxidised cellulose nanofibre (TOCNF) concentration on the formation of gel network and its bulk properties. The oscillatory frequency sweep quantifies the gel consistency, which we anticipate is dominated by fibre-fibre interactions, whereas the oscillatory strain sweep characterises bulk flow properties which are dominated by viscosity.

At the lowest concentration (0.09 wt.%), fibres interact very weakly and possess relative motion. Gels at this concentration exhibit a transitional behaviour without strong evidence of material yielding (i.e. no linear viscoelastic region, LVR). Upon increasing the fibre concentration to 0.29 wt.%, the fibres are sufficiently interacting to demonstrate a well-defined LVR with a clear yielding behaviour (as shown in the strain sweep and complex viscosity as a function of strain). Gels containing at least 0.48 wt.% possess a stronger network, as evidenced by higher zero-shear viscosity and by higher G' values. The increase in entanglements at these concentrations also means that the network is becoming less flexible as shown by the yielding of the gels at lower strains.

The formation of the fibre network can also be observed through the evolution of the viscosity profile at increasing concentrations. Cellulose suspensions, whether nano- or micro- fibrillated, are known for their shear-thinning behaviour as the individual fibres can rearrange following the direction of shear. At a sufficient fibre concentration (0.29 wt.% and above), the complex viscosity demonstrates two shear-thinning regimes of the gel separated by a region of weaker strain dependence. This behaviour was also observed for other forms of nanocellulose [46, 50-52]. In microfibrillated cellulose, a plateau region was seen, related to a transitional structure which exists between low and high shear structures. At low shear rates, nanofibres orient along the shear direction causing a decrease in viscosity. Upon reaching the critical shear strain (transition region), the low shear structure breaks down causing an increase in the floc size pre-empting the formation of a new high shear structure. Past this critical strain range, these

large flocs are broken into smaller flocs which can move relative to each other [46, 50-52].

This transformational behaviour was showed in TOCNF systems by birefringence [33]. TOCNFs re-orient accordingly to shear to produce intermediate structures. Provided that there is enough fibre to make a transitional structure, then and only then a viscosity plateau is reached. This indicates that at 0.09 wt.%, the gel does not possess enough fibre to exhibit this plateau behaviour. However, in more concentrated gels (>2 wt.%), we observe a change in the behaviour of the plateau itself. The plateau is extended and in the second shear-thinning stage the viscosity gradient decreases compared to the lower concentrations (0.29 – 1 wt. %). This reveals that larger flocs are formed which hinders movement of the gel.

The transitional behaviour highlighted in 0.09 wt.% is also validated by estimating the average number of contact points per fibre through the Crowding Factor Theory [53]. The crowding factor N is defined as the number of fibres present in a sphere wherein the diameter of the sphere is equal to the length of the fibre. The crowding factor (N) can be defined and calculated with the following equations:

$$N = \frac{2}{3} C_v \left(\frac{L}{d} \right)^2 \quad (2)$$

$$N \cong \frac{4\pi n_c^3}{3(n_c-1)} \quad (3)$$

$$N \cong 4n_c^2 \quad (4)$$

Where C_v is the fibre concentration by volume, L and d are the fibre average length and diameter, respectively, and n_c is the number of contact points per fibre. A minimum n_c of 3 is required to have sufficient contact in order to sustain a network.

At this critical concentration of 0.09 wt.%, $63 \leq N \leq 125$ by estimating fibre length range between 1000nm to 1400nm (DLS measurements) and an average diameter of 2.5nm (from AFM measurement). Assuming a constraint of $n_c \gg 1$ (Simplifying Eqn. 3 to Eqn.4), the estimated number of contact points per fibre lies between $3.98 \leq n_c \leq 5.58$. This indicates that the fibres possess slightly higher than the minimum contact points required for stable network formation and have restricted relative motion resulting into

the observed rheological values ($G' > G''$ in frequency sweep). These are characteristics of a gel.

We also investigated the effect of cyclical stress on the 1wt.% nanocellulose gel to observe its stress relaxation and network recovery behaviour. This was evaluated via a step strain test. The thixotropy of TOCNF gels is due to the non-covalent physical bonding with surrounding fibres. The gels respond to changes in strains as the fibres re-assemble, quickly reforming the gel. On all high strain intervals, the gels possess a viscous dominant behaviour ($G'' > G'$) with both G' and G'' showing reproducible values throughout the test. At low strain intervals, the elastic-dominated behaviour of gel allows quick re-formation; however some degradation in G'' is observed. This hysteretic dependence of G'' may indicate overall structuring of the fibres during the test, or a consolidation of the fibre network during the measurement that results in different viscous dissipation of the gel at lower strains.

2.6 CONCLUSION

TEMPO-mediated oxidation is an efficient oxidation process for producing cellulose nanofibres of a small diameter (2-5nm) [8, 10] and high surface charge (COOH). In aqueous suspensions, these elongated nanofibres colloids form cellulosic gels above a critical concentration. Most previous studies on TEMPO-oxidised cellulose nanofibres (TOCNFs) have focussed on the rheological properties, aspect ratio quantification, and production from different substrates or its usability for various applications[25-27, 43]. Very few- if any – have analysed cellulose nanofibres in terms of colloidal and interfacial chemistry[24, 44]. In this study, we analysed the gelation and colloidal stability of TEMPO-oxidised cellulose nanofibres (TOCNF) by investigating the effect of concentration, pH, and salt content on rheology from a colloids and interfacial perspective. Gel rheology is examined in terms of nanofiber fibre stability, surface charge (pH) and double layer thickness (NaCl). TOCNFs are elongated and flexible nanofibres forming entangled polymer solutions at low concentrations which transition to gels at higher nanofibre concentrations. This is evidenced by the transition at 0.1 wt.% as measured by rheology and correlation with network theory (Crowding factor). pH and salt strongly influence the colloidal stability of the gels and water is released as the gel

collapses. The protonation of the carboxylate groups via the reduction in pH led to a lower surface charge and reduced the amount of water bound to the nanofibers. Increasing ionic strength via salt addition induces charge shielding by compression of the electrical double layer between adjacent fibres, also leading to water release. TOCNFs are colloidal gels- interacting colloidal suspensions of elongated flexible charged particles. The stability of the nanofibres results from the overlap and entanglement of the high aspect ratio fibres combined with electrostatic stabilisation of the pendant COO^- groups. Relating the mechanism of TOCNF gel formation to the well-established colloid and interface science enables specific applications in food, biomedical and as rheology modifier to be efficiently engineered from first principles.

2.7 ACKNOWLEDGMENTS

This work was funded by the ARC Bioprocessing Advance Manufacturing Industry Research Transformation Hub IH13100016, Visy, Norske Skog, Orora, CHH/Oji Paper, and Australian Paper and Circa. Many thanks to Australian Paper for providing the pulp.

2.8 REFERENCES

1. Klemm, D., et al., *Cellulose: Fascinating Biopolymer and Sustainable Raw Material*. Angewandte Chemie International Edition, 2005. **44**(22): p. 3358-3393.
2. Dufresne, A., *Nanocellulose From Nature to High Performance Tailored Materials*. 2012: De Gruyter.
3. Lin, N. and A. Dufresne, *Nanocellulose in biomedicine: Current status and future prospect*. European Polymer Journal, 2014. **59**: p. 302-325.
4. Varanasi, S., R. He, and W. Batchelor, *Estimation of cellulose nanofibre aspect ratio from measurements of fibre suspension gel point*. Cellulose, 2013. **20**(4): p. 1885-1896.
5. Zhang, L., et al., *Effect of cellulose nanofiber dimensions on sheet forming through filtration*. Cellulose, 2012. **19**(2): p. 561-574.
6. Saito, T., et al., *Cellulose Nanofibers Prepared by TEMPO-Mediated Oxidation of Native Cellulose*. Biomacromolecules, 2007. **8**(8): p. 2485-2491.
7. Saito, T. and A. Isogai, *TEMPO-Mediated Oxidation of Native Cellulose. The Effect of Oxidation Conditions on Chemical and Crystal Structures of the Water-Insoluble Fractions*. Biomacromolecules, 2004. **5**(5): p. 1983-1989.
8. Isogai, A., T. Saito, and H. Fukuzumi, *TEMPO-oxidized cellulose nanofibers*. Nanoscale, 2011. **3**(1): p. 71-85.
9. Nechyporchuk, O., M.N. Belgacem, and F. Pignon, *Current Progress in Rheology of Cellulose Nanofibril Suspensions*. Biomacromolecules, 2016. **17**(7): p. 2311-2320.
10. Fukuzumi, H., et al., *Transparent and High Gas Barrier Films of Cellulose Nanofibers Prepared by TEMPO-Mediated Oxidation*. Biomacromolecules, 2009. **10**(1): p. 162-165.
11. Li, Q., et al., *Nanocellulose Life Cycle Assessment*. ACS Sustainable Chemistry & Engineering, 2013. **1**(8): p. 919-928.
12. Weishaupt, R., et al., *TEMPO-Oxidized Nanofibrillated Cellulose as a High Density Carrier for Bioactive Molecules*. Biomacromolecules, 2015. **16**(11): p. 3640-3650.
13. Rees, A., et al., *3D Bioprinting of Carboxymethylated-Periodate Oxidized Nanocellulose Constructs for Wound Dressing Applications*. BioMed Research International, 2015. **2015**: p. 7.
14. Zander, N.E., et al., *Metal Cation Cross-Linked Nanocellulose Hydrogels as Tissue Engineering Substrates*. ACS Applied Materials & Interfaces, 2014. **6**(21): p. 18502-18510.
15. Cheng, J., M. Park, and J. Hyun, *Thermoresponsive hybrid hydrogel of oxidized nanocellulose using a polypeptide crosslinker*. Cellulose, 2014. **21**(3): p. 1699-1708.
16. Park, M., D. Lee, and J. Hyun, *Nanocellulose-alginate hydrogel for cell encapsulation*. Carbohydrate Polymers, 2015. **116**: p. 223-228.
17. Bulota, M. and M. Hughes, *Toughening mechanisms in poly(lactic) acid reinforced with TEMPO-oxidized cellulose*. Journal of Materials Science, 2012. **47**(14): p. 5517-5523.

18. Fujisawa, S., et al., *Superior Reinforcement Effect of TEMPO-Oxidized Cellulose Nanofibrils in Polystyrene Matrix: Optical, Thermal, and Mechanical Studies*. *Biomacromolecules*, 2012. **13**(7): p. 2188-2194.
19. Hakalahti, M., et al., *Effect of interfibrillar PVA bridging on water stability and mechanical properties of TEMPO/NaClO₂ oxidized cellulosic nanofibril films*. *Carbohydrate Polymers*, 2015. **126**: p. 78-82.
20. Saito, T. and A. Isogai, *Wet Strength Improvement of TEMPO-Oxidized Cellulose Sheets Prepared with Cationic Polymers*. *Industrial & Engineering Chemistry Research*, 2007. **46**(3): p. 773-780.
21. Dimic-Misic, K., P.A.C. Gane, and J. Paltakari, *Micro- and Nanofibrillated Cellulose as a Rheology Modifier Additive in CMC-Containing Pigment-Coating Formulations*. *Industrial & Engineering Chemistry Research*, 2013. **52**(45): p. 16066-16083.
22. Sun, X., et al., *Cellulose Nanofibers as a Modifier for Rheology, Curing and Mechanical Performance of Oil Well Cement*. *Scientific Reports*, 2016. **6**: p. 31654.
23. Jiang, F. and Y.-L. Hsieh, *Super water absorbing and shape memory nanocellulose aerogels from TEMPO-oxidized cellulose nanofibrils via cyclic freezing-thawing*. *Journal of Materials Chemistry A*, 2014. **2**(2): p. 350-359.
24. Usov, I., et al., *Understanding nanocellulose chirality and structure-properties relationship at the single fibril level*. *Nat Commun*, 2015. **6**.
25. Ishii, D., T. Saito, and A. Isogai, *Viscoelastic Evaluation of Average Length of Cellulose Nanofibers Prepared by TEMPO-Mediated Oxidation*. *Biomacromolecules*, 2011. **12**(3): p. 548-550.
26. Jowkarderis, L. and T.G.M. van de Ven, *Intrinsic viscosity of aqueous suspensions of cellulose nanofibrils*. *Cellulose*, 2014. **21**(4): p. 2511-2517.
27. Jowkarderis, L. and T.G.M. van de Ven, *Rheology of semi-dilute suspensions of carboxylated cellulose nanofibrils*. *Carbohydrate Polymers*, 2015. **123**: p. 416-423.
28. Rees, D.A. and W.E. Scott, *Polysaccharide conformation. Part VI. Computer model-building for linear and branched pyranoglycans. Correlations with biological function. Preliminary assessment of inter-residue forces in aqueous solution. Further interpretation of optical rotation in terms of chain conformation*. *Journal of the Chemical Society B: Physical Organic*, 1971(0): p. 469-479.
29. Li, L., *Thermal Gelation of Methylcellulose in Water: Scaling and Thermoreversibility*. *Macromolecules*, 2002. **35**(15): p. 5990-5998.
30. Bekkour, K., D. Sun-Waterhouse, and S.S. Wadhwa, *Rheological properties and cloud point of aqueous carboxymethyl cellulose dispersions as modified by high or low methoxyl pectin*. *Food Research International*, 2014. **66**: p. 247-256.
31. Benslimane, A., et al., *Thermal gelation properties of carboxymethyl cellulose and bentonite-carboxymethyl cellulose dispersions: Rheological considerations*. *Applied Clay Science*, 2016. **132**: p. 702-710.
32. Fang, Y., et al., *Multiple Steps and Critical Behaviors of the Binding of Calcium to Alginate*. *The Journal of Physical Chemistry B*, 2007. **111**(10): p. 2456-2462.

33. Lasseuguette, E., D. Roux, and Y. Nishiyama, *Rheological properties of microfibrillar suspension of TEMPO-oxidized pulp*. *Cellulose*, 2008. **15**(3): p. 425-433.
34. Saito, T., et al., *Self-aligned integration of native cellulose nanofibrils towards producing diverse bulk materials*. *Soft Matter*, 2011. **7**(19): p. 8804-8809.
35. Dong, H., et al., *Cation-Induced Hydrogels of Cellulose Nanofibrils with Tunable Moduli*. *Biomacromolecules*, 2013. **14**(9): p. 3338-3345.
36. Fernandez-Nieves, A. and A.M. Puertas, *Rheology of Soft Materials*, in *Fluids, Colloids and Soft Materials*, H.M. Wyss, Editor. 2016, John Wiley & Sons, Inc. p. 149-163.
37. Shinoda, R., et al., *Relationship between Length and Degree of Polymerization of TEMPO-Oxidized Cellulose Nanofibrils*. *Biomacromolecules*, 2012. **13**(3): p. 842-849.
38. Maloney, T.C., *Network swelling of TEMPO-oxidized nanocellulose*, in *Holzforschung*. 2015. p. 207.
39. Besbes, I., S. Alila, and S. Boufi, *Nanofibrillated cellulose from TEMPO-oxidized eucalyptus fibres: Effect of the carboxyl content*. *Carbohydrate Polymers*, 2011. **84**(3): p. 975-983.
40. Moberg, T., et al., *Rheological properties of nanocellulose suspensions: effects of fibril/particle dimensions and surface characteristics*. *Cellulose*, 2017. **24**(6): p. 2499-2510.
41. Lapasin, R., *Rheological Characterization of Hydrogels*, in *Polysaccharide Hydrogels: Characterization and Biomedical Applications*, P. Matricardi, F. Alhaique, and T. Coviello, Editors. 2016, CRC Press. p. 96-97.
42. Mason, T.G., et al., *Osmotic pressure and viscoelastic shear moduli of concentrated emulsions*. *Physical Review E*, 1997. **56**(3): p. 3150-3166.
43. Besbes, I., M.R. Vilar, and S. Boufi, *Nanofibrillated cellulose from Alfa, Eucalyptus and Pine fibres: Preparation, characteristics and reinforcing potential*. *Carbohydrate Polymers*, 2011. **86**(3): p. 1198-1206.
44. Fall, A.B., et al., *Colloidal Stability of Aqueous Nanofibrillated Cellulose Dispersions*. *Langmuir*, 2011. **27**(18): p. 11332-11338.
45. Lowys, M.P., J. Desbrières, and M. Rinaudo, *Rheological characterization of cellulosic microfibril suspensions. Role of polymeric additives*. *Food Hydrocolloids*, 2001. **15**(1): p. 25-32.
46. Saarikoski, E., et al., *Flocculated flow of microfibrillated cellulose water suspensions: an imaging approach for characterisation of rheological behaviour*. *Cellulose*, 2012. **19**(3): p. 647-659.
47. Tanaka, R., et al., *Determination of nanocellulose fibril length by shear viscosity measurement*. *Cellulose*, 2014. **21**(3): p. 1581-1589.
48. Naderi, A., T. Lindström, and T. Pettersson, *The state of carboxymethylated nanofibrils after homogenization-aided dilution from concentrated suspensions: a rheological perspective*. *Cellulose*, 2014. **21**(4): p. 2357-2368.
49. Raj, P., et al., *Effect of cationic polyacrylamide on the processing and properties of nanocellulose films*. *Journal of Colloid and Interface Science*, 2015. **447**: p. 113-119.
50. Agoda-Tandjawa, G., et al., *Rheological characterization of microfibrillated cellulose suspensions after freezing*. *Carbohydrate Polymers*, 2010. **80**(3): p. 677-686.

51. Iotti, M., et al., *Rheological Studies of Microfibrillar Cellulose Water Dispersions*. Journal of Polymers and the Environment, 2011. **19**(1): p. 137-145.
52. Karppinen, A., et al., *Flocculation of microfibrillated cellulose in shear flow*. Cellulose, 2012. **19**(6): p. 1807-1819.
53. Kerekes, R.J. and C.J. Schell, *Characterization of Fibre Flocculation Regimes by a Crowding Factor*. Journal of Pulp and Paper Science, 1992. **18**(1): p. J32-J38.

THIS PAGE HAS BEEN INTENTIONALLY LEFT BLANK

CHAPTER 3

**EFFECTS OF FIBRE DIMENSION AND
CHARGE DENSITY ON NANOCELLULOSE
GELS**

THIS PAGE HAS BEEN INTENTIONALLY LEFT BLANK

CHAPTER 3 EFFECTS OF FIBRE DIMENSION AND CHARGE DENSITY ON NANOCELLULOSE GELS

3.1	ABSTRACT.....	81
3.1.1	HYPOTHESIS.....	81
3.1.2	EXPERIMENTS.....	81
3.1.3	FINDINGS.....	81
3.1.4	KEYWORDS	82
3.2	INTRODUCTION	82
3.3	METHODOLOGY.....	83
3.3.1	MATERIALS	83
3.3.2	TEMPO-MEDIATED OXIDATION.....	84
3.3.3	DETERMINING SOLIDS CONCENTRATION	84
3.3.4	CONDUCTOMETRIC TITRATION.....	84
3.3.5	RHEOLOGICAL MEASUREMENT	85
3.3.6	ATOMIC FORCE MICROSCOPY (AFM)	85
3.3.7	FIBRELAB	85
3.4	RESULTS	86
3.4.1	FIBRE DIMENSIONS.....	86
3.4.2	RHEOLOGICAL MEASUREMENTS.....	88
3.4.3	EFFECT OF PULP SOURCE.....	89
3.4.4	EFFECT OF CHARGE DENSITY	91
3.5	DISCUSSION.....	93
3.5.1	EFFECT OF PULP FIBRES ON NANOCELLULOSE FIBRE DIMENSIONS.....	93
3.5.2	EFFECT OF NANOFIBRE DIMENSIONS AND SURFACE CHARGE ON GEL RHEOLOGY	94
3.6	CONCLUSION	96
3.7	ACKNOWLEDGMENTS	97
3.8	REFERENCES	98

THIS PAGE HAS BEEN INTENTIONALLY LEFT BLANK

Effects of Fibre Dimension and Charge Density on Nanocellulose Gels

Llyza Mendoza¹, Thilina Gunawardhana¹, Warren Batchelor¹ and Gil Garnier^{1,}*

¹Bioresource Processing Research Institute of Australia (BioPRIA), Department of Chemical Engineering, Monash University, VIC 3800, Australia

²School of Chemistry, Monash University, Clayton, VIC 3800, Australia

*E-mail: gil.garnier@monash.edu

3.1 ABSTRACT

3.1.1 HYPOTHESIS

Carboxylated cellulose nanofibres can produce gels at low concentrations. The effect of pulp source on the nanocellulose fibre dimension and gel rheology are studied. It is hypothesised that fibre length and surface charge influence aspects of the gel rheological properties.

3.1.2 EXPERIMENTS

TEMPO (2,2,6,6-tetramethylpiperidine-1-oxyl)- mediated oxidised cellulose nanofibres from never-dried hardwood and softwood pulp and containing different charge levels were produced and characterized. Steady-state and dynamic rheological studies were performed to ascertain the effects of pulp type on gel behaviour and properties.

3.1.3 FINDINGS

Nanocellulose fibres extracted from softwood (SW-TOCN) and hardwood (HW-TOCN) pulp exhibit similar widths but different length dimensions as shown via AFM analysis. Rheological measurements show that the dynamic moduli (G' and G'') of nanocellulose gels are independent of pulp source and are mostly influenced by fibre concentration. Differences in the steady-state behaviour (i.e. viscosity) at constant surface charge can be attributed to differences in fibre length. Increasing the surface charge density influences the critical strain and the viscosity at the percolation concentration (0.1 wt.%) due to higher electrostatic interactions.

3.1.4 KEYWORDS

nanocellulose, gel, fibre dimension, rheology, TEMPO-mediated oxidation, atomic force microscopy

3.2 INTRODUCTION

Cellulose nanofibres are long semi-flexible fibrils derived from the disintegration of wood pulp via various chemical, enzymatic, and mechanical treatments [1]. Chemical methods, such as TEMPO-mediated oxidation, selectively introduce carboxylate moieties on the cellulose fibril surface. The high electrostatic repulsion between the individual fibrils assists in the liberation of TEMPO-oxidised cellulose nanofibres (TOCNs) upon mechanical disintegration [2]. The ease of scale-up of TEMPO-mediated oxidation has led to the establishment of pilot-scale production and its availability as a commercial product [3]. Applications of TOCNs extend far beyond pulp and paper. TOCNs have shown great performance as reinforcing agent in plastics, [4, 5], in biomedical applications [6-11], pharmaceuticals [12], catalysis [13], superabsorbents [14, 15], and flexible electronics [16].

Nanocellulose is typically found as a suspension or a gel with water as continuous phase. Rheology is the technique of choice to quantify nanocellulose flow behaviour and properties. For instance, the flow behaviour of semi-flexible nanocellulose fibrils can be related to the length and width of the fibrils. The studies of Tanaka, Saito [17] and Jowkarderis and van de Ven [18], related shear and intrinsic viscosities of dilute TOCN suspensions to equations of flow for rigid rod-like particles to determine fibre aspect ratio. Varanasi, He [19], on the other hand, utilised yield stress measurements to determine the fibre gel point and correlate it to the aspect ratio via the crowding factor theory.

The bulk properties of nanocellulose gels and suspensions have been investigated in several rheological studies. In particular, TOCNs possess high aspect ratio [2] which form percolated networks even at low solid concentrations [20]. TOCNs and similarly surface-charged nanocellulose suspensions form gels which exhibit pseudoplastic and thixotropic behaviour due to their inherent fibril assembly and restructuring which

occurs during material deformation [20-22]. The presence of high surface charges leading to their colloidal stability was also investigated in several studies [20, 23-25]. Local flow phenomenon in nanocellulose such as wall slip, shear-banding, and other flow instabilities which may affect the accuracy of rheological measurements were analysed [12, 21]. Simulation and numerical modelling have mainly focused on understanding the mechanism of shear-thinning in nanocellulose [26, 27]. However, studies on the effects of fibre dimensions and surface charges, on the nanocellulose gel rheological properties are very limited. Only one known study has related nanocellulose aspect ratio to the changes in the fibre percolation as observed by changes in viscosity [28].

This study aims at quantifying the effect of fibre dimension and surface charge on the rheological properties of nanocellulose gels. Fibre dimension was varied with the pulp source by oxidising softwood and hardwood kraft pulp from *Pinus Radiata* and *Eucalyptus sp.* respectively. The objectives are two-fold. First, to understand the relationship between the initial fibre size on the dimensions of the resulting nanocellulose; second to quantify the effect of nanocellulose fibre dimension on gel rheology. Differences are analysed through steady-state shear and oscillatory rheological measurements via cone and plate geometry. In steady-state shear, changes in the signature double yielding-behaviour and zero-shear viscosity will be observed, whereas in oscillatory measurements variations in the key parameters such as the dynamic (G' and G'') moduli and the critical strain γ_c are examined.

3.3 METHODOLOGY

3.3.1 MATERIALS

Hardwood (*Eucalyptus sp.*) kraft pulp of approximately 10 wt.% solids was supplied by Australian Paper, Maryvale, Australia. Softwood (*Pinus Radiata*) kraft pulp containing 17.7wt.% solids was supplied by Oji Fibre Solutions, Kinleith, New Zealand. 2,2,6,6-Tetramethylpiperidine-1-oxyl (TEMPO) and sodium bromide (NaBr) were purchased from Sigma-Aldrich. Hydrochloric acid (HCl) and Sodium Hydroxide (NaOH) were diluted for solutions as required and were purchased from ACL Laboratories and Merck,

respectively. 12 w/v% Sodium Hypochlorite (NaClO) was purchased from Thermo Fisher Scientific and used as received. All chemicals were analytical grade.

3.3.2 TEMPO-MEDIATED OXIDATION

The TEMPO-mediated oxidation process employed is based on the method of Saito and Isogai [2]. Wood pulp containing 10 dry g fibre was suspended in 2500mL water containing 0.4g TEMPO and 2.5g NaBr. The 12 w/v% NaClO solution was initially adjusted to pH 10 via addition of 36% HCl before the reaction. To initiate the oxidation process, NaClO was added drop-wise to the suspension whilst stirred. Varying amounts of NaClO was added depending on the desired carboxylate group density. The primary oxidant content was varied between 3.3 mmol NaClO .g⁻¹ fibre to 12.5 mmol NaClO .g⁻¹ fibre for hardwood and constant 6.5 mmol NaClO .g⁻¹ fibre for softwood. The pH of the reaction was maintained at 10 through the addition of 0.5M NaOH. The oxidation process was maintained until no pH change was observed. The oxidised fibres were recovered through filtration and stored refrigerated (4°C). The oxidised pulp was then dispersed in deionised water to a desired concentration (0.1 wt.% to 1 wt.%). Fibrillation was accomplished through a high-pressure homogeniser (GEA Niro Soavi Homogerniser Panda) at 1000 bar for two passes.

3.3.3 DETERMINING SOLIDS CONCENTRATION

The solids concentration of all samples (i.e. gel or pulp) were determined through drying. The sample was weighed before (w_i) and after (w_d) drying. Sample moisture was evaporated by drying in an oven at 105° for at least 6 hours. The solids content was calculated as:

$$\text{solids content (\%)} = \frac{w_d}{w_i} \times 100 \% \quad (1)$$

3.3.4 CONDUCTOMETRIC TITRATION

The carboxylate group content was measured by conductometric titration as reported in [29]. Oxidised pulp samples (approx. 30 mg dry weight) were suspended in 40mL deionised water. 40µL 1% NaCl was added to the suspended sample. The pH of the suspended sample was adjusted between 2.5 – 3 with 0.5M HCl prior to titration.

Titration was accomplished by controlled addition of 0.1M NaOH using a Mettler Toledo T5 titrator. The conductivity of the sample was monitored throughout the titration progress. The carboxyl group content (mmol COO⁻Na⁺ .g⁻¹ fibre) was determined with:

$$CC = \frac{c(V_2 - V_1)}{w} \times 1000 \quad (2)$$

Where V_1 and V_2 pertain to the amount of titrant required to neutralise the carboxylic groups (in L), c is the NaOH concentration (mol/L), and w is the sample weight (g).

3.3.5 RHEOLOGICAL MEASUREMENT

Rheological testing was performed with an Anton Paar MCR302 rheometer. A cone (0.997°) and plate (49.975 mm) geometry were selected. Testing was done at ambient temperature (25°C). A solvent trap was used to ensure stable temperature during measurements. Viscosity was measured at shear rate ranging from 0.5 to 100 s⁻¹. Oscillatory strain sweep was performed from 0.01 to 100% at a constant 1 Hz frequency. Frequency sweep was measured from 0.1 to 100 rad/s and at various suitable shear stresses at the linear viscoelastic region (LVR) wherein the dynamic moduli (G' and G'') are independent of the shear stress. All measurements were done in triplicates and the most representative result is presented.

3.3.6 ATOMIC FORCE MICROSCOPY (AFM)

AFM imaging was performed using a JPK Nanowizard 3 to determine fibre length and width. A 0.001 wt.% nanocellulose dispersion was spin coated (Laurell technologies, WS-400BZ-6NPP/LITE) at 2500rpm onto a plasma coated glass slide. Images were obtained in intermittent contact mode using Brüker NCHV model cantilevers. Fibre widths were obtained from the reported height of single fibres on the surface due to convolution effects. Fibre lengths were estimated by placing segmented lines on the AFM images through an imaging software (Fiji).

3.3.7 FIBRELAB

Fibre dimensions (length and width) of the unrefined and unoxidised hardwood and softwood samples have been obtained via the Kajaani Fibre Lab (Valmet). Dilute

suspensions (~ 0.05 wt.%) were utilised for size analysis. Image analysis from the Fibrelab software is primarily capable of detecting large fibres more than fines.

3.4 RESULTS

The effect of fibre dimensions, using never-dried bleached kraft pulp of softwood and hardwood, on the dimensions and charge density of cellulose nanofibres resulting from TEMPO-mediated oxidation pre-treatment and homogenization is first studied. Secondly, the rheological properties of the gel formed are quantified to understand the effect of nanocellulose dimensions and surface charge (i.e. extent of oxidation).

3.4.1 FIBRE DIMENSIONS

The distributions of fibre length and width of never-dried unrefined softwood and hardwood kraft pulps are shown in Figure 1. On average, hardwood pulp has shorter and narrower fibres than softwood; length and width distributions are also much narrower (Tables I and II). However, the fibre average aspect ratio (L/W) are nearly identical for both fibres, with hardwood $L/W = 36$ and softwood $L/W = 42$.

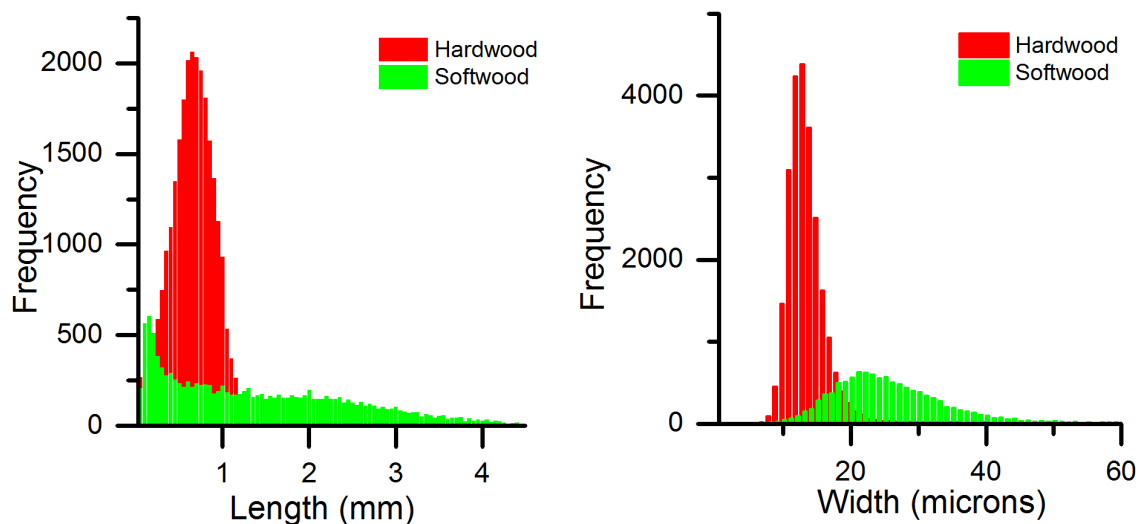


Figure 1. Population length and width distributions for hardwood and softwood bleached kraft pulp fibres.

The fibre size distributions of TEMPO-oxidised cellulose nanofibres produced from hardwood (HW-TOCN) and softwood (SW-TOCN) pulp containing different surface charges are shown in Figure 2. The nanocellulose produced in all cases have the width

distribution in the nano-scale- as expected from TEMPO-mediated oxidation. Length distributions, on the other hand, have changed post- chemical oxidation and mechanical fibrillation. For both fibre types and their varying surface charge levels, the mean length decreased drastically as shown in Tables I and II. On average, hardwood-nanocellulose (HW-TOCN) are wider and longer than softwood-nanocellulose (SW-TOCN) at similar surface charge ($1 \text{ mmol COO}^- \cdot \text{g}^{-1}$ fibre) as shown in Tables I and II. Moreover, length and width distributions for HW-TOCNs are slightly broader than for SW-TOCNs. When surface charge is modified in HW-TOCNs, length and width dimension distributions and mean values are very similar.

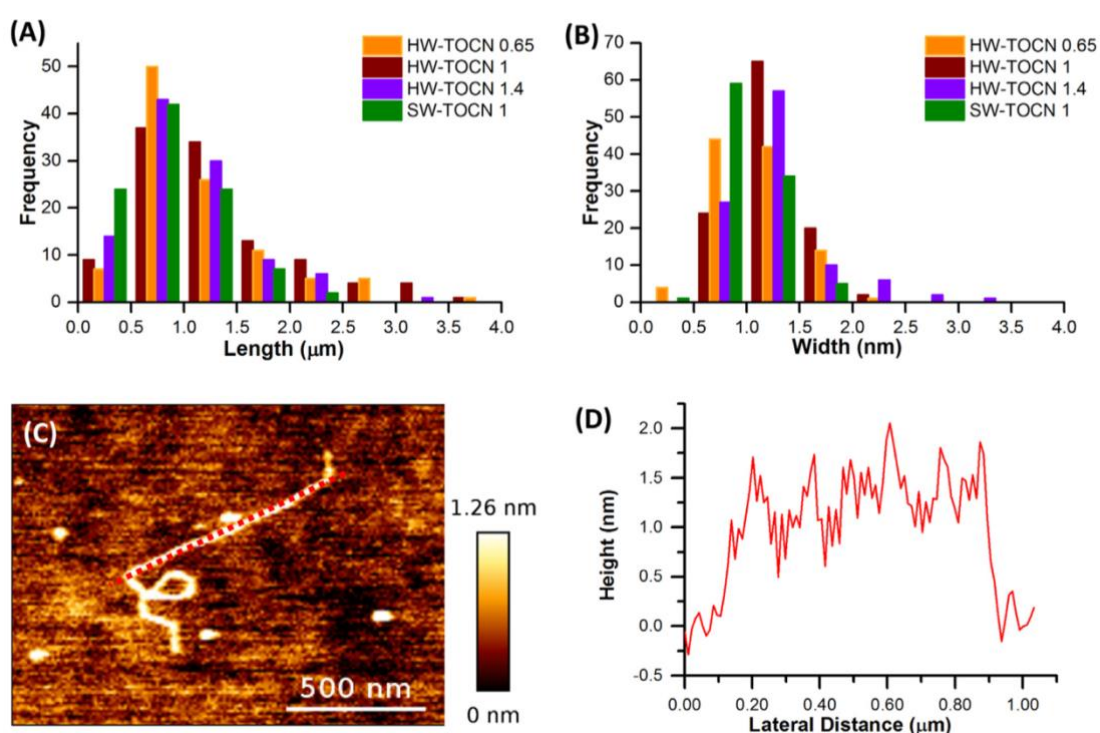


Figure 2. Nanocellulose fibres produced from softwood and hardwood bleached kraft pulp. Width (A) and length (B) distributions for nanocellulose produced from softwood ($1 \text{ mmol COO}^- \cdot \text{g}^{-1}$) and hardwood (0.65, 1, and $1.4 \text{ mmol} \cdot \text{g}^{-1}$) at various surface charges. (C) and (D) AFM image of a single HW-TOCN fibre with surface topology shown.

Table I. Fibre length statistics of hardwood and softwood kraft pulp and the nanocellulose fibres produced from those.

Pulp Type	Surface Charge (mmol COO ⁻ .g ⁻¹)	Mean Length (μ m)	Standard Deviation (μ m)	Population (# of fibres)
Hardwood	0	620	260	26327
HW - TOCN	0.65	1.16	0.62	105
	1.00	1.30	0.73	111
	1.40	1.02	0.53	103
Softwood	0	1420	1130	13070
SW-TOCN	1.00	0.85	0.42	99

Table II. Fibre width statistics of hardwood and softwood bleached kraft pulp and the nanocellulose fibres produced from those.

Pulp Source	Surface Charge (mmol COO ⁻ .g ⁻¹)	Mean Width (nm)	Standard Deviation (nm)	Population (# of fibres)
Hardwood	0	17240	4253	24441
HW - TOCN	0.65	1.06	0.37	105
	1.00	1.24	0.33	111
	1.40	1.29	0.47	103
Softwood	0	34060	9028	10799
SW-TOCN	1.00	0.97	0.30	99

3.4.2 RHEOLOGICAL MEASUREMENTS

Oscillatory rheology is an ideal technique to characterise the elastic and viscous behaviour of nanocellulose gels at varying conditions. For instance, the rheology of nanocellulose gels produced from softwood pulp at increasing fibre concentration is shown in Figure 3. The elastic modulus G' pertains to the solid-like behaviour whereas the viscous modulus G'' characterises the liquid-like behaviour of the gel. At the linear viscoelastic region (LVR), G' and G'' are independent of the shear strain. When $G' > G''$, the elastic behaviour of the nanocellulose gel is dominant at a particular strain. At the critical strain γ_c , the gel moduli (G' and G'') deviates from the LVR and is at the onset of

yielding. Consequently, at even higher strains when $G'' > G'$, the gel possesses a viscous dominant behaviour.

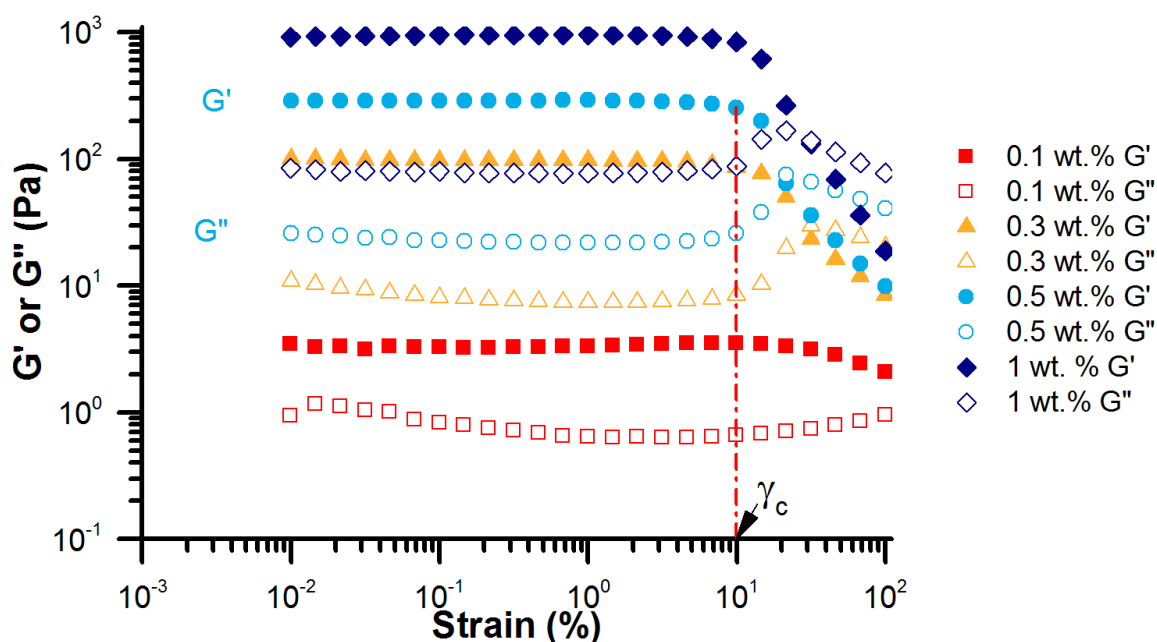


Figure 3. Oscillatory strain measurement for nanocellulose gels made from bleached softwood fibres ($1 \text{ mmol} \cdot \text{g}^{-1}$) as a function of solids concentration. Important spectral rheological data including the G' and G'' at the linear viscoelastic region (LVR), and the critical strain γ_c are identified for the 0.5 wt.% gel used as example. Measurements were done at 25°C , 1Hz.

3.4.3 EFFECT OF PULP SOURCE

The effect of initial pulp source on the dynamic moduli (G' and G'') at various solid concentrations is shown in Figure 4A. At constant charge density ($1 \text{ mmol COO}^- \cdot \text{g}^{-1}$ fibre), the elastic moduli (G') of nanocellulose gels derived from hardwood and softwood sources are very similar. The differences in the viscous moduli (G'') observed between HW-TOCN and SW-TOCN are within the error margins. Moreover, for both types of pulp, γ_c is constant across all solids contents as shown in Figure 4B. However, SW-TOCN possess consistently higher γ_c at all tested concentrations.

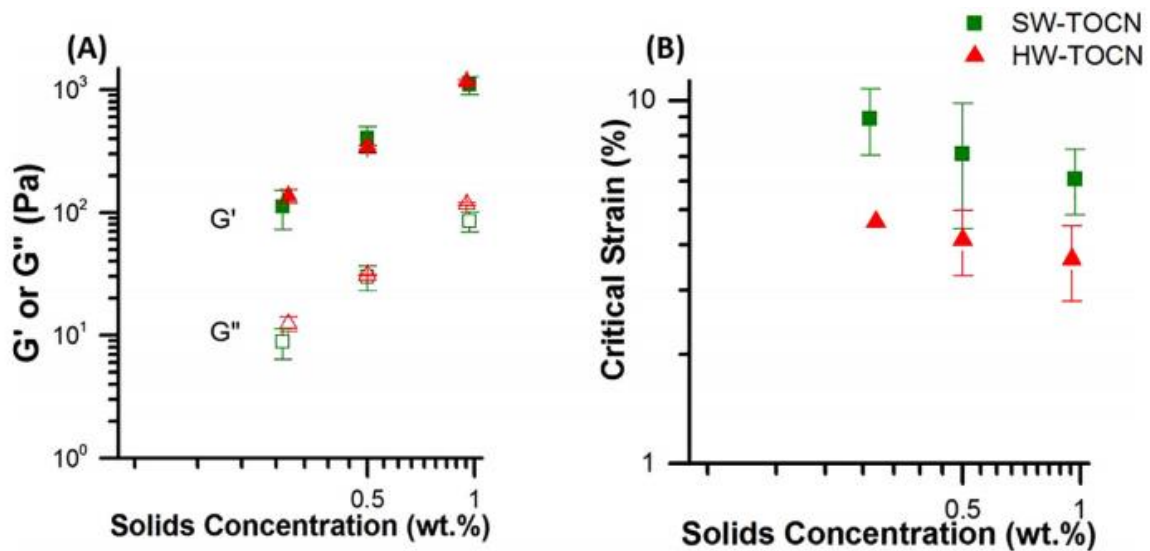


Figure 4. (A) Dynamic Moduli (G' and G'') of nanocellulose gels produced from unrefined softwood and hardwood as a function of solids concentration at constant charge density (1 mmol. .g^{-1}). (B) Critical Strain of SW-TOCN and HW-TOCN as a function of solids concentration.

The difference of pulp source on the resultant nanocellulose gels viscosity profile is highlighted in Figure 5. SW-TOCN and HW-TOCN both display similar viscosity values and linear shear-thinning behaviour at 0.1 wt.%. On the other hand, the double yielding behaviour is observed for HW-TOCN and SW-TOCN at concentrations equal or greater than 0.3 wt.%. The major difference in nanocellulose produced from hardwood and softwood pulp sources is emphasized at the semi-dilute concentrations (0.3 wt.% to 1 wt.%) wherein SW-TOCN viscosity decreases at a steeper gradient at both double yielding regions than HW-TOCNs.

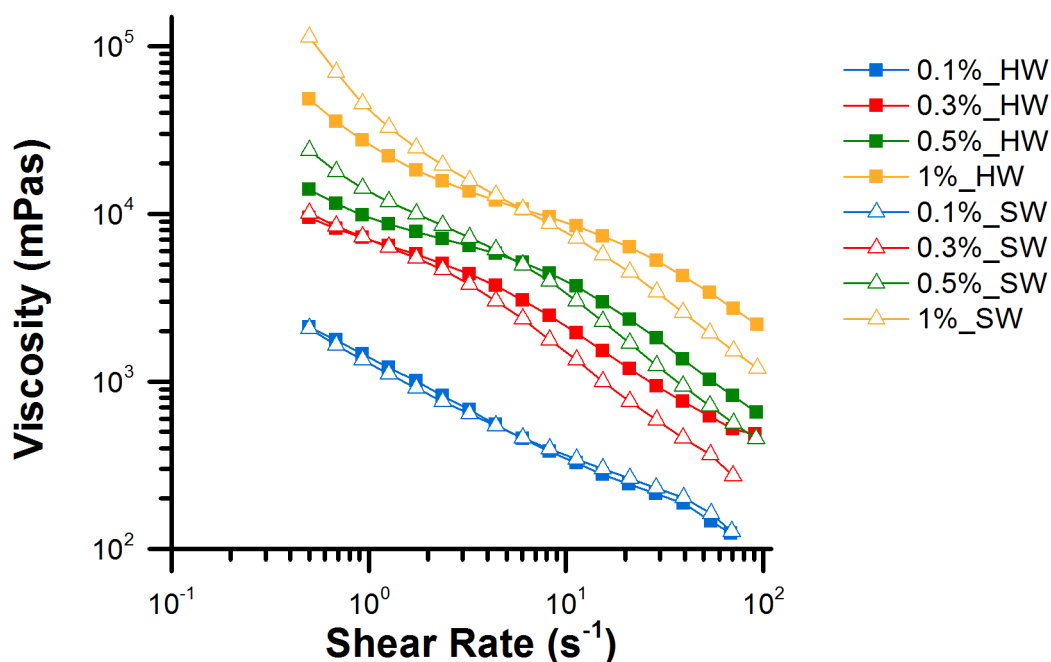


Figure 5. Viscosity Profile of TOCNs from hardwood (solid symbol) and softwood (open symbol) as a function of concentration for constant charge density ($1 \text{ mmol} \cdot \text{g}^{-1}$). Measurements were done at 25°C .

3.4.4 EFFECT OF CHARGE DENSITY

The effect of charge density on the dynamic rheological properties of nanocellulose gels produced from hardwood is shown in Figure 6. Gels with the lowest carboxylate content ($0.65 \text{ mmol} \cdot \text{g}^{-1}$) consistently report the lowest G' and G'' values. However, gels containing either 1 or $1.4 \text{ mmol} \cdot \text{g}^{-1}$ show similar G' . On the other hand, G'' values were also observed to increase with increasing carboxylate content at all solids concentrations. Critical strain γ_c does not vary significantly up to a charge density of $1 \text{ mmol} \cdot \text{g}^{-1}$. At the highest surface charge tested ($1.4 \text{ mmol} \cdot \text{g}^{-1}$), γ_c decreases linearly with increasing fibre content.

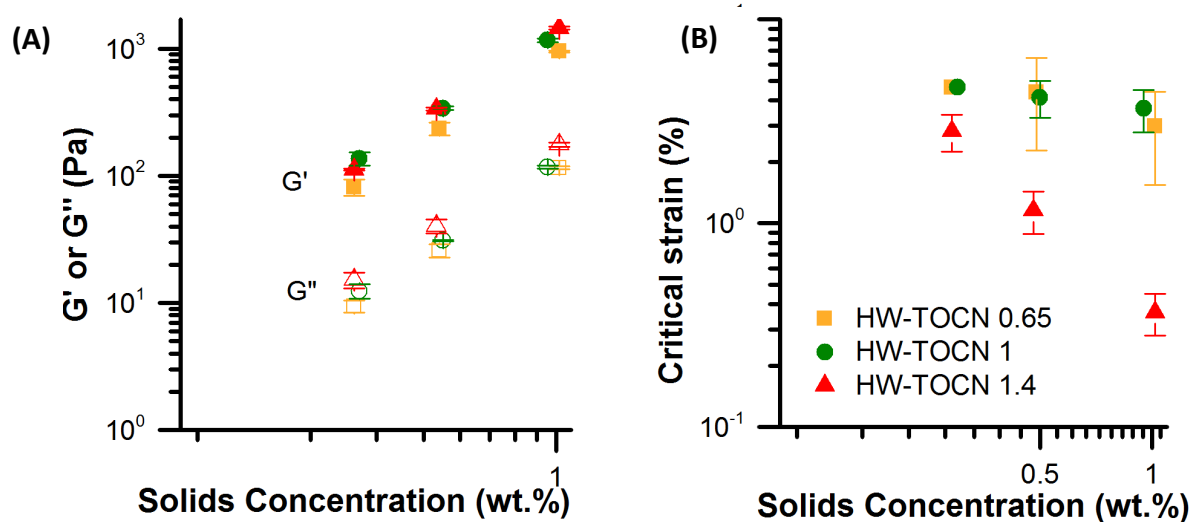


Figure 6. The effect of charge density on the (A) dynamic moduli at LVR and (B) critical strain of HW-TOCN nanocellulose gels at different solids concentrations. Yellow symbols for 0.65mmol.g⁻¹, green symbols for 1mmol.g⁻¹ and red symbols for 1.4 mmol.g⁻¹. Measurements were done at 25°C, 1Hz.

The viscosity profile of nanocellulose gels produced from hardwood at different surface charges is shown in Figure 7. All HW-TOCN gels containing at least 0.3 wt.% possess a double yielding behaviour. At a given concentration past 0.3 wt.%, the differences in the absolute viscosity values are minimal and could be attributed to small variations in actual nanocellulose content in the tested samples. However, at 0.1 wt.%, the gel containing the lowest surface charge at 0.65 mmol .g⁻¹ is significantly less viscous than at 1 and 1.4 mmol .g⁻¹.

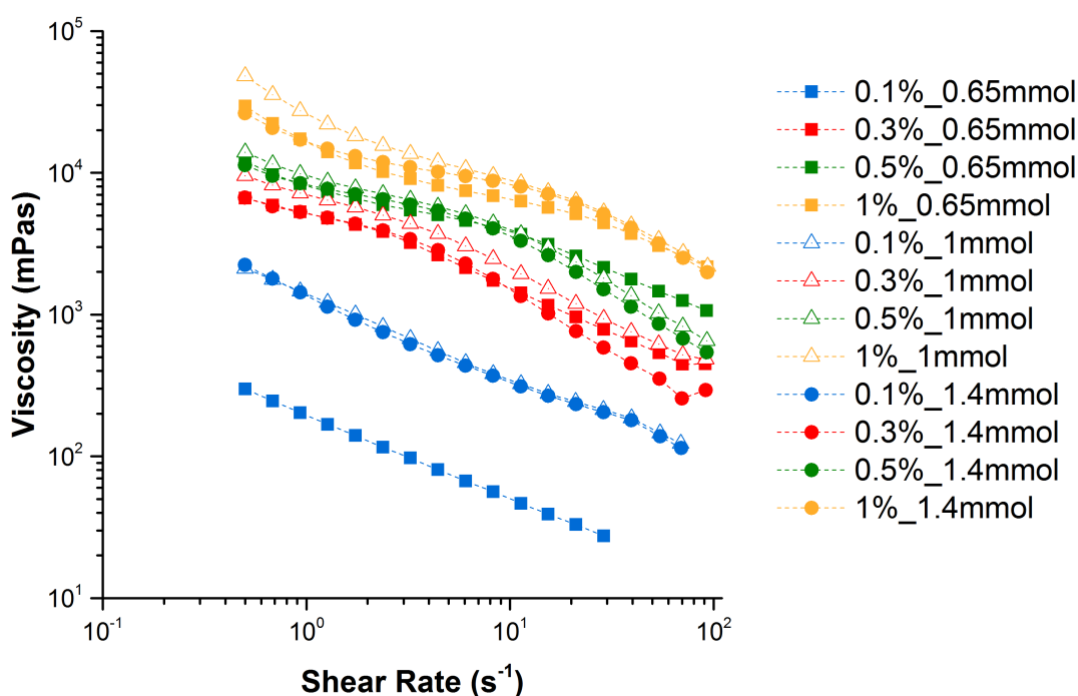


Figure 7. Viscosity Profile for HW-TOCNs at three levels of charge density (0.65, 1, and 1.4 mmol. g⁻¹) and different solids content. Measurements were done at 25°C.

3.5 DISCUSSION

3.5.1 EFFECT OF PULP FIBRES ON NANOCELLULOSE FIBRE DIMENSIONS

Cellulose fibres vary in fibre dimension and chemical composition depending on the original wood source and the pulping process used. The most widely-used process to produce cellulosic fibres is through a combination of kraft chemical pulping followed by bleaching. This process removes most of the lignin and hemicellulose that occur in different amounts and compositions in softwood (*Pinus Radiata*), and hardwood (*Eucalyptus sp.*) [30, 31]. However, traces of lignin and hemicellulose still remain within the bleached cellulose pulp which impact the TEMPO-mediated oxidation process. The softwood pulp used in this study required a higher primary oxidant content (6.5 mmol NaClO .g⁻¹ fibre) than the hardwood pulp (5 mmol NaClO .g⁻¹ fibre) to achieve the same surface charge (1 mmol COO⁻.g⁻¹ fibre).

The original width and length of the never-dried bleached hardwood and softwood fibres are vastly different (Figure 1) – softwood fibres are approximately twice as long and thick

on average compared to hardwood fibres (Tables I and II). The combination of TEMPO-mediated oxidation and high-pressure homogenisation results in nanocellulose fibres with dimensions multiple orders of magnitude smaller. This chemical and mechanical treatment has effectively liberated elementary fibrils from both hardwood and softwood pulp sources, evident by the similar widths of the HW-TOCN and SW-TOCN fibres in the order of nanometers [15]. Due to the high energy required for mechanical fibrillation (i.e. 1000 bar pressure), it is possible that further delamination occurred resulting in a fibre mean width less than the currently accepted elementary fibril dimensions consisting a 6x6 chain array. Since individual cellulose chains are assembled into fibrils by H-bonding along their length, the high-pressure homogenisation could have created shear forces strong enough to liberate thinner fibrils. The widths measured support previous studies. For instance, Usov et al. [32] reported AFM measurements visualising single cellulose chains and 2x2 cellulose nanofibrils with average widths of 0.44 and 0.84 nm, respectively. In addition, Geng et al. [33] described a mean width value of 2.35nm (at a surface charge of 980 $\mu\text{mol. g}^{-1}$); however, width distributions showed a large proportion of fibres thinner than 2 nm. When comparing lengths of the HW-TOCN and SW-TOCN fibres, cleavage is evident for both pulp sources, attributed to the preferential oxidation of the weak amorphous regions subsequently cleaved under intense mechanical fibrillation [34]. This is evident in the XRD spectra (Supporting Information) as the small reduction in the crystalline index (CI) could not account for the large degree of fibrillation which we have observed. On average, the resulting HW-TOCNs are longer than SW-TOCNs (1.30 μm versus 0.85 μm) for a surface charge of 1 mmol $\text{COO}^- \cdot \text{g}^{-1}$.

3.5.2 EFFECT OF NANOFIBRE DIMENSIONS AND SURFACE CHARGE ON GEL RHEOLOGY

TEMPO-oxidised nanocellulose are characterised by two key parameters: physical dimensions (length and width) and surface charge. For TOCNs, provided sufficient electrostatic repulsion and mechanical fibrillation, width is determined by the elementary fibril width which is similar for hardwood and softwood pulp [35]. Length, on the other hand, can vary depending on the processing conditions [2]. The change in length of a semi-flexible fibre affects the extent and ability of entanglement. For SW-

TOCN and HW-TOCN, the difference in fibre lengths is most evident at the onset (i.e. critical strain values) of yielding and steady-state shear (i.e. viscosity) behaviour. Across all concentrations, the shorter SW-TOCNs consistently yielded at higher strains than HW-TOCNs. This might be due to a longer persistence length, related to the flexibility and stiffness of the crystalline domains of softwood, affecting nanofibre conformation upon shear [32]. Nanocellulose gels exhibit shear-thinning response which is generally understood to be due to the alignment of fibres along the shear direction. As seen in Figure 5, for concentrations ranging between 0.3 and 1 wt.%, SW-TOCNs have steeper viscosity gradients than HW-TOCNs due to easier alignment of the shorter fibres. However, this difference does not seem to affect the percolation threshold which is identified as the concentration wherein there is no double yielding behaviour [20]. The double-yielding phenomenon in nanocellulose is attributed to the reorientation of fibres from an isotropic (i.e. randomly oriented) state to partial alignment in the direction of flow. At high fibre concentrations, higher shear rates are required to disrupt any remaining isotropic micro-domains, which leads to a further decrease in viscosity [36]. For both softwood and hardwood-based nanocellulose, the percolation concentration is 0.1 wt.%. Moreover, the dynamic moduli in the LVR region are not significantly different from both pulp types and are primarily concentration-dependent (Figure 4A).

Effective surface charge arising from the nanocellulose carboxylate groups dictates the colloidal stability of the gels [20]. HW-TOCN gel with the lowest charge density (0.65 mmol.g^{-1}) has lower moduli than HW-TOCN gels of higher charge density (Figure 6A). A higher surface charge creates stronger and more stable gels due to higher electrostatic repulsion. The gel critical strain is affected by the variation in the surface charges (Figure 6B). At 1.4 mmol.g^{-1} , the critical strain decreases at increasing concentration. This is not a direct effect of the fibre dimensions as we should observe some differences between 0.65 mmol.g^{-1} and 1 mmol.g^{-1} . The observations at 1.4 mmol.g^{-1} can be attributed to the repulsive charges among fibres which act as lubricant allowing fibres to slide past each other [37]. Hence, the combination of high surface charge and high fibre concentration results in stronger repelling, partially hydrated fibres per unit volume, which reduces the required minimum strain for yielding. Comparing three levels of carboxylation (Figure 7) reveals a significant impact on viscosity at the percolation threshold. At 0.1 wt %

concentration, the reduction in the surface charge to 0.65 mmol.g^{-1} results in an order of magnitude reduction in gel viscosity, possibly due to the less constrained nature of the fibre interactions. A fibre containing low surface charge is expected to have less interactions with other neighbouring fibres as it has a lower effective electrical double layer.

3.6 CONCLUSION

TEMPO-oxidised cellulose nanofibres (TOCNs) are semi-flexible fibrils derived from the primary alcohol oxidation of cellulose. Previous studies have primarily focussed on integrating TOCNs into other compatible materials to improve their bulk properties [4, 5, 10, 14]. Some fundamental studies have been conducted, aiming to understand the colloidal stability [20, 23], local flow phenomenon [12, 21], and model rheological behaviour [26, 27]. The effect of different process conditions (i.e. bleach content and pH, primary oxidant) have been explored previously [2, 38, 39], however little is known on how the fibre source and its dimensions affect the rheological properties of nanocellulose gels. This study analysed the effect of wood pulp source and the resulting nanocellulose fibre dimensions on the rheology of nanocellulose gels. Kraft pulped and bleached hardwood (*Eucalyptus sp.*) and softwood (*Pinus Radiata*) contained fibres with significantly different dimensions ($L = 0.6 \text{ mm}$, $W = 17 \text{ }\mu\text{m}$ and $L = 1.4 \text{ mm}$, $W = 34 \text{ }\mu\text{m}$, respectively) but similar aspect ratios (36 and 42 respectively). However, the initial fibre size has minimal effect on the degree of fibrillation, resulting in hardwood and softwood nanocellulose fibers (HW-TOCN and SW-TOCN) with similar widths in the order of nanometers, indicating elementary fibrils. In terms of length, HW-TOCN fibres are longer than SW-TOCN ($L = 1.3 \text{ }\mu\text{m}$ and $L = 0.9 \text{ }\mu\text{m}$, respectively). The decrease in length from initial macro-fibres for both pulp sources is attributed to the preferential oxidation at weak amorphous regions cleaved under intense mechanical fibrillation. This difference in length affects the onset of yielding (ie. critical strain) and the evolution of the viscosity curves at increasing solids content. This is particularly evident via rheology at the semi-dilute concentrations (0.3 wt.% to 1 wt.%) – shorter SW-TOCN fibres display a steeper viscosity gradient in contrast to HW-TOCNs. Surface charge also impacts the rheological properties at the percolation threshold – for 0.1 wt.% HW-TOCN, increasing the surface charge from 0.65 to at least 1 mmol .g^{-1} results in higher viscosity due to greater

electrostatic interactions. However, at higher concentrations, fibre length and surface charge have minimal effect, and instead the gel dynamic rheological properties (G' and G'') are primarily affected by fibre concentration. These results indicate that, at fibre concentrations greater than the percolation threshold, nanocellulose gels can be produced with similar properties regardless of pulp source and minimal surface charge. This is a key finding beneficial for engineering nanocellulose gels for any specific biomedical or rheology application.

3.7 ACKNOWLEDGMENTS

This work was funded by the ARC Bioprocessing Advance Manufacturing Industry Research Transformation (BAMI) Hub IH13100016, Visy, Norske Skog, Orora, CHH/Oji Paper, Australian Paper and Circa. Many thanks to Australian Paper and Oji Fibre Solutions for providing the pulp. Paul Banham (Norske Skog) for Fibrelab results. Dr. Rico Tabor for his insightful discussion about colloids and rheology. Dr. Vikram Raghuwanshi and Dr. Jisheng Ma (Monash X-ray Platform) for their assistance in performing XRD measurements. This research used equipment (Bruker D8 Discover) funded by Australian Research Council grant LE13010007.

3.8 REFERENCES

1. Quennouz, N., et al., *Rheology of cellulose nanofibrils in the presence of surfactants*. Soft Matter, 2016. **12**(1): p. 157-164.
2. Isogai, A., T. Saito, and H. Fukuzumi, *TEMPO-oxidized cellulose nanofibers*. Nanoscale, 2011. **3**(1): p. 71-85.
3. Reiner, R.S. and A.W. Rudie, *Experiences with Scaling-Up Production of TEMPO-Grade Cellulose Nanofibrils*, in *Nanocelluloses: Their Preparation, Properties, and Applications*. 2017, American Chemical Society. p. 227-245.
4. Fujisawa, S., et al., *Superior Reinforcement Effect of TEMPO-Oxidized Cellulose Nanofibrils in Polystyrene Matrix: Optical, Thermal, and Mechanical Studies*. Biomacromolecules, 2012. **13**(7): p. 2188-2194.
5. Bulota, M. and M. Hughes, *Toughening mechanisms in poly(lactic) acid reinforced with TEMPO-oxidized cellulose*. Journal of Materials Science, 2012. **47**(14): p. 5517-5523.
6. Morimune-Moriya, S., et al., *Hydroxyapatite formation on oxidized cellulose nanofibers in a solution mimicking body fluid*. Polym J, 2015. **47**(2): p. 158-163.
7. Cheng, J., M. Park, and J. Hyun, *Thermoresponsive hybrid hydrogel of oxidized nanocellulose using a polypeptide crosslinker*. Cellulose, 2014. **21**(3): p. 1699-1708.
8. Zander, N.E., et al., *Metal Cation Cross-Linked Nanocellulose Hydrogels as Tissue Engineering Substrates*. ACS Applied Materials & Interfaces, 2014. **6**(21): p. 18502-18510.
9. Feng, J., et al., *Antimicrobial activity of silver nanoparticles in situ growth on TEMPO-mediated oxidized bacterial cellulose*. Cellulose, 2014. **21**(6): p. 4557-4567.
10. Kim, S.-S., et al., *High-Fidelity Bioelectronic Muscular Actuator Based on Graphene-Mediated and TEMPO-Oxidized Bacterial Cellulose*. Advanced Functional Materials, 2015. **25**(23): p. 3560-3570.
11. Shimotoyodome, A., et al., *Regulation of Postprandial Blood Metabolic Variables by TEMPO-Oxidized Cellulose Nanofibers*. Biomacromolecules, 2011. **12**(10): p. 3812-3818.
12. Nechyporchuk, O., M.N. Belgacem, and F. Pignon, *Concentration effect of TEMPO-oxidized nanofibrillated cellulose aqueous suspensions on the flow instabilities and small-angle X-ray scattering structural characterization*. Cellulose, 2015. **22**(4): p. 2197-2210.
13. Azetsu, A., et al., *Direct Synthesis of Gold Nanocatalysts on TEMPO-oxidized Pulp Paper Containing Aldehyde Groups*. 2013. Vol. 8. 2013.
14. Isobe, N., et al., *TEMPO-oxidized cellulose hydrogel as a high-capacity and reusable heavy metal ion adsorbent*. Journal of Hazardous Materials, 2013. **260**: p. 195-201.
15. Jiang, F. and Y.-L. Hsieh, *Super water absorbing and shape memory nanocellulose aerogels from TEMPO-oxidized cellulose nanofibrils via cyclic freezing-thawing*. Journal of Materials Chemistry A, 2014. **2**(2): p. 350-359.
16. Koga, H., et al., *Transparent, Conductive, and Printable Composites Consisting of TEMPO-Oxidized Nanocellulose and Carbon Nanotube*. Biomacromolecules, 2013. **14**(4): p. 1160-1165.

17. Tanaka, R., et al., *Influence of Flexibility and Dimensions of Nanocelluloses on the Flow Properties of Their Aqueous Dispersions*. *Biomacromolecules*, 2015. **16**(7): p. 2127-2131.
18. Jowkarderis, L. and T.G.M. van de Ven, *Intrinsic viscosity of aqueous suspensions of cellulose nanofibrils*. *Cellulose*, 2014. **21**(4): p. 2511-2517.
19. Varanasi, S., R. He, and W. Batchelor, *Estimation of cellulose nanofibre aspect ratio from measurements of fibre suspension gel point*. *Cellulose*, 2013. **20**(4): p. 1885-1896.
20. Mendoza, L., et al., *Gelation mechanism of cellulose nanofibre gels: A colloids and interfacial perspective*. *Journal of Colloid and Interface Science*, 2018. **509**(Supplement C): p. 39-46.
21. Nazari, B., et al., *Rheology of cellulose nanofibers suspensions: Boundary driven flow*. *Journal of Rheology*, 2016. **60**(6): p. 1151-1159.
22. Iotti, M., et al., *Rheological Studies of Microfibrillar Cellulose Water Dispersions*. *Journal of Polymers and the Environment*, 2011. **19**(1): p. 137-145.
23. Nordenström, M., et al., *Formation of Colloidal Nanocellulose Glasses and Gels*. *Langmuir*, 2017. **33**(38): p. 9772-9780.
24. Martoia, F., et al., *Micro-mechanics of electrostatically stabilized suspensions of cellulose nanofibrils under steady state shear flow*. *Soft Matter*, 2016. **12**(6): p. 1721-1735.
25. Jowkarderis, L. and T.G.M. van de Ven, *Rheology of semi-dilute suspensions of carboxylated cellulose nanofibrils*. *Carbohydrate Polymers*, 2015. **123**: p. 416-423.
26. Puisto, A., et al., *Modeling the rheology of nanocellulose suspensions*. *Nordic Pulp & Paper Research Journal*, 2012. **27**(2): p. 277-281.
27. Puisto, A., et al., *Modeling the viscosity and aggregation of suspensions of highly anisotropic nanoparticles*. *The European Physical Journal E*, 2012. **35**(1): p. 6.
28. Moberg, T., et al., *Rheological properties of nanocellulose suspensions: effects of fibril/particle dimensions and surface characteristics*. *Cellulose*, 2017. **24**(6): p. 2499-2510.
29. da Silva Perez, D., S. Montanari, and M.R. Vignon, *TEMPO-Mediated Oxidation of Cellulose III*. *Biomacromolecules*, 2003. **4**(5): p. 1417-1425.
30. Martínez, P., M. Pereira, and R.T. Mendonça, *Retention and Structure of Xylans from Eucalyptus Globulus Genotypes with Different Pulpwood Characteristics*. *Journal of Wood Chemistry and Technology*, 2015. **35**(2): p. 129-136.
31. Cruz, N., et al., *Impact of the Chemical Composition of Pinus radiata Wood on its Physical and Mechanical Properties Following Thermo-Hygro-mechanical Densification*. 2018. Vol. 13. 2018.
32. Usov, I., et al., *Understanding nanocellulose chirality and structure-properties relationship at the single fibril level*. *Nature Communications*, 2015. **6**: p. 7564.
33. Geng, L., et al., *Understanding the Mechanistic Behavior of Highly Charged Cellulose Nanofibers in Aqueous Systems*. *Macromolecules*, 2018. **51**(4): p. 1498-1506.
34. Zimmermann, R., et al., *Oxidation and structural changes in NMMO-regenerated cellulose films*. *Cellulose*, 2016. **23**(6): p. 3535-3541.
35. Chinga-Carrasco, G., Y. Yu, and O. Diserud, *Quantitative Electron Microscopy of Cellulose Nanofibril Structures from Eucalyptus and Pinus radiata Kraft Pulp Fibers*. *Microscopy and Microanalysis*, 2011. **17**(4): p. 563-571.

36. Lasseuguette, E., D. Roux, and Y. Nishiyama, *Rheological properties of microfibrillar suspension of TEMPO-oxidized pulp*. Cellulose, 2008. **15**(3): p. 425-433.
37. Hubbe, M.A., et al., *Rheology of Nanocellulose-rich Aqueous Suspensions: A Review*. 2017. Vol. 12. 2017.
38. de Nooy, A.E.J., A.C. Besemer, and H. van Bekkum, *Highly selective tempo mediated oxidation of primary alcohol groups in polysaccharides*. Recueil des Travaux Chimiques des Pays-Bas, 1994. **113**(3): p. 165-166.
39. Benhamou, K., et al., *Control of size and viscoelastic properties of nanofibrillated cellulose from palm tree by varying the TEMPO-mediated oxidation time*. Carbohydrate Polymers, 2014. **99**(Supplement C): p. 74-83.

THIS PAGE HAS BEEN INTENTIONALLY LEFT BLANK

THIS PAGE HAS BEEN INTENTIONALLY LEFT BLANK

CHAPTER 4

CARBOXYLATED NANOCCELLULOSE FOAMS

AS SUPERABSORBENTS

THIS PAGE HAS BEEN INTENTIONALLY LEFT BLANK

CHAPTER 4 CARBOXYLATED NANOCELLULOSE FOAMS AS SUPERABSORBENTS

4.1	ABSTRACT.....	107
4.1.1	HYPOTHESIS.....	107
4.1.2	EXPERIMENTS.....	107
4.1.3	FINDINGS.....	107
4.1.4	KEYWORDS	108
4.2	INTRODUCTION	108
4.3	METHODOLOGY	110
4.3.1	MATERIALS	110
4.3.2	TEMPO-MEDIATED OXIDATION	110
4.3.3	PREPARATION OF NANOCELLULOSE FOAMS.....	111
4.3.4	DETERMINING SOLIDS CONCENTRATION	111
4.3.5	DETERMINING THE CARBOXYLATE CONTENT OF NANOCELLULOSE.....	111
4.3.6	MEASUREMENT OF ABSORPTION CAPACITY.....	112
4.3.7	IMAGING OF NANOCELLULOSE STRUCTURE	112
4.3.8	MERCURY POROSIMETRY.....	112
4.4	RESULTS	113
4.4.1	EFFECT OF GEL SOLIDS CONCENTRATION	113
4.4.2	EFFECT OF SURFACE CHARGE.....	114
4.4.3	EFFECT OF FREEZING RATE.....	115
4.4.4	ABSORPTION OF SALINE.....	116
4.5	DISCUSSION	117
4.5.1	EFFECT OF FOAM AND FIBRE PROPERTIES ON SUPERABSORBENT CAPACITY	117
4.5.2	SWELLING KINETICS OF NANOCELLULOSE FOAMS	119
4.5.3	EFFECT OF FREEZING RATE AND ABSORBATE ON SUPERABSORBENT CAPACITY	120
4.6	CONCLUSION	121
4.7	ACKNOWLEDGMENTS	123
4.8	REFERENCES	124

THIS PAGE HAS BEEN INTENTIONALLY LEFT BLANK

Carboxylated Nanocellulose Foams as Superabsorbents

Llyza Mendoza¹, Laila Hossain¹, Emma Downey¹, Camilla Scales¹, Warren Batchelor¹, Gil Garnier^{1,}*

¹Bioresource Processing Research Institute of Australia (BioPRIA), Department of Chemical Engineering, Monash University, VIC 3800, Australia

²School of Chemistry, Monash University, Clayton, VIC 3800, Australia

*E-mail: gil.garnier@monash.edu

4.1 ABSTRACT

4.1.1 HYPOTHESIS

Carboxylated nanocellulose fibres formed into foam structures can demonstrate superabsorption capacity. Their performance can be engineered by changing process variables.

4.1.2 EXPERIMENTS

TEMPO-oxidised cellulose nanofibres of varying concentration and surface charge are produced from hardwood kraft pulp. Foams were prepared through a 2-step freezing and lyophilisation process. The absorption capacity of water and saline solution (0.9wt.%) were measured as a function of time and related to the foam structure.

4.1.3 FINDINGS

The absorption capacity of nanocellulose foams can be manipulated from initial gel properties and processing conditions. Pore structure and distribution of nanocellulose foams are dictated by fibre content and charge density and freezing rate. The best performing foams are at 0.3-0.5 wt.%, with a carboxylate concentration of 1.2 mmol/g and frozen at -86°C before freeze-drying, which can absorb 120 g H₂O/ g fibre. Fibre surface charge influences the absorption capacity of the foams by dictating the amount of participating carboxylate groups. Absorption capacity in saline (60 g/g) is lower than in deionised water (120 g/g); but is only slightly lower than that of a commercial polyacrylic acid (PAA) SAPs (80g/g). Nanocellulose foams are attractive renewable

alternatives for superabsorbent applications, contributing to a reduction of plastic microspheres.

4.1.4 KEYWORDS

Superabsorbent, TEMPO-mediated oxidation, nanocellulose, foam, structure

4.2 INTRODUCTION

Superabsorbent polymer (SAP) hydrogels contain cross-linked network of hydrophilic polymers capable of absorbing large volumes of water [1]. Upon contact with water, the glassy polymers hydrate to form a three-dimensional network which does not dissolve due to the presence of cross-linking [2]. The swelling of these polymer networks is driven by the difference in osmotic pressure inside and outside the gel caused by the movement of the counterions in the system. The high absorption of water molecules is due to a high concentration of COO^- groups able to form hydrogen bonding with water molecules [3]. Although commercial SAPs are usually known for applications in personal care and hygiene products, these materials are also increasingly utilised in agriculture and horticulture [4], biomedical products [5-7], and even wastewater treatment [8, 9]. Currently, the majority of superabsorbent products in the market is synthesised from acrylic and acrylamide polymers from petrochemicals which exhibit poor environmental degradability. This lack of sustainability has driven research towards developing alternatives which are renewably sourced and biodegradable.

There are many reports of superabsorbents made from biopolymers in literature. Natural-based SAPs, such as chitosan, gelatine, carrageenan and starch, have been modified to increase water absorption [10, 11]. Cellulose, the most abundant biopolymer, has also been studied for its desirable characteristics: biodegradability, renewability, and innate hydrophilicity [12]. Cellulose can be processed into porous materials such as foams [13, 14] and different synthesis methods have been explored to functionalise cellulose as a superabsorbent hydrogel [12]. Among those are foam and hydrogel composites made with carboxymethyl cellulose [15-19] and hydroxyethyl cellulose [20, 21] used in combination with other polymers and nanoparticles. Another strategy is to graft side groups such as butanetetracarboxyl, acrylic, and acrylamide

groups onto the cellulose backbone which results in large absorption of water (~ 720 g/g) [22, 23]. Functionalising the cellulose hydroxyl groups can significantly increase water interactions.

Another method of producing foams is through the production of nanocellulose and manufacture of foams via ice-templating followed by sublimation or via supercritical drying [24]. TEMPO-mediated oxidation is alternative method of functionalising cellulose fibres [25]. This oxidation process selectively converts the primary alcohol (C6) groups into carboxylate groups. The added electrostatic repulsion produces nano-scale fibres upon mechanical fibrillation. Brodin and Theliander initially tested the superabsorbent characteristics of TEMPO-oxidised nanocellulose by varying different process conditions such as pulp types, composition, and oxidation severity [26-29]. Jiang and Hsieh investigated the production of nanocellulose aerogels via cyclic freeze-thawing process and also introduced functionalisation to create oleophilic foams [30-32]. However, the effects of varying foam properties by changing the fibre density were not explored nor related to composite structure. There are limited studies on the effect of processing conditions (i.e. freezing rate) on the performance of nanocellulose foams. Moreover, the kinetics of nanocellulose foam swelling remain unknown.

In this study, we produced nanocellulose superabsorbent foams via a two-step process: (1) TEMPO-mediated oxidation/high-pressure homogenisation to produce a nanocellulose hydrogel [33, 34] and (2) freeze-drying the hydrogel to produce nanocellulose foams. The aim of this study is to understand the relationship between process variables (freezing rate) and nanocellulose properties (surface charge and fibre concentration) to the resulting foam structure and absorption characteristics. The swelling kinetics of the foams is also determined. Insight into the mechanism of superabsorbency of these carboxylated nanocellulose foams is demonstrated.

4.3 METHODOLOGY

4.3.1 MATERIALS

Bleached Eucalyptus Kraft (BEK) pulp, containing approximately 10 wt.% solids, was obtained from Australian Paper, Maryvale, Australia. 2,2,6,6-Tetramethylpiperidine-1-oxyl (TEMPO) and sodium bromide (NaBr) were purchased from Sigma-Aldrich. Hydrochloric acid (HCl) and Sodium Hydroxide (NaOH) were diluted for solutions as required and were purchased from ACL Laboratories and Merck, respectively. 12 w/v% Sodium Hypochlorite (NaClO) was purchased from Thermo Fisher Scientific and used as received. Commercial sodium polyacrylate superabsorbent (HySORB R 8130) was provided by BASF.

4.3.2 TEMPO-MEDIATED OXIDATION

The TEMPO-mediated oxidation process employed is based on a previously developed method [25]. 100g BEK pulp was suspended in 2500mL water containing 0.4g TEMPO and 2.5g NaBr. The 12 w/v% NaClO solution was initially adjusted to pH 10 via addition of 36 w/v% HCl. To produce high surface charged fibres, 75mL NaClO (5mmol NaClO/g cellulose) was added drop-wise to the suspension whilst stirred. Lower surface charged fibres were produced by adding a lower amount of the primary oxidant (50mL NaClO, 3.33mmol/g). The pH of the reaction was maintained at 10 through the addition of 0.5M NaOH. The oxidation process is deemed to be complete when the pH change is negligible. The oxidised fibres were recovered through filtration and stored refrigerated (2-8°C).

The TEMPO-oxidised pulp is then dispersed in deionised water at a desired concentration. Fibrillation is accomplished through a high-pressure homogeniser (GEA Niro Soavi Homogeniser Panda) at 1000 bar. Suspensions which contain less than 1wt.% TEMPO-oxidised pulp is homogenised with two passes. More concentrated suspensions are homogenised with only one pass.

4.3.3 PREPARATION OF NANOCELLULOSE FOAMS

Nanocellulose foams were prepared by spreading 15 g gel in a 50mm petri dish and freezing at either in a freezer for at least 12 hours (-20°C, -80°C) or in liquid nitrogen (-196°C). For freezing at -196°C, the samples were placed in a cold-proof container and liquid nitrogen was poured in ensuring full immersion for 4-5 minutes. Once frozen, all samples were freeze-dried (Christ Alpha 2-4 LD Plus) for 2 days.

4.3.4 DETERMINING SOLIDS CONCENTRATION

The solids concentration of any sample (i.e. hydrogel or pulp) is determined through oven drying. The sample is weighed before (w_i) and after (w_d) drying, where the sample moisture is evaporated in a ventilated oven at 105°C for at least 4 hours. The solids content is determined through the following equation:

$$\text{Solids content (\%)} = \frac{w_d}{w_i} \times 100 \% \quad (1)$$

4.3.5 DETERMINING THE CARBOXYLATE CONTENT OF NANOCELLULOSE

The carboxylate content of the nanocellulose fibre is determined via conductometric titration [35]. 0.1 dry g oxidised pulp is suspended in 40mL deionised water. 100µL 1 wt.% NaCl is added to the suspension to increase base sample conductivity. The sample pH is then lowered to pH 2.5-3 to protonate all of the carboxylate groups prior to the beginning of titration. Sample titration is initiated by the addition of 0.1 mL/min NaOH (Mettler Toledo T5 titrator). The conductivity is monitored throughout the progress of the titration. The amount of carboxylate groups is then calculated through the following equation:

$$\text{Carboxylate Content} \left(\frac{\text{mmol}}{\text{g}} \right) = \frac{c(V_2 - V_1)}{w} \times 1000 \quad (2)$$

where V_2 and V_1 pertain to the required amount of titrant to neutralise the carboxylic groups (plateau region in the titration curve), c is the NaOH concentration (mol/L), and w is the dry sample weight.

4.3.6 MEASUREMENT OF ABSORPTION CAPACITY

The freeze-dried fibres are then allowed to be in contact with deionised water or 0.9 wt.% NaCl solution for reabsorption. The foams were repeatedly taken out of immersion and weighed. Intake of water by the foam is measured in regular intervals up to 2 hours. The free swell capacity W is then calculated through the following equation:

$$\text{Free Swell Capacity, } W = \frac{m_t - m_i}{m_i} \quad (3)$$

Where m_t is the mass of the swollen foam at a particular time interval and m_i is the initial mass of the foam. The results are reported as the average and standard deviation of 3 replicates.

4.3.7 IMAGING OF NANOCELLULOSE STRUCTURE

Nanocellulose foams were imaged by optical microscopy (Nikon Eclipse Ni-E Upright Microscope) in bright-field mode at 5x magnification.

4.3.8 MERCURY POROSIMETRY

The pore size distribution, porosity (total and at $P = 1\text{atm}$), and pore surface area were determined for selected nanocellulose foams via mercury porosimetry (Micromeritics Autopore IV). Nanocellulose foams were cut in small cubes ($0.5 \times 0.5 \times 0.5 \text{ cm}$) by a laser cutter (Epilog Laser Helix). The samples were prepared by initially de-gassing (24 hours, 100°C) followed by testing. Two replicates per sample were tested. In all measurements, the contact angle at the Hg-Foam interface is assumed to be 130° and a testing pressure range from 0.1 to 60,000 psia is applied. The desired values are calculated via the Washburn Equation:

$$D = \frac{-4\gamma \cos \theta}{P} \quad (4)$$

Where D is the pore diameter, γ is the surface tension of mercury, θ is the contact angle between the pore wall and mercury, and P is the applied pressure. Important values are reported at either as a result of considering 1 atm (14.7 psia) intrusion pressure or at total maximum porosimetry pressure (60,000 psia / 4082atm).

4.4 RESULTS

The effect of initial gel properties such as the solids concentration and surface charge on the structure and morphology as well as the absorption behaviour of the foams is initially studied (frozen at -80°C). The effect of freezing rate is then analysed. Lastly, the best performing foam in distilled water is tested with saline and compared against a commercial SAP.

4.4.1 EFFECT OF GEL SOLIDS CONCENTRATION

Figure 1 shows the free swell capacity (FSC) of nanocellulose foams in deionised water as a function of the initial gel solids concentration in deionised water. In all cases, the initial rapid swelling is followed by a slower absorption process in the 2 hour testing period. There is no significant difference between the performance of foams produced from 0.3 wt.% and 0.5 wt.% (overlapping error bars). Measurement error also increases at lower initial gel concentrations. However, increasing the fibre concentration in gel from 0.5 wt. % to 1 and 3 wt. % resulted in a decrease in the FSC values.

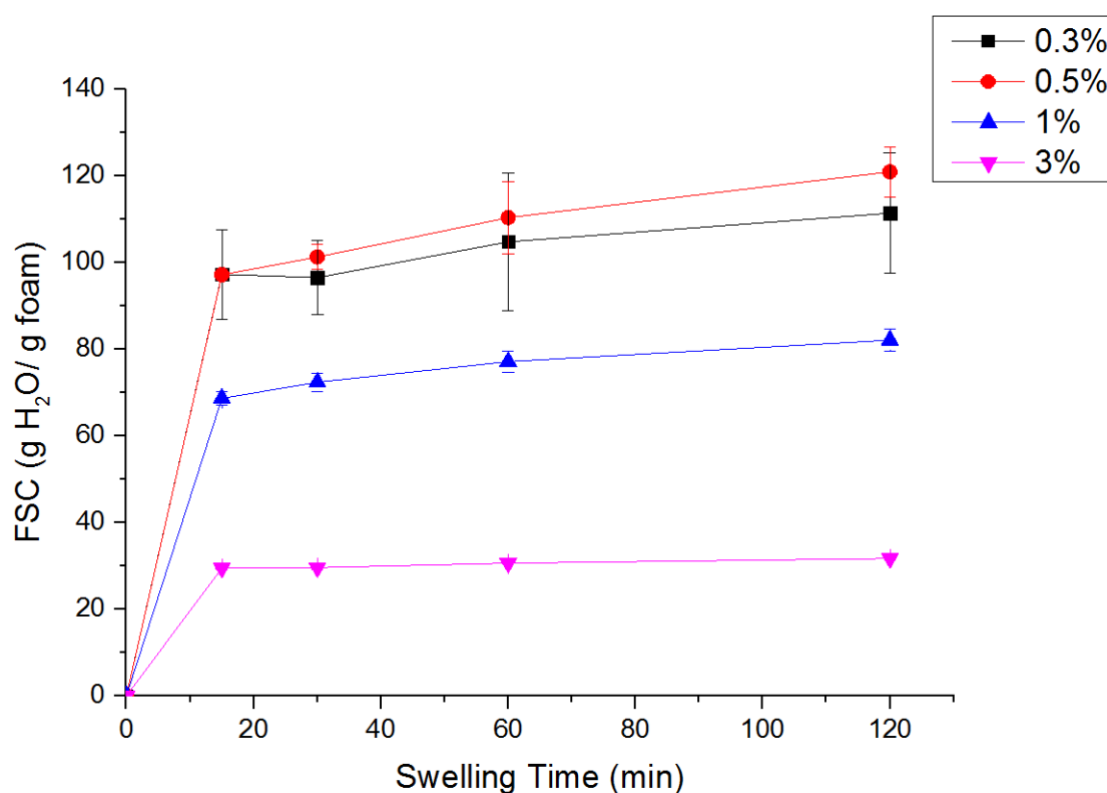


Figure 1. Free Swell Capacity (FSC) in deionised water of Nanocellulose Foams (-80°C) at different solids concentrations as a function of swelling time.

The pore size distribution of nanocellulose foams was measured by mercury porosimetry as a function of the initial gel solids concentration as shown in Figure 2A. Calculated foam properties for each of the nanocellulose foams is also summarised in Figures 2B and 2C. At increasing initial gel solids concentration, the foam bulk density consistently increases. Foam porosity is calculated at two pressure levels (1 atm and at 4082 atm) to signify pores accessible at atmospheric pressure and the total maximum pore volume, respectively. Total foam porosity is similar (>94%) across all original gel concentrations; however, porosity at 1 atm is halved when the solids content is increased by an order of magnitude. The total pore surface area also decreased with increasing gel solids concentration.

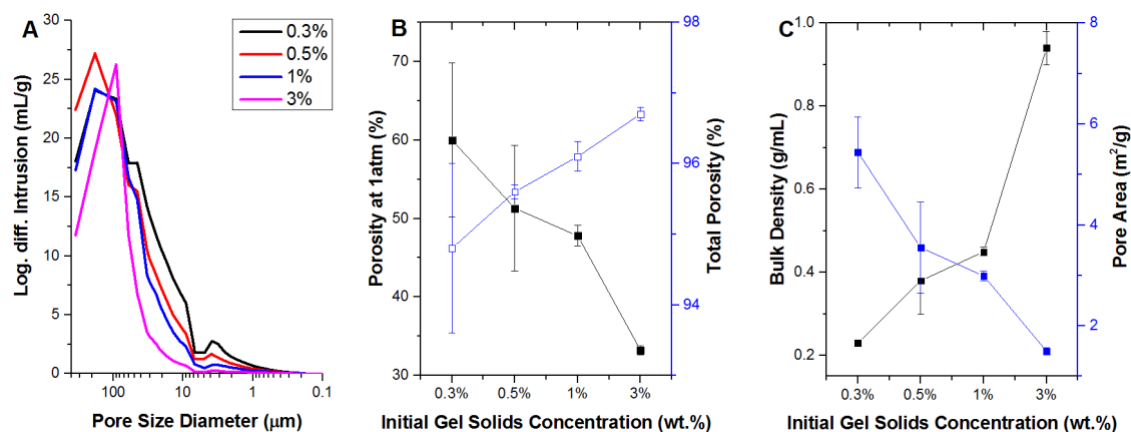


Figure 2. (A) Pore Size Distribution of Nanocellulose Foams (-80°C) at different solids concentrations. Foam properties such as (B) porosity (1 atm^a and total^b), (C) bulk density and pore area derived from mercury porosimetry. Further details on porosimetry data and related calculations are provided in the Supplementary Information.

Notes:

$$^a\text{Porosity at 1 atm is calculated by: } \text{Porosity (1 atm)} = \left(1 - \frac{\text{Bulk Density (1 atm)}}{\text{Skeletal Density}}\right) \times 100\%$$

$$^b\text{Total porosity is calculated by: } \text{Total Porosity} = \left(\frac{\text{Pore Volume}}{\text{Skeletal Volume} + \text{Pore Volume}}\right) \times 100\%.$$

4.4.2 EFFECT OF SURFACE CHARGE

Figure 2 shows the effect of the nanocellulose carboxylate group content on the foam absorption capacity. Lowering the carboxylate group from 1.2 mmol/g to 0.65 mmol/g resulted in lower absorption values for all concentrations tested.

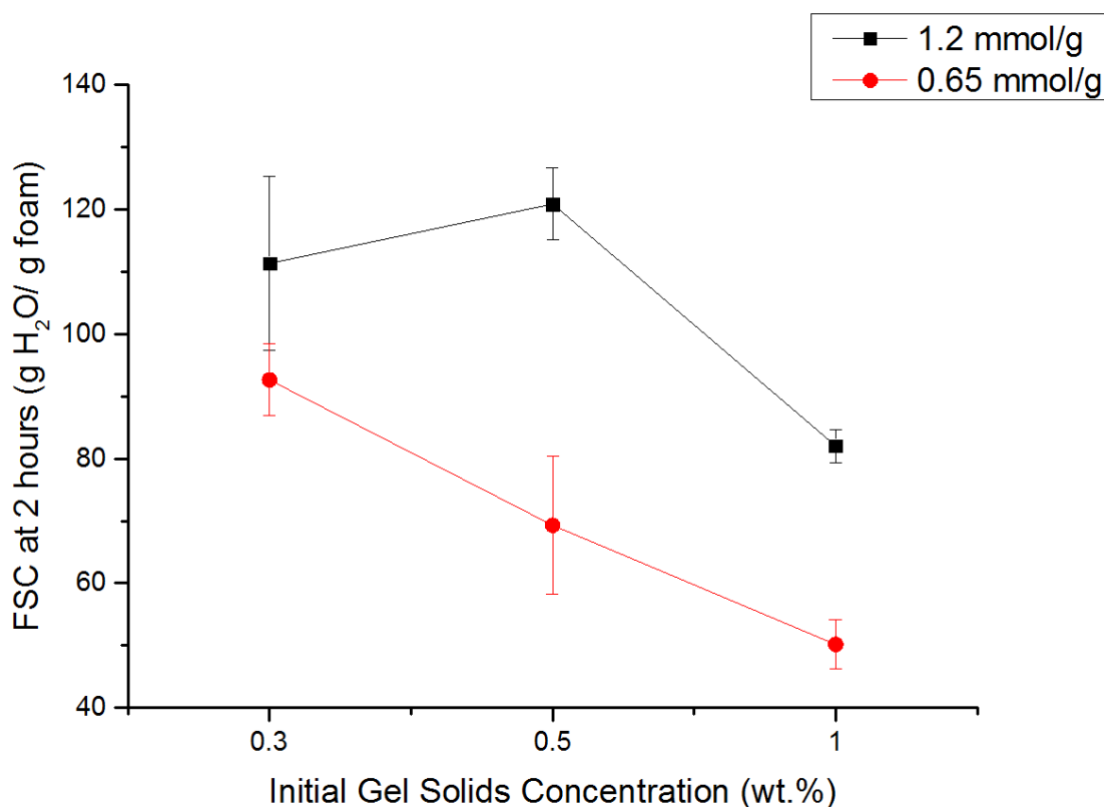


Figure 3. Effect of cellulose fibre surface charge of Nanocellulose Foams (-80°C) at different solids concentration on FSC in deionised water

4.4.3 EFFECT OF FREEZING RATE

The formation of nanocellulose foams is a two-step process which includes freezing of the nanocellulose gels and sublimation of the frozen water. In this study, the effect of freezing rate is studied by freezing at different temperatures (-20°C, -80°C, -196°C). The freezing rate will be the slowest at -20°C whereas freezing at -196°C will be the fastest. The lyophilisation step is kept constant in this study. The effect of freezing rate on the performance of nanocellulose foams in absorbing deionised water is shown in Figure 4A. Aside from 0.3 wt.%, foams processed at -80°C has performed slightly better than -20°C. Freezing rate was modified to control foam morphology. Freezing at the lowest rate (-20°C) results in sheet-like structures with interspersed pores (Figure 4B) whereas at the fastest freezing rate (-196°C), the pores formed are more uniform (Figure 4D). At -80°C, the structure formed is a combination of those from the two freezing rates (Figure 4C).

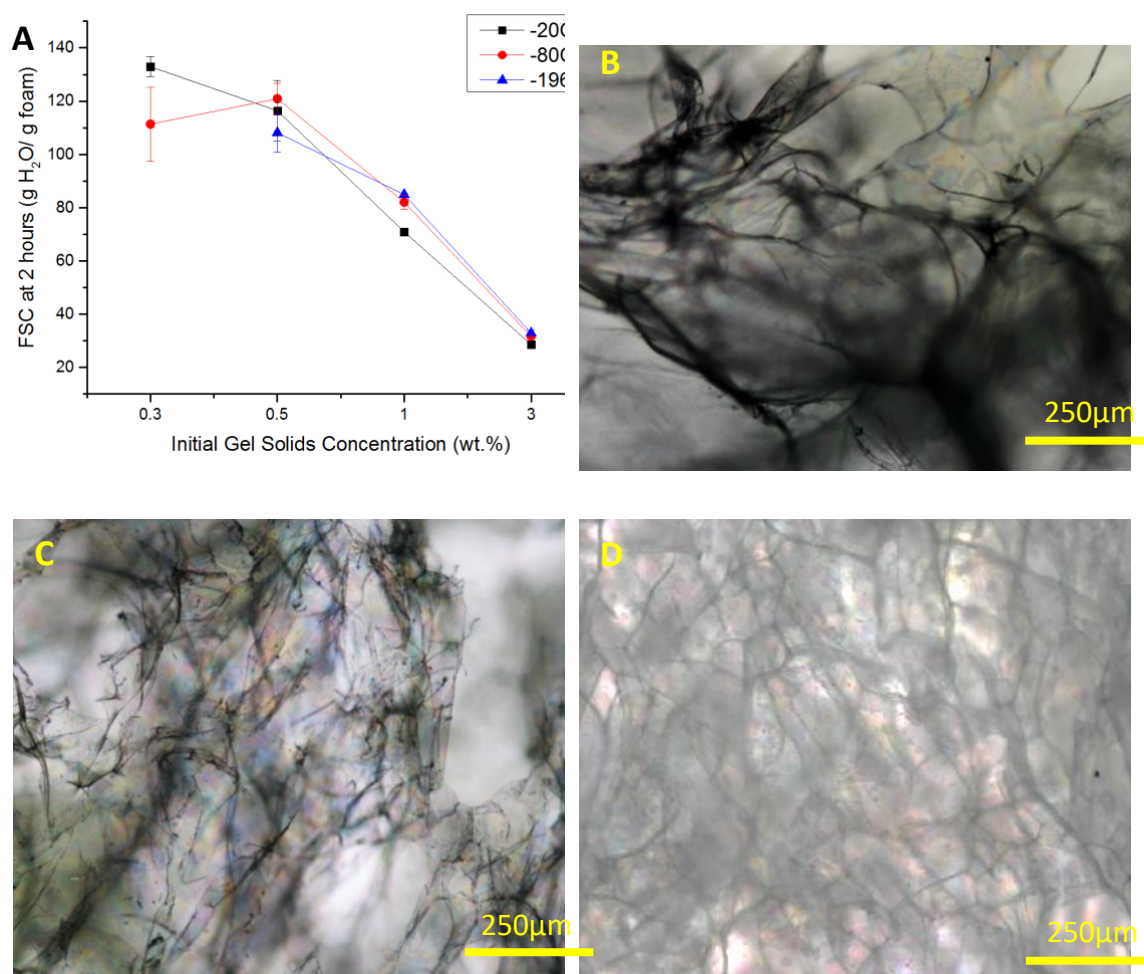


Figure 4. (A) The Effect of Freezing Rate (initial freezing at -20°C, -80°C, and 196°C) on the FSC in deionised water. Optical microscopy illustrating the effect of freezing at (B) -20°C (C) -80°C, and (D) -196°C on the morphology of nanocellulose foams.

4.4.4 ABSORPTION OF SALINE

Figure 5 shows the FSC of nanocellulose foam in 0.9 wt.% saline. For all foams, lower FSC values are recorded in saline than in deionised water. Absorption after 2 hours is very similar for all concentrations tested with capacity ranging between 50 g/g to 70 g/g. The saline absorption capacity of nanocellulose foams were slightly lower to those of commercial SAP (80 g/g).

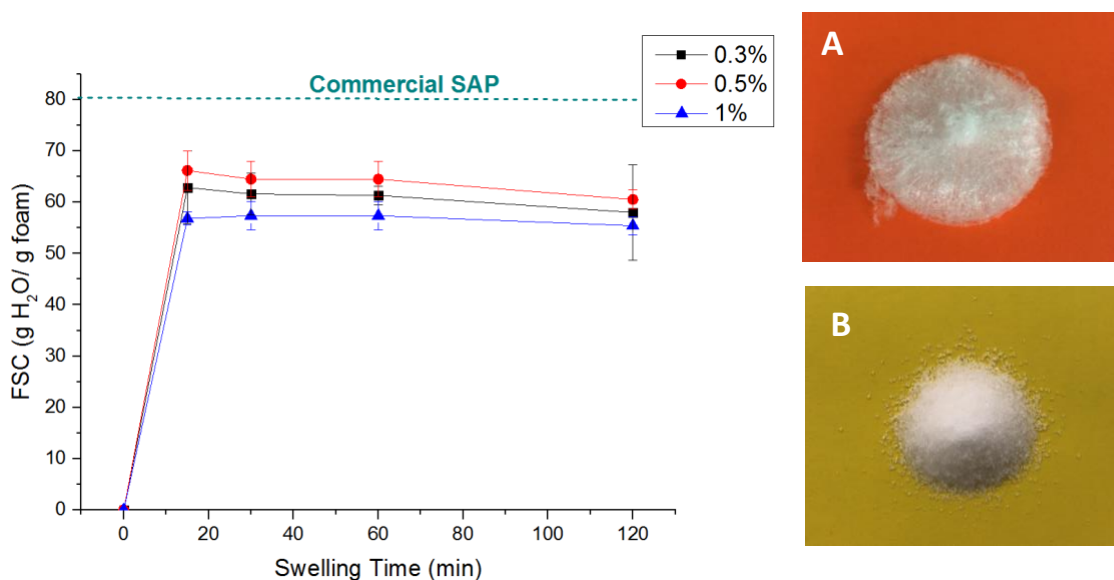


Figure 5. FSC of nanocellulose (-80°C) in 0.9 wt.% saline as a function of swelling time compared against the equilibrium absorption capacity of a commercial SAP polymer. Images showing a (A) NC foam and (B) commercial SAP polymer.

4.5 DISCUSSION

4.5.1 EFFECT OF FOAM AND FIBRE PROPERTIES ON SUPERABSORBENT CAPACITY

In this study, fibre properties, including the initial solids concentration and surface charge, are varied to determine the effect on the superabsorption performance of nanocellulose gels. When the initial gel solids concentration was varied from 0.3 wt.% to 0.5 wt.% (-80°C), FSC values were similar. However, further increase in the fibre concentration (0.5 wt.% to 3 wt.%) resulted in lower FSC values due to the limited availability of the foam internal structure because of a narrower pore distribution (Figure 2). The percentage of accessible pores, quantified by the porosity at 1 atm, decreases with increasing initial solids concentration. For instance, increasing the fibre density by an order of magnitude (0.3 wt.% to 3 wt.%) resulted in halving ($\sim 50\%$ decrease) the available pores at 1 atm. However, the high absorption capacity of nanocellulose cannot be explained merely by the available pore volume shown in Figure 6. For instance, the foam from 0.5 wt.% gel, which is capable of absorbing 120 g/g, has a calculated volume of easily accessible pores of 1.4 mL/g foam (at 1 atm) and a total pore volume of 29 mL/g foam. The available pore volume cannot solely take into account such a large absorption. This means that the 0.5 wt.% foam structure needs to

significantly expand by a factor four its initial volume. The absorption capacity of nanocellulose can be attributed largely to the swelling of the fibre network leading to physical entrapment of liquid water loosely held between nanofibres by capillary forces. This is in contrast to the absorption mechanism of conventional polyacrylic SAPs which are composed of longer polymer chains ($DP = \sim 20,000$ [36], compared to nanocellulose $DP = \sim 600$ [37]) with a higher density of COO^- groups participating in hydrogen bonding with water.

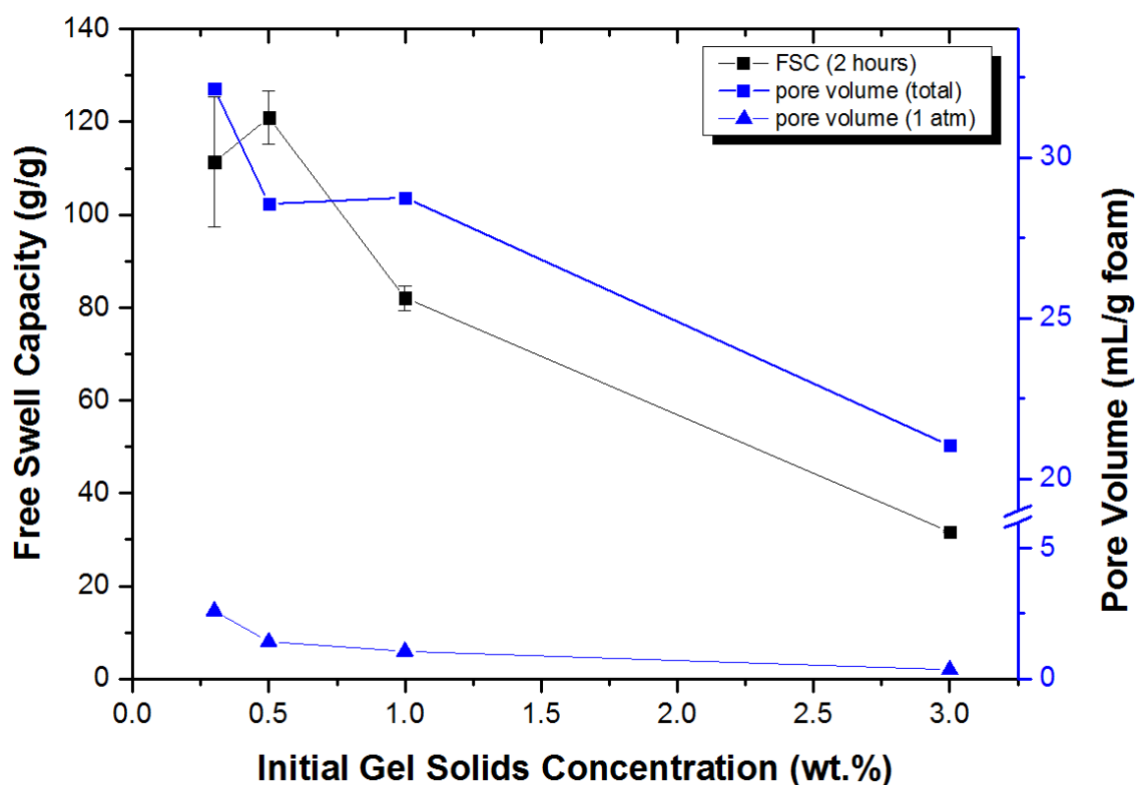


Figure 6. Effect of the initial gel solids content on the superabsorbent nanocellulose foam FSC ($-80^{\circ}C$) in deionised water (2 hours) and available pore volume at 1atm and total pore volume from mercury porosimetry

Fibre surface charge is indicative of the amount of COO^- groups which participate to water absorption. Fibrous structures with a higher concentration of COO^- groups can be expected to have higher absorption and FSC values. Nanocellulose fibres have a theoretical and demonstrated upper carboxylate limit of 1.6 mmol/g fibre [38]. Our fibres contain 1.2 mmol COO^- /g fibre, indicating near-complete oxidation of the C6 hydroxyl group. Doubling the carboxylate content on the cellulose polymer resulted in an increase in the absorption capacity (19 g/g to 51 g/g), as shown in Figure 3.

4.5.2 SWELLING KINETICS OF NANOCELLULOSE FOAMS

The swelling of nanocellulose foams over time can be characterised by two distinct regimes: (a) the initial rapid uptake of absorbate and (b) the asymptotic increase of absorption towards the equilibrium absorption capacity W_{∞} (Figure 1) [39]. Swelling kinetic parameters such as the equilibrium absorption capacity W_{∞} (g/g) and swelling rate constant k_s (g/g min) describing the swelling kinetics of the foams can be estimated by assuming a second order rate of swelling of absorption W (g/g) at swelling time t (min) as derived by Schott [40]:

$$\frac{dW}{dt} = k_s(W_{\infty} - W)^2 \quad (5)$$

Eqn. 5. can be linearised by setting the following conditions: $W= 0$ at $t = 0$ and $W= W$ at $t = t$, resulting in Equation 4:

$$\frac{t}{W} = A + Bt \quad (6)$$

Where:

$$B = \frac{1}{W_{\infty}} \quad (7)$$

$$A = \frac{1}{\left(\frac{dW}{dt}\right)_0} \quad (8)$$

$$k_s = \frac{1}{AW_{\infty}^2} \quad (9)$$

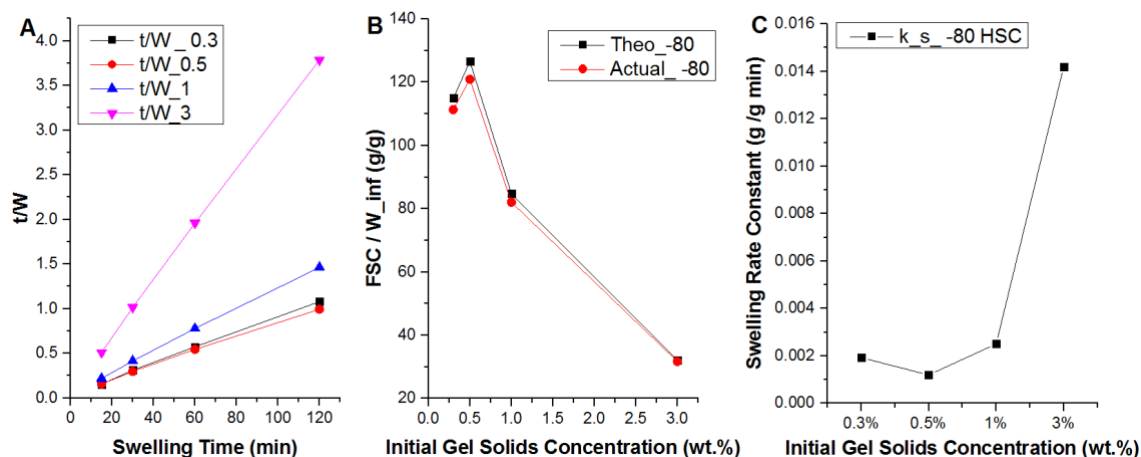


Figure 7. Calculated Swelling Kinetic Parameters of Nanocellulose Foams (-80°C): (A) Linearisation of FSC by Schott's Equation (B) Equilibrium Absorption Capacity W_{∞} and (C) Swelling Rate Constant

Linearising equation (6) by plotting t/W versus t provides good fit with the experiments ($R^2 > 0.99$) (Figure 7A). This suggests that the second-order kinetic assumption with respect to capacity is indicative either of a bimolecular mechanism (water-cellulose) or of a system with diffusion constraints. The actual absorption capacity at 2 hours is close to the theoretical capacity W_{∞} , which indicates that the foams reach saturation within the testing period (Figure 7B). In all concentrations tested, at least 90% of the theoretical capacity was reached within the first 30 minutes of testing – independent of the initial gel concentration. The foam swelling rate constant is constant between 0.3 wt.% to 1 wt.% and increased dramatically at 3 wt.% (Figure 7C). The increase in the swelling rate constant at increasing solids content can be due to saturation reached much faster because of smaller pores and numerous inaccessible carboxylate groups leading to an overall lower free swell capacity.

4.5.3 EFFECT OF FREEZING RATE AND ABSORBATE ON SUPERABSORBENT CAPACITY

The freezing rate of nanocellulose before lyophilisation dictates either nucleation or crystal growth of ice in the gel influencing the nanocellulose porous structure [41]. Freezing at -20°C promotes the crystallisation of larger ice crystals as the degree of supercooling is low [41]. Hence, large pores are produced in certain regions where the ice crystals are formed, and individual fibres are aggregated forming sheet-like

structures together, as seen from Figure 4B. Freezing at a faster rate (-80°C) led to an intermediate state wherein there are still sheets formed with the hornified fibres producing a more uniform structure. Vitrification of the network structure is promoted by freezing at a much faster rate (-196°C) producing a more homogeneous pore structure. This is due to the fibre spacing present within the gel structure (electrostatic repulsion) being maintained upon foam formation. In this instance, the higher rate of freezing promoted the rapid nucleation of smaller ice crystals leading to a more homogenous pore structure [42]. The foams produced at -196°C however were brittle and difficult to handle in contrast to those treated at -20°C and -80°C. Other studies have corroborated with our findings and also reported brittle foams produced from freezing in liquid nitrogen [30, 43]. Hence, it was rather difficult to test low solids content foams such as 0.3 wt.%; these results were omitted from Figure 4A. Although, the morphologies of nanocellulose structures are visibly affected by the freezing rate, the absorption capacity remains similar. This could be due to the hornified fibres in foams prepared at -20°C and -80°C that separate partially while swelling.

The lower values of absorption in saline compared to deionised water is due to the charge shielding from the ions. This reduces the interaction with the COO⁻ groups and the water molecules. The saline capacity of the nanocellulose foams is similar to those reported by Theliander *et al.* with FSCs ranging between 30 to 60 g/g [26-29]. The performance of the nanocellulose foams is slightly lower in contrast to a granulated commercial polyacrylic acid SAP. Further optimising the method to produce the foams may yield similar performance to commercial SAPs.

4.6 CONCLUSION

Cellulose-based superabsorbents were investigated as sustainable substitutes for the current acrylic acid and acrylamide-based SAPs. While numerous studies have examined cellulose-based superabsorbents using various methodologies, few have analysed the SAP structure-performance relationship of TEMPO-oxidised nanocellulose foams [26-29, 44]. In particular, the effect of fibre content and processing conditions (ie. freezing conditions) were not investigated. Moreover, the kinetics and mechanism of absorption

for nanocellulose have not been studied. TEMPO-mediated oxidation produces charged nanocellulose fibres capable of forming cellulosic colloidal gels. The carboxylate groups of TEMPO-oxidised nanocellulose can be exploited for superabsorption. In this study, the potential of TEMPO-oxidised fibres as a superabsorbent polymer is demonstrated. The effect of fibre properties and processing conditions on the resulting nanocellulose foam morphology and its superabsorption performance is determined. Nanocellulose foam density is dictated by the initial gel solids concentration. The best performing foams are at 0.3-0.5 wt.% frozen at -80°C which are capable of absorbing 110-120g/g H_2O . In general, a higher solids concentration produces foams with a narrower pore size distribution and a lower porosity leading to a decreased absorption performance. Nanocellulose foams follow a pseudo-second order absorption kinetics which is affected by foam density. Freezing temperature affects the foam network structure by dictating whether ice nucleation or crystallisation dominates, expanding or not the fibrous structure. A homogeneous porous structure is formed at the fastest freezing rate (-196°C) whereas uneven sheet-like formations were observed at lower freezing rates (-20°C , -80°C). The free swell capacity remained unaffected even with differences in morphology. Changing the absorbate from deionised water to 0.9 wt.% NaCl, mimicking bodily fluids, resulted in the decrease of free swell capacity (FSC) values due to charge shielding. However, the nanocellulose foam performance in saline is already comparable with granulated polyacrylamide SAPs which have been optimised over the last 3 decades. With the results already achieved, the clear link between process-structure-properties and a robust optimization methodology, matching the properties of the current commercial polyacrylic superabsorbent polymers has become a realistic target for cellulose composites. Absorption behaviour in saline can be further improved by blending nanocellulose with biopolymers and optimising the shape and microstructure of foams. Nanocellulose foams has emerged as a high performance, renewable and biodegradable superabsorbent material for biomedical, personal care and environmental applications.

4.7 ACKNOWLEDGMENTS

This work was funded by the ARC Bioprocessing Advance Manufacturing Industry Research Transformation (BAMI) Hub IH13100016, Visy, Norske Skog, Orora, CHH/Oji Paper, Australian Paper and Circa. Special thanks to Anthony De Girolamo (Monash University) for running the porosimetry experiments.

4.8 REFERENCES

1. Gross, J.R., *The Evolution of Absorbent Materials*, in *Studies in Polymer Science*, L. Brannon-Peppas and R.S. Harland, Editors. 1990, Elsevier. p. 3-22.
2. Omidian, H., et al., *A model for the swelling of superabsorbent polymers*. *Polymer*, 1998. **39**(26): p. 6697-6704.
3. Warson, H., *Modern Superabsorbent Polymer Technology*, ed. F.L. Buchholz and A.T. Graham. Vol. 49. 2000, New York: Wiley-VCH.
4. Chen, P., et al., *Synthesis of superabsorbent polymers by irradiation and their applications in agriculture*. *Journal of Applied Polymer Science*, 2004. **93**(4): p. 1748-1755.
5. Rogers, J.V., et al., *Use of superabsorbent polymer gels for surface decontamination of Bacillus anthracis spores*. *Letters in Applied Microbiology*, 2009. **48**(2): p. 180-186.
6. Wiegand, C., et al., *Superabsorbent polymer-containing wound dressings have a beneficial effect on wound healing by reducing PMN elastase concentration and inhibiting microbial growth*. *Journal of Materials Science : Materials in Medicine*, 2011. **22**(11): p. 2583-90.
7. Lavoine, N. and L. Bergström, *Nanocellulose-based foams and aerogels: processing, properties, and applications*. *Journal of Materials Chemistry A*, 2017. **5**(31): p. 16105-16117.
8. Ferfera-Harrar, H., N. Aouaz, and N. Dairi, *Environmental-sensitive chitosan-g-polyacrylamide/carboxymethylcellulose superabsorbent composites for wastewater purification I: synthesis and properties*. *Polymer Bulletin*, 2016. **73**(3): p. 815-840.
9. Dalaran, M., et al., *Study on a novel polyampholyte nanocomposite superabsorbent hydrogels: Synthesis, characterization and investigation of removal of indigo carmine from aqueous solution*. *Desalination*, 2011. **279**(1): p. 170-182.
10. Serna-Cock, L. and M.A. Guancha-Chalapud, *Natural fibers for hydrogels production and their applications in agriculture*. *Acta Agronómica*, 2017. **66**: p. 495-505.
11. Xu, X., et al., *Synthesis and Properties of an Ecofriendly Superabsorbent Composite by Grafting the Poly(acrylic acid) onto the Surface of Dopamine-Coated Sea Buckthorn Branches*. *Industrial & Engineering Chemistry Research*, 2015. **54**(13): p. 3268-3278.
12. Hubbe, M.A., et al., *Enhanced Absorbent Products Incorporating Cellulose and Its Derivatives: A Review*, in *BioResources*. 2013. p. 6556-+.
13. Gavillon, R. and T. Budtova, *Aerocellulose: New Highly Porous Cellulose Prepared from Cellulose–NaOH Aqueous Solutions*. *Biomacromolecules*, 2008. **9**(1): p. 269-277.
14. Sescousse, R., R. Gavillon, and T. Budtova, *Aerocellulose from cellulose–ionic liquid solutions: Preparation, properties and comparison with cellulose–NaOH and cellulose–NMMO routes*. *Carbohydrate Polymers*, 2011. **83**(4): p. 1766-1774.
15. Djafari Petroudy, S.R., J. Ranjbar, and E. Rasooly Garmaroody, *Eco-friendly superabsorbent polymers based on carboxymethyl cellulose strengthened by TEMPO-mediated oxidation wheat straw cellulose nanofiber*. *Carbohydrate Polymers*, 2018. **197**: p. 565-575.

16. Olad, A., et al., *Slow-release NPK fertilizer encapsulated by carboxymethyl cellulose-based nanocomposite with the function of water retention in soil*. Materials Science and Engineering: C, 2018. **90**: p. 333-340.
17. Olad, A., et al., *Synthesis, characterization, and swelling kinetic study of porous superabsorbent hydrogel nanocomposite based on sulfonated carboxymethylcellulose and silica nanoparticles*. Journal of Porous Materials, 2018. **25**(5): p. 1325-1335.
18. Raafat, A.I., M. Eid, and M.B. El-Arnaouty, *Radiation synthesis of superabsorbent CMC based hydrogels for agriculture applications*. Nuclear Instruments and Methods in Physics Research Section B: Beam Interactions with Materials and Atoms, 2012. **283**: p. 71-76.
19. Wang, Z., et al., *Synthesis and swelling behaviors of carboxymethyl cellulose-based superabsorbent resin hybridized with graphene oxide*. Carbohydrate Polymers, 2017. **157**: p. 48-56.
20. Adair, A., A. Kaesaman, and P. Klinpituksa, *Superabsorbent materials derived from hydroxyethyl cellulose and bentonite: Preparation, characterization and swelling capacities*. Polymer Testing, 2017. **64**: p. 321-329.
21. Fekete, T., et al., *Synthesis and characterization of superabsorbent hydrogels based on hydroxyethylcellulose and acrylic acid*. Carbohydrate Polymers, 2017. **166**: p. 300-308.
22. Kono, H. and S. Fujita, *Biodegradable superabsorbent hydrogels derived from cellulose by esterification crosslinking with 1,2,3,4-butanetetracarboxylic dianhydride*. Carbohydrate Polymers, 2012. **87**(4): p. 2582-2588.
23. Dai, H. and H. Huang, *Enhanced Swelling and Responsive Properties of Pineapple Peel Carboxymethyl Cellulose-g-poly(acrylic acid-co-acrylamide) Superabsorbent Hydrogel by the Introduction of Carclazte*. Journal of Agricultural and Food Chemistry, 2017. **65**(3): p. 565-574.
24. Long, L.-Y., Y.-X. Weng, and Y.-Z. Wang, *Cellulose Aerogels: Synthesis, Applications, and Prospects*. Polymers, 2018. **10**(6): p. 623.
25. Saito, T., et al., *Cellulose Nanofibers Prepared by TEMPO-Mediated Oxidation of Native Cellulose*. Biomacromolecules, 2007. **8**(8): p. 2485-2491.
26. Brodin, P.W. and H. Theliander, *Absorbent materials based on kraft pulp: Preparation and material characterization*. BioResources, 2012. **7**(2): p. 1666-1686.
27. Brodin, F.W. and H. Theliander, *A comparison of softwood and birch kraft pulp fibers as raw materials for production of TEMPO-oxidized pulp, MFC and superabsorbent foam*. Cellulose, 2013. **20**(6): p. 1-14.
28. Brodin, F.W., Y. Sonavane, and H. Theliander, *Preparation of absorbent foam based on softwood kraft pulp: Advancing from gram to kilogram scale*. BioResources, 2013. **8**(2): p. 2099-2117.
29. Brodin, F.W., et al., *Reinforced absorbent material: A cellulosic composite of TEMPO-oxidized MFC and CTMP fibres*. Cellulose, 2012. **19**(4): p. 1413-1423.
30. Jiang, F. and Y.-L. Hsieh, *Super water absorbing and shape memory nanocellulose aerogels from TEMPO-oxidized cellulose nanofibrils via cyclic freezing-thawing*. Journal of Materials Chemistry A, 2014. **2**(2): p. 350-359.
31. Jiang, F. and Y.-L. Hsieh, *Amphiphilic superabsorbent cellulose nanofibril aerogels*. Journal of Materials Chemistry A, 2014. **2**(18): p. 6337-6342.
32. Jiang, F. and Y.-L. Hsieh, *Self-assembling of TEMPO Oxidized Cellulose Nanofibrils As Affected by Protonation of Surface Carboxyls and Drying Methods*. ACS Sustainable Chemistry & Engineering, 2016. **4**(3): p. 1041-1049.

33. Mendoza, L., et al., *Effects of fibre dimension and charge density on nanocellulose gels*. Journal of Colloid and Interface Science, 2018. **525**: p. 119-125.
34. Mendoza, L., et al., *Gelation mechanism of cellulose nanofibre gels: A colloids and interfacial perspective*. Journal of Colloid and Interface Science, 2018. **509**: p. 39-46.
35. da Silva Perez, D., S. Montanari, and M.R. Vignon, *TEMPO-Mediated Oxidation of Cellulose III*. Biomacromolecules, 2003. **4**(5): p. 1417-1425.
36. Fujita, H., K. Mitsuhashi, and T. Homma, *Viscosities of sodium polyacrylate in aqueous sodium chloride*. Journal of Colloid Science, 1954. **9**(5): p. 466-478.
37. Isogai, A., T. Saito, and H. Fukuzumi, *TEMPO-oxidized cellulose nanofibers*. Nanoscale, 2011. **3**(1): p. 71-85.
38. Okita, Y., T. Saito, and A. Isogai, *Entire Surface Oxidation of Various Cellulose Microfibrils by TEMPO-Mediated Oxidation*. Biomacromolecules, 2010. **11**(6): p. 1696-1700.
39. Shi, X., W. Wang, and A. Wang, *pH-responsive sodium alginate-based superporous hydrogel generated by an anionic surfactant micelle templating*. Carbohydrate Polymers, 2013. **94**(1): p. 449-455.
40. Schott, H., *Swelling kinetics of polymers*. Journal of Macromolecular Science, Part B, 1992. **31**(1): p. 1-9.
41. Li, W.L., K. Lu, and J.Y. Walz, *Freeze casting of porous materials: review of critical factors in microstructure evolution*. International Materials Reviews, 2012. **57**(1): p. 37-60.
42. Martoia, F., et al., *Cellulose nanofibril foams: Links between ice-templating conditions, microstructures and mechanical properties*. Materials & Design, 2016. **104**: p. 376-391.
43. Erlandsson, J., et al., *On the mechanism behind freezing-induced chemical crosslinking in ice-templated cellulose nanofibril aerogels*. Journal of Materials Chemistry A, 2018. **6**(40): p. 19371-19380.
44. Ma, J., X. Li, and Y. Bao, *Advances in cellulose-based superabsorbent hydrogels*. RSC Advances, 2015. **5**(73): p. 59745-59757.

THIS PAGE HAS BEEN INTENTIONALLY LEFT BLANK

THIS PAGE HAS BEEN INTENTIONALLY LEFT BLANK

CHAPTER 5

NANOCELLULOSE FOR GEL

ELECTROPHORESIS

THIS PAGE HAS BEEN INTENTIONALLY LEFT BLANK

CHAPTER 5 NANOCELLULOSE FOR GEL ELECTROPHORESIS

5.1	ABSTRACT	133
5.1.1	HYPOTHESIS	133
5.1.2	EXPERIMENTS	133
5.1.3	FINDINGS	133
5.1.4	KEYWORDS	134
5.2	INTRODUCTION	134
5.3	METHODOLOGY	135
5.3.1	MATERIALS	135
5.3.2	FORMULATION AND CASTING OF NANOCELLULOSE GEL SLABS	136
5.3.3	ELECTROPHORESIS EXPERIMENTS	136
5.3.4	CHARACTERISATION OF CROSS-LINKED NANOCELLULOSE	137
5.4	RESULTS	137
5.4.1	GEL CROSS-LINKING BY BORIC ACID-CATALYSED AMIDE FORMATION	137
5.4.2	EFFECT OF THE CROSS-LINKER CHAIN LENGTH	138
5.4.3	EFFECT OF CROSS-LINKER CONCENTRATION	140
5.4.4	EFFECT OF ELECTROPHORESIS VOLTAGE	141
5.5	DISCUSSION	142
5.5.1	GEL CROSS-LINKING AND GEL SLAB FORMATION	142
5.5.2	EFFECT OF CROSS-LINKER TYPE	143
5.5.3	EFFECT OF CROSS-LINKER CONCENTRATION	144
5.5.4	EFFECT OF ELECTROPHORESIS VOLTAGE	144
5.5.5	DEVELOPMENT PERSPECTIVES	145
5.6	CONCLUSION	146
5.7	ACKNOWLEDGMENTS	146
5.8	REFERENCES	147

THIS PAGE HAS BEEN INTENTIONALLY LEFT BLANK

Nanocellulose for Gel Electrophoresis

Llyza Mendoza¹, Thilina Gunawardhana¹, Warren Batchelor¹, Gil Garnier^{1,}*

¹Bioresource Processing Research Institute of Australia (BioPRIA), Department of Chemical Engineering, Monash University, VIC 3800, Australia

²School of Chemistry, Monash University, Clayton, VIC 3800, Australia

*E-mail: gil.garnier@monash.edu

5.1 ABSTRACT

5.1.1 HYPOTHESIS

Cellulose nanofibres produced by TEMPO-mediated oxidation can form gels. This study presents a proof-of-concept for gel electrophoresis with nanocellulose (NC).

5.1.2 EXPERIMENTS

TEMPO-oxidised cellulose nanofibre dispersion is chemically cross-linked by inducing amide linkages to produce electrophoresis gel slabs for electrophoretic separation. Nanocellulose gel slabs 1 cm thick containing Tris/Borate/EDTA (TBE) buffer were casted. Different cross-linker types and ratios are investigated to assess the migration of conventional electrophoresis tracking dyes.

5.1.3 FINDINGS

Tracking dyes (bromophenol blue and orange G) can diffuse within the gel at different rates and therefore separate. Changing the cross-linker length from EDA to HMDA (C2- to C6-chain) increases the overall network pore size resulting in a faster migration rate for both bromophenol blue and orange G. Increasing the cross-linker concentration stabilises the HMDA-NC gel (no extension) during the electrophoresis run without any effect on the dye migration rate. Increasing the voltage increases the migration rates for both orange G and bromophenol blue. Further development is required to cast the gels evenly and to prevent bubble formation during the cross-linking process. This will enable to effectively separate mixtures of proteins. Nanocellulose gels can become a novel substrate for sustainable biomedical separation and diagnostics by electrophoresis.

5.1.4 KEYWORDS

Gel electrophoresis, nanocellulose, TEMPO-mediated oxidation

5.2 INTRODUCTION

Electrophoresis is a widely used method in molecular biology to separate and identify individual macromolecules from a mixture by the difference in their mobility under an electric field. Negatively charged macromolecules, such as nucleic acids or coated proteins, are fractionated based on their structure, charge, conformation and size as they move towards the anode. Shorter molecules travel faster than longer ones as they can easily migrate through the pores of the gel medium [1]. Initial development of electrophoresis technique began with the work of Arne Tiselius in 1931 separating colloids (human serum) under an electric field [2]. Zone electrophoresis, which utilises substrates such as paper, starch, gel, agarose, cellulose acetate or polyacrylamide to act as a sieve to separate a mixture into components as bands, was then developed (1940-1950s)[3]. At present, conventional separation of macromolecules such as DNA or RNA is achieved through agarose and polyacrylamide gels. A mixture of large DNA molecules (200-30,000 bp)[1, 4] is often separated through horizontally casted agarose gels because of their larger pores. The neutral charge of the agarose gel network does not interact with the molecules to separate [5]. Separation of smaller protein-based molecules (RNA) (5-1,000 bp)[6] is performed typically with a polyacrylamide gel as its pore size is smaller and its structure can better be controlled [7]. However, safety issues arise with the use of the acrylamide monomer as it is classified as a neurotoxin [8, 9]. There is a need to develop safer and effective alternatives.

Nanocellulose (NC) fibres are high aspect ratio fibrils derived from cellulose-based sources such as wood or bacteria [10]. Isolation of nanocellulose from various sources can be achieved through a combination of chemical and mechanical processes [11]. One of the most common methods to produce nanocellulose is the TEMPO-mediated oxidation wherein the regio-selective carboxylation of the C6 alcohol of the *D*-glucose monomer provides the necessary electrostatic repulsion to produce nanofibres upon

fibrillation [12]. The combination of nanofibrils with high surface charge and high aspect ratio produces viscous colloidal gels even at low solids content [13].

Studies on the characterisation and application development of nanocellulose have grown exponentially over the last decade. Rheological studies have elucidated their gelation mechanism, achievable property range and even flow instability phenomena [13-18]. Many applications are also being developed ranging from pulp and paper strength additive, agriculture, wastewater to biomedical applications [19-24]. In the biomedical field, nanocellulose composite films and membranes have been developed for protein interaction, passivation and immobilisation for advanced separation purposes [25-30]. Nanocellulose gels have also been used as scaffold structures with tuneable properties suitable for cell culture and tissue engineering [31-34]. Nanocellulose gels were investigated for protein and drug release [35, 36]. However, only one study has investigated nanocellulose composite films for electrochemical-based ion-exchange for DNA oligomers [37]. To the best of our knowledge, nanocellulose hydrogels have never been studied as an electrophoretic material before.

This study investigates the potential of nanocellulose gels as electrophoresis substrates. Gel slabs are casted by chemically cross-linking nanocellulose fibres with diamine cross-linkers. The effect of cross-linker properties such as chain length and concentration on the migration of two model tracking dyes is evaluated. The effects of electrophoresis conditions (voltage) on the migration behaviour are also studied. The last section presents a perspective of nanocellulose gels development for DNA and protein mixture separation.

5.3 METHODOLOGY

5.3.1 MATERIALS

A 0.82 wt.% TEMPO-oxidised cellulose nanofibre suspension (containing 1.5mmol COO⁻/g fibre) was purchased from the Process Development Center, University of Maine. Hexamethylenediamine (HMDA) and ethylenediamine (EDA) were bought from Sigma-Aldrich. Glycerol, Orange G and Bromophenol blue was purchased from Merck.

Tris/Borate/EDTA (TBE) 10x buffer was bought from Bio-Rad. All chemicals were used as received and were analytical grade.

5.3.2 FORMULATION AND CASTING OF NANOCELLULOSE GEL SLABS

A 50mL nanocellulose suspension is mixed with 5 mL 10x TBE buffer under nitrogen gas. The cross-linker (EDA or HMDA) is then added rapidly under thorough agitation. Once a uniform colour is reached, the suspension is immediately poured in a 7cm x 10cm transparent gel caster (Bio-Rad Sub-Cell GT UV Transparent Mini-Gel Tray). The gel is then cured at 80°C for 1 hour in an oven. The cross-linked gel is taken out of the oven and cooled at 4°C. The sample wells are then stamped before running an electrophoresis experiment. Table I summarises the ratio of amine to carboxylate group studied:

Table I. Cross-linker type and ratios for the different casted nanocellulose gel slabs

Cross-linker Type	Ratio (mol NH ₂ : mol COO ⁻)
EDA (C2)	8:1, 12:1
HMDA (C6)	4:1, 6:1, 8:1

Nanocellulose gels cross-linked with EDA and HMDA are referred to as EDA-NC and HMDA-NC, respectively.

5.3.3 ELECTROPHORESIS EXPERIMENTS

Electrophoresis was performed using a Bio-Rad Wide Mini SubCell GT system. The gel is submerged in 1x TBE buffer. Samples (tracking dyes) were loaded at various sample wells of the gel. The tracking dye was prepared by mixing the following: 0.25g bromophenol blue, 0.15g Orange G, 6mL 50% glycerol, 4 mL milliQ water. Tracking dyes were utilised to monitor the progression of electrophoresis. Orange G represents the smaller protein molecules and hence migrates faster in contrast to bromophenol blue. The 0.2mL formulated tracking dye is diluted to a total 1mL prior to electrophoresis. 20µL of the dilute tracking dye was added in 3 different regions (left, centre, right) in the gel. The voltage is set at various levels (50, 75, and 100V) for the electrophoresis to start. The migration rate of tracking dye front is measured visually by the naked eye at 30-minute intervals, for at least 3 hours or until the orange G dye reached the end of the gel.

5.3.4 CHARACTERISATION OF CROSS-LINKED NANOCELLULOSE

The characterisation of the cross-linking reaction is performed through ATR- FTIR using the Agilent Cary 630 FTIR Spectrometer. The gels are firstly frozen at -80°C then freeze-dried to sublimate all of the water. The HMDA-/ EDA- NC samples were ground and then tested for the FTIR spectra (4000 cm^{-1} to 450 cm^{-1})

5.4 RESULTS

5.4.1 GEL CROSS-LINKING BY BORIC ACID-CATALYSED AMIDE FORMATION

Nanocellulose gel slabs were prepared through boric acid catalysed amide formation between the carboxylate groups of nanocellulose and amine groups of di-amine cross-linkers followed by 80°C curing. The appearance of amide bonds, indicating the cross-linking of nanocellulose gel slabs, is shown in the FTIR spectra (Figure 1). The spectra of the neat nanocellulose gel displays the representative peaks of the pendant carboxylate group (COO^-) at 3331 cm^{-1} and 1601 cm^{-1} corresponding to the O-H stretch and C=O stretch, respectively. The transformation from an O-H bond to N-H bond shows a change in the transmission intensity but no peak shift for HMDA-NC and EDA-NC gels. The C=O stretch peak shifts in the amide cross-linked gels for both HMDA-NC and EDA-NC gels. Curing the gels at 80°C produces larger peaks at all areas of interest. Figure 2 shows a cross-linked 8:1 EDA-NC gel.

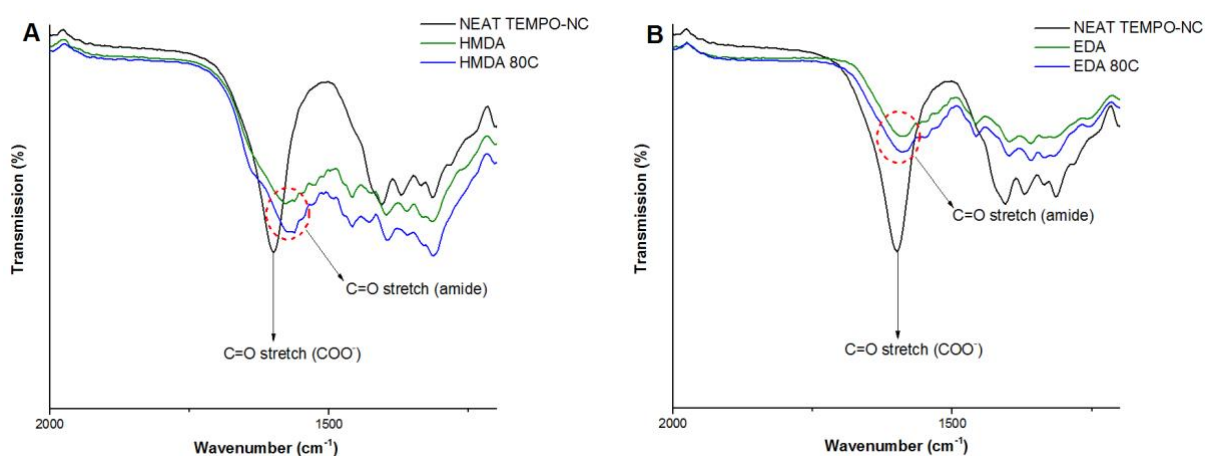


Figure 1. FTIR spectra evolution of cross-linking of nanocellulose gel slabs with 8:1 (A) HMDA and (B) EDA. Room temperature and 80°C reactions catalysed by boric acid.

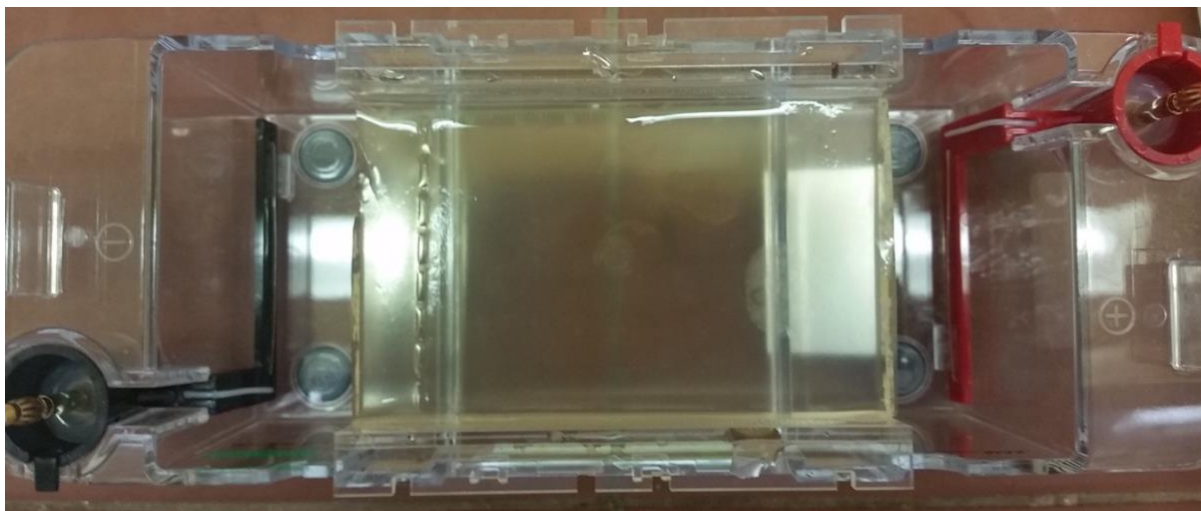


Figure 2. A casted 8:1 EDA-NC gel placed on a horizontal electrophoresis system.

5.4.2 EFFECT OF THE CROSS-LINKER CHAIN LENGTH

The amine-crosslinkers used in this study vary in the length of the carbon backbone. Ethylenediamine (EDA) is a C2-chain whereas hexamethylenediamine (HMDA) has a 6-carbon chain. The effect of amine cross-linker chain length (C2 vs C6) on the migration rate of the tracking dyes in the nanocellulose gel is shown in Figure 3. Images of EDA- and HMDA- NC gels at different time intervals during electrophoresis are shown in Figure 4 and supplementary information, respectively. The migration rate of both tracking dyes decreases with EDA compared to HMDA. The migration of bromophenol blue reduces from 0.23 to 0.14 mm .min⁻¹ (at 100V). Similarly, orange G travels at a rate of 0.43 mm .min⁻¹ in HMDA-NC whereas it slows down to 0.32mm .min⁻¹ in EDA-NC. Moreover, migration behaviour differs between the two cross-linker types. In HMDA-gels, the tracking dyes travels more linearly throughout the electrophoresis run. The tracking dye behaviour in EDA-NC gels is less linear as a plateau region is observed between 60 -120 mins.

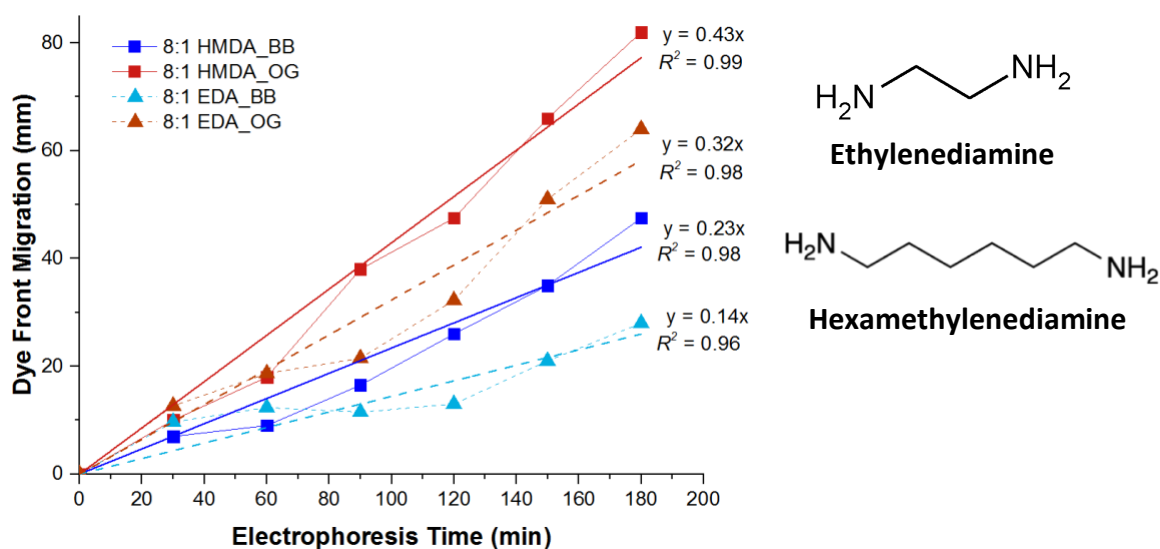
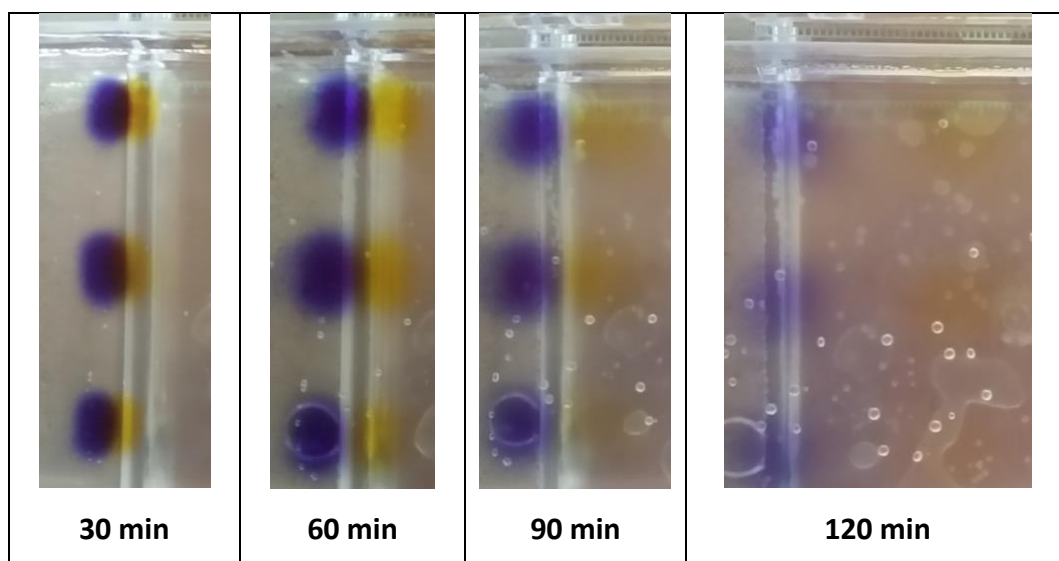


Figure 3. Migration of Bromophenol Blue (BB) and Orange G (OG) dyes in HMDA- (8:1) and EDA- (8:1) cross-linked nanocellulose gel slabs. Bold lines indicate trend lines and faint lines indicate the actual migration behaviour of tracking dyes. Chemical structures of EDA and HMDA. Electrophoresis voltage constant at 100V.



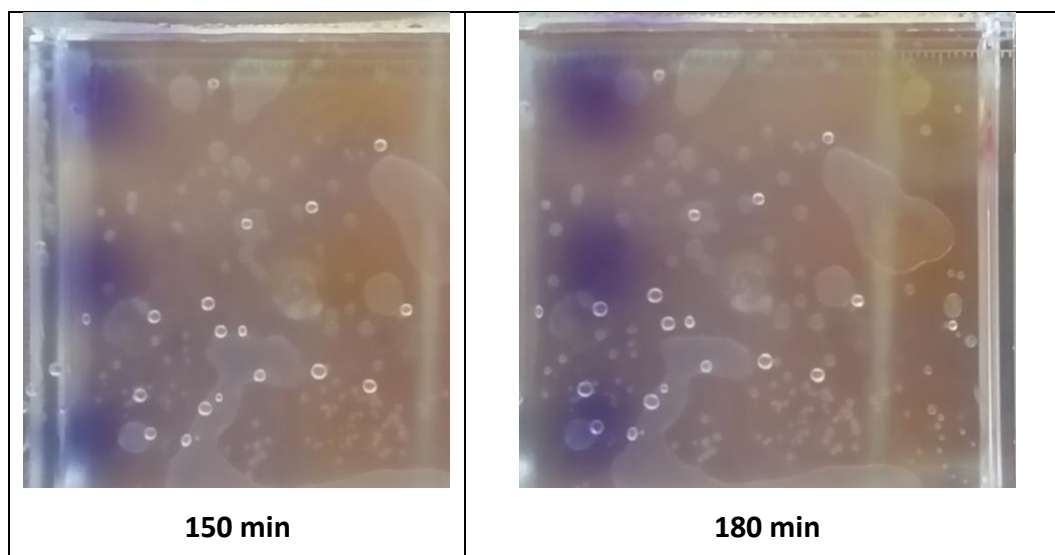


Figure 4. Migration of Tracking Dyes at 30 min intervals in 8:1 EDA-NC gel. Electrophoresis voltage constant at 100V.

5.4.3 EFFECT OF CROSS-LINKER CONCENTRATION

Figure 5 shows the effect of cross-linker concentration on the mobility of bromophenol blue and orange G during electrophoresis for EDA-NC and HMDA-NC gels. For both cross-linker types, the increase in the cross-linker concentration has no effect on the migration behaviour and rate of either bromophenol blue or orange G. Gel stability and ease of handling however increases with cross-linker concentration, particularly with HMDA. All gels tested become increasingly stiffer with higher cross-linker concentration. Increasing the cross-linker concentration from 2:1 onwards maintains gel stability throughout the electrophoresis run. However, all EDA-NC gels tested are very unstable with the gels extending and retracting at both sides of the cell during electrophoresis.

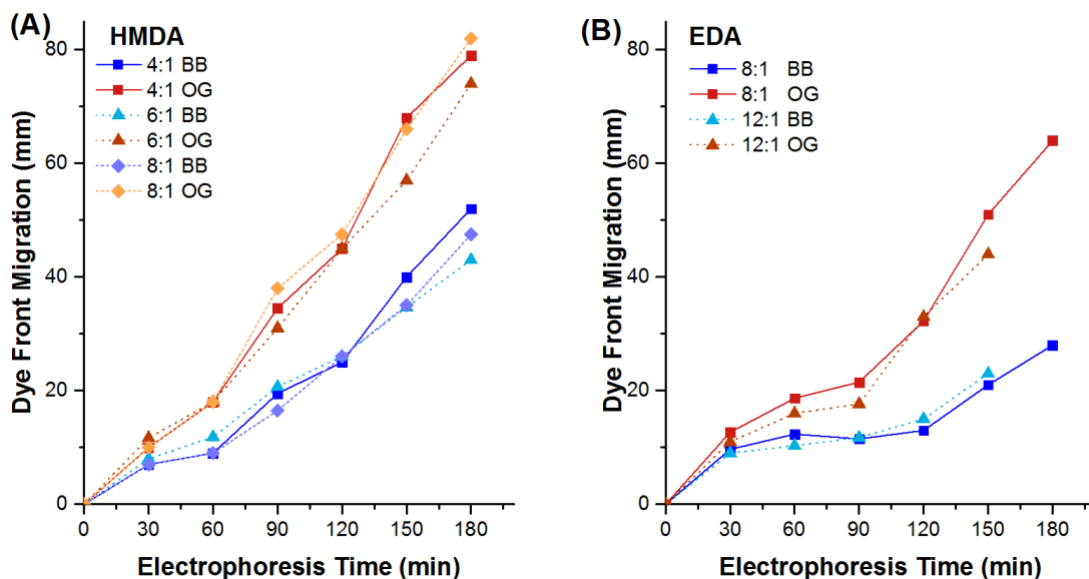


Figure 5. Migration of Bromophenol Blue (BB) and Orange G (OG) in a (A) HMDA cross-linked and (B) EDA cross-linked nanocellulose gel at various NH_2 : COO^- concentrations. Electrophoresis voltage constant at 100V.

5.4.4 EFFECT OF ELECTROPHORESIS VOLTAGE

Varying the electrophoresis voltage changes the migration rate for 8:1 HMDA-NC gel as shown in Figure 4. Increasing the voltage from 50V to 100V results in almost tripling and doubling the migration rate of orange G and bromophenol blue, respectively. Moreover, the separation gap between both dyes becomes larger with increasing voltage.

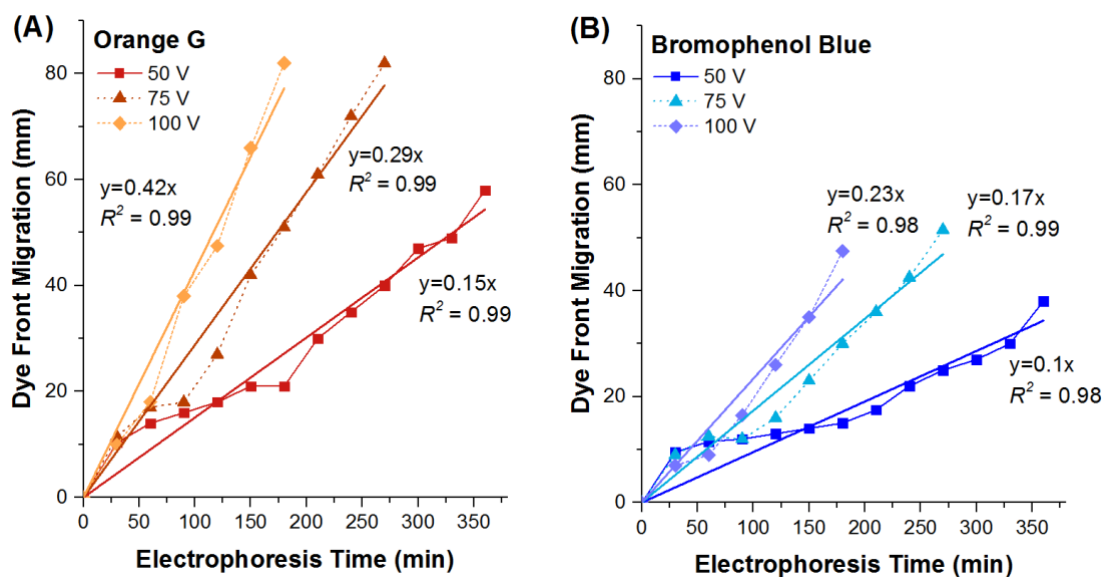


Figure 6. Migration of (A) Orange G (OG) and (B) Bromophenol Blue (BB) in an 8:1 HMDA cross-linked nanocellulose gel at different electrophoresis voltages. The linear trendlines were added with a y-intercept set at zero. The slope represents the average migration rate under various voltages.

5.5 DISCUSSION

5.5.1 GEL CROSS-LINKING AND GEL SLAB FORMATION

TEMPO-oxidised cellulose nanofibres (TOCNs) can form a suspension or colloidal gel depending on the combination of fibre length and concentration [13, 38]. The nanocellulose suspension selected in this study has a concentration of 0.82wt.% and still exhibits primarily liquid-like behaviour. At this initial state, the nanocellulose fibres are not sufficiently entangled to form the stable 3D-network of a gel. Introducing cross-links is therefore necessary to produce a uniform gel slab which remains stable under electrophoretic conditions.

TOCNs contain COO^- groups which can be cross-linked to improve dimensional stability and form a stable gel. Cross-linking can be achieved either by physical or chemical means [39]. Physical cross-linking of TEMPO-nanocellulose can be accomplished with divalent (Ca^{2+} , Zn^{2+} , Cu^{2+}) or trivalent (Al^{3+} , Fe^{3+}) cations which coordinate with the COO^- groups to induce chain-chain association similar to pectins and alginates. This results in very stiff gels [40]. These cations, however, are prone to movement and can leave the gel upon the introduction of electrical current. This can lead to gel instability and collapse. Moreover, as the individual fibres are not completely neutralised in this type of cross-linking, their negative charges induce nanocellulose fibre migration during electrophoresis. Temperature and pressure have recently been reported as a trigger for nanocellulose gelation. Nonetheless, the increased gel strength and stability achieved may not be sufficient for electrophoresis operations [41, 42].

Chemical cross-linking, on the other hand, provides a more stable network as the fibres are permanently bridged with a cross-linker. Carboxylic acid groups in different substances can be bridged by amine-based cross-linkers to induce amide bond formation. Amide formation is not spontaneous under ambient conditions as the carboxylic acid is deprotonated to form an ammonium carboxylate salt. Conversion to amide requires heat to overcome the activation energy with water as a by-product to be driven off for the reaction to progress [43]. Hence, when either EDA or HMDA is added to TOCNs at ambient conditions, no cross-linking occurs.

Different catalysts and co-reactants are required to produce amides at ambient conditions. For instance, coupling agents such as 1-ethyl-3-(3-dimethylaminopropyl) carbodiimide (EDC) combined with *N*-hydroxysuccinimide (NHS) is a common reaction system [44]. Boric acid, a component in DNA electrophoresis buffers, can also act as a catalyst to trigger carboxylate group – amine cross-linking to produce amide bonds [45, 46]. Amide formation in TOCNs with boric acid is triggered at room temperature as shown in Figure 1. The change in the representative spectra of COO⁻ groups indicates the formation of amide bonds at room temperature. Full conversion is not achieved as a stronger FTIR signal is shown after the gel is cured at 80°C for 1 hour. This increased amide formation is also demonstrated by the higher stability and ease of handling of the cured gel.

5.5.2 EFFECT OF CROSS-LINKER TYPE

The effect of two types of diamine cross-linkers on the gel slab formation and tracking dye migration behaviour is investigated. Ethylenediamine and hexamethylenediamine are both diamine compounds which only differ in the length of the hydrocarbon backbone. EDA and HMDA consist of 2 and 6 carbon chain, respectively. The cross-linker chain length determines the cross-linking likelihood, bond rigidity, and average pore mesh of the resulting three-dimensional network formed by the nanocellulose fibres. A longer cross-linker is able to bridge more effectively individual nanocellulose fibres separated by repelling electrostatic forces. It is therefore expected that a longer chain cross-linker will produce a more stable gel. HMDA-NC gels are stronger than EDA-NC gels, similarly reported in [47]. In this investigation, we extend the idea of stability from just producing a self-standing gel to maintaining its structural integrity whilst immersed in an electrophoretic environment. At constant NH₂: COO⁻ ratio of 8:1, EDA-NC gels extended and contracted at different time periods throughout the electrophoresis experiment. This is in contrast with HMDA-NC which remains unchanged. The change in gel shape (extension and contraction) can be attributed to the lack of stiffness of EDA-NC gels as fibre mobility is less restricted than for HMDA-NC gels. Another reason might be that the diamine terminated cross-linkers have not fully formed amide bonds at both

ends, resulting in a net positive charge on the fibre surface leading to the increased electrophoretic movement observed.

The migration rate and behaviour of orange G and bromophenol blue are also affected by HMDA and EDA. Both tracking dyes display lower migration rates in EDA-NC gels. The small chain length in EDA resulted in smaller network pores upon cross-linking in contrast to HMDA. The change in the cross-linker length impacts the migration rate as it decreases by 25.6% and 39.1% in orange G and bromophenol blue, respectively. Moreover, non-linearity in the dyes migration rates are observed for EDA-NC gels. A plateau region in the electrophoresis run is observed wherein there is very little movement (Figure 3). This can be attributed to the movement of the tracking dyes relative to the gel dimensional instability (extension) resulting in net zero movement.

5.5.3 EFFECT OF CROSS-LINKER CONCENTRATION

Modifying the cross-linker concentration (NH₂: COO⁻ ratio) influences the stability of the gels. The higher cross-linker concentration for HMDA-gels forms gel slabs which are more stable: they are easier to handle (i.e. stronger) and do not deform (no dimensional extension) during the electrophoresis testing. This is due to the formation of more crosslinking junctions. However, for EDA-gels, increasing the cross-linker concentration does not improve the gel stability during electrophoresis. Gel extension is still observed even at higher cross-linker concentrations (12:1). Furthermore, the amount of cross-linker concentration does not affect the migration rate of the tracking dyes (Figure 5). For all HMDA gels (4:1 to 8:1), the tracking dyes travel at similar rates. Similarly, the migration behaviour in EDC gels does not change significantly. This indicates that the network pore sizes have not changed significantly with the increase in cross-linker concentration.

5.5.4 EFFECT OF ELECTROPHORESIS VOLTAGE

The electrophoresis voltage dictates the migration rate and the degree of separation between molecules and dyes. A higher electrophoresis voltage indicates a faster migration rate which may affect the quality of separation as it can cause smearing or

distortion of bands. In cross-linked nanocellulose gels, the tracking dyes travel the slowest at 50V and fastest at 100V (Figure 6). Doubling the voltage from 50V to 100V results in tripling of the migration rate of orange G and doubling for bromophenol blue. Moreover, at increasing voltage the gap between orange G and bromophenol blue increases.

5.5.5 DEVELOPMENT PERSPECTIVES

There are four main development issues to resolve for consistent and effective separation with nanocellulose gel electrophoresis:

- *Bubble formation during casting.* The presence of bubbles can inhibit the effective separation of tracking dyes or proteins due to the absence of current within the bubbles in contrast to the gel which carries the current. Distortion of the separation bands was observed as the dyes are dragged around the bubbles. Hence, there is a need to engineer casting methods to suit nanocellulose gels which may include mixing under vacuum prior to gelation. A well stamp can also be integrated with the caster upon curing such that wells are always well-formed.
- *Nanocellulose gels for substitution of SDS-PAGE.* Trials on casting ultra-thin (0.75mm) nanocellulose gels to mimic SDS-PAGE (sodium dodecyl sulphate-polyacrylamide gel) for RNA separation were attempted. Concentrated solutions of Al^{3+} and Ca^{2+} cations, which are known to physically cross-link nanocellulose gels, were each applied to the casting plate via plasma-coating and spin-coating techniques. However, uneven precipitation of cations and SDS-nanocellulose interactions prevented even gelation.
- *Investigation of kinetics.* The kinetics and extent of the amide cross-linking reaction can be investigated to optimise casting methods.
- *Optimisation of nanocellulose type.* Nanocellulose properties such as aspect ratio and surface charge can be modified for optimisation of the pore size network to enable enhanced separation. This is best achieved by testing gels from cellulose nanocrystals and bacterial cellulose.

5.6 CONCLUSION

Nanocellulose gels have been increasingly studied for applications spanning agriculture [20, 21], personal care and hygiene [48], and biomedicine as tissue engineering scaffolds [10, 31, 34] and drug delivery media [35]. In this study, we report a proof-of-concept for utilising nanocellulose gels as novel electrophoresis media. Nanocellulose gels were investigated as an electrophoretic material by understanding the fundamentals which govern electrophoretic separation. Gels from TEMPO- oxidised cellulose nanofibres were chemically cross-linked by diamines to form slabs for horizontal gel electrophoresis. We demonstrated the feasibility of boric acid catalysed amide formation between the carboxylate pendant groups of the nanocellulose fibres with diamine terminated cross-linkers. Curing (80°C) enhanced the cross-linking for increased gel stability (handleability and minimal deformation during electrophoresis). The pore size of the gel network was varied with the carbon chain length of the diamine cross-linker molecule. This affected the migration rates for both the bromophenol blue and orange G dyes. Gel stability was also influenced as shorter cross-linkers (i.e. EDA) produced unstable gels which extend and retract at both ends of the cell during electrophoresis; this is due to incomplete junctions of the short diamine and the lack of gel stiffness. Increasing the cross-linker concentration increased gel stability and handleability whilst migration rate and behaviour remained constant. Increasing the electrophoresis voltage increased the migration rate and separation gap between bromophenol blue and orange G. Further optimisation is required for developing nanocellulose gels as robust and consistent electrophoretic materials. This especially involves process improvement for producing bubble-free and homogeneous gels. Nanocellulose gels have the potential to become the next generation of efficient and safe electrophoretic media for diagnostic and biomolecule separation.

5.7 ACKNOWLEDGMENTS

This work was funded by the ARC Bioprocessing Advance Manufacturing Industry Research Transformation (BAMI) Hub IH13100016, Visy, Norske Skog, Orora, CHH/Oji Fibre Solutions, Australian Paper and Circa. Special thanks to Maheshi Udugama (Monash University) for advice and discussions regarding electrophoresis.

5.8 REFERENCES

1. Armstrong, J.A. and J.R. Schulz, *Agarose Gel Electrophoresis*, in *Current Protocols Essential Laboratory Techniques*. 2008.
2. Tiselius, A., *A new apparatus for electrophoretic analysis of colloidal mixtures*. Transactions of the Faraday Society, 1937. **33**(0): p. 524-531.
3. Gordon, M.J., et al., *Capillary Electrophoresis*. Science, 1988. **242**(4876): p. 224-228.
4. Voytas, D., *Agarose Gel Electrophoresis*. Current Protocols in Molecular Biology, 2000. **51**(1): p. 2.5A.1-2.5A.9.
5. Royse, V.L. and D.M. Jensen, *Development of an agarose gel electrophoresis technique for determining alpha-amylase isoenzymes*. Clinical Chemistry, 1984. **30**(3): p. 387-390.
6. Chory, J. and J.D. Pollard, *Separation of Small DNA Fragments by Conventional Gel Electrophoresis*. Current Protocols in Molecular Biology, 1999. **47**(1): p. 2.7.1-2.7.8.
7. Bravo, R., *CHAPTER 1 - Two-Dimensional Gel Electrophoresis: A Guide for the Beginner*, in *Two-dimensional Gel Electrophoresis of Proteins*, J.E. Celis and R. Bravo, Editors. 1984, Academic Press. p. 3-36.
8. Friedman, M., *Chemistry, Biochemistry, and Safety of Acrylamide. A Review*. Journal of Agricultural and Food Chemistry, 2003. **51**(16): p. 4504-4526.
9. Westermeier, R., *Electrophoresis*, in *Electrophoresis in Practice: A guide to methods and applications of DNA and protein separations* W. R, Editor. 2005. p. 16.
10. Abitbol, T., et al., *Nanocellulose, a tiny fiber with huge applications*. Current Opinion in Biotechnology, 2016. **39**: p. 76-88.
11. Klemm, D., et al., *Cellulose: Fascinating Biopolymer and Sustainable Raw Material*. Angewandte Chemie International Edition, 2005. **44**(22): p. 3358-3393.
12. Isogai, A., T. Saito, and H. Fukuzumi, *TEMPO-oxidized cellulose nanofibers*. Nanoscale, 2011. **3**(1): p. 71-85.
13. Mendoza, L., et al., *Gelation mechanism of cellulose nanofibre gels: A colloids and interfacial perspective*. Journal of Colloid and Interface Science, 2018. **509**: p. 39-46.
14. Jowkarderis, L. and T.G.M. van de Ven, *Intrinsic viscosity of aqueous suspensions of cellulose nanofibrils*. Cellulose, 2014. **21**(4): p. 2511-2517.
15. Jowkarderis, L. and T.G.M. van de Ven, *Rheology of semi-dilute suspensions of carboxylated cellulose nanofibrils*. Carbohydrate Polymers, 2015. **123**: p. 416-423.
16. Lasseguette, E., D. Roux, and Y. Nishiyama, *Rheological properties of microfibrillar suspension of TEMPO-oxidized pulp*. Cellulose, 2008. **15**(3): p. 425-433.
17. Nechyporchuk, O., M.N. Belgacem, and F. Pignon, *Rheological properties of micro-/nanofibrillated cellulose suspensions: Wall-slip and shear banding phenomena*. Carbohydrate Polymers, 2014. **112**(Supplement C): p. 432-439.
18. Nechyporchuk, O., M.N. Belgacem, and F. Pignon, *Concentration effect of TEMPO-oxidized nanofibrillated cellulose aqueous suspensions on the flow instabilities and small-angle X-ray scattering structural characterization*. Cellulose, 2015. **22**(4): p. 2197-2210.

19. Hakalahti, M., et al., *Effect of interfibrillar PVA bridging on water stability and mechanical properties of TEMPO/NaClO₂ oxidized cellulosic nanofibril films*. Carbohydrate Polymers, 2015. **126**: p. 78-82.
20. Zhang, H., et al., *Cellulose Anionic Hydrogels Based on Cellulose Nanofibers As Natural Stimulants for Seed Germination and Seedling Growth*. Journal of Agricultural and Food Chemistry, 2017. **65**(19): p. 3785-3791.
21. Kabir, S.M.F., et al., *Cellulose-based hydrogel materials: chemistry, properties and their prospective applications*. Progress in Biomaterials, 2018. **7**(3): p. 153-174.
22. Boufi, S., et al., *Nanofibrillated cellulose as an additive in papermaking process: A review*. Carbohydrate Polymers, 2016. **154**: p. 151-166.
23. Gatenholm, P. and D. Klemm, *Bacterial Nanocellulose as a Renewable Material for Biomedical Applications*. MRS Bulletin, 2011. **35**(3): p. 208-213.
24. Sharma, P.R., et al., *Nanocellulose from Spinifex as an Effective Adsorbent to Remove Cadmium(II) from Water*. ACS Sustainable Chemistry & Engineering, 2018. **6**(3): p. 3279-3290.
25. Gustafsson, S., L. Manukyan, and A. Mihranyan, *Protein–Nanocellulose Interactions in Paper Filters for Advanced Separation Applications*. Langmuir, 2017. **33**(19): p. 4729-4736.
26. Vuoriluoto, M., et al., *Control of Protein Affinity of Bioactive Nanocellulose and Passivation Using Engineered Block and Random Copolymers*. ACS Applied Materials & Interfaces, 2016. **8**(8): p. 5668-5678.
27. Malho, J.-M., et al., *Enhanced Plastic Deformations of Nanofibrillated Cellulose Film by Adsorbed Moisture and Protein-Mediated Interactions*. Biomacromolecules, 2015. **16**(1): p. 311-318.
28. Xu, C., D.O. Carlsson, and A. Mihranyan, *Feasibility of using DNA-immobilized nanocellulose-based immunoadsorbent for systemic lupus erythematosus plasmapheresis*. Colloids and Surfaces B: Biointerfaces, 2016. **143**: p. 1-6.
29. Uth, C., et al., *A Chemoenzymatic Approach to Protein Immobilization onto Crystalline Cellulose Nanoscaffolds*. Angewandte Chemie International Edition, 2014. **53**(46).
30. Kuzmenko, V., et al., *Universal method for protein bioconjugation with nanocellulose scaffolds for increased cell adhesion*. Materials Science and Engineering: C, 2013. **33**(8): p. 4599-4607.
31. Zander, N.E., et al., *Metal Cation Cross-Linked Nanocellulose Hydrogels as Tissue Engineering Substrates*. ACS Applied Materials & Interfaces, 2014. **6**(21): p. 18502-18510.
32. Leppiniemi, J., et al., *3D-Printable Bioactivated Nanocellulose–Alginate Hydrogels*. ACS Applied Materials & Interfaces, 2017. **9**(26): p. 21959-21970.
33. Mondragon, G., et al., *Bionanocomposites based on gelatin matrix and nanocellulose*. European Polymer Journal, 2015. **62**: p. 1-9.
34. Liu, J., et al., *Development of nanocellulose scaffolds with tunable structures to support 3D cell culture*. Carbohydrate Polymers, 2016. **148**: p. 259-271.
35. Müller, A., et al., *The Biopolymer Bacterial Nanocellulose as Drug Delivery System: Investigation of Drug Loading and Release using the Model Protein Albumin*. Journal of Pharmaceutical Sciences, 2013. **102**(2): p. 579-592.
36. Müller, A., et al., *Loading of bacterial nanocellulose hydrogels with proteins using a high-speed technique*. Carbohydrate Polymers, 2014. **106**: p. 410-413.

37. Razaq, A., et al., *High-Capacity Conductive Nanocellulose Paper Sheets for Electrochemically Controlled Extraction of DNA Oligomers (Conductive Nanocellulose for Extraction of DNA)*. PLoS ONE, 2011. **6**(12): p. e29243.
38. Mendoza, L., et al., *Effects of fibre dimension and charge density on nanocellulose gels*. Journal of Colloid and Interface Science, 2018. **525**: p. 119-125.
39. Hunger, K., et al., *Investigation of cross-linked and additive containing polymer materials for membranes with improved performance in pervaporation and gas separation*. Membranes, 2012. **2**(4): p. 727-763.
40. Braccini, I. and S. Pérez, *Molecular Basis of Ca²⁺-Induced Gelation in Alginates and Pectins: The Egg-Box Model Revisited*. Biomacromolecules, 2001. **2**(4): p. 1089-1096.
41. Schmitt, J., et al., *TEMPO-oxidised cellulose nanofibrils; probing the mechanisms of gelation via small angle X-ray scattering*. Physical Chemistry Chemical Physics, 2018. **20**(23): p. 16012-16020.
42. Suenaga, S. and M. Osada, *Self-Sustaining Cellulose Nanofiber Hydrogel Produced by Hydrothermal Gelation without Additives*. ACS Biomaterials Science & Engineering, 2018. **4**(5): p. 1536-1545.
43. Valeur, E. and M. Bradley, *Amide bond formation: beyond the myth of coupling reagents*. Chemical Society Reviews, 2009. **38**(2): p. 606-631.
44. Orelma, H., et al., *CMC-Modified Cellulose Biointerface for Antibody Conjugation*. Biomacromolecules, 2012. **13**(4): p. 1051-1058.
45. Mylavarapu, R.K., et al., *Boric Acid Catalyzed Amidation in the Synthesis of Active Pharmaceutical Ingredients*. Organic Process Research & Development, 2007. **11**(6): p. 1065-1068.
46. Sabatini, M.T., L.T. Boulton, and T.D. Sheppard, *Borate esters: Simple catalysts for the sustainable synthesis of complex amides*. Science Advances, 2017. **3**(9).
47. Syverud, K., et al., *Controlling the elastic modulus of cellulose nanofibril hydrogels—scaffolds with potential in tissue engineering*. Cellulose, 2015. **22**(1): p. 473-481.
48. Mendoza, L., et al., *Carboxylated nanocellulose foams as superabsorbents*. Journal of Colloid and Interface Science, 2019. **538**: p. 433-439.

THIS PAGE HAS BEEN INTENTIONALLY LEFT BLANK

CHAPTER 6

CONCLUSIONS AND PERSPECTIVES

THIS PAGE HAS BEEN INTENTIONALLY LEFT BLANK

CHAPTER 6 **CONCLUSIONS AND PERSPECTIVES**

6.1 CONCLUSIONS 155

 6.1.1 NANOCELLULOSE GEL SELF-ASSEMBLY, STABILITY, AND RHEOLOGICAL PROPERTIES155

 6.1.2 DEVELOPMENT OF NANOCELLULOSE FOAMS FOR SUPERABSORBENT APPLICATIONS.....156

 6.1.3 DEVELOPMENT OF NANOCELLULOSE FOR ELECTROPHORESIS157

6.2 PERSPECTIVES..... 157

THIS PAGE HAS BEEN INTENTIONALLY LEFT BLANK

Conclusions and Perspectives

6.1 CONCLUSIONS

The primary goal of this dissertation is to present a step-wise understanding of the fundamentals of nanocellulose gels and to utilise this knowledge to develop new applications. This was achieved by answering the research objectives of this study via in-depth rheological characterisation of nanocellulose gels and studying these gels for two different applications.

6.1.1 NANOCELLULOSE GEL SELF-ASSEMBLY, STABILITY, AND RHEOLOGICAL PROPERTIES

The rheological properties of nanocellulose gels were mapped as well as the variables which affects those and their stability. The self-assembly of TEMPO-oxidised nanocellulose into colloidal gels was explained as the increased entanglement of the nanocellulose fibres combined with electrostatic stabilisation brought by high density of carboxylate groups. This was determined via rheological characterisation as a function of solids concentration and relating it with the network theory (crowding factor analysis) in addition to observing the colloidal stability of the gel as a function of pH and salt content. In Chapter 3, the effect of the starting wood pulp source and charge density on nanocellulose fibre dimensions and its effect on rheology is quantified. Kraft hardwood and softwood pulp were utilised to produce nanofibres of differing average lengths and surface charges. It has been determined that this difference in average length affects the yielding behaviour (critical strain and viscosity) of gels. Surface charge primarily influences the rheological behaviour of nanocellulose gel at the percolation threshold of 0.1 wt.%. At higher concentrations (0.3 wt.% and higher), gel rheological properties are independent of fibre length and surface charge. Table 1 summarises the effect of different process variables studied to the rheological behaviour of nanocellulose gels.

Table I. The effect of key process variables to the rheological behaviour of nanocellulose gels

Variables	Viscosity	G' and G''	Critical Strain	Colloidal Stability
Solids Content	✓✓	✓✓	✓ (at 1.4 mmol/g)	-
Charge Density	✓ (at 0.1 wt.%)	✗	✓	-
pH	-	-	-	✓
Salt	-	-	-	✓
Pulp Source	✓	✗	✓	-

Note: ✓✓ strongly influences, ✓ influences, - not studied, ✗ does not influence

6.1.2 DEVELOPMENT OF NANOCELLULOSE FOAMS FOR SUPERABSORBENT APPLICATIONS

Nanocellulose foams were produced from freeze-lyophilisation process and tested for their superabsorbent capacity. The effect of fibre content, surface charge, and processing condition on the foam morphology and absorption capacity were investigated. The gel fibre content influences foam density and pore size distribution. A denser nanocellulose foam resulted in lower porosity values leading to a decreased absorption. Freezing temperature affects foam morphology by dictating whether the present water within the gel promotes ice nucleation or crystallisation. Freezing at the fastest rate (-196°C) produced a homogeneous but brittle structure whereas at lower freezing rates (-20°C and -80°C) sheet-like formations were observed. Nanocellulose foam absorption were also studied and determined to follow pseudo second-order kinetics highly dependent on foam density. This study demonstrated that an optimised foam containing 0.3 wt.% to 0.5 wt.% fibre and frozen at -80°C, is capable of absorbing 110-120g/g H₂O and 60g/g saline.

6.1.3 DEVELOPMENT OF NANOCELLULOSE FOR ELECTROPHORESIS

A novel application is demonstrated by utilising nanocellulose gels as electrophoresis media. TEMPO-oxidised nanocellulose fibres which contain carboxylate groups were chemically cross-linked by boric-acid catalysed formation of amide linkages with di-amine cross-linkers. The cross-linking reaction produced gel slabs which can perform horizontal gel electrophoresis. It was also showed that curing (80°C, 1 hour) is beneficial in enhancing the cross-linking resulting in better handleability and minimal deformation during electrophoresis. Varying the carbon chain length of the di-amine crosslinker (EDA vs. HMDA) modified the network pore size affecting the migration rate of bromophenol blue and orange G. Dimensional stability during electrophoresis run was affected when a shorter cross-linker chain (EDA) is utilised due to incomplete junctions and the lack of gel stiffness. Increase in cross-linker concentration, particularly for HMDA, improved gel stability and handleability whilst maintaining tracking dye behaviour and migration rate. Electrophoretic voltage can be modified with nanocellulose gels in order to tune the separation of bromophenol blue and orange G.

6.2 PERSPECTIVES

In this dissertation, the structure-property relationship of nanocellulose gels were established via intensive rheological testing and observing the influence in the colloidal stability of the effect of various variables. To progress on, an interesting avenue is to pursue further research on understanding the interactions of nanocellulose with other bio-polymers such as hemicellulose, starch, pectin, and chitosan. This will underpin the behaviour of nanocellulose in hydrogel composites as many applications require mixtures of polymers to have better characteristics and performance.

The two applications demonstrated in this work displays the immense potential in utilising nanocellulose gels. These works present new direct avenues of investigation. Optimisation of shape and incorporation of other biopolymers may further increase the absorption capacity of nanocellulose foams. Re-engineering the casting methods for gel electrophoresis can promote the development of nanocellulose as a separation media.

Hence, this indicates that further studies in nanocellulose gels will lead to progress in the use and commercialisation of sustainable and renewable materials.

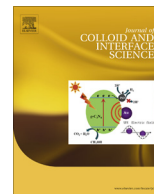
THIS PAGE HAS BEEN INTENTIONALLY LEFT BLANK

THIS PAGE HAS BEEN INTENTIONALLY LEFT BLANK

APPENDIX I

**PUBLICATIONS INCLUDED IN THESIS IN
THEIR PUBLISHED FORMAT**

THIS PAGE HAS BEEN INTENTIONALLY LEFT BLANK

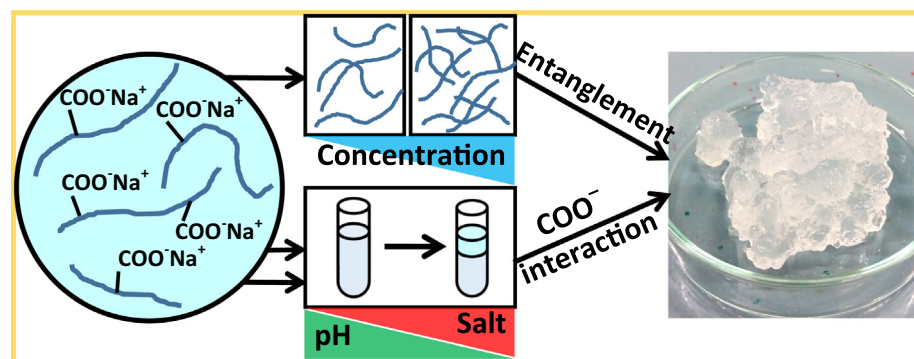


Regular Article

Gelation mechanism of cellulose nanofibre gels: A colloids and interfacial perspective

Llyza Mendoza^a, Warren Batchelor^a, Rico F. Tabor^b, Gil Garnier^{a,*}^a Bioresource Processing Research Institute of Australia (BioPRIA), Department of Chemical Engineering, Monash University, VIC 3800, Australia^b School of Chemistry, Monash University, VIC 3800, Australia

GRAPHICAL ABSTRACT



ARTICLE INFO

Article history:

Received 23 May 2017

Revised 24 August 2017

Accepted 24 August 2017

Available online 1 September 2017

Keywords:

Nanocellulose

TEMPO-mediated oxidation

Hydrogels

Colloids

Rheology

AFM

ABSTRACT

Hypothesis: Nanocellulose gels form a new category of sustainable soft materials of industrial interest for a wide range of applications. There is a need to map the rheological properties and understand the mechanism which provides the colloidal stability and gelation of these nanofibre suspensions.

Experiments: TEMPO (2,2,6,6-tetramethylpiperidine-1-oxyl)-oxidised cellulose nanofibre gels were investigated at different fibre concentrations, pH and ionic strength. Dynamic and cyclic rheological studies was performed to quantify gel behaviour and properties. Gels were produced at different pH and salt contents to map and understand colloidal stability of the nanocellulose gel.

Findings: Rheology indicates gelation as a transitional state starting at a fibre concentration of 0.1 wt.%. The colloidal stability of the nanocellulose gel network is controlled by pH and salt, whereas fibre concentration mainly dictates the dynamic rheological properties. Decreasing pH and adding salt destabilises the gel network by eluting bound water which is correlated with the decrease in electrostatic repulsion between fibres. The gelation and colloidal stability of these nanocellulose gels is driven by electrostatic forces and the entanglement ability of the fibrous system to overlap.

Crown Copyright © 2017 Published by Elsevier Inc. All rights reserved.

1. Introduction

Cellulose fibrils of nano-scale width – referred to as nanocellulose – can be extracted from plants and bacterial sources through a variety of mechanical and chemical methods [1,2]. Nanocellulose exhibits exceptional characteristics such as high tensile strength,

* Corresponding author.

E-mail address: gil.garnier@monash.edu (G. Garnier).

ease of functionalisation, combined with its expected biological characteristics: renewability, biocompatibility, biodegradability and low toxicity [3–5]. Isogai et al. developed the TEMPO-mediated oxidation process which utilises a nitroxyl catalyst (TEMPO, 2,2,6,6-tetramethylpiperidine-1-oxyl) to convert the primary alcohol groups of the cellulose D-glucose units into carboxylate groups. This provides the necessary electrostatic repulsion which allows the liberation of nanocellulose fibres [6–8]. TEMPO-oxidised cellulose nanofibres (TOCNFs) macroscopically appear as viscous and stable colloidal suspensions even at low solids content (1–2 wt.%) [9]. This surface modification produces nanofibres 3–4 nm in width and several microns in length [8,10] and is currently considered among the most effective methods for producing nanocellulose [11]. Recent TOCNF studies have focussed on biomedical applications such as drug delivery [12], wound dressing [13], tissue engineering substrate [14] and cell encapsulation [15,16], engineering reinforcement materials in plastics and paper [17–20], rheology modifier [21,22], and the development of novel materials such as aerogels [23]. Previous studies on the properties of TOCNFs investigated the structure at the individual fibril level [24], determining the fibre aspect ratio through rheological measurements [25,26] and modelling properties at the dilute and semi-dilute concentration regimes [26,27]. However, there is poor understanding on what drives the gelation and provides the colloidal stability in TOCNFs. Limited studies have analysed the properties of nanofiber cellulose gels from a colloidal and interfacial perspective.

Polysaccharides, owing to their high degrees of polymerisation and hydrogen bonding ability, can form hydrogels through physical interactions. κ -carrageenan undergoes a coil-to-helix structural transformation as a response to temperature changes and forms gels [28]. Thermo-responsive polysaccharides, which contain methyl or other short hydrophobic groups such as methylcellulose and carboxymethylcellulose, gel through the formation of specific hydrogen bonding combined with hydrophobic associations within the cellulose backbone [29–31]. Alginates, on the other hand, require coordinating cations (i.e. Ca^{2+}) to bridge consecutive alginate polymers which induces gelation [32]. However, none of these gelation mechanisms can describe the gelation of TOCNFs. This type of nanocellulose has been known to form stable gels without the aid of temperature nor cations [27,33]. Although it is recognized that modification of its rheological properties, resulting in stiff and self-standing gels, can be achieved by manipulating pH and the addition of cations [14,34,35].

The objective of this study is to characterise the gelation mechanism of TOCNFs. These fibres, possessing nano-scale diameter and micro-scale length and strong surface charges, can be viewed as flexible colloidal particles of high aspect ratio able to interact, deform and entangle. It is desired to quantify fibre-fibre interactions and determine the factors which affect the stability of the fibres by modifying surface charge and electrical double layer thickness. This is achieved by combining rheology, atomic force microscopy (AFM) and qualitative imaging. Rheology is a well-established method to quantify the viscoelastic characteristics of complex soft materials such as gels. It provides an insight to the state of the gel network by controlled macroscopic deformation [36]. Through rheology, we can monitor the gelation state and properties of TOCNFs as a function of different variables. AFM and light scattering allows the imaging of the cellulose nanofibres enabling us to resolve the fibre dimensions. The combination of these techniques allows us to explore the source of the exceptional colloidal stability and properties of these gels.

To understand the gelation of TOCNFs, we characterised the range of viscoelastic properties in the dilute to semi-dilute range. Their rheological behaviour provides insight into how the fibres organize into a network. The effect of pH and salt on the colloidal

stability of the gels was determined and analysed in terms of colloids and interfacial chemistry. We aim at relating the mechanism of cellulose nanofibre gel properties to the well-established colloid and interface science to efficiently engineer applications in food, biomedical and as rheology modifier.

2. Materials and methods

2.1. Materials

Bleached Eucalyptus Kraft (BEK) pulp of approximately 10 wt.% solids was supplied by Australian Paper, Maryvale, Australia. 2,2,6,6-Tetramethylpiperidine-1-oxyl (TEMPO) and sodium bromide (NaBr) were purchased from Sigma-Aldrich. Hydrochloric acid (HCl) and Sodium Hydroxide (NaOH) were diluted for solutions as required and were purchased from ACL Laboratories and Merck, respectively. 12 w/v% Sodium Hypochlorite (NaClO) was purchased from Thermo Fisher Scientific and used as received.

2.2. TEMPO-mediated oxidation

The TEMPO-mediated oxidation process employed is based on the method of Saito and Isogai [6]. 100 g BEK pulp was suspended in 2500 mL water containing 0.4 g TEMPO and 2.5 g NaBr. The 12 w/v% NaClO solution was initially adjusted to pH 10 via addition of 36% HCl. To initiate the oxidation process, 75 mL NaClO was added drop-wise to the suspension whilst stirred. The pH of the reaction was maintained at 10 through the addition of 0.5 M NaOH. The oxidation process was maintained for 2 h. The oxidised fibres were recovered through filtration and stored refrigerated (4 °C).

The oxidised pulp was then dispersed in deionised water to a desired concentration. Fibrillation was accomplished through a high-pressure homogeniser (GEA Niro Soavi Homogeniser Panda) at 1000 bar. Suspensions which contain less than 1 wt.% TEMPO-oxidised pulp was homogenised for two passes. More concentrated suspensions were homogenised with only one pass. TEMPO-oxidised cellulose nanofibres (TOCNFs) possess an average length of several microns and diameter of 3–4 nm [8,10].

2.3. Determining solids concentration

The solids concentration of all samples (i.e. gel or pulp) were determined through drying. The sample was weighed before (w_i) and after (w_d) drying. Sample moisture was evaporated by drying in an oven at 105° for at least 4 h. The solids content was calculated with:

$$\text{solids content}(\%) = \frac{w_d}{w_i} \times 100\% \quad (1)$$

2.4. Rheology

All rheological testing of the gels were performed with an Anton Paar MCR302 rheometer. A cone (0.997°) and plate (49.975 mm) geometry were selected. Testing was done at ambient temperature (25 °C). To ensure stable temperature during the testing, a solvent trap was used.

Viscosity was measured at shear rate ranging from 0.5 to 100 s^{-1} . Oscillatory strain sweep was performed from 0.01 to 100% at a constant 1 Hz frequency. Frequency sweep was measured from 0.1 to 100 rad/s and at 0.1% strain. All measurements were in triplicates. A thixotropic loop test was performed with a 1 wt.% gel by varying the shear stress between the LVR (0.1%, 1 Hz) and the yielded region (10%, 1 Hz) for 5 cycles.

2.5. Visualising the effect of pH and ionic strength

The effect of pH and salt content on the gel structure was observed qualitatively. The pH of the gels was increased and decreased by adding 0.5 M NaOH and 1 M HCl, respectively. The salt content of the gel was varied between 8.9 mM and 68.5 mM by the addition of 3 M NaCl. The gels were then loaded into test tubes and centrifuged at 4000 rpm for 20 min to separate any released water. The experiment was done in triplicates. Fibre ratio is then calculated as the ratio between the final and initial gel height. The gels were imaged with a black background to enhance visualisation.

2.6. Dynamic light scattering

A DLS measurement (Nanobrook Omni Particle Size Analyser) was performed with a dilute (0.03 wt.%) suspension to estimate fibre length.

2.7. Atomic force microscopy (AFM) imaging

AFM imaging was performed using a JPK Nanowizard 3 to determine fibre diameter and morphology. Samples were prepared by spin coating (Laurell technologies, WS-400BZ-6NPP/LITE) a 0.01 wt.% CNF dispersion onto glass microscope slides. Images were obtained in intermittent contact mode using Brüker NCHV model cantilevers. Due to convolution effects from the finite size of the AFM tip, fibre diameters were obtained from the reported height of single fibres on the surface.

3. Results

3.1. Fibre dimensions and morphology

To characterise the fibre dimensions, atomic force microscopy (AFM) imaging was used, with results shown in Fig. 1. From the

images of spin-coated and dried fibres, it is clear that the fibres are quite monodisperse in diameter, with reported diameters from AFM height measurements of 2–3 nm. Previous reports have shown a similar diameter distribution [8,10]. The fibre lengths are, as expected from previous literature protocols [8,37], more variable and typically the fibres are several microns in length. These fibres have been shown to swell in water depending on their counterion present with the carboxylate pendant group. A Na⁺ counterion was shown to have a higher fibre swelling in contrast to H⁺ [38].

3.2. Effect of pH and ionic strength

The effect of pH and ionic strength on gel is shown in Fig. 2. Varying both variables resulted in the gel losing its homogeneous structure with the formation of heterogeneous clumps in a dilute water matrix. Hence, rheological measurements were not completed due to the phase separation (i.e. release of water) resulting in inaccurate measurements. To visualise the effect of both variables, the gels were placed in tubes and centrifuged to observe any eluted water. Fig. 2A shows the effect of varying the pH of gels. TOCNF gels have an original pH of 7.4. Adding acid (pH<7) increases the amount of water eluted from the gel. The fibres forming the gel become heterogeneously distributed and compact as pH is decreased- indicated by the whitish appearance. However, increasing the pH does not have any observable effects on gel.

Fig. 2B shows the effect of salt concentration on gel stability. The addition of up to 17.4 mM NaCl did not affect nanocellulose gel stability; water is however released over this concentration. The addition of 34.7 mM and 68.5 mM NaCl released increasing amounts of water, respectively. The water released by the gel at the highest salt concentration is comparable to the gel at pH 2.

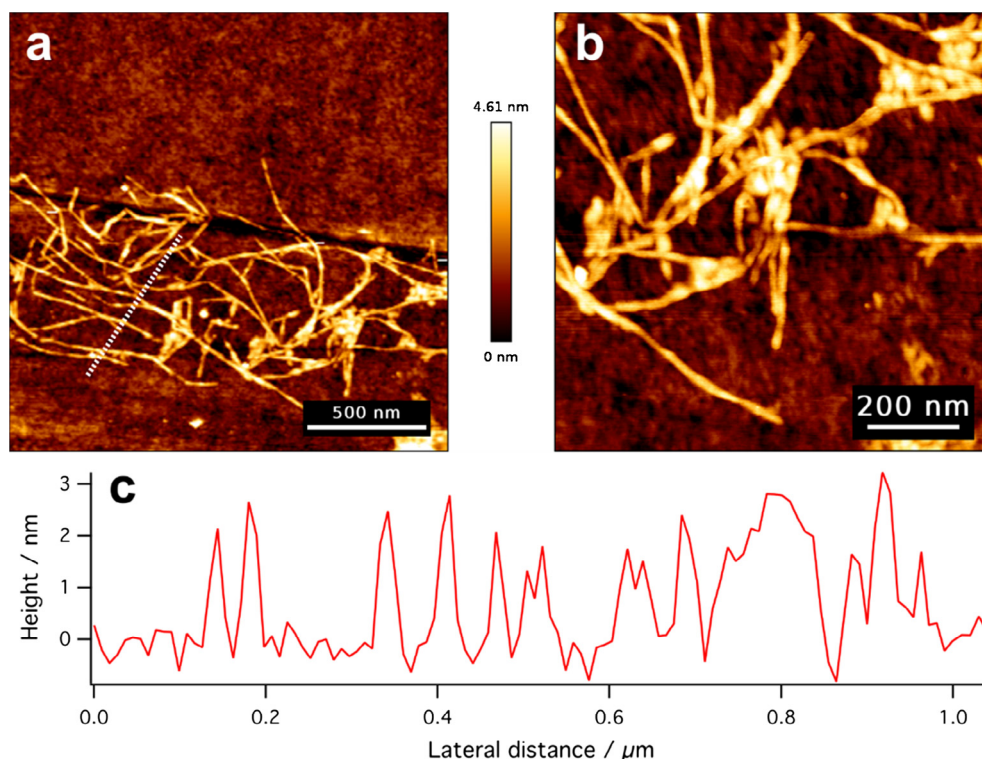


Fig. 1. AFM images of TOCNF spin coated onto a glass slide. (a, b) AFM height images of the fibres at different image sizes. (c) A cross-sectional profile of the surface topology at the point indicated by the white dotted line in (a) showing that the height (diameter) of individual fibres in the dry state is 2–3 nm.

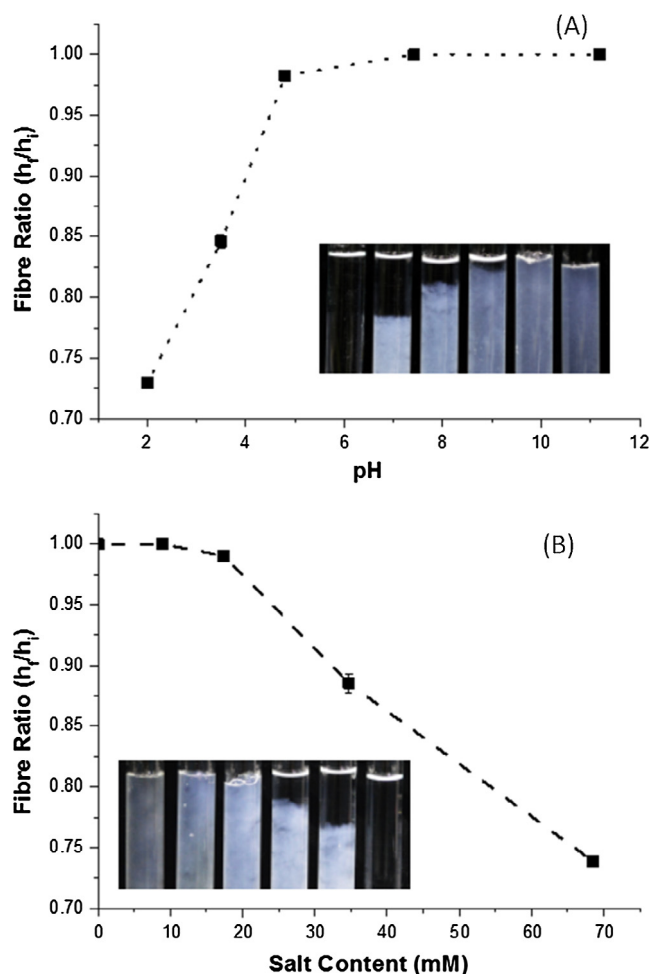


Fig. 2. The effect of (A) pH and (B) salt on the stability of 1 wt.% TEMPO-oxidised cellulose nanofibre gels. Fibre ratio is calculated as the ratio between the final height of gel after centrifugation and the total gel height. Insets show water released from gels at different conditions with pure water as reference.

3.3. Effect of fibre concentration

We measured the effect of fibre concentration on gel properties by rheology. Rheology is an effective method to characterise the behaviour of soft matter such as gels. Rheological measurements can be performed in two modes: steady-shear or oscillatory flow. The effect of shear rate and nanofibre concentration on TOCNF dispersion complex viscosity are presented in Fig. 3. Gel viscosity decreases with shear, denoting shear-thinning behaviour in line with expectation [9,39,40]. Higher zero-shear viscosities are observed with increasing TOCNF concentrations. Gels containing at least 0.29 wt.% TOCNF possess clear yield points, indicating that these are true gels. Indeed, we see some evidence for two yielding zones in the viscosity curves at higher fibre concentrations (discussed later), whereas gels containing less TOCNF (0.09%) have a linearly decreasing viscosity profile.

In oscillatory rheology, the gels are subjected to an increasing oscillating strain (strain sweep) at a constant frequency or vice versa (frequency sweep). In a strain sweep, the range of viscoelastic behaviour can be quantified for gels. The elastic modulus G' describes the solid-like behaviour of TOCNF gel whereas the loss or viscous modulus G'' defines the liquid-like behaviour of the material. Fig. 4 shows the rheological spectra of gels as a function of concentration. At low shear stresses, gels possess a linear viscoelastic region (LVR) wherein the elastic modulus G' and viscous

modulus G'' are independent of the shear stress. Within this region, G' is dominant over G'' , indicating that the material is acting consistently solid-like; elastic behaviour dominates over viscous behaviour. At a critical shear stress, the gel yields as shown by the decrease in G' , and then reaches a “cross-over point” where G'' becomes dominant and the gel begins to flow. Past this critical stress, the viscous regime dominates ($G'' > G'$) indicating that the network structure has yielded and begins to behave as a non-Newtonian shear thinning fluid. Gels containing a fibre content of at least 0.29 wt.% possess a distinct linear viscoelastic region and a yield point. For 0.09 wt.%, the linear viscoelastic region is significantly lengthened, and the cross-over point is not observed in the selected strain range.

The frequency sweep shows the time-dependent behaviour of TOCNF gels at increasing concentrations (Fig. 5). The G' and G'' values are non-intersecting for concentrations of at least 0.29 wt.% where G' increases gradually with angular frequency. This slight increase in the moduli is common for weak physically cross-linked gels [41]. For the higher concentration samples a minimum in G'' is apparent across the tested frequency range. This minimum has been related to the viscous relaxations which occur between the low and high frequencies: at low frequency, the fibres undergo glasslike rearrangement; at high frequency, the contribution of the solvent viscosity is increasingly important [42].

The thixotropic behaviour of the TOCNF gels was tested through a step strain test. The strain is varied by setting the strain (at constant frequency) either within the LVR region or outside. Similar to the oscillatory amplitude sweep, when $G' > G''$ the gel is behaving solid-like and vice versa. Fig. 6 shows the self-healing behaviour of a 1 wt.% nanocellulose gel. At low strain (0.1%), the gel is acting more solid-like. But once the strain (10%) is increased past the yield point, the gel immediately responds and flows in a viscous manner. Gel behaviour is reversible and changes between elastic-dominated and viscous-dominated regimes instantaneously.

4. Discussion

The discussion is divided into two sections: (1) the effect of pH and ionic strength (electrostatic stabilisation) and (2) the effect of fibre concentration (fibre overlap and entanglement).

4.1. Factors influencing gel stability

4.1.1. Effect of pH

pH affects the level of dissociation of the carboxylic groups, thus changing the density and strength of fibre-fibre interactions. The TOCNF gels produced typically have a pH of 7.4, indicating that most of the pendant groups present are in the sodium carboxylate form as the carboxylic acid pKa is much lower at 4.8. Upon lowering pH, the gel destabilises resulting in the agglomeration of fibres, appearing as semi-translucent aggregates accompanied by the release of water. This was previously observed by Besbes et al. [43] wherein the transmittance of the nanocellulose gels decreased drastically at lower pH indicating fibre agglomeration and destabilisation of the gels. The protonation of the carboxylic groups at low pH decreases the surface potential and electrostatic repulsion allowing the fibres to come in closer contact [44], as shown by the increase in fibres compaction (Fig. 2A). This is likely a result of Van der Waals forces becoming dominant when insufficient charge repulsion is present between the fibres. Another consequence of low pH is the release of water from the gel (Fig. 2A). The change in the counter-ion group from a Na^+ to H^+ drastically decreases the individual fibre and network swelling of TEMPO-oxidised nanocellulose [38]. These evidences prove that electrostatic stabilisation of the ionised COO^- groups conferred by the

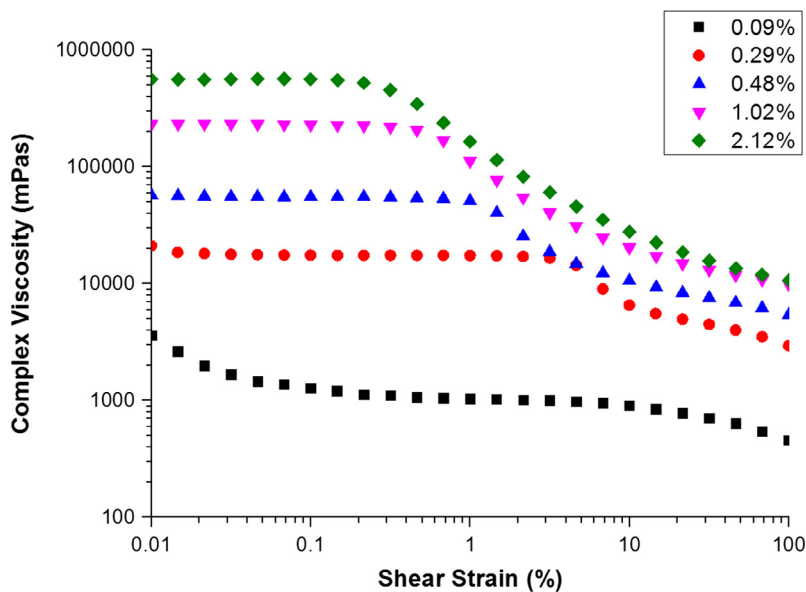


Fig. 3. Complex viscosity profile of shear-thinning TEMPO-oxidised cellulose nanofibre gels at various concentrations derived from dynamic strain sweep measurements (25 °C). A yield point is clearly evident for fibre concentrations of 0.29% and above.

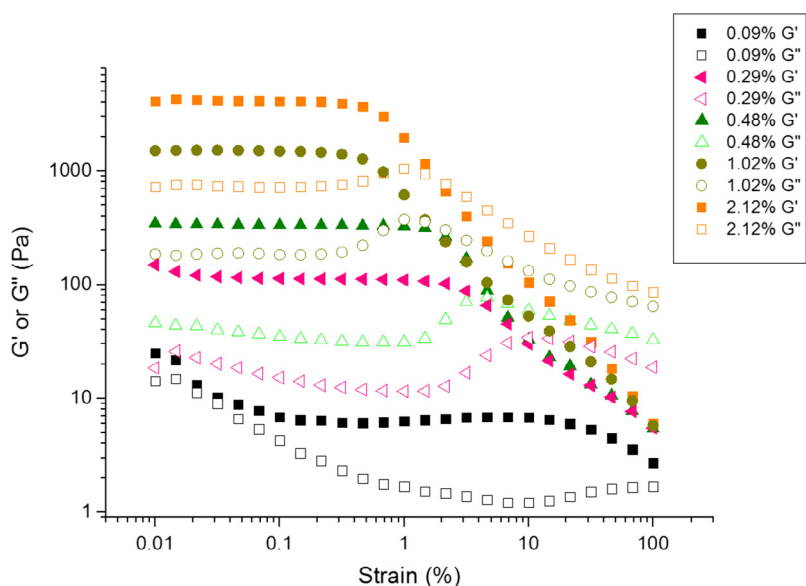


Fig. 4. Viscoelastic properties of TEMPO-oxidised cellulose nanofibre gels at different fibre concentrations: dynamic strain sweep (25 °C) at a frequency of 1 Hz. Filled symbols indicate elastic moduli whereas unfilled symbols indicate loss moduli.

TEMPO-oxidised cellulose nanofibres govern gel stability and formation.

4.1.2. Effect of ionic strength

Salt addition also causes the gel to release water, however not to the same extent as pH (Fig. 2B). Increasing the salt concentration reduces the electrical double layer, which causes an imbalance of the attractive and repulsive forces required for a stable colloid. The double layer thickness is estimated as a function of ionic strength with the Gouy-Chapman equation (Fig. 7). The double layer thickness (1 exponential or 63% decay) ranging from 1.2 to 3.2 nm is similar in magnitude to the diameter of the nanofibers (3–4 nm) [8,10]. Hence, for TEMPO-oxidised nanocellulose fibres, a charge is required in order to form stable network gels.

There is divergence in opinion regarding the effect of ionic strength on the rheological properties of cellulose suspensions.

Some studies claimed that the addition of monovalent salts (e.g. NaCl) to cellulose suspensions can increase both flow (viscosity) and dynamic (G' and G'') rheological properties [45,46]. These microfibrillated cellulose solutions studied were not carboxylated (bearing only OH- groups), which could potentially be a different regime. Both studies linked the increase in rheological properties to the enhanced screening of electrostatic repulsion leading to improved H-bonding between cellulose microfibrils. However, in these studies the microfibrillated cellulose suspensions were not surface modified (only containing OH- groups); hence, the increase in ionic strength allows improved H-bonding between the cellulose microfibrils which results in increased rheological properties. Other studies reported the opposite effect – a decreased viscosity with an increase in ionic strength [26,47,48], however the main difference is these fibres had polarizable groups (carboxylated or carboxymethylated). Carboxylate (~ -75 mV) and car-

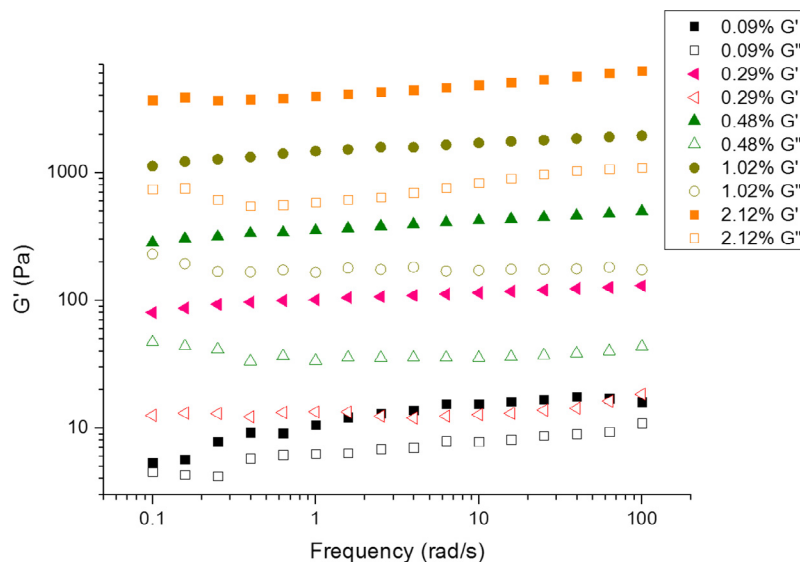


Fig. 5. Viscoelastic properties of TEMPO-oxidised cellulose nanofibre gels as at different fibre concentrations: dynamic frequency sweep (25 °C) at 0.1% strain.

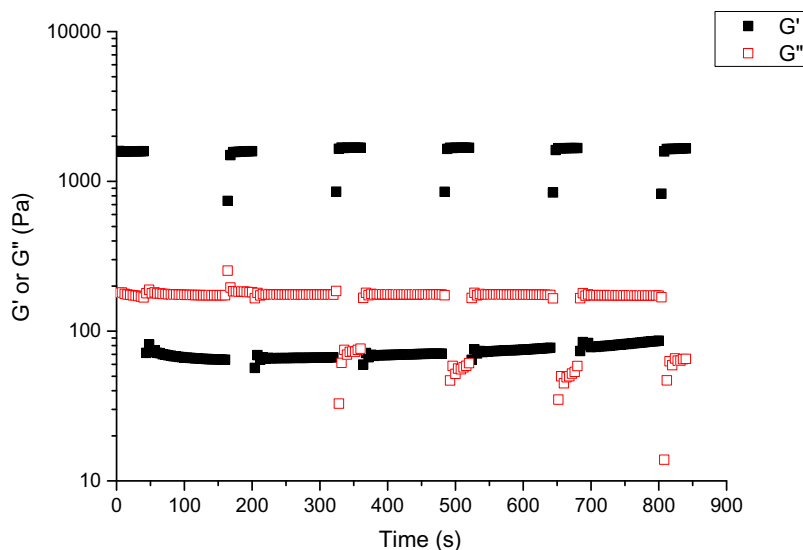


Fig. 6. Rheological properties of 1 wt.% TEMPO-oxidised cellulose nanofibre gel in a step strain test: strain has been varied between 0.1% and 10% at constant 1 Hz and 25 °C for 5 cycles.

boxymethyl groups ($\sim 590 \mu\text{eq/g}$) have a higher surface potential than the hydroxyl groups ($\sim -25 \text{ mV}$) on nanocellulose [8,48,49] leading to higher electrostatic repulsive force between fibres and a different form of fibre-fibre interaction. The screening of these forces results in the collapse of the existing fibre network leading to decreased gel strength properties, as reported.

4.2. Factors governing gel formation and behaviour

4.2.1. Effect of fibre concentration

We utilised rheology to understand the effect of TEMPO-oxidised cellulose nanofibre (TOCNF) concentration on the formation of gel network and its bulk properties. The oscillatory frequency sweep quantifies the gel consistency, which we anticipate is dominated by fibre-fibre interactions, whereas the oscillatory strain sweep characterises bulk flow properties which are dominated by viscosity.

At the lowest concentration (0.09 wt.%), fibres interact very weakly and possess relative motion. Gels at this concentration exhibit a transitional behaviour without strong evidence of material yielding (i.e. no linear viscoelastic region, LVR). Upon increasing the fibre concentration to 0.29 wt.%, the fibres are sufficiently interacting to demonstrate a well-defined LVR with a clear yielding behaviour (as shown in the strain sweep and complex viscosity as a function of strain). Gels containing at least 0.48 wt.% possess a stronger network, as evidenced by higher zero-shear viscosity and by higher G' values. The increase in entanglements at these concentrations also means that the network is becoming less flexible as shown by the yielding of the gels at lower strains.

The formation of the fibre network can also be observed through the evolution of the viscosity profile at increasing concentrations. Cellulose suspensions, whether nano- or micro-fibrillated, are known for their shear-thinning behaviour as the individual fibres can rearrange following the direction of shear. At a sufficient fibre concentration (0.29 wt.% and above), the com-

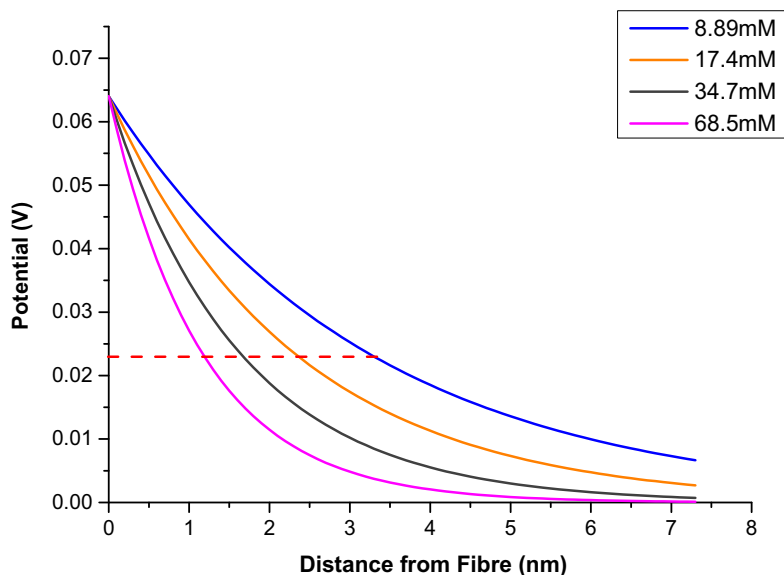


Fig. 7. Effect of ionic strength on the electrical double layer of TOCNF fibres estimated from the Gouy-Chapman equation (reference pH of original gel: 7.4). Dashed line indicates 63% decrease in surface charge corresponding to decreased double layer thickness at increased ionic strength.

plex viscosity demonstrates two shear-thinning regimes of the gel separated by a region of weaker strain dependence. This behaviour was also observed for other forms of nanocellulose [46,50–52]. In microfibrillated cellulose, a plateau region was seen, related to a transitional structure which exists between low and high shear structures. At low shear rates, nanofibres orient along the shear direction causing a decrease in viscosity. Upon reaching the critical shear strain (transition region), the low shear structure breaks down causing an increase in the floc size pre-empting the formation of a new high shear structure. Past this critical strain range, these large flocs are broken into smaller flocs which can move relative to each other [46,50–52].

This transformational behaviour was showed in TOCNF systems by birefringence [33]. TOCNFs re-orient accordingly to shear to produce intermediate structures. Provided that there is enough fibre to make a transitional structure, then and only then a viscosity plateau is reached. This indicates that at 0.09 wt.%, the gel does not possess enough fibre to exhibit this plateau behaviour. However, in more concentrated gels (>2 wt.%), we observe a change in the behaviour of the plateau itself. The plateau is extended and in the second shear-thinning stage the viscosity gradient decreases compared to the lower concentrations (0.29–1 wt.%). This reveals that larger flocs are formed which hinders movement of the gel.

The transitional behaviour highlighted in 0.09 wt.% is also validated by estimating the average number of contact points per fibre through the Crowding Factor Theory [53]. The crowding factor N is defined as the number of fibres present in a sphere wherein the diameter of the sphere is equal to the length of the fibre. The crowding factor (N) can be defined and calculated with the following equations:

$$N = \frac{2}{3} C_v \left(\frac{L}{d} \right)^2 \quad (2)$$

$$N \cong \frac{4\pi n_c^3}{3(n_c - 1)} \quad (3)$$

$$N \cong 4n_c^2 \quad (4)$$

where C_v is the fibre concentration by volume, L and d are the fibre average length and diameter, respectively, and n_c is the number of

contact points per fibre. A minimum n_c of 3 is required to have sufficient contact in order to sustain a network.

At this critical concentration of 0.09 wt.%, $63 \leq N \leq 125$ by estimating fibre length range between 1000 nm and 1400 nm (DLS measurements) and an average diameter of 2.5 nm (from AFM measurement). Assuming a constraint of $n_c \gg 1$ (Simplifying Eqs. (3) to (4)), the estimated number of contact points per fibre lies between $3.98 \leq n_c \leq 5.58$. This indicates that the fibres possess slightly higher than the minimum contact points required for stable network formation and have restricted relative motion resulting into the observed rheological values ($G' > G''$ in frequency sweep). These are characteristics of a gel.

We also investigated the effect of cyclical stress on the 1 wt.% nanocellulose gel to quantify stress relaxation and network recovery behaviour. This was evaluated via a step strain test. The thixotropy of TOCNF gels is due to the non-covalent physical bonding with surrounding fibres. The gels respond to changes in strains as the fibres re-assemble, quickly reforming the gel. On all high strain intervals, the gels possess a viscous dominant behaviour ($G'' > G'$) with both G' and G'' showing reproducible values throughout the test. At low strain intervals, the elastic-dominated behaviour of gel allows quick re-formation; however some degradation in G'' is observed. This hysteretic dependence of G'' may indicate overall structuring of the fibres during the test, or a consolidation of the fibre network during the measurement that results in different viscous dissipation of the gel at lower strains.

5. Conclusion

TEMPO-mediated oxidation is an efficient oxidation process for producing cellulose nanofibres of a small diameter (2–5 nm) [8,10] and high surface charge (COOH). In aqueous suspensions, these elongated nanofibres colloids form cellulosic gels above a critical concentration. Most previous studies on TEMPO-oxidised cellulose nanofibres (TOCNFs) have focussed on the rheological properties, aspect ratio quantification, and production from different substrates or its usability for various applications [25–27,43]. Very few- if any - have analysed cellulose nanofibres in terms of colloidal and interfacial chemistry [24,44]. In this study, we analysed the gelation and colloidal stability of TEMPO-oxidised cellulose nanofibres (TOCNF) by investigating the effect of concentration, pH, and salt content on rheology from a colloids and interfacial

perspective. Gel rheology is examined in terms of nanofiber fibre stability, surface charge (pH) and double layer thickness (NaCl). TOCNFs are elongated and flexible nanofibres forming entangled polymer solutions at low concentrations which transition to gels at higher nanofibre concentrations. This is evidenced by the transition at 0.1 wt.% as measured by rheology and correlation with network theory (Crowding factor). pH and salt strongly influence the colloidal stability of the gels and water is released as the gel collapses. The protonation of the carboxylate groups via the reduction in pH led to a lower surface charge and reduced the amount of water bound to the nanofibers. Increasing ionic strength via salt addition induces charge shielding by compression of the electrical double layer between adjacent fibres, also leading to water release. TOCNFs are colloidal gels- interacting colloidal suspensions of elongated flexible charged particles. The stability of the nanofibres results from the overlap and entanglement of the high aspect ratio fibres combined with electrostatic stabilisation of the pendant COO⁻ groups. Relating the mechanism of TOCNF gel formation to the well-established colloid and interface science enables specific applications in food, biomedical and as rheology modifier to be efficiently engineered from first principles.

Acknowledgments

This work was funded by the ARC Bioprocessing Advance Manufacturing Industry Research Transformation Hub IH13100016, Visy, Norske Skog, Orora, CHH/Oji Paper, and Australian Paper and Circa. Many thanks to Australian Paper for providing the pulp.

References

- [1] D. Klemm et al., Cellulose: fascinating biopolymer and sustainable raw material, *Angewandte Chemie Internat. Edit.* 44 (22) (2005) 3358–3393.
- [2] A. Dufresne, *Nanocellulose From Nature to High Performance Tailored Materials*, 2012: De Gruyter.
- [3] N. Lin, A. Dufresne, *Nanocellulose in biomedicine: current status and future prospect*, *Eur. Polymer J.* 59 (2014) 302–325.
- [4] S. Varanasi, R. He, W. Batchelor, Estimation of cellulose nanofibre aspect ratio from measurements of fibre suspension gel point, *Cellulose* 20 (4) (2013) 1885–1896.
- [5] L. Zhang et al., Effect of cellulose nanofiber dimensions on sheet forming through filtration, *Cellulose* 19 (2) (2012) 561–574.
- [6] T. Saito et al., Cellulose nanofibers prepared by TEMPO-Mediated oxidation of native cellulose, *Biomacromol* 8 (8) (2007) 2485–2491.
- [7] T. Saito, A. Isogai, TEMPO-mediated oxidation of native cellulose. The effect of oxidation conditions on chemical and crystal structures of the water-insoluble fractions, *Biomacromol* 5 (5) (2004) 1983–1989.
- [8] A. Isogai, T. Saito, H. Fukuzumi, TEMPO-oxidized cellulose nanofibers, *Nanoscale* 3 (1) (2011) 71–85.
- [9] O. Nechyporchuk, M.N. Belgacem, F. Pignon, Current progress in rheology of cellulose nanofibril suspensions, *Biomacromol* 17 (7) (2016) 2311–2320.
- [10] H. Fukuzumi et al., Transparent and high gas barrier films of cellulose nanofibers prepared by TEMPO-mediated oxidation, *Biomacromol* 10 (1) (2009) 162–165.
- [11] Q. Li et al., Nanocellulose life cycle assessment, *ACS Sustain. Chem. Eng.* 1 (8) (2013) 919–928.
- [12] R. Weishaupt et al., TEMPO-oxidized nanofibrillated cellulose as a high density carrier for bioactive molecules, *Biomacromol* 16 (11) (2015) 3640–3650.
- [13] A. Rees et al., 3D Bioprinting of carboxymethylated-periodate oxidized nanocellulose constructs for wound dressing applications, *BioMed Res. Internat.* 2015 (2015) 7.
- [14] N.E. Zander et al., Metal cation cross-linked nanocellulose hydrogels as tissue engineering substrates, *ACS Appl. Mater. Interfaces.* 6(21) (2014) 18502–18510.
- [15] J. Cheng, M. Park, J. Hyun, Thermoresponsive hybrid hydrogel of oxidized nanocellulose using a polypeptide crosslinker, *Cellulose* 21 (3) (2014) 1699–1708.
- [16] M. Park, D. Lee, J. Hyun, Nanocellulose-alginate hydrogel for cell encapsulation, *Carbohydr. Polym.* 116 (2015) 223–228.
- [17] M. Bulota, M. Hughes, Toughening mechanisms in poly(lactic) acid reinforced with TEMPO-oxidized cellulose, *J. Mater. Sci.* 47 (14) (2012) 5517–5523.
- [18] S. Fujisawa et al., Superior reinforcement effect of TEMPO-oxidized cellulose nanofibrils in polystyrene matrix: optical, thermal, and mechanical studies, *Biomacromol* 13 (7) (2012) 2188–2194.
- [19] M. Hakalahti et al., Effect of interfibrillar PVA bridging on water stability and mechanical properties of TEMPO/NaClO₂ oxidized cellulosic nanofibril films, *Carbohydr. Polym.* 126 (2015) 78–82.
- [20] T. Saito, A. Isogai, Wet strength improvement of TEMPO-oxidized cellulose sheets prepared with cationic polymers, *Ind. Eng. Chem. Res.* 46 (3) (2007) 773–780.
- [21] K. Dimic-Misic, P.A.C. Gane, J. Paltakari, Micro- and nanofibrillated cellulose as a rheology modifier additive in CMC-containing pigment-coating formulations, *Ind. Eng. Chem. Res.* 52 (45) (2013) 16066–16083.
- [22] X. Sun et al., Cellulose nanofibers as a modifier for rheology, curing and mechanical performance of oil well cement, *Sci. Rep.* 6 (2016) 31654.
- [23] F. Jiang, Y.-L. Hsieh, Super water absorbing and shape memory nanocellulose aerogels from TEMPO-oxidized cellulose nanofibrils via cyclic freezing-thawing, *J. Mater. Chem. A* 2 (2) (2014) 350–359.
- [24] I. Usov, Understanding nanocellulose chirality and structure-properties relationship at the single fibril level, *Nat Commun.* (2015) 6.
- [25] D. Ishii, T. Saito, A. Isogai, Viscoelastic evaluation of average length of cellulose nanofibers prepared by TEMPO-mediated oxidation, *Biomacromol* 12 (3) (2011) 548–550.
- [26] L. Jowkarderis, T.G.M. van de Ven, Intrinsic viscosity of aqueous suspensions of cellulose nanofibrils, *Cellulose* 21 (4) (2014) 2511–2517.
- [27] L. Jowkarderis, T.G.M. van de Ven, Rheology of semi-dilute suspensions of carboxylated cellulose nanofibrils, *Carbohydr. Polym.* 123 (2015) 416–423.
- [28] D.A. Rees, W.E. Scott, Polysaccharide conformation, Part VI. Computer model-building for linear and branched pyranoglycans. Correlations with biological function. Preliminary assessment of inter-residue forces in aqueous solution, Further interpretation of optical rotation in terms of chain conformation, *J. Chem. Soc. B: Phys. Organ.* 1971 0 p. 469–79.
- [29] L. Li, Thermal gelation of methylcellulose in water: scaling and thermoreversibility, *Macromolecules* 35 (15) (2002) 5990–5998.
- [30] K. Bekkour, D. Sun-Waterhouse, S.S. Wadhwa, Rheological properties and cloud point of aqueous carboxymethyl cellulose dispersions as modified by high or low methoxyl pectin, *Food Res. Int.* 66 (2014) 247–256.
- [31] A. Benslimane et al., Thermal gelation properties of carboxymethyl cellulose and bentonite-carboxymethyl cellulose dispersions: rheological considerations, *Appl. Clay Sci.* 132 (2016) 702–710.
- [32] Y. Fang et al., Multiple steps and critical behaviors of the binding of calcium to alginate, *J. Phys. Chem. B* 111 (10) (2007) 2456–2462.
- [33] E. Lasseguette, D. Roux, Y. Nishiyama, Rheological properties of microfibrillar suspension of TEMPO-oxidized pulp, *Cellulose* 15 (3) (2008) 425–433.
- [34] T. Saito et al., Self-aligned integration of native cellulose nanofibrils towards producing diverse bulk materials, *Soft Matter* 7 (19) (2011) 8804–8809.
- [35] H. Dong et al., Cation-induced hydrogels of cellulose nanofibrils with tunable moduli, *Biomacromol* 14 (9) (2013) 3338–3345.
- [36] A. Fernandez-Nieves, A.M. Puertas, Rheology of Soft Materials, in *Fluids, Colloids and Soft Materials*, H.M. Wyss, Editor. 2016, John Wiley & Sons, Inc. p. 149–163.
- [37] R. Shinoda et al., Relationship between length and degree of polymerization of TEMPO-oxidized cellulose nanofibrils, *Biomacromol* 13 (3) (2012) 842–849.
- [38] T.C. Maloney, Network swelling of TEMPO-oxidized nanocellulose, in *Holzforchung*, 2015. p. 207.
- [39] I. Besbes, S. Alila, S. Boufi, Nanofibrillated cellulose from TEMPO-oxidized eucalyptus fibres: effect of the carboxyl content, *Carbohydr. Polym.* 84 (3) (2011) 975–983.
- [40] T. Moberg et al., Rheological properties of nanocellulose suspensions: effects of fibril/particle dimensions and surface characteristics, *Cellulose* 24 (6) (2017) 2499–2510.
- [41] R. Lapasin, Rheological Characterization of Hydrogels, in *Polysaccharide Hydrogels: Characterization and Biomedical Applications*, P. Matricardi, F. Alhaique, and T. Coviello, Editors. 2016, CRC Press. p. 96–97.
- [42] T.G. Mason et al., Osmotic pressure and viscoelastic shear moduli of concentrated emulsions, *Phys. Rev. E* 56 (3) (1997) 3150–3166.
- [43] I. Besbes, M.R. Vilar, S. Boufi, Nanofibrillated cellulose from Alfa, Eucalyptus and pine fibres: preparation, characteristics and reinforcing potential, *Carbohydr. Polym.* 86 (3) (2011) 1198–1206.
- [44] A.B. Fall et al., Colloidal stability of aqueous nanofibrillated cellulose dispersions, *Langmuir* 27 (18) (2011) 11332–11338.
- [45] M.P. Lowys, J. Desbrières, M. Rinaudo, Rheological characterization of cellulosic microfibril suspensions. Role of polymeric additives, *Food Hydrocolloids* 15 (1) (2001) 25–32.
- [46] E. Saarikoski et al., Flocculated flow of microfibrillated cellulose water suspensions: an imaging approach for characterisation of rheological behaviour, *Cellulose* 19 (3) (2012) 647–659.
- [47] R. Tanaka et al., Determination of nanocellulose fibril length by shear viscosity measurement, *Cellulose* 21 (3) (2014) 1581–1589.
- [48] A. Naderi, T. Lindström, T. Pettersson, The state of carboxymethylated nanofibrils after homogenization-aided dilution from concentrated suspensions: a rheological perspective, *Cellulose* 21 (4) (2014) 2357–2368.
- [49] P. Raj et al., Effect of cationic polyacrylamide on the processing and properties of nanocellulose films, *J. Colloid Interface Sci.* 447 (2015) 113–119.
- [50] G. Agoda-Tandjawa et al., Rheological characterization of microfibrillated cellulose suspensions after freezing, *Carbohydr. Polym.* 80 (3) (2010) 677–686.
- [51] M. Iotti et al., Rheological studies of microfibrillar cellulose water dispersions, *J. Polym. Environ.* 19 (1) (2011) 137–145.
- [52] A. Karppinen et al., Flocculation of microfibrillated cellulose in shear flow, *Cellulose* 19 (6) (2012) 1807–1819.
- [53] R.J. Kerekes, C.J. Schell, Characterization of fibre flocculation regimes by a crowding factor, *J. Pulp Pap. Sci.* 18 (1) (1992) J32–J38.



Regular Article

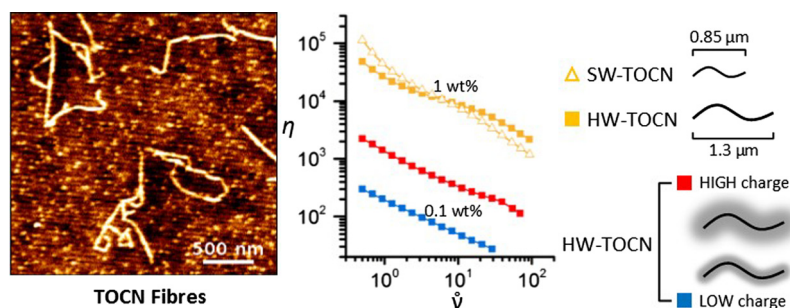
Effects of fibre dimension and charge density on nanocellulose gels

Llyza Mendoza, Thilina Gunawardhana, Warren Batchelor, Gil Garnier*



Bioresource Processing Research Institute of Australia (BioPRIA), Department of Chemical Engineering, Monash University, VIC 3800, Australia

GRAPHICAL ABSTRACT



ARTICLE INFO

Article history:

Received 7 March 2018

Revised 16 April 2018

Accepted 17 April 2018

Available online 18 April 2018

Keywords:

Nanocellulose

Gel

Fibre dimension

Rheology

TEMPO-mediated oxidation

Atomic force microscopy

ABSTRACT

Hypothesis: Carboxylated cellulose nanofibres can produce gels at low concentrations. The effect of pulp source on the nanocellulose fibre dimension and gel rheology are studied. It is hypothesised that fibre length and surface charge influence aspects of the gel rheological properties.

Experiments: TEMPO (2,2,6,6-tetramethylpiperidine-1-oxyl)- mediated oxidised cellulose nanofibres from never-dried hardwood and softwood pulp and containing different charge levels were produced and characterized. Steady-state and dynamic rheological studies were performed to ascertain the effects of pulp type on gel behavior and properties.

Findings: Nanocellulose fibres extracted from softwood (SW-TOCN) and hardwood (HW-TOCN) pulp exhibit similar widths but different length dimensions as shown via AFM analysis. Rheological measurements show that the dynamic moduli (G' and G'') of nanocellulose gels are independent of pulp source and are mostly influenced by fibre concentration. Differences in the steady-state behavior (i.e. viscosity) at constant surface charge can be attributed to differences in fibre length. Increasing the surface charge density influences the critical strain and the viscosity at the percolation concentration (0.1 wt%) due to higher electrostatic interactions.

Crown Copyright © 2018 Published by Elsevier Inc. All rights reserved.

1. Introduction

Cellulose nanofibres are long semi-flexible fibrils derived from the disintegration of wood pulp via various chemical and mechanical treatments [1]. Chemical methods, such as TEMPO-mediated oxidation, selectively introduce carboxylate moieties on the

cellulose fibril surface. The high electrostatic repulsion between the individual fibrils assists in the liberation of TEMPO-oxidised cellulose nanofibres (TOCNs) upon mechanical disintegration [2]. The ease of scale-up of TEMPO-mediated oxidation has led to the establishment of pilot-scale production and its availability as a commercial product [3]. Applications of TOCNs extend far beyond pulp and paper. TOCNs have shown great performance as reinforcing agent in plastics, [4,5], in biomedical applications [6–11], pharmaceuticals [12], catalysis [13], superabsorbents [14,15], and flexible electronics [16].

* Corresponding author.

E-mail address: gil.garnier@monash.edu (G. Garnier).

Nanocellulose is typically found as a suspension or a gel with water as continuous phase. Rheology is the technique of choice to quantify nanocellulose behavior and properties. For instance, the flow behavior of semi-flexible nanocellulose fibrils can be related to the length and width of the fibrils. The studies of Tanaka et al. [17] and Jowkarderis and van de Ven [18], related shear and intrinsic viscosities of dilute TOCN suspensions to equations of flow for rigid rod-like particles to determine fibre aspect ratio. Varanasi et al. [19], on the other hand, utilised yield stress measurements to determine the fibre gel point and correlate it to the aspect ratio via the crowding factor theory.

The bulk properties of nanocellulose gels and suspensions have been investigated in several rheological studies. In particular, TOCNs possess high aspect ratio [2] which form percolated networks even at low solid concentrations [20]. TOCNs and similarly surface-charged nanocellulose suspensions form gels which exhibit pseudoplastic and thixotropic behavior due to their inherent fibril assembly and restructuring which occurs during material deformation [20–22]. The presence of high surface charges leading to their colloidal stability was also investigated in several studies [20,23–25]. Local flow phenomenon in nanocellulose such as wall slip, shear-banding, and other flow instabilities which may affect the accuracy of rheological measurements were analysed [12,21]. Simulation and numerical modelling have mainly focused on understanding the mechanism of shear-thinning in nanocellulose [26,27]. However, studies on the effects of fibre dimensions and surface charges, on the nanocellulose gel rheological properties are very limited. Only one known study has related nanocellulose aspect ratio to the changes in the fibre percolation as observed by changes in viscosity [28].

This study aims at quantifying the effect of fibre dimension and surface charge on the rheological properties of nanocellulose gels. Fibre dimension was varied with the pulp source by oxidising softwood and hardwood kraft pulp from *Pinus Radiata* and *Eucalyptus* sp. respectively. The objectives are two-fold. First, to understand the relationship between the initial fibre size on the dimensions of the resulting nanocellulose; second to quantify the effect of nanocellulose fibre dimension on gel rheology. Differences are analysed through steady-state shear and oscillatory rheological measurements via cone and plate geometry. In steady-state shear, changes in the signature double yielding-behavior and zero-shear viscosity will be observed, whereas in oscillatory measurements variations in the key parameters such as the dynamic (G' and G'') moduli and the critical strain γ_c are examined.

2. Methodology

2.1. Materials

Hardwood (*Eucalyptus* sp.) kraft pulp of approximately 10 wt% solids was supplied by Australian Paper, Maryvale, Australia. Softwood (*Pinus Radiata*) kraft pulp containing 17.7 wt% solids was supplied by Oji Fibre Solutions, Kinleith, New Zealand. 2,2,6,6-tetra methylpiperidine-1-oxyl (TEMPO) and sodium bromide (NaBr) were purchased from Sigma-Aldrich. Hydrochloric acid (HCl) and Sodium Hydroxide (NaOH) were diluted for solutions as required and were purchased from ACL Laboratories and Merck, respectively. 12 w/v% Sodium Hypochlorite (NaClO) was purchased from Thermo Fisher Scientific and used as received. All chemicals were analytical grade.

2.2. TEMPO-mediated oxidation

The TEMPO-mediated oxidation process employed is based on the method of Isogai et al. [2]. Wood pulp containing 10 dry g fibre

was suspended in 2500 mL water containing 0.4 g TEMPO and 2.5 g NaBr. The 12 w/v% NaClO solution was initially adjusted to pH 10 via addition of 36% HCl before the reaction. To initiate the oxidation process, NaClO was added drop-wise to the suspension whilst stirred. Varying amounts of NaClO was added depending on the desired carboxylate group density. The primary oxidant content was varied between 3.3 mmol NaClO·g⁻¹ fibre to 12.5 mmol NaClO·g⁻¹ fibre for hardwood and constant 6.5 mmol NaClO·g⁻¹ fibre for softwood. The pH of the reaction was maintained at 10 through the addition of 0.5 M NaOH. The oxidation process was maintained until no pH change was observed. The oxidised fibres were recovered through filtration and stored refrigerated (4 °C). The oxidised pulp was then dispersed in deionised water to a desired concentration (0.1–1 wt%). Fibrillation was accomplished through a high-pressure homogeniser (GEA Niro Soavi Homogener Panda) at 1000 bar for two passes.

2.3. Determining solids concentration

The solids concentration of all samples (i.e. gel or pulp) were determined through drying. The sample was weighed before (w_i) and after (w_d) drying. Sample moisture was evaporated by drying in an oven at 105° for at least 6 h. The solids content was calculated as:

$$\text{solidscontent}(\%) = \frac{w_d}{w_i} \times 100\% \quad (1)$$

2.4. Conductometric titration

The carboxylate group content was measured by conductometric titration as reported in [29]. Oxidised pulp samples (approx. 30 mg dry weight) were suspended in 40 mL deionised water. 40 μ L 1% NaCl was added to the suspended sample. The pH of the suspended sample was adjusted between 2.5 and 3 prior to titration with 0.5 M HCl. Titration was accomplished by controlled addition of 0.1 M NaOH using a Mettler Toledo T5 titrator. The conductivity of the sample was monitored throughout the titration progress. The carboxyl group content (mmol COO⁻Na⁺·g⁻¹ fibre) was determined with:

$$CC = \frac{c(V_2 - V_1)}{w} \times 1000 \quad (2)$$

where V_1 and V_2 pertain to the amount of titrant required to neutralise the carboxylic groups (in L), c is the NaOH concentration (mol/L), and w is the sample weight (g).

2.5. Rheological measurement

Rheological testing was performed with an Anton Paar MCR302 rheometer. A cone (0.997°) and plate (49.975 mm) geometry were selected. Testing was done at ambient temperature (25 °C). A solvent trap was used to ensure stable temperature during measurements. Viscosity was measured at shear rate ranging from 0.5 to 100 s⁻¹. Oscillatory strain sweep was performed from 0.01 to 100% at a constant 1 Hz frequency. Frequency sweep was measured from 0.1 to 100 rad/s and at various suitable shear stresses at the linear viscoelastic region (LVR) wherein the dynamic moduli (G' and G'') are independent of the shear stress. All measurements were done in triplicates and the most representative result is presented.

2.6. Atomic force microscopy (AFM)

AFM imaging was performed using a JPK Nanowizard 3 to determine fibre length and width. A 0.001 wt% nanocellulose dispersion

was spin coated (Laurell technologies, WS-400BZ-6NPP/LITE) at 2500 rpm onto a plasma coated glass slide. Images were obtained in intermittent contact mode using Brüker NCHV model cantilevers. Fibre widths were obtained from the reported height of single fibres on the surface due to convolution effects. Fibre lengths were estimated by placing segmented lines on the AFM images through an imaging software (Fiji).

2.7. Fibrelab

Fibre dimensions (length and width) of the unrefined and unoxidised hardwood and softwood samples have been obtained via the Kajaani Fibre Lab (Valmet). Dilute suspensions (~ 0.05 wt%) were utilised for size analysis. Image analysis from the Fibrelab software is primarily capable of detecting large fibres more than fines.

3. Results

The effect of fibre dimensions, using never-dried bleached kraft pulp of softwood and hardwood, on the dimensions and charge density of cellulose nanofibres resulting from TEMPO-mediated oxidation pre-treatment and homogenization is first studied. Secondly, the rheological properties of the gel formed are quantified to understand the effect of nanocellulose dimensions and surface charge (i.e. extent of oxidation).

3.1. Fibre dimensions

The distributions of fibre length and width of never-dried unrefined softwood and hardwood kraft pulps are shown in Fig. 1. On average, hardwood pulp has shorter and narrower fibres than softwood; length and width distributions are also much narrower (Tables 1 and 2). However, the fibre average aspect ratio (L/W) are nearly identical for both fibres, with hardwood $L/W = 36$ and softwood $L/W = 42$.

The fibre size distributions of TEMPO-oxidised cellulose nanofibres produced from hardwood (HW-TOCN) and softwood (SW-TOCN) pulp containing different surface charges are shown in Fig. 2. The nanocellulose produced in all cases have the width distribution in the nano-scale- as expected from TEMPO-mediated oxidation. Length distributions, on the other hand, have changed post- chemical oxidation and mechanical fibrillation. For both fibre types and their varying surface charge levels, the mean length decreased drastically as shown in Tables 1 and 2. On average, hardwood-nanocellulose (HW-TOCN) are wider and longer than softwood-nanocellulose (SW-TOCN) at similar surface charge ($1 \text{ mmol COO}^- \cdot \text{g}^{-1}$ fibre) as shown in Tables 1 and 2. Moreover,

length and width distributions for HW-TOCNs are slightly broader than for SW-TOCNs. When surface charge is modified in HW-TOCNs, length and width dimension distributions and mean values are very similar.

3.2. Rheological measurements

Oscillatory rheology is an ideal technique to characterize the elastic and viscous behavior of nanocellulose gels at varying conditions. For instance, the rheology of nanocellulose gels produced from softwood pulp at increasing fibre concentration is shown in Fig. 3. The elastic modulus G' pertains to the solid-like behavior whereas the viscous modulus G'' characterizes the liquid-like behavior of the gel. At the linear viscoelastic region (LVR), G' and G'' are independent of the shear strain. When $G' > G''$, the elastic behavior of the nanocellulose gel is dominant at a particular strain. At the critical strain γ_c , the gel moduli (G' and G'') deviates from the LVR and is at the onset of yielding. Consequently, at even higher strains when $G'' > G'$, the gel possesses a viscous dominant behavior.

3.2.1. Effect of pulp source

The effect of initial pulp source on the dynamic moduli (G' and G'') at various solid concentrations is shown in Fig. 4A. At constant charge density ($1 \text{ mmol COO}^- \cdot \text{g}^{-1}$ fibre), the elastic moduli (G') of nanocellulose gels derived from hardwood and softwood sources are very similar. The differences in the viscous moduli (G'') observed between HW-TOCN and SW-TOCN are within the error margins. Moreover, for both types of pulp, γ_c is constant across all solids contents as shown in Fig. 4B. However, SW-TOCN possess consistently higher γ_c at all tested concentrations.

The difference of pulp source on the resultant nanocellulose gels viscosity profile is highlighted in Fig. 5. SW-TOCN and HW-TOCN both display similar viscosity values and linear shear-thinning behavior at 0.1 wt%. On the other hand, the double yielding behavior is observed for HW-TOCN and SW-TOCN at concentrations equal or greater than 0.3 wt%. The major difference in nanocellulose produced from hardwood and softwood pulp sources is emphasized at the semi-dilute concentrations (0.3–1 wt%) wherein SW-TOCN viscosity decreases at a steeper gradient at both double yielding regions than HW-TOCNs.

3.2.2. Effect of charge density

The effect of charge density on the dynamic rheological properties of nanocellulose gels produced from hardwood is shown in Fig. 6. Gels with the lowest carboxylate content ($0.65 \text{ mmol} \cdot \text{g}^{-1}$) consistently report the lowest G' and G'' values. However, gels

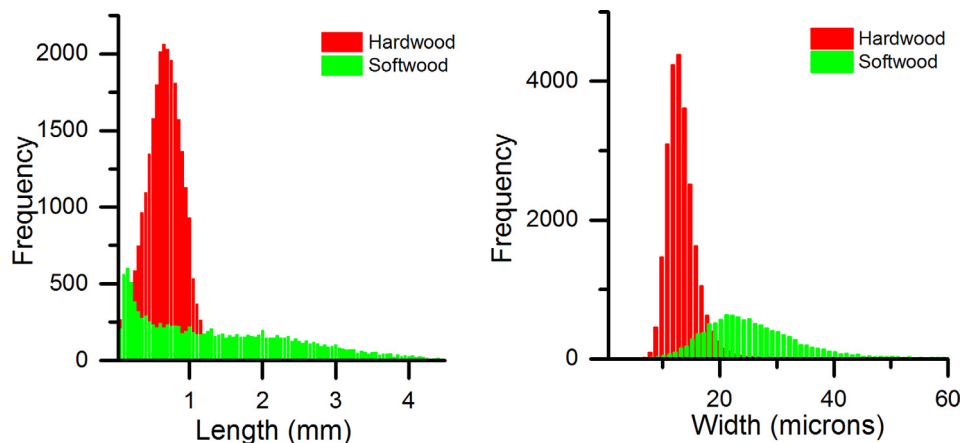


Fig. 1. Population Length and width distributions for hardwood and softwood bleached kraft pulp fibres.

Table 1
Fibre length statistics of hardwood and softwood kraft pulp and the nanocellulose fibres produced from those.

Pulp type	Surface charge (mmol COO ⁻ .g ⁻¹)	Mean length (μm)	Standard deviation (μm)	Population (# of fibres)
Hardwood	0	620	260	26,327
HW – TOCN	0.65	1.16	0.62	105
	1.00	1.30	0.73	111
	1.40	1.02	0.53	103
Softwood	0	1420	1130	13,070
SW-TOCN	1.00	0.85	0.42	99

Table 2
Fibre width statistics of hardwood and softwood bleached kraft pulp and the nanocellulose fibres produced from those.

Pulp source	Surface charge (mmol COO ⁻ .g ⁻¹)	Mean width (nm)	Standard deviation (nm)	Population (# of fibres)
Hardwood	0	17,240	4253	24,441
HW – TOCN	0.65	1.06	0.37	105
	1.00	1.24	0.33	111
	1.40	1.29	0.47	103
Softwood	0	34,060	9028	10,799
SW-TOCN	1.00	0.97	0.30	99

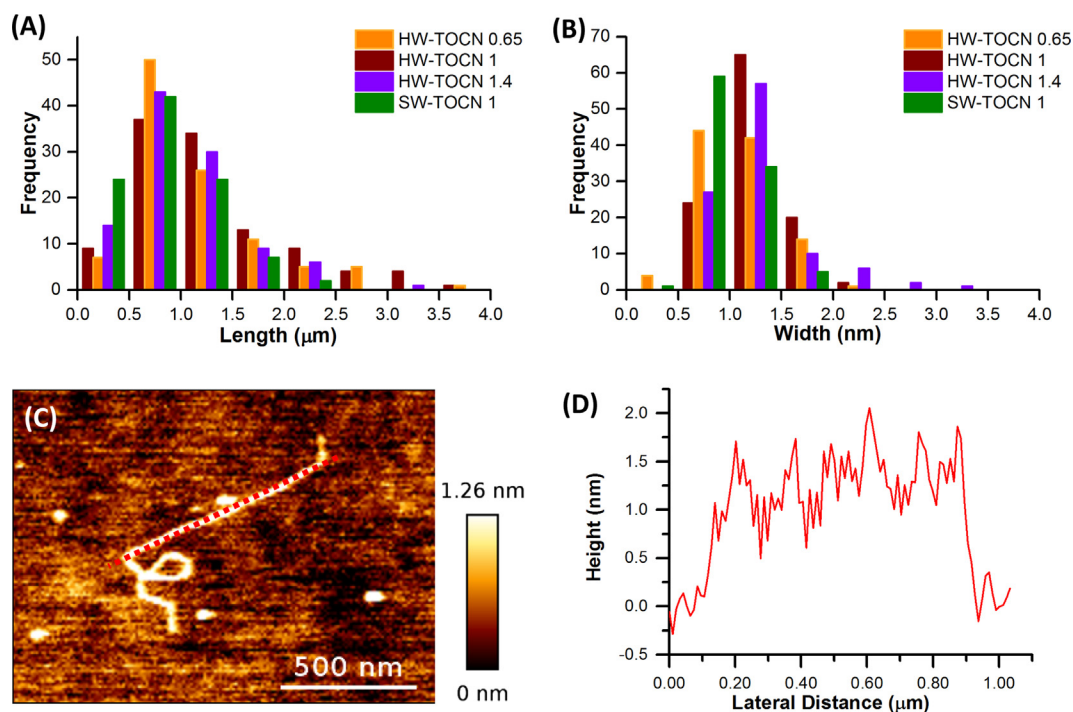


Fig. 2. Nanocellulose fibres produced from softwood and hardwood bleached kraft pulp. Width (A) and length (B) distributions for nanocellulose produced from softwood (1mmol COO⁻.g⁻¹) and hardwood (0.65, 1, and 1.4 mmol.g⁻¹) at various surface charges. (C) and (D) AFM image of a single HW-TOCN fibre with surface topology shown.

containing either 1 or 1.4 mmol.g⁻¹ show similar G' . On the other hand, G'' values were also observed to increase with increasing carboxylate content at all solids concentrations. Critical strain γ_c does not vary significantly up to a charge density of 1 mmol.g⁻¹. At the highest surface charge tested (1.4 mmol.g⁻¹), γ_c decreases linearly with increasing fibre content.

The viscosity profile of nanocellulose gels produced from hardwood at different surface charges is shown in Fig. 7. All HW-TOCN gels containing at least 0.3 wt% possess a double yielding behavior. At a given concentration past 0.3 wt%, the differences in the absolute viscosity values are minimal and could be attributed to small variations in actual nanocellulose content in the tested samples. However, at 0.1 wt%, the gel containing the lowest surface charge at 0.65 mmol.g⁻¹ is significantly less viscous than at 1 and 1.4 mmol.g⁻¹.

4. Discussion

4.1. Effect of pulp fibres on nanocellulose fibre dimensions

Cellulose fibres vary in fibre dimension and chemical composition depending on the original wood source and the pulping process used. The most widely-used process to produce cellulosic fibres is through a combination of kraft chemical pulping followed by bleaching. This process removes most of the lignin and hemicellulose that occur in different amounts and compositions in softwood (*Pinus Radiata*), and hardwood (*Eucalyptus* sp.) [30,31]. However, traces of lignin and hemicellulose still remain within the bleached cellulose pulp which impact the TEMPO-mediated oxidation process. The softwood pulp used in this study required a higher primary oxidant content (6.5 mmol NaClO.g⁻¹ fibre) than

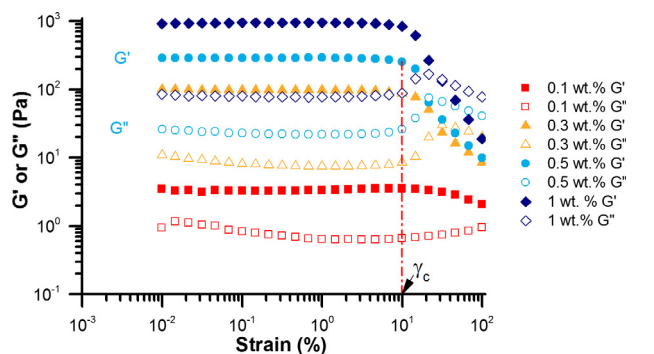


Fig. 3. Oscillatory strain measurement for nanocellulose gels made from bleached softwood fibres ($1 \text{ mmol}\cdot\text{g}^{-1}$) as a function of solids concentration. Important spectral rheological data including the G' and G'' at the linear viscoelastic region (LVR), and the critical strain γ_c are identified for the 0.5 wt% gel used as example. Measurements were done at 25°C , 1 Hz.

the hardwood pulp ($5 \text{ mmol NaClO}\cdot\text{g}^{-1}$ fibre) to achieve the same surface charge ($1 \text{ mmol COO}^-\cdot\text{g}^{-1}$ fibre).

The original width and length of the never-dried bleached hardwood and softwood fibres are vastly different (Fig. 1) – softwood fibres are approximately twice as long and thick on average compared to hardwood fibres (Tables 1 and 2). The combination of TEMPO-mediated oxidation and high-pressure homogenisation results in nanocellulose fibres with dimensions multiple orders of magnitude smaller. This chemical and mechanical treatment has effectively liberated elementary fibrils from both hardwood and softwood pulp sources, evident by the similar widths of the HW-TOCN and SW-TOCN fibres in the order of nanometers [15]. Due to the high energy required for mechanical fibrillation (i.e. 1000 bar pressure), it is possible that further delamination occurred resulting in a fibre mean width less than the currently accepted elementary fibril dimensions consisting a 6×6 chain array. Since individual cellulose chains are assembled into fibrils by H-bonding along their length, the high-pressure homogenisation could have created shear forces strong enough to liberate thinner fibrils. The widths measured support previous studies. For instance, Usov et al. [32] reported AFM measurements visualising single cellulose chains and 2×2 cellulose nanofibrils with average widths of 0.44 and 0.84 nm, respectively. In addition, Geng et al. [33] described a mean width value of 2.35 nm (at a surface charge of $980 \mu\text{mol}\cdot\text{g}^{-1}$); however, width distributions showed a large proportion of fibres thinner than 2 nm. When comparing lengths of the HW-TOCN and SW-TOCN fibres, cleavage is evident for both

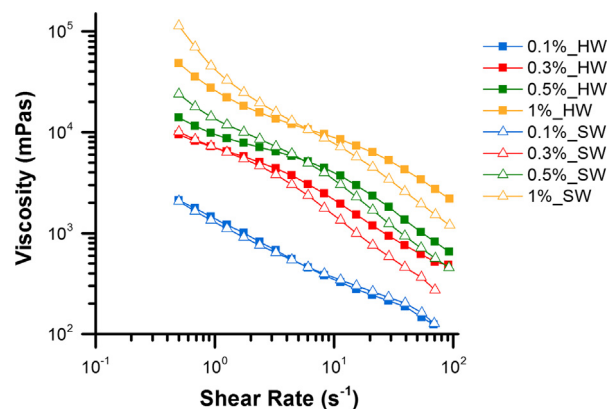


Fig. 5. Viscosity Profile of TOCNs from hardwood (solid symbol) and softwood (open symbol) as a function of concentration for constant charge density ($1 \text{ mmol}\cdot\text{g}^{-1}$). Measurements were done at 25°C .

pulp sources, attributed to the preferential oxidation of the weak amorphous regions subsequently cleaved under intense mechanical fibrillation [34]. This is evident in the XRD spectra (Supporting Information) as the small reduction in the crystalline index (CI) could not account for the large degree of fibrillation which we have observed. On average, the resulting HW-TOCNs are longer than SW-TOCNs ($1.30 \mu\text{m}$ versus $0.85 \mu\text{m}$) for a surface charge of $1 \text{ mmol COO}^-\cdot\text{g}^{-1}$.

4.2. Effect of nanofibre dimensions and surface charge on gel rheology

TEMPO-oxidised nanocellulose are characterized by two key parameters: physical dimensions (length and width) and surface charge. For TOCNs, provided sufficient electrostatic repulsion and mechanical fibrillation, width is determined by the elementary fibril width which is similar for hardwood and softwood pulp [35]. Length, on the other hand, can vary depending on the processing conditions [2]. The change in length of a semi-flexible fibre affects the extent and ability of entanglement. For SW-TOCN and HW-TOCN, the difference in fibre lengths is most evident at the onset (i.e. critical strain values) of yielding and steady-state shear (i.e. viscosity) behavior. Across all concentrations, the shorter SW-TOCNs consistently yielded at higher strains than HW-TOCNs. This might be due to a longer persistence length, related to the flexibility and stiffness of the crystalline domains of softwood, affecting nanofibre conformation upon shear [32].

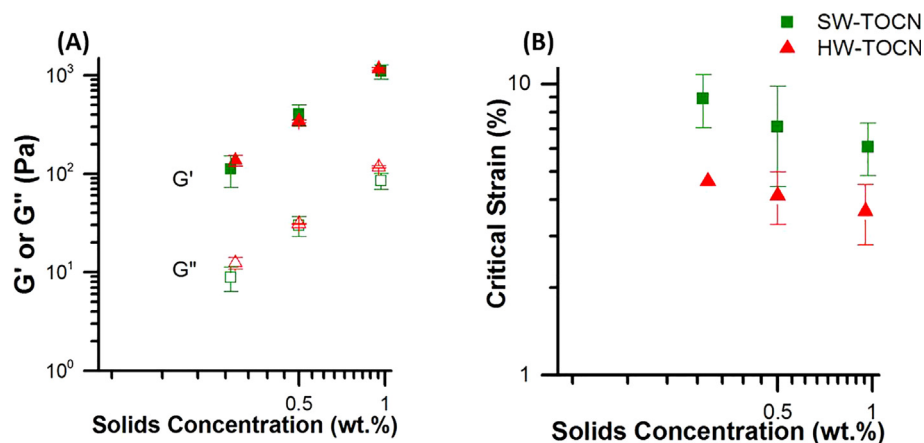


Fig. 4. (A) Dynamic Moduli (G' and G'') of nanocellulose gels produced from unrefined softwood and hardwood as a function of solids concentration at constant charge density ($1 \text{ mmol}\cdot\text{g}^{-1}$). (B) Critical Strain of SW-TOCN and HW-TOCN as a function of solids concentration.

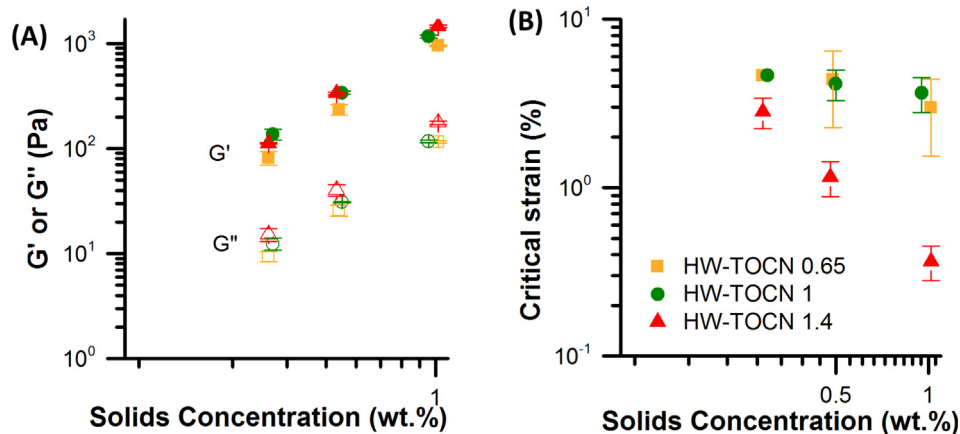


Fig. 6. The effect of charge density on the (A) dynamic moduli at LVR and (B) critical strain of HW-TOCN nanocellulose gels at different solids concentrations. Yellow symbols for 0.65 mmol.g⁻¹, green symbols for 1 mmol.g⁻¹ and red symbols for 1.4 mmol.g⁻¹. Measurements were done at 25 °C, 1 Hz.

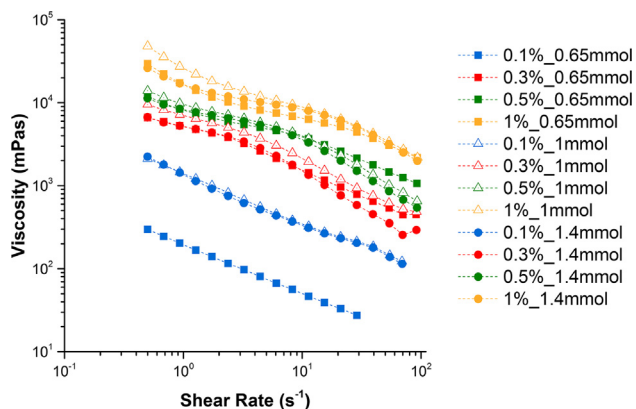


Fig. 7. Viscosity Profile for HW-TOCNs at three levels of charge density (0.65, 1, and 1.4 mmol.g⁻¹) and different solids content. Measurements were done at 25 °C.

Nanocellulose gels exhibit shear-thinning response which is generally understood to be due to the alignment of fibres along the shear direction. As seen in Fig. 5, for concentrations ranging between 0.3 and 1 wt%, SW-TOCNs have steeper viscosity gradients than HW-TOCNs due to easier alignment of the shorter fibres. However, this difference does not seem to affect the percolation threshold which is identified as the concentration wherein there is no double yielding behavior [20]. The double-yielding phenomenon in nanocellulose is attributed to the reorientation of fibres from an isotropic (i.e. randomly oriented) state to partial alignment in the direction of flow. At high fibre concentrations, higher shear rates are required to disrupt any remaining isotropic micro-domains, which leads to a further decrease in viscosity [36]. For both softwood and hardwood-based nanocellulose, the percolation concentration is 0.1 wt%. Moreover, the dynamic moduli in the LVR region are not significantly different from both pulp types and are primarily concentration-dependent (Fig. 4A).

Effective surface charge arising from the nanocellulose carboxylate groups dictates the colloidal stability of the gels [20]. HW-TOCN gel with the lowest charge density (0.65 mmol.g⁻¹) has lower moduli than HW-TOCN gels of higher charge density (Fig. 6A). A higher surface charge creates stronger and more stable gels due to higher electrostatic repulsion. The gel critical strain is affected by the variation in the surface charges (Fig. 6B). At 1.4 mmol.g⁻¹, the critical strain decreases at increasing concentration. This is not a direct effect of the fibre dimensions as we should observe some differences between 0.65 mmol.g⁻¹ and 1 mmol.g⁻¹.

The observations at 1.4 mmol.g⁻¹ can be attributed to the repulsive charges among fibres which act as lubricant allowing fibres to slide past each other [37]. Hence, the combination of high surface charge and high fibre concentration results in stronger repelling, partially hydrated fibres per unit volume, which reduces the required minimum strain for yielding. Comparing three levels of carboxylation (Fig. 7) reveals a significant impact on viscosity at the percolation threshold. At 0.1 wt% concentration, the reduction in the surface charge to 0.65 mmol.g⁻¹ results in an order of magnitude reduction in gel viscosity, possibly due to the less constrained nature of the fibre interactions. A fibre containing low surface charge is expected to have less interactions with other neighbouring fibres as it has a lower effective electrical double layer.

5. Conclusion

TEMPO-oxidised cellulose nanofibres (TOCNs) are semi-flexible fibrils derived from the primary alcohol oxidation of cellulose-based sources. Previous studies have primarily focussed on integrating TOCNs into other compatible materials to improve their bulk properties [4,5,10,14]. Some fundamental studies have been conducted, aiming to understand the colloidal stability [20,23], local flow phenomenon [12,21], and model rheological behavior [26,27]. The effect of different process conditions (i.e. bleach content and pH, primary oxidant) have been explored previously [2,38,39], however little is known on how the fibre source and its dimensions affect the rheological properties of nanocellulose gels. This study analysed the effect of wood pulp source and the resulting nanocellulose fibre dimensions on the rheology of nanocellulose gels. Kraft pulped and bleached hardwood (*Eucalyptus* sp.) and softwood (*Pinus Radiata*) contained fibres with significantly different dimensions ($L = 0.6$ mm, $W = 17$ μ m and $L = 1.4$ mm, $W = 34$ μ m, respectively) but similar aspect ratios (36 and 42 respectively). However, the initial fibre size has minimal effect on the degree of fibrillation, resulting in hardwood and softwood nanocellulose fibers (HW-TOCN and SW-TOCN) with similar widths in the order of nanometers, indicating elementary fibrils. In terms of length, HW-TOCN fibres are longer than SW-TOCN ($L = 1.3$ μ m and $L = 0.9$ μ m, respectively). The decrease in length from initial macro-fibres for both pulp sources is attributed to the preferential oxidation at weak amorphous regions cleaved under intense mechanical fibrillation. This difference in length affects the onset of yielding (i.e. critical strain) and the evolution of the viscosity curves at increasing solids content. This is particularly evident via rheology at the semi-dilute concentrations (0.3–1 wt%) – shorter SW-TOCN fibres display a steeper viscosity gradient in con-

trast to HW-TOCNs. Surface charge also impacts the rheological properties at the percolation threshold – for 0.1 wt% HW-TOCN, increasing the surface charge from 0.65 to at least 1 mmol·g⁻¹ results in higher viscosity due to greater electrostatic interactions. However, at higher concentrations, fibre length and surface charge have minimal effect, and instead the gel dynamic rheological properties (G' and G'') are primarily affected by fibre concentration. These results indicate that, at fibre concentrations greater than the percolation threshold, nanocellulose gels can be produced with similar properties regardless of pulp source and minimal surface charge. This is a key finding beneficial for engineering nanocellulose gels for any specific biomedical or rheology application.

Acknowledgments

This work was funded by the ARC Bioprocessing Advance Manufacturing Industry Research Transformation (BAMI) Hub IH13100016, Visy, Norske Skog, Orora, CHH/Oji Paper, Australian Paper and Circa. Many thanks to Australian Paper and Oji Fibre Solutions for providing the pulp. Paul Banham (Norske Skog) for Fibrelab results. Dr. Rico Tabor for his insightful discussion about colloids and rheology. Dr. Vikram Raghuvanshi and Dr. Jisheng Ma (Monash X-ray Platform) for their assistance in performing XRD measurements. This research used equipment (Bruker D8 Discover) funded by Australian Research Council grant LE130100072.

Appendix A. Supplementary material

Supplementary data associated with this article can be found, in the online version, at <https://doi.org/10.1016/j.jcis.2018.04.077>.

References

- [1] N. Quennouz et al., Rheology of cellulose nanofibrils in the presence of surfactants, *Soft Matter* 12 (1) (2016) 157–164.
- [2] A. Isogai, T. Saito, H. Fukuzumi, TEMPO-oxidized cellulose nanofibers, *Nanoscale* 3 (1) (2011) 71–85.
- [3] R.S. Reiner, A.W. Rudie, Experiences with scaling-up production of TEMPO-grade cellulose nanofibrils, in: *Nanocelluloses: Their Preparation, Properties, and Applications*, American Chemical Society, 2017, pp. 227–245.
- [4] S. Fujisawa et al., Superior reinforcement effect of TEMPO-oxidized cellulose nanofibrils in polystyrene matrix: optical, thermal, and mechanical studies, *Biomacromolecules* 13 (7) (2012) 2188–2194.
- [5] M. Bulota, M. Hughes, Toughening mechanisms in poly(lactic) acid reinforced with TEMPO-oxidized cellulose, *J. Mater. Sci.* 47 (14) (2012) 5517–5523.
- [6] S. Morimune-Moriya et al., Hydroxyapatite formation on oxidized cellulose nanofibers in a solution mimicking body fluid, *Polym. J.* 47 (2) (2015) 158–163.
- [7] J. Cheng, M. Park, J. Hyun, Thermoresponsive hybrid hydrogel of oxidized nanocellulose using a polypeptide crosslinker, *Cellulose* 21 (3) (2014) 1699–1708.
- [8] N.E. Zander et al., Metal cation cross-linked nanocellulose hydrogels as tissue engineering substrates, *ACS Appl. Mater. Interfaces* 6 (21) (2014) 18502–18510.
- [9] J. Feng et al., Antimicrobial activity of silver nanoparticles in situ growth on TEMPO-mediated oxidized bacterial cellulose, *Cellulose* 21 (6) (2014) 4557–4567.
- [10] S.-S. Kim et al., High-Fidelity bioelectronic muscular actuator based on graphene-mediated and TEMPO-oxidized bacterial cellulose, *Adv. Funct. Mater.* 25 (23) (2015) 3560–3570.
- [11] A. Shimotodome et al., Regulation of postprandial blood metabolic variables by TEMPO-oxidized cellulose nanofibers, *Biomacromolecules* 12 (10) (2011) 3812–3818.
- [12] O. Nechyporchuk, M.N. Belgacem, F. Pignon, Concentration effect of TEMPO-oxidized nanofibrillated cellulose aqueous suspensions on the flow instabilities and small-angle X-ray scattering structural characterization, *Cellulose* 22 (4) (2015) 2197–2210.
- [13] A. Azetsu et al., Direct synthesis of gold nanocatalysts on TEMPO-oxidized pulp paper containing aldehyde groups, 8 (2013).
- [14] N. Isobe et al., TEMPO-oxidized cellulose hydrogel as a high-capacity and reusable heavy metal ion adsorbent, *J. Hazard. Mater.* 260 (2013) 195–201.
- [15] F. Jiang, Y.-L. Hsieh, Super water absorbing and shape memory nanocellulose aerogels from TEMPO-oxidized cellulose nanofibrils via cyclic freezing-thawing, *J. Mater. Chem. A* 2 (2) (2014) 350–359.
- [16] H. Koga et al., Transparent, conductive, and printable composites consisting of TEMPO-oxidized nanocellulose and carbon nanotube, *Biomacromolecules* 14 (4) (2013) 1160–1165.
- [17] R. Tanaka et al., Influence of flexibility and dimensions of nanocelluloses on the flow properties of their aqueous dispersions, *Biomacromolecules* 16 (7) (2015) 2127–2131.
- [18] L. Jowkarderis, T.G.M. van de Ven, Intrinsic viscosity of aqueous suspensions of cellulose nanofibrils, *Cellulose* 21 (4) (2014) 2511–2517.
- [19] S. Varanasi, R. He, W. Batchelor, Estimation of cellulose nanofibre aspect ratio from measurements of fibre suspension gel point, *Cellulose* 20 (4) (2013) 1885–1896.
- [20] L. Mendoza et al., Gelation mechanism of cellulose nanofibre gels: a colloids and interfacial perspective, *J. Colloid Interface Sci.* 509 (2018) 39–46.
- [21] B. Nazari et al., Rheology of cellulose nanofibers suspensions: boundary driven flow, *J. Rheol.* 60 (6) (2016) 1151–1159.
- [22] M. Iotti et al., Rheological Studies of microfibrillar cellulose water dispersions, *J. Polym. Environ.* 19 (1) (2011) 137–145.
- [23] M. Nordenström et al., Formation of colloidal nanocellulose glasses and gels, *Langmuir* 33 (38) (2017) 9772–9780.
- [24] F. Martoia et al., Micro-mechanics of electrostatically stabilized suspensions of cellulose nanofibrils under steady state shear flow, *Soft Matter* 12 (6) (2016) 1721–1735.
- [25] L. Jowkarderis, T.G.M. van de Ven, Rheology of semi-dilute suspensions of carboxylated cellulose nanofibrils, *Carbohydr. Polym.* 123 (2015) 416–423.
- [26] A. Puiisto et al., Modeling the rheology of nanocellulose suspensions, *Nord. Pulp Pap. Res. J.* 27 (2) (2012) 277–281.
- [27] A. Puiisto et al., Modeling the viscosity and aggregation of suspensions of highly anisotropic nanoparticles, *Eur. Phys. J. E* 35 (1) (2012) 6.
- [28] T. Moberg et al., Rheological properties of nanocellulose suspensions: effects of fibril/particle dimensions and surface characteristics, *Cellulose* 24 (6) (2017) 2499–2510.
- [29] D. da Silva Perez, S. Montanari, M.R. Vignon, TEMPO-mediated oxidation of cellulose III, *Biomacromolecules* 4 (5) (2003) 1417–1425.
- [30] P. Martínez, M. Pereira, R.T. Mendonça, Retention and structure of xylans from eucalyptus globulus genotypes with different pulpwood characteristics, *J. Wood Chem. Technol.* 35 (2) (2015) 129–136.
- [31] N. Cruz et al., Impact of the chemical composition of pinus radiata wood on its physical and mechanical properties following thermo-hygro-mechanical densification, 13 (2018).
- [32] I. Usov et al., Understanding nanocellulose chirality and structure-properties relationship at the single fibril level, *Nat. Commun.* 6 (2015) 7564.
- [33] L. Geng et al., Understanding the mechanistic behavior of highly charged cellulose nanofibers in aqueous systems, *Macromolecules* 51 (4) (2018) 1498–1506.
- [34] R. Zimmermann et al., Oxidation and structural changes in NMMO-regenerated cellulose films, *Cellulose* 23 (6) (2016) 3535–3541.
- [35] G. Chinga-Carrasco, Y. Yu, O. Diserud, Quantitative electron microscopy of cellulose nanofibril structures from eucalyptus and pinus radiata kraft pulp fibers, *Microsc. Microanal.* 17 (4) (2011) 563–571.
- [36] E. Lasseguette, D. Roux, Y. Nishiyama, Rheological properties of microfibrillar suspension of TEMPO-oxidized pulp, *Cellulose* 15 (3) (2008) 425–433.
- [37] M.A. Hubbe et al., Rheology of Nanocellulose-rich Aqueous Suspensions: A Review, 12 (2017)
- [38] A.E.J. de Nooy, A.C. Besemer, H. van Bekkum, Highly selective tempo mediated oxidation of primary alcohol groups in polysaccharides, *Recl. Trav. Chim. Pays-Bas* 113 (3) (1994) 165–166.
- [39] K. Benhamou et al., Control of size and viscoelastic properties of nanofibrillated cellulose from palm tree by varying the TEMPO-mediated oxidation time, *Carbohydr. Polym.* 99 (Supplement C) (2014) 74–83.

Effects of Fibre Dimension and Charge Density on Nanocellulose Gels – Supplementary Information

Llyza Mendoza¹, Thilina Gunawardhana¹, Warren Batchelor¹ and Gil Garnier^{1,}*

¹Bioresource Processing Research Institute of Australia (BioPRIA), Department of Chemical Engineering, Monash University, VIC 3800, Australia

*Email: gil.garnier@monash.edu

X-Ray Diffraction (XRD) Analysis

The crystallinity of several TEMPO-mediated oxidised cellulose samples (pre- and post-homogenised) was measured by XRD analysis (Bruker D8 Discover). Approximately 0.25 dry grams of sample is casted on a silicone tray and dried in an oven at 40°C. The casted sheets are then frozen at -86°C (Labec -86°C Freezer) and then lyophilised (Christ Beta 1-8 LD plus) to remove any residual moisture. The XRD measurement was performed using Cu K α ($\lambda = 1.5148 \text{ \AA}$) radiation with a step size 0.02° at 2θ between 10° and 30°. The crystallinity index (CI) for each sample is calculated with the following relationship:

$$CI (\%) = \frac{I_{002} - I_{am}}{I_{002}} \times 100\%$$

where I_{002} is the intensity of crystalline cellulose ($2\theta = 22.5^\circ$) and I_{am} is the intensity of the amorphous region ($2\theta = 18^\circ$). Figure S1 illustrates the resulting XRD results for the pre- and post-homogenised samples.

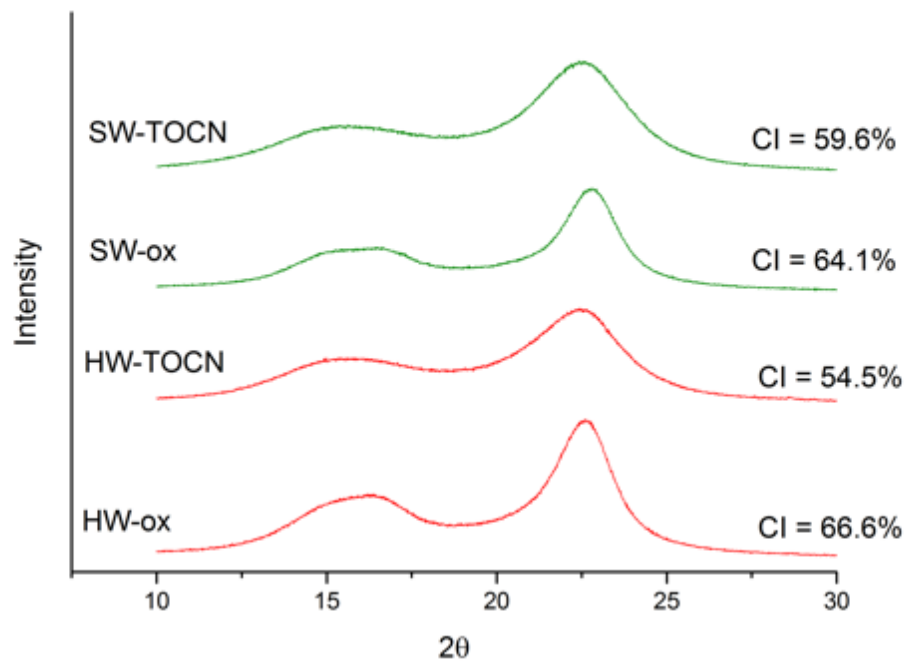


Figure S1. X-ray diffraction spectra of pre-homogenised (SW-ox, HW-ox) and post-homogenised softwood (SW-TOCN) and hardwood (HW-TOCN) pulp.



Contents lists available at ScienceDirect

Journal of Colloid and Interface Science

journal homepage: www.elsevier.com/locate/jcis

Regular Article

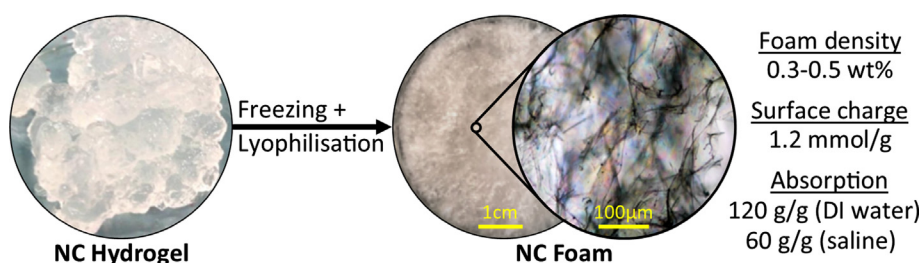
Carboxylated nanocellulose foams as superabsorbents

Llyza Mendoza, Laila Hossain, Emma Downey, Camilla Scales, Warren Batchelor, Gil Garnier*



Bioresource Processing Research Institute of Australia (BioPRIA), Department of Chemical Engineering, Monash University, VIC 3800, Australia

GRAPHICAL ABSTRACT



ARTICLE INFO

Article history:

Received 25 October 2018
 Revised 29 November 2018
 Accepted 30 November 2018
 Available online 1 December 2018

Keywords:

Superabsorbent
 TEMPO-mediated oxidation
 Nanocellulose
 Foam
 Structure

ABSTRACT

Hypothesis: Carboxylated nanocellulose fibres formed into foam structures can demonstrate superabsorption capacity. Their performance can be engineered by changing process variables.

Experiments: TEMPO-oxidised cellulose nanofibres of varying concentration and surface charge are produced from hardwood kraft pulp. Foams were prepared through a 2-step freezing and lyophilisation process. The absorption capacity of water and saline solution (0.9 wt%) were measured as a function of time and related to the foam structure.

Findings: The absorption capacity of nanocellulose foams can be manipulated from initial gel properties and processing conditions. Pore structure and distribution of nanocellulose foams are dictated by fibre content and charge density and freezing rate. The best performing foams are at 0.3–0.5 wt%, with a carboxylate concentration of 1.2 mmol/g and frozen at -86°C before freeze-drying, which can absorb 120 g $\text{H}_2\text{O/g}$ fibre. Fibre surface charge influences the absorption capacity of the foams by dictating the amount of participating carboxylate groups. Absorption capacity in saline (60 g/g) is lower than in deionised water (120 g/g); but is only slightly lower than that of a commercial polyacrylic acid (PAA) SAPs (80 g/g). Nanocellulose foams are attractive renewable alternatives for superabsorbent applications, contributing to a reduction of plastic microspheres.

Crown Copyright © 2018 Published by Elsevier Inc. All rights reserved.

1. Introduction

Superabsorbent polymer (SAP) hydrogels contain cross-linked network of hydrophilic polymers capable of absorbing large volumes of water [1]. Upon contact with water, the glassy polymers hydrate to form a three-dimensional network which does not dissolve due to the presence of cross-linking [2]. The swelling of these

polymer networks is driven by the difference in osmotic pressure inside and outside the gel caused by the movement of the counterions in the system. The high absorption of water molecules is due to a high concentration of COO^- groups able to form hydrogen bonding with water molecules [3]. Although commercial SAPs are usually known for applications in personal care and hygiene products, these materials are also increasingly utilised in agriculture and horticulture [4], biomedical products [5–7], and even wastewater treatment [8,9]. Currently, the majority of superabsorbent products in the market is synthesised from acrylic and acrylamide

* Corresponding author.

E-mail address: gil.garnier@monash.edu (G. Garnier).

polymers from petrochemicals which exhibit poor environmental degradability. This lack of sustainability has driven research towards developing alternatives which are renewably sourced and biodegradable.

There are many reports of superabsorbents made from natural polymers in literature. Natural-based SAPs, such as chitosan, gelatine, carrageenan and starch, have been modified to increase water absorption [10,11]. Cellulose, the most abundant biopolymer, has also been studied for its desirable characteristics: biodegradability, renewability, and innate hydrophilicity [12]. Cellulose can be processed into porous materials such as foams [13,14] and different synthesis methods have been explored to functionalise cellulose as a superabsorbent hydrogel [12]. Among those are foam and hydrogel composites made with carboxymethyl cellulose [15–19] and hydroxyethyl cellulose [20,21] used in combination with other polymers and nanoparticles. Another strategy is to graft side groups such as butanetetracarboxyl, acrylic, and acrylamide groups onto the cellulose backbone which results in large absorption of water (~720 g/g) [22,23]. Functionalising the cellulose hydroxyl groups can significantly increase water interactions.

Another method of producing foams is through the production of nanocellulose and manufacture of foams via ice-templating followed by sublimation or via supercritical drying [24]. TEMPO-mediated oxidation is alternative method of functionalising cellulose fibres [25]. This oxidation process selectively converts the primary alcohol (C6) groups into carboxylate groups. The added electrostatic repulsion produces nano-scale fibres upon mechanical fibrillation. Brodin and Theliander initially tested the superabsorbent characteristics of TEMPO-oxidised nanocellulose by varying different process conditions such as pulp types, composition, and oxidation severity [26–29]. Jiang and Hsieh investigated the production of nanocellulose aerogels via cyclic freeze-thawing process and also introduced functionalisation to create oleophilic foams [30–32]. However, the effects of varying foam properties by changing the fibre density were not explored nor related to composite structure. There are limited studies on the effect of processing conditions (i.e. freezing rate) on the performance of nanocellulose foams. Moreover, the kinetics of nanocellulose foam swelling remain unknown.

In this study, we produced nanocellulose superabsorbent foams via a two-step process: (1) TEMPO-mediated oxidation/high-pressure homogenisation to produce a nanocellulose hydrogel [33,34] and (2) freeze-drying the hydrogel to produce nanocellulose foams. The aim of this study is to understand the relationship between process variables (freezing rate) and nanocellulose properties (surface charge and fibre concentration) to the resulting foam structure and absorption characteristics. The swelling kinetics of the foams is also determined. Insight into the mechanism of superabsorbency of these carboxylated nanocellulose foams is demonstrated.

2. Methodology

2.1. Materials

Bleached Eucalyptus Kraft (BEK) pulp, containing approximately 10 wt% solids, was obtained from Australian Paper, Maryvale, Australia. 2,2,6,6-Tetramethylpiperidine-1-oxyl (TEMPO) and sodium bromide (NaBr) were purchased from Sigma-Aldrich. Hydrochloric acid (HCl) and Sodium Hydroxide (NaOH) were diluted for solutions as required and were purchased from ACL Laboratories and Merck, respectively. 12 w/v% Sodium Hypochlorite (NaClO) was purchased from Thermo Fisher Scientific and used as received. Commercial sodium polyacrylate superabsorbent (HySORB R 8130) was provided by BASF.

2.2. TEMPO-mediated oxidation

The TEMPO-mediated oxidation process employed is based on a previously developed method [25]. 100 g BEK pulp was suspended in 2500 mL water containing 0.4 g TEMPO and 2.5 g NaBr. The 12 w/v% NaClO solution was initially adjusted to pH 10 via addition of 36 w/v% HCl. To produce high surface charged fibres, 75 mL NaClO (5 mmol NaClO/g cellulose) was added drop-wise to the suspension whilst stirred. Lower surface charged fibres were produced by adding a lower amount of the primary oxidant (50 mL NaClO, 3.33 mmol/g). The pH of the reaction was maintained at 10 through the addition of 0.5 M NaOH. The oxidation process is deemed to be complete when the pH change is negligible. The oxidised fibres were recovered through filtration and stored refrigerated (2–8 °C).

The TEMPO-oxidised pulp is then dispersed in deionised water at a desired concentration. Fibrillation is accomplished through a high-pressure homogeniser (GEA Niro Soavi Homogeniser Panda) at 1000 bar. Suspensions which contain less than 1 wt% TEMPO-oxidised pulp is homogenised with two passes. More concentrated suspensions are homogenised with only one pass.

2.3. Preparation of nanocellulose foams

Nanocellulose foams were prepared by spreading 15 g gel in a 50 mm petri dish and freezing at either in a freezer for at least 12 h (–20 °C, –80 °C) or in liquid nitrogen (–196 °C). For freezing at –196 °C, the samples were placed in a cold-proof container and liquid nitrogen was poured in ensuring full immersion for 4–5 min. Once frozen, all samples were freeze-dried (Christ Alpha 2–4 LD Plus) for 2 days.

2.4. Determining solids concentration

The solids concentration of any sample (i.e. hydrogel or pulp) is determined through oven drying. The sample is weighed before (w_i) and after (w_d) drying, where the sample moisture is evaporated in a ventilated oven at 105 °C for at least 4 h. The solids content is determined through the following equation:

$$\text{Solids content (\%)} = \frac{w_d}{w_i} \times 100\% \quad (1)$$

2.5. Determining the carboxylate content of nanocellulose

The carboxylate content of the nanocellulose fibre is determined via conductometric titration [35]. 0.1 dry g oxidised pulp is suspended in 40 mL deionised water. 100 μ L 1 wt% NaCl is added to the suspension to increase base sample conductivity. The sample pH is then lowered to pH 2.5–3 to protonate all of the carboxylate groups prior to the beginning of titration. Sample titration is initiated by the addition of 0.1 mL/min NaOH (Mettler Toledo T5 titrator). The conductivity is monitored throughout the progress of the titration. The amount of carboxylate groups is then calculated through the following equation:

$$\text{Carboxylate Content} \left(\frac{\text{mmol}}{\text{g}} \right) = \frac{c(V_2 - V_1)}{w} \times 100 \quad (2)$$

where V_2 and V_1 pertain to the required amount of titrant to neutralise the carboxylic groups (plateau region in the titration curve), c is the NaOH concentration (mol/L), and w is the dry sample weight.

2.6. Measurement of absorption capacity

The freeze-dried fibres are then allowed to be in contact with deionised water or 0.9 wt% NaCl solution for reabsorption. The foams were repeatedly taken out of immersion and weighed.

Intake of water by the foam is measured in regular intervals up to 2 h. The free swell capacity W is then calculated through the following equation:

$$\text{Free Swell Capacity, } W = \frac{m_t - m_i}{m_i} \quad (3)$$

where m_t is the mass of the swollen foam at a particular time interval and m_i is the initial mass of the foam. The results are reported as the average and standard deviation of 3 replicates.

2.7. Imaging of nanocellulose structure

Nanocellulose foams were imaged by optical microscopy (Nikon Eclipse Ni-E Upright Microscope) in bright-field mode at 5x magnification.

2.8. Mercury porosimetry

The pore size distribution, porosity (total and at $P = 1$ atm), and pore surface area were determined for selected nanocellulose foams via mercury porosimetry (Micromeritics Autopore IV). Nanocellulose foams were cut in small cubes ($0.5 \times 0.5 \times 0.5$ cm) by a laser cutter (Epilog Laser Helix). The samples were prepared by initially de-gassing (24 h, 100°C) followed by testing. Two replicates per sample were tested. In all measurements, the contact

angle at the Hg-Foam interface is assumed to be 130° and a testing pressure range from 0.1 to 60,000 psia is applied. The desired values are calculated via the Washburn Equation:

$$D = \frac{-4\gamma \cos \theta}{P} \quad (4)$$

where D is the pore diameter, γ is the surface tension of mercury, θ is the contact angle between the pore wall and mercury, and P is the applied pressure. Important values are reported at either as a result of considering 1 atm (14.7 psia) intrusion pressure or at total maximum porosimetry pressure (60,000 psia/4082 atm).

3. Results

The effect of initial gel properties such as the solids concentration and surface charge on the structure and morphology as well as the absorption behaviour of the foams is initially studied (frozen at -80°C). The effect of freezing rate is then analysed. Lastly, the best performing foam in distilled water is tested with saline and compared against a commercial SAP.

3.1. Effect of gel solids concentration

Fig. 1 shows the free swell capacity (FSC) of nanocellulose foams in deionised water as a function of the initial gel solids concentration in deionised water. In all cases, the initial rapid swelling is followed by a slower absorption process in the 2 h testing period. There is no significant difference between the performance of foams produced from 0.3 wt% and 0.5 wt% (overlapping error bars). Measurement error also increases at lower initial gel concentrations. However, increasing the fibre concentration in gel from 0.5 wt% to 1 and 3 wt% resulted in a decrease in the FSC values.

The pore size distribution of nanocellulose foams was measured by mercury porosimetry as a function of the initial gel solids concentration is shown in Fig. 2A. Calculated foam properties for each of the nanocellulose foams is also summarised in Fig. 2B and C. At increasing initial gel solids concentration, the foam bulk density consistently increases. Foam porosity is calculated at two pressure levels (1 atm and at 4082 atm) to signify pores accessible at atmospheric pressure and the total maximum pore volume, respectively. Total foam porosity is similar (>94%) across all original gel concentrations; however, porosity at 1 atm is halved when the solids content is increased by an order of magnitude. The total pore surface area also decreased with increasing gel solids concentration.

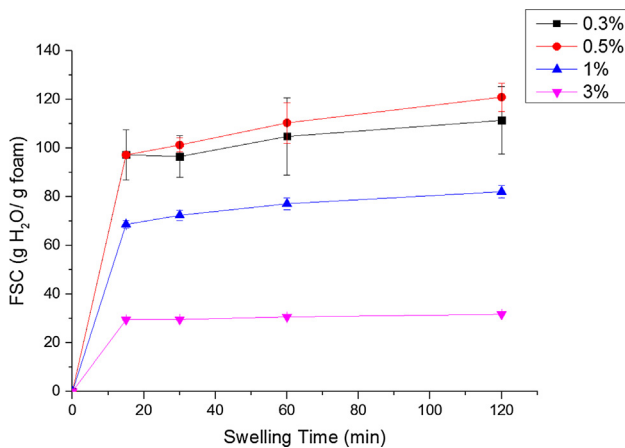


Fig. 1. Free Swell Capacity (FSC) in deionised water of nanocellulose foams (-80°C) at different solids concentrations as a function of swelling time.

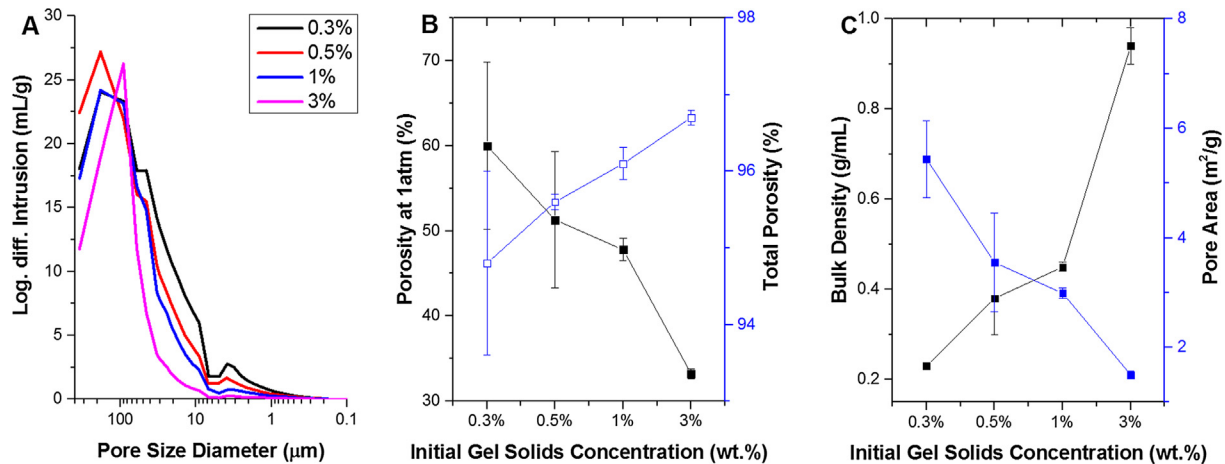


Fig. 2. (A) Pore size distribution of nanocellulose foams (-80°C) at different solids concentrations. Foam properties such as (B) porosity (1 atm^a and total^b), (C) bulk density and pore area derived from mercury porosimetry. Further details on porosimetry data and related calculations are provided in the Supplementary Information. Notes: ^aPorosity at 1 atm is calculated by: $\text{Porosity (1atm)} = \left(1 - \frac{\text{Bulk Density (1atm)}}{\text{Skeletal Density}}\right) \times 100\%$. ^bTotal porosity is calculated by: $\text{Total Porosity} = \left(\frac{\text{Pore Volume}}{\text{Skeletal Volume} + \text{Pore Volume}}\right) \times 100\%$.

3.2. Effect of surface charge

Fig. 3 shows the effect of the nanocellulose carboxylate group content on the foam absorption capacity. Lowering the carboxylate group from 1.2 mmol/g to 0.65 mmol/g resulted in lower absorption values for all concentrations tested.

3.3. Effect of freezing rate

The formation of nanocellulose foams is a two-step process which includes freezing of the nanocellulose gels and sublimation

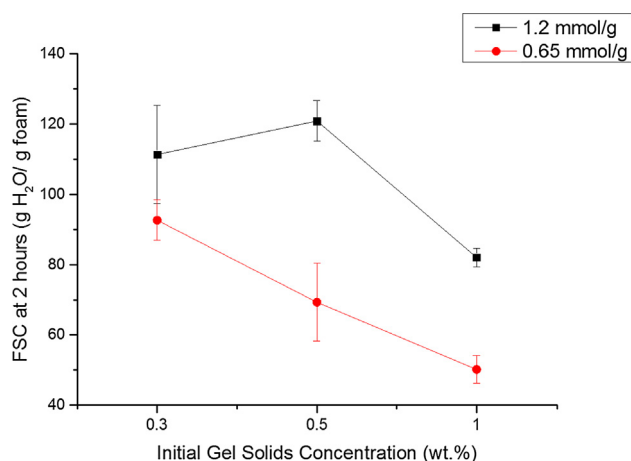


Fig. 3. Effect of cellulose fibre surface charge of nanocellulose foams (-80°C) at different solids concentration on FSC in deionised water.

of the frozen water. In this study, the effect of freezing rate is studied by freezing at different temperatures (-20°C , -80°C , -196°C). The freezing rate will be the slowest at -20°C whereas freezing at -196°C will be the fastest. The lyophilisation step is kept constant in this study. The effect of freezing rate on the performance of nanocellulose foams in absorbing deionised water is shown in Fig. 4A. Aside from 0.3 wt%, foams processed at -80°C has performed slightly better than -20°C . Freezing rate was modified to control foam morphology. Freezing at the lowest rate (-20°C) results in sheet-like structures with interspersed pores (Fig. 4B) whereas at the fastest freezing rate (-196°C), the pores formed are more uniform (Fig. 4D). At -80°C , the structure formed is a combination of those from the two freezing rates (Fig. 4C).

3.4. Absorption of saline

Fig. 5 shows the FSC of nanocellulose foam in 0.9 wt% saline. For all foams, lower FSC values are recorded in saline than in deionised water. Absorption after 2 h is very similar for all concentrations tested with capacity ranging between 50 g/g and 70 g/g. The saline absorption capacity of nanocellulose foams were slightly lower to those of commercial SAP (80 g/g).

4. Discussion

4.1. Effect of foam and fibre properties on superabsorbent capacity

In this study, fibre properties, including the initial solids concentration and surface charge, are varied to determine the effect on the superabsorption performance of nanocellulose gels. When the initial gel solids concentration was varied from 0.3 wt% to

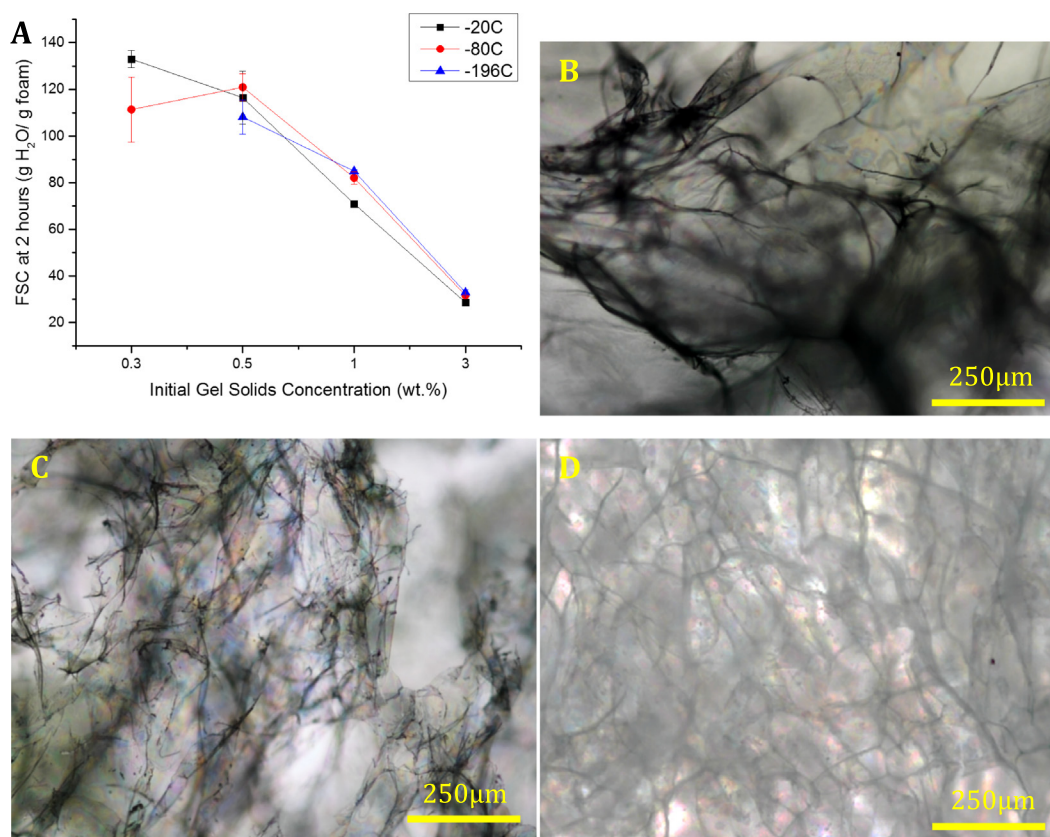


Fig. 4. (A) The effect of freezing rate (initial freezing at -20°C , -80°C , and -196°C) on the FSC in deionised water. Optical microscopy illustrating the effect of freezing at (B) -20°C (C) -80°C , and (D) -196°C on the morphology of nanocellulose foams.

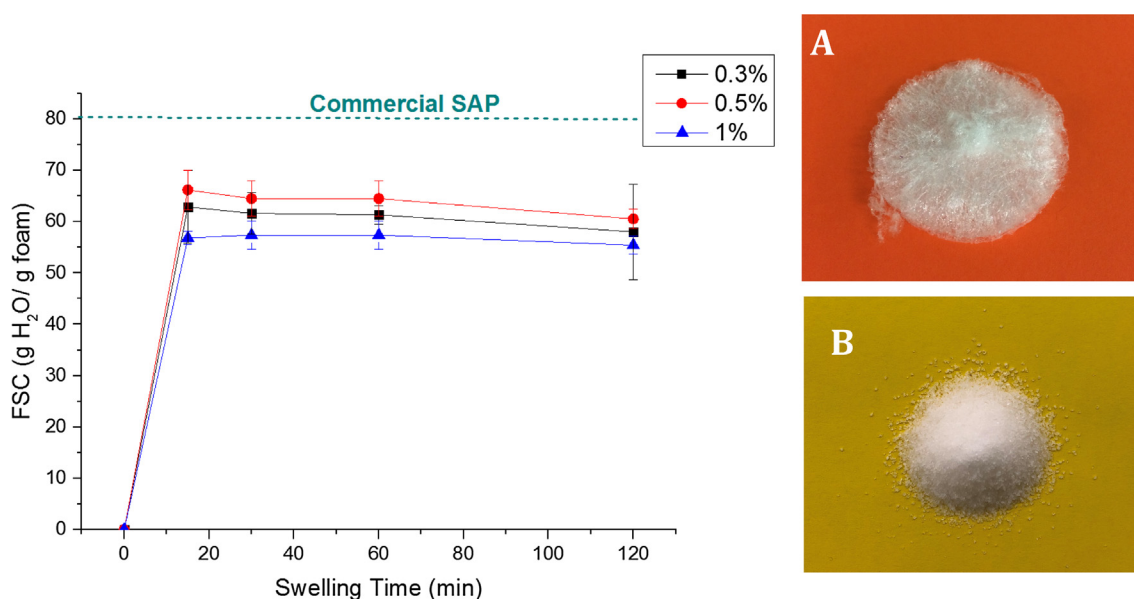


Fig. 5. FSC of nanocellulose (-80°C) in 0.9 wt% saline as a function of swelling time compared against the equilibrium absorption capacity of a commercial SAP polymer. Images showing a (A) NC foam and (B) commercial SAP polymer.

0.5 wt% (-80°C), FSC values were similar. However, further increase in the fibre concentration (0.5 wt% to 3 wt%) resulted in lower FSC values due to the limited availability of the foam internal structure because of a narrower pore distribution (Fig. 2). The percentage of accessible pores, quantified by the porosity at 1 atm, decreases with increasing initial solids concentration. For instance, increasing the fibre density by an order of magnitude (0.3 wt% to 3 wt%) resulted in halving ($\sim 50\%$ decrease) the available pores at 1 atm. However, the high absorption capacity of nanocellulose cannot be explained merely by the available pore volume shown in Fig. 6. For instance, the foam from 0.5 wt% gel, which is capable of absorbing 120 g/g, has a calculated volume of easily accessible pores of 1.4 mL/g foam (at 1 atm) and a total pore volume of 29 mL/g foam. The available pore volume cannot solely take into account such a large absorption. This means that the 0.5 wt% foam structure needs to significantly expand by a factor four its initial volume. The absorption capacity of nanocellulose can be attributed largely to the swelling of the fibre network leading to physical entrapment of liquid water loosely held between nanofibres by capillary forces. This is in contrast to the absorption mechanism

of conventional polyacrylic SAPs which are composed of longer polymer chains ($DP = \sim 20,000$ [36], compared to nanocellulose $DP = \sim 600$ [37]) with a higher density of COO^- groups participating in hydrogen bonding with water.

Fibre surface charge is indicative of the amount of COO^- groups which participate to water absorption. Fibrous structures with a higher concentration of COO^- groups can be expected to have higher absorption and FSC values. Nanocellulose fibres have a theoretical and demonstrated upper carboxylate limit of 1.6 mmol/g fibre [38]. Our fibres contain 1.2 mmol COO^- /g fibre, indicating near-complete oxidation of the C6 hydroxyl group. Doubling the carboxylate content on the cellulose polymer resulted in an increase in the absorption capacity (19 g/g to 51 g/g), as shown in Fig. 3.

4.2. Swelling kinetics of nanocellulose foams

The swelling of nanocellulose foams over time can be characterised by two distinct regimes: (a) the initial rapid uptake of absorbate and (b) the asymptotic increase of absorption towards the equilibrium absorption capacity W_{∞} (Fig. 1) [39]. Swelling kinetic parameters such as the equilibrium absorption capacity W_{∞} (g/g) and swelling rate constant k_s (g/g min) describing the swelling kinetics of the foams can be estimated by assuming a second order rate of swelling of absorption W (g/g) at swelling time t (min) as derived by Schott [40]:

$$\frac{dW}{dt} = k_s(W_{\infty} - W)^2 \quad (5)$$

Eq. (5) can be linearised by setting the following conditions: $W = 0$ at $t = 0$ and $W = W$ at $t = t$, resulting in Eq. (4):

$$\frac{t}{W} = A + Bt \quad (6)$$

where:

$$B = \frac{1}{W_{\infty}} \quad (7)$$

$$A = \frac{1}{\left(\frac{dW}{dt}\right)_0} \quad (8)$$

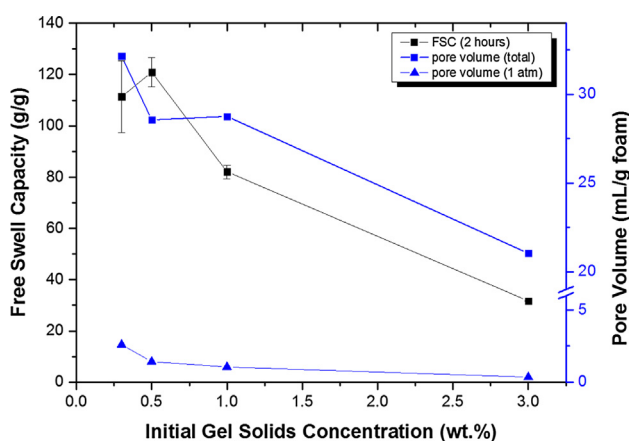


Fig. 6. Effect of the initial gel solids content on the superabsorbent nanocellulose foam FSC (-80°C) in deionised water (2 h) and available pore volume at 1 atm and total pore volume from mercury porosimetry.

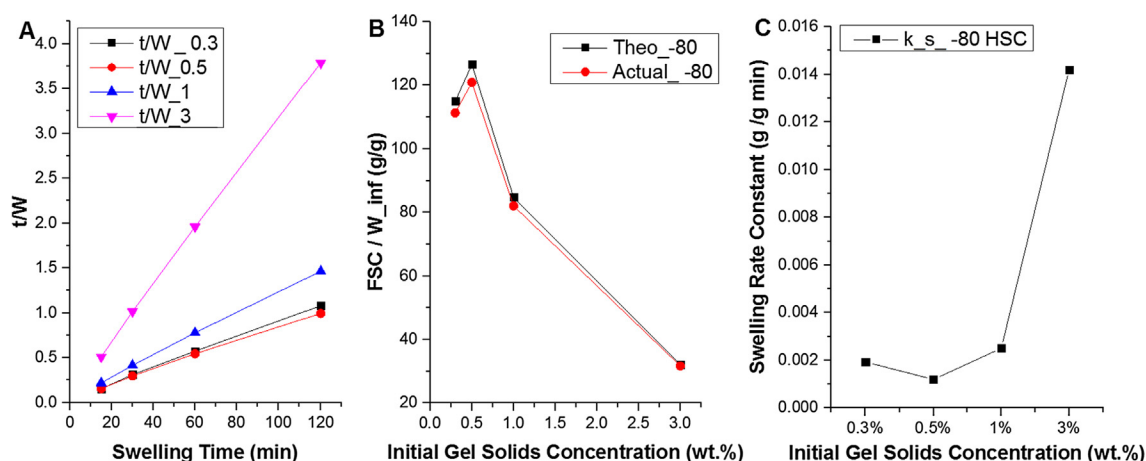


Fig. 7. Calculated swelling kinetic parameters of nanocellulose foams ($-80\text{ }^{\circ}\text{C}$): (A) Linearisation of FSC by Schott's equation (B) equilibrium absorption capacity W_{∞} and (C) swelling rate constant.

$$k_s = \frac{1}{AW_{\infty}^2} \quad (9)$$

Linearising Eq. (6) by plotting t/W versus t provides good fit with the experiments ($R^2 > 0.99$) (Fig. 7A). This suggests that the second-order kinetic assumption with respect to capacity is indicative either of a bimolecular mechanism (water-cellulose) or of a system with diffusion constraints. The actual absorption capacity at 2 h is close to the theoretical capacity W_{∞} , which indicates that the foams reach saturation within the testing period (Fig. 7B). In all concentrations tested, at least 90% of the theoretical capacity was reached within the first 30 min of testing – independent of the initial gel concentration. The foam swelling rate constant is constant between 0.3 wt% and 1 wt% and increased dramatically at 3 wt% (Fig. 7C). The increase in the swelling rate constant at increasing solids content can be due to saturation reached much faster because of smaller pores and numerous inaccessible carboxylate groups leading to an overall lower free swell capacity.

4.3. Effect of freezing rate and absorbate on superabsorbent capacity

The freezing rate of nanocellulose before lyophilisation dictates either nucleation or crystal growth of ice in the gel influencing the nanocellulose porous structure [41]. Freezing at $-20\text{ }^{\circ}\text{C}$ promotes the crystallisation of larger ice crystals as the degree of supercooling is low [41]. Hence, large pores are produced in certain regions where the ice crystals are formed, and individual fibres are aggregated forming sheet-like structures together, as seen from Fig. 4B. Freezing at a faster rate ($-80\text{ }^{\circ}\text{C}$) led to an intermediate state wherein there are still sheets formed with the hornified fibres producing a more uniform structure. Vitrification of the network structure is promoted by freezing at a much faster rate ($-196\text{ }^{\circ}\text{C}$) producing a more homogeneous pore structure. This is due to the fibre spacing present within the gel structure (electrostatic repulsion) being maintained upon foam formation. In this instance, the higher rate of freezing promoted the rapid nucleation of smaller ice crystals leading to a more homogenous pore structure [42]. The foams produced at $-196\text{ }^{\circ}\text{C}$ however were brittle and difficult to handle in contrast to those treated at $-20\text{ }^{\circ}\text{C}$ and $-80\text{ }^{\circ}\text{C}$. Other studies have corroborated with our findings and also reported brittle foams produced from freezing in liquid nitrogen [30,43]. Hence, it was rather difficult to test low solids content foams such as 0.3 wt%; these results were omitted from Fig. 4A. Although, the morphologies of nanocellulose structures are visibly affected by the freezing rate, the absorption capacity remains similar. This

could be due to the hornified fibres in foams prepared at $-20\text{ }^{\circ}\text{C}$ and $-80\text{ }^{\circ}\text{C}$ that separate partially while swelling.

The lower values of absorption in saline compared to deionised water is due to the charge shielding from the ions. This reduces the interaction with the COO^- groups and the water molecules. The saline capacity of the nanocellulose foams is similar to those reported by Theliander et al. with FSCs ranging between 30 and 60 g/g [26–29]. The performance of the nanocellulose foams is slightly lower in contrast to a granulated commercial polyacrylic acid SAP. Further optimising the method to produce the foams may yield similar performance to commercial SAPs.

5. Conclusion

Cellulose-based superabsorbents were investigated as sustainable substitutes for the current acrylic acid and acrylamide-based SAPs. While numerous studies have examined cellulose-based superabsorbents using various methodologies, few have analysed the SAP structure-performance relationship of TEMPO-oxidised nanocellulose foams [26–29,44]. In particular, the effect of fibre content and processing conditions (ie. freezing conditions) were not investigated. Moreover, the kinetics and mechanism of absorption for nanocellulose have not been studied. TEMPO-mediated oxidation produces charged nanocellulose fibres capable of forming cellulosic colloidal gels. The carboxylate groups of TEMPO-oxidised nanocellulose can be exploited for superabsorption. In this study, the potential of TEMPO-oxidised fibres as a superabsorbent polymer is demonstrated. The effect of fibre properties and processing conditions on the resulting nanocellulose foam morphology and its superabsorption performance is determined. Nanocellulose foam density is dictated by the initial gel solids concentration. The best performing foams are at 0.3–0.5 wt% frozen at $-80\text{ }^{\circ}\text{C}$ which are capable of absorbing 110–120 g/g H_2O . In general, a higher solids concentration produces foams with a narrower pore size distribution and a lower porosity leading to a decreased absorption performance. Nanocellulose foams follow a pseudo-second order absorption kinetics which is affected by foam density. Freezing temperature affects the foam network structure by dictating whether ice nucleation or crystallisation dominates, expanding or not the fibrous structure. A homogeneous porous structure is formed at the fastest freezing rate ($-196\text{ }^{\circ}\text{C}$) whereas uneven sheet-like formations were observed at lower freezing rates ($-20\text{ }^{\circ}\text{C}$, $-80\text{ }^{\circ}\text{C}$). The free swell capacity remained unaffected even with differences in morphology. Changing the absorbate from deionised water to 0.9 wt% NaCl, mimicking bodily fluids, resulted in

the decrease of free swell capacity (FSC) values due to charge shielding. However, the nanocellulose foam performance in saline is already comparable with granulated polyacrylamide SAPs which have been optimised over the last 3 decades. With the results already achieved, the clear link between process-structure-properties and a robust optimization methodology, matching the properties of the current commercial polyacrylic superabsorbent polymers has become a realistic target for cellulose composites. Absorption behaviour in saline can be further improved by blending nanocellulose with biopolymers and optimising the shape and microstructure of foams. Nanocellulose foams has emerged as a high performance, renewable and biodegradable superabsorbent material for biomedical, personal care and environmental applications.

Acknowledgments

This work was funded by the ARC Bioprocessing Advance Manufacturing Industry Research Transformation (BAMI) Hub IH13100016, Visy, Norske Skog, Orora, Oji Fibre Solutions, Australian Paper and Circa. Special thanks to Anthony De Girolamo (Monash University) for running the porosimetry experiments.

Appendix A. Supplementary material

Supplementary data to this article can be found online at <https://doi.org/10.1016/j.jcis.2018.11.112>.

References

- [1] J.R. Gross, in: *Studies in Polymer Science*, Elsevier, 1990, p. 3.
- [2] H. Omidian, S.A. Hashemi, P.G. Sammes, I. Meldrum, *Polymer* 39 (1998) 6697.
- [3] H. Warson, *Modern Superabsorbent Polymer Technology*, Wiley-VCH, New York, 2000.
- [4] P. Chen, W.A. Zhang, W. Luo, Y.e. Fang, *J. Appl. Polym. Sci.* 93 (2004) 1748.
- [5] J.V. Rogers, W.R. Richter, Y.W. Choi, A.K. Judd, *Lett. Appl. Microbiol.* 48 (2009) 180.
- [6] C. Wiegand, M. Abel, P. Ruth, U.C. Hipler, *J. Mater. Sci.: Mater. Med.* 22 (2011) 2583.
- [7] N. Lavoine, L. Bergström, *J. Mater. Chem. A* 5 (2017) 16105.
- [8] H. Ferfera-Harrar, N. Aouaz, N. Dairi, *Polym. Bull.* 73 (2016) 815.
- [9] M. Dalaran, S. Emik, G. Güçlü, T.B. İyim, S. Özgümüş, *Desalination* 279 (2011) 170.
- [10] L. Serna-Cock, M.A. Guancha-Chalapud, *Acta Agronómica* 66 (2017) 495.
- [11] X. Xu, B. Bai, C. Ding, H. Wang, Y. Suo, *Ind. Eng. Chem. Res.* 54 (2015) 3268.
- [12] M.A. Hubbe, A. Ayoub, J. Daystar, R. Venditti, J. Pawlak, in: (Ed.)²(Eds.) *BioResources*, 2013, p. 6556.
- [13] R. Gavillon, T. Budtova, *Biomacromolecules* 9 (2008) 269.
- [14] R. Sescousse, R. Gavillon, T. Budtova, *Carbohydr. Polym.* 83 (2011) 1766.
- [15] S.R. Djafari Petroudy, J. Ranjbar, E. Rasooly Garmaroody, *Carbohydr. Polym.* 197 (2018) 565.
- [16] A. Olad, H. Zebhi, D. Salari, A. Mirmohseni, A. Reyhani Tabar, *Mater. Sci. Eng.: C* 90 (2018) 333.
- [17] A. Olad, H. Zebhi, D. Salari, A. Mirmohseni, A. Reyhanitabar, *J. Porous Mater.* 25 (2018) 1325.
- [18] A.I. Raafat, M. Eid, M.B. El-Arnaouty, *Nucl. Instrum. Methods Phys. Res., Sect. B* 283 (2012) 71.
- [19] Z. Wang, A. Ning, P. Xie, G. Gao, L. Xie, X. Li, A. Song, *Carbohydr. Polym.* 157 (2017) 48.
- [20] A. Adair, A. Kaesaman, P. Klinpituksa, *Polym. Test.* 64 (2017) 321.
- [21] T. Fekete, J. Borsa, E. Takács, L. Wojnárovits, *Carbohydr. Polym.* 166 (2017) 300.
- [22] H. Kono, S. Fujita, *Carbohydr. Polym.* 87 (2012) 2582.
- [23] H. Dai, H. Huang, *J. Agric. Food. Chem.* 65 (2017) 565.
- [24] L.-Y. Long, Y.-X. Weng, Y.-Z. Wang, *Polymers* 10 (2018) 623.
- [25] T. Saito, S. Kimura, Y. Nishiyama, A. Isogai, *Biomacromolecules* 8 (2007) 2485.
- [26] P.W. Brodin, H. Theliander, *BioResources* 7 (2012) 1666.
- [27] F.W. Brodin, H. Theliander, *Cellulose* 20 (2013) 1.
- [28] F.W. Brodin, Y. Sonavane, H. Theliander, *BioResources* 8 (2013) 2099.
- [29] F.W. Brodin, K. Lund, H. Brelid, H. Theliander, *Cellulose* 19 (2012) 1413.
- [30] F. Jiang, Y.-L. Hsieh, *J. Mater. Chem. A* 2 (2014) 350.
- [31] F. Jiang, Y.-L. Hsieh, *J. Mater. Chem. A* 2 (2014) 6337.
- [32] F. Jiang, Y.-L. Hsieh, *ACS Sustain. Chem. Eng.* 4 (2016) 1041.
- [33] L. Mendoza, T. Gunawardhana, W. Batchelor, G. Garnier, *J. Colloid Interface Sci.* 525 (2018) 119.
- [34] L. Mendoza, W. Batchelor, R.F. Tabor, G. Garnier, *J. Colloid Interface Sci.* 509 (2018) 39.
- [35] D. da Silva Perez, S. Montanari, M.R. Vignon, *Biomacromolecules* 4 (2003) 1417.
- [36] H. Fujita, K. Mitsuhashi, T. Homma, *J. Colloid Sci.* 9 (1954) 466.
- [37] A. Isogai, T. Saito, H. Fukuzumi, *Nanoscale* 3 (2011) 71.
- [38] Y. Okita, T. Saito, A. Isogai, *Biomacromolecules* 11 (2010) 1696.
- [39] X. Shi, W. Wang, A. Wang, *Carbohydr. Polym.* 94 (2013) 449.
- [40] H. Schott, *J. Macromol. Sci., Part B* 31 (1992) 1.
- [41] W.L. Li, K. Lu, J.Y. Walz, *Int. Mater. Rev.* 57 (2012) 37.
- [42] F. Martoña, T. Cochereau, P.J.J. Dumont, L. Orgéas, M. Terrien, M.N. Belgacem, *Mater. Des.* 104 (2016) 376.
- [43] J. Erlandsson, T. Pettersson, T. Ingverud, H. Granberg, P.A. Larsson, M. Malkoch, L. Wågberg, *J. Mater. Chem. A* 6 (2018) 19371.
- [44] J. Ma, X. Li, Y. Bao, *RSC Adv.* 5 (2015) 59745.

Carboxylated Nanocellulose Foams as Superabsorbents

Llyza Mendoza¹, Laila Hossain¹, Emma Downey¹, Camilla Scales¹, Warren Batchelor¹, Gil Garnier^{1,*}

¹Bioresource Processing Research Institute of Australia (BioPRIA), Department of Chemical Engineering,
Monash University, VIC 3800, Australia

*Email: gil.garnier@monash.edu

Mercury Porosimetry Analysis

The foam structure was analysed by mercury porosimetry (Micromeritics Autopore IV). Table 1 summarises the important values calculated from the porosimetry data. Each parameter has been calculated as an average of 2 sample measurements. The equations below summarise the calculation for the total porosity.

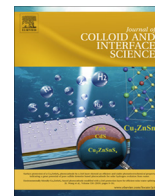
Table S1. Mercury Porosimetry Values for Nanocellulose Foams

<i>Parameter</i>	<i>0.3 wt.%</i>	<i>0.5 wt.%</i>	<i>1 wt.%</i>	<i>3 wt.%</i>
Total Hg Intrusion Volume (mL/g)	32.1 ± 0.4	28.5 ± 0.8	27.1 ± 2.0	21.2 ± 0.1
Skeletal Density (g/mL)	0.6 ± 0.2	0.8 ± 0.04	0.87 ± 0.01	1.4 ± 0.05
Total Porosity (%)	94.8 ± 1.2	95.6 ± 0.1	96.1 ± 0.21	96.7 ± 0.1
Bulk Density at 14.7 psia (1atm) (g/mL)	0.2 ± 0.0	0.38 ± 0.08	0.45 ± 0.01	0.9 ± 0.04
Porosity at 1 atm (%)	60.0 ± 9.8	51.3 ± 8.0	47.8 ± 1.3	33.2 ± 0.6
Total Pore Area (m ² /g)	5.4 ± 0.7	3.55 ± 0.9	3.1 ± 0.1	1.5 ± 0.07

$$\text{Total Porosity (\%)} = \left(\frac{\text{Pore Volume (mL)}}{\text{Pore Volume (mL)} + \text{Skeletal Volume (mL)}} \right) \times 100\%$$

$$\text{Pore Volume (mL)} = \text{Total Hg Intrusion Volume} \left(\frac{\text{mL}}{\text{g}} \right) \times \text{Sample Mass (g)}$$

$$\text{Skeletal Volume (mL)} = \frac{\text{Sample Mass (g)}}{\text{Skeletal Density} \left(\frac{\text{g}}{\text{mL}} \right)}$$



Regular Article

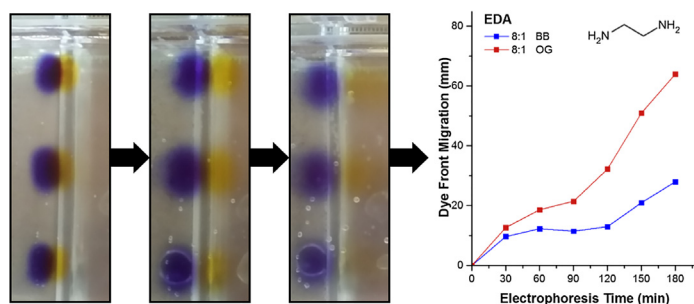
Nanocellulose for gel electrophoresis

Llyza Mendoza, Thilina Gunawardhana, Warren Batchelor, Gil Garnier*

Bioresource Processing Research Institute of Australia (BioPRIA), Department of Chemical Engineering, Monash University, VIC 3800, Australia



GRAPHICAL ABSTRACT



ARTICLE INFO

Article history:

Received 14 December 2018

Revised 3 January 2019

Accepted 4 January 2019

Available online 5 January 2019

Keywords:

Gel electrophoresis

Nanocellulose

TEMPO-mediated oxidation

ABSTRACT

Hypothesis: Cellulose nanofibres produced by TEMPO-mediated oxidation can form gels. This study presents a proof-of-concept for gel electrophoresis with nanocellulose (NC).

Experiments: TEMPO-oxidised cellulose nanofibre dispersion is chemically cross-linked by inducing amide linkages to produce gel slabs for electrophoretic separation. Nanocellulose gel slabs 1 cm thick containing Tris/Borate/EDTA (TBE) buffer were casted. Different cross-linker types and ratios are investigated to assess the migration of conventional electrophoresis tracking dyes.

Findings: Tracking dyes (bromophenol blue and orange G) can diffuse within the gel at different rates and therefore separate. Changing the cross-linker length from EDA to HMDA (C₂- to C₆-chain) increases the overall network pore size resulting in a faster migration rate for both bromophenol blue and orange G. Increasing the cross-linker concentration stabilises the HMDA-NC gel (no extension) during the electrophoresis run without any effect on the dye migration rate. Increasing the voltage increases the migration rates for both orange G and bromophenol blue. Further development is required to cast the gels evenly and to prevent bubble formation during the cross-linking process. This will enable to effectively separate mixtures of proteins. Nanocellulose gels can become a novel substrate for sustainable biomedical separation and diagnostics by electrophoresis.

Crown Copyright © 2019 Published by Elsevier Inc. All rights reserved.

1. Introduction

Electrophoresis is a widely used method in molecular biology to separate and identify individual macromolecules from a mixture by the difference in their mobility under an electric field. Nega-

tively charged macromolecules, such as nucleic acids or coated proteins, are fractionated based on their structure, charge, conformation and size as they move towards the anode. Shorter molecules travel faster than longer ones as they can easily migrate through the pores of the gel medium [1]. Initial development of electrophoresis technique began with the work of Arne Tiselius in 1931, separating colloids (human serum) under an electric field [2]. Zone electrophoresis, which utilises substrates such as paper,

* Corresponding author.

E-mail address: gil.garnier@monash.edu (G. Garnier).

starch, gel, agarose, cellulose acetate or polyacrylamide to act as a sieve to separate a mixture into components as bands, was then developed (1940–1950s) [3]. At present, conventional separation of macromolecules such as DNA or RNA is achieved through agarose and polyacrylamide gels. A mixture of large DNA molecules (200–30,000 bp) [1,4] is often separated through horizontally casted agarose gels because of their larger pores. The neutral charge of the agarose gel network does not interact with the molecules to separate [5]. Separation of smaller protein-based molecules (RNA) (5–1000 bp) [6] is performed typically with a polyacrylamide gel as its pore size is smaller and its structure can better be controlled [7]. However, safety issues arise with the use of the acrylamide monomer as it is classified as a neurotoxin [8,9]. There is a need to develop safer and effective alternatives.

Nanocellulose (NC) fibres are high aspect ratio fibrils derived from cellulose-based sources such as wood or bacteria [10]. Isolation of nanocellulose from various sources can be achieved through a combination of chemical and mechanical processes [11]. One of the most common methods to produce nanocellulose is the TEMPO-mediated oxidation wherein the regio-selective carboxylation of the C6 alcohol of the *D*-glucose monomer provides the necessary electrostatic repulsion to produce nanofibres upon fibrillation [12]. The combination of nanofibrils with high surface charge and high aspect ratio produces viscous colloidal gels even at low solids content [13].

Studies on the characterisation and application development of nanocellulose have grown exponentially over the last decade. Rheological studies have elucidated their gelation mechanism, achievable property range and even flow instability phenomena [13–18]. Many applications are also being developed ranging from pulp and paper strength additive, agriculture, wastewater to biomedical applications [19–24]. In the biomedical field, nanocellulose composite films and membranes have been developed for protein interaction, passivation and immobilisation for advanced separation purposes [25–30]. Nanocellulose gels have also been used as scaffold structures with tuneable properties suitable for cell culture and tissue engineering [31–34]. Nanocellulose gels were investigated for protein and drug release [35,36]. However, only one study has investigated nanocellulose composite films for electrochemical-based ion-exchange for DNA oligomers [37]. To the best of our knowledge, nanocellulose hydrogels have never been studied as an electrophoretic material before.

This study investigates the potential of nanocellulose gels as electrophoresis substrates. Gel slabs are casted by chemically cross-linking nanocellulose fibres with diamine cross-linkers. The effect of cross-linker properties such as chain length and concentration on the migration of two model tracking dyes is evaluated. The effects of electrophoresis conditions (voltage) on the migration behaviour are also studied. The last section presents a perspective of nanocellulose gels development for DNA and protein mixture separation.

2. Methodology

2.1. Materials

A 0.82 wt% TEMPO-oxidised cellulose nanofibre suspension (containing 1.5 mmol COO⁻/g fibre) was purchased from the Process Development Center, University of Maine. Hexamethylenediamine (HMDA) and ethylenediamine (EDA) were bought from Sigma-Aldrich. Glycerol, Orange G and Bromophenol blue was purchased from Merck. Tris/Borate/EDTA (TBE) 10x buffer was bought from Bio-Rad. All chemicals were used as received and were analytical grade.

2.2. Formulation and casting of nanocellulose gel slabs

A 50 mL nanocellulose suspension is mixed with 5 mL 10x TBE buffer under nitrogen gas. The cross-linker (EDA or HMDA) is then added rapidly under thorough agitation. Once a uniform colour is reached, the suspension is immediately poured in a 7 cm × 10 cm transparent gel caster (Bio-Rad Sub-Cell GT UV Transparent Mini-Gel Tray). The gel is then cured at 80 °C for 1 h in an oven. The cross-linked gel is taken out of the oven and cooled at 4 °C. The sample wells are then stamped before running an electrophoresis experiment. Table 1 summarises the ratio of amine to carboxylate group studied:

Nanocellulose gels cross-linked with EDA and HMDA are referred to as EDA-NC and HMDA-NC, respectively.

2.3. Electrophoresis experiments

Electrophoresis was performed using a Bio-Rad Wide Mini Sub-Cell GT system. The gel is submerged in 1x TBE buffer. Samples (tracking dyes) were loaded at various sample wells of the gel. The tracking dye was prepared by mixing the following: 0.25 g bromophenol blue, 0.15 g Orange G, 6 mL 50% glycerol, 4 mL milliQ water. Tracking dyes were utilised to monitor the progression of electrophoresis. Orange G represents the smaller protein molecules and hence migrates faster in contrast to bromophenol blue. The 0.2 mL formulated tracking dye is diluted to a total 1 mL prior to electrophoresis. 20 µL of the dilute tracking dye was added in 3 different regions (left, centre, right) in the gel. The voltage is set at various levels (50, 75, and 100 V) for the electrophoresis to start. The migration rate of tracking dye front is measured visually by the naked eye at 30-minute intervals, for at least 3 h or until the orange G dye reached the end of the gel.

2.4. Characterisation of cross-linked nanocellulose

The characterisation of the cross-linking reaction is performed through ATR-FTIR using the Agilent Cary 630 FTIR Spectrometer. The gels are firstly frozen at –80 °C then freeze-dried to sublimate all of the water. The HMDA-/EDA-NC samples ground and then tested for the FTIR spectra (4000–450 cm⁻¹).

3. Results

3.1. Gel cross-linking by boric acid-catalysed amide formation

Nanocellulose gel slabs were prepared through boric acid catalysed amide formation between the carboxylate groups of nanocellulose and amine groups of di-amine cross-linkers followed by 80 °C curing. The appearance of amide bonds, indicating the cross-linking of nanocellulose gel slabs, is shown in the FTIR spectra (Fig. 1). The spectra of the neat nanocellulose gel displays the representative peaks of the pendant carboxylate group (COO⁻) 1601 cm⁻¹ corresponding to the C=O stretch, respectively. The C=O stretch peak shifts in the amide cross-linked gels for both HMDA-NC and EDA-NC gels. Curing the gels at 80 °C produces larger peaks at all areas of interest. Fig. 2 shows a cross-linked 8:1 EDA-NC gel.

Table 1
Cross-linker type and ratios for the different casted nanocellulose gel slabs.

Cross-linker type	Ratio (mol NH ₂ : mol COO ⁻)
EDA (C2)	8:1, 12:1
HMDA (C6)	4:1, 6:1, 8:1

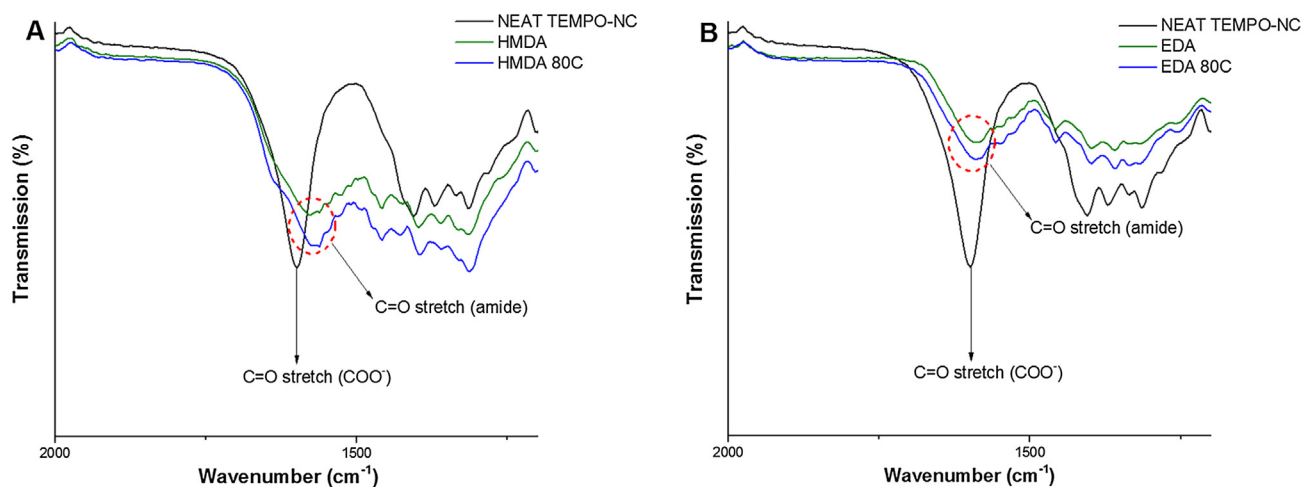


Fig. 1. FTIR spectra evolution of cross-linking of nanocellulose gel slabs with 8:1 (A) HMDA and (B) EDA. Room temperature and 80 °C reactions catalysed by boric acid.

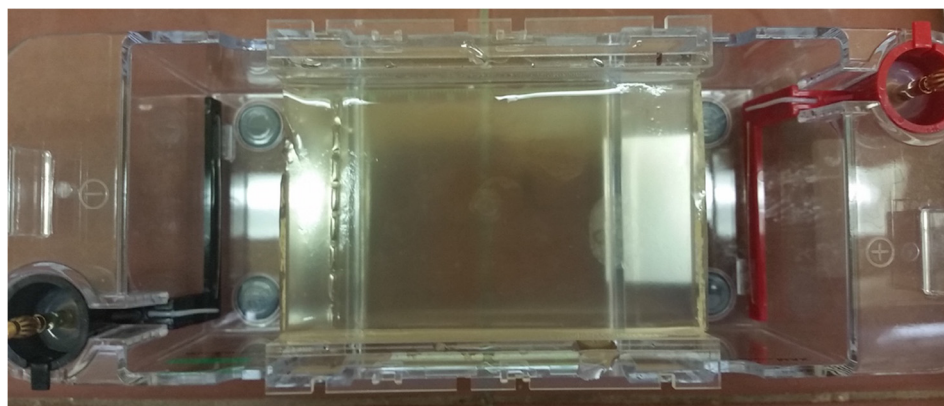


Fig. 2. A casted 8:1 EDA-NC gel placed on a horizontal electrophoresis system.

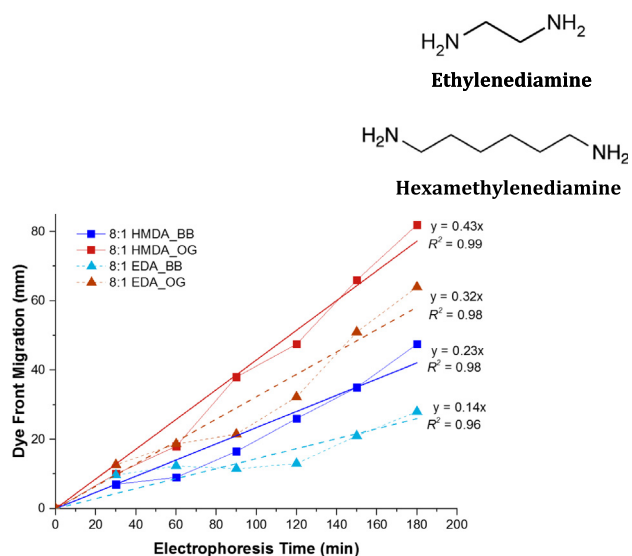


Fig. 3. Migration of Bromophenol Blue (BB) and Orange G (OG) dyes in HMDA-(8:1) and EDA-(8:1) cross-linked nanocellulose gel slabs. Bold lines indicate trend lines and faint lines indicate the actual migration behaviour of tracking dyes. Chemical structures of EDA and HMDA. Electrophoresis voltage constant at 100 V.

3.2. Effect of the cross-linker chain length

The amine-crosslinkers used in this study vary in the length of the carbon backbone. Ethylenediamine (EDA) is a C2-chain whereas hexamethylenediamine (HMDA) has a 6-carbon chain. The effect of amine cross-linker chain length (C2 vs C6) on the migration rate of the tracking dyes in the nanocellulose gel is shown in Fig. 3. Images of EDA- and HMDA-NC gels at different time intervals during electrophoresis are shown in Fig. 4 and supplementary information, respectively. The migration rate of both tracking dyes decreases in EDA-NC compared to HMDA-NC. The migration of bromophenol blue reduces from 0.23 to 0.14 mm min⁻¹ (at 100 V). Similarly, orange G travels at a rate of 0.43 mm min⁻¹ in HMDA-NC whereas it slows down to 0.32 mm min⁻¹ in EDA-NC. Moreover, migration behaviour differs between the two cross-linker types. In HMDA-gels, the tracking dyes travels more linearly throughout the electrophoresis run. The tracking dye behaviour in EDA-NC gels is less linear as a plateau region is observed between 60 and 120 mins.

3.3. Effect of cross-linker concentration

Fig. 5 shows the effect of cross-linker concentration on the mobility of bromophenol blue and orange G during electrophoresis for EDA-NC and HMDA-NC gels. For both cross-linker types, the

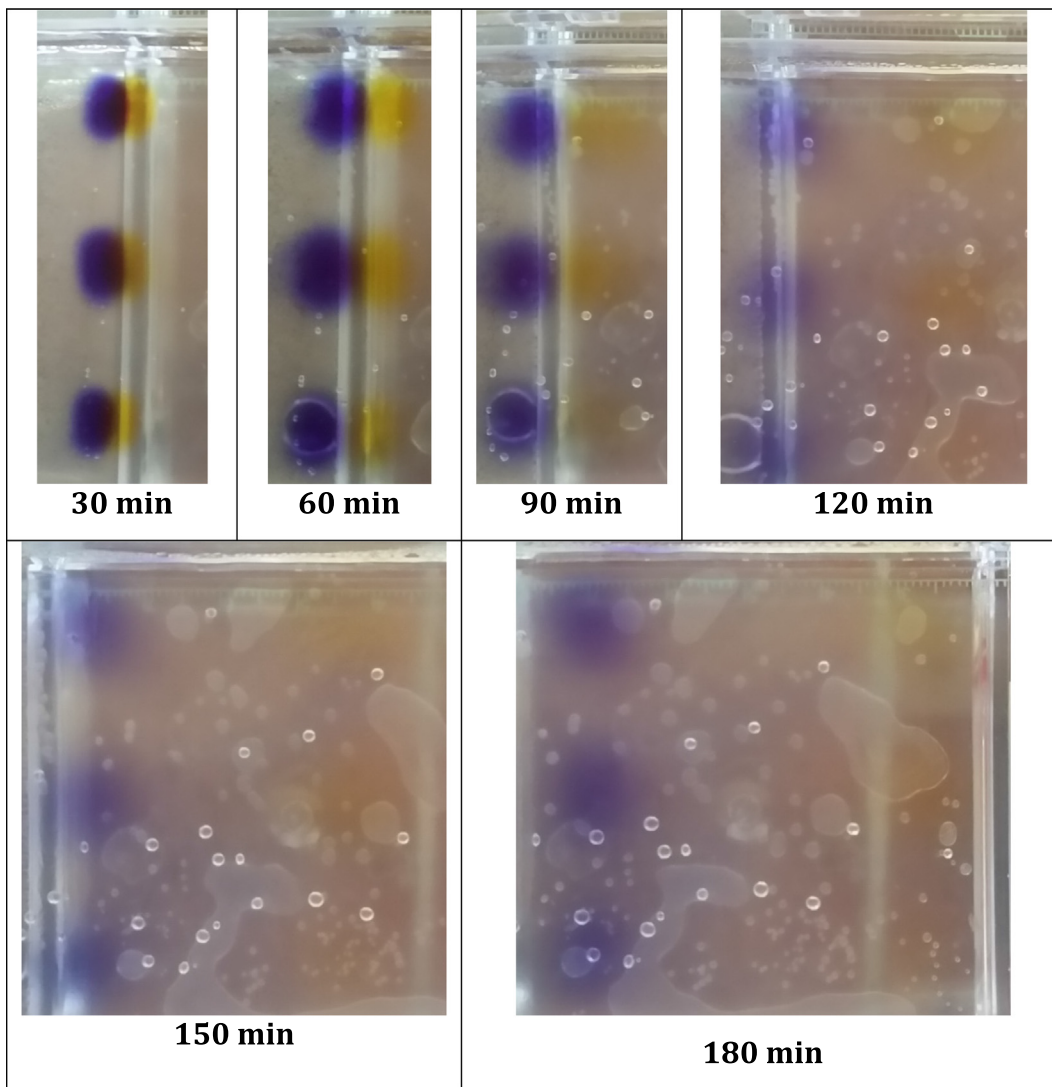


Fig. 4. Migration of Tracking Dyes at 30 min intervals in 8:1 EDA-NC gel. Electrophoresis voltage constant at 100 V.

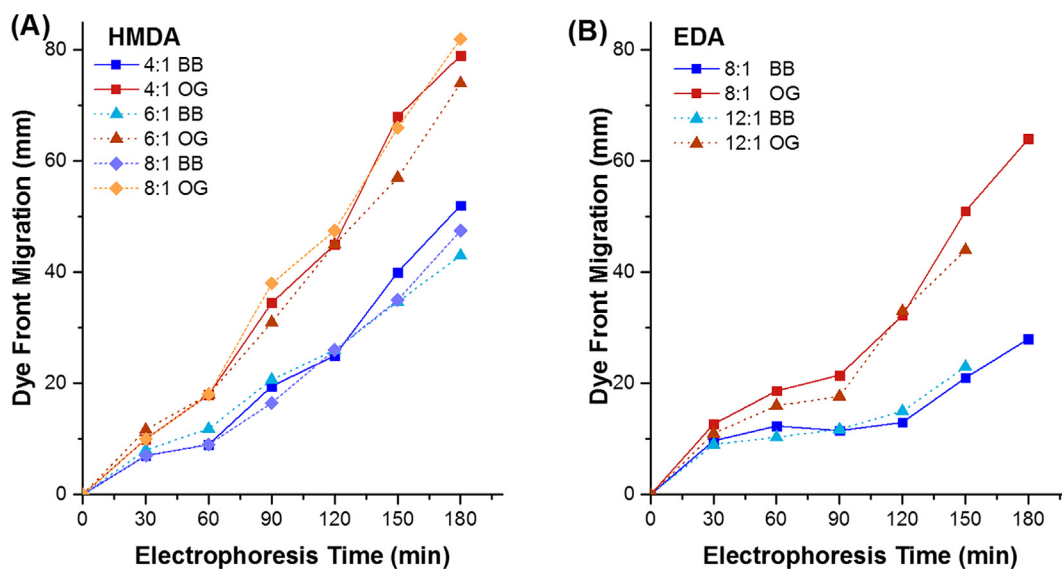


Fig. 5. Migration of Bromophenol Blue (BB) and Orange G (OG) in a (A) HMDA cross-linked and (B) EDA cross-linked nanocellulose gel at various NH_2 : COO^- concentrations. Electrophoresis voltage constant at 100 V.

increase in the cross-linker concentration has no effect on the migration behaviour and rate of either bromophenol blue or orange G. Gel stability and ease of handling however increases with cross-linker concentration, particularly with HMDA. All gels tested become increasingly stiffer with higher cross-linker concentration. Increasing the cross-linker concentration from 2:1 onwards maintains gel stability throughout the electrophoresis run. However, all EDA-NC gels tested are very unstable with the gels extending and retracting at both sides of the cell during electrophoresis.

3.4. Effect of electrophoresis voltage

Varying the electrophoresis voltage changes the migration rate for 8:1 HMDA-NC gel as shown in Fig. 6. Increasing the voltage from 50 V to 100 V results in almost tripling and doubling the migration rate of orange G and bromophenol blue, respectively. Moreover, the separation gap between both dyes becomes larger with increasing voltage.

4. Discussion

4.1. Gel cross-linking and gel slab formation

TEMPO-oxidised cellulose nanofibres (TOCNs) can form a suspension or colloidal gel depending on the combination of fibre length and concentration [13,38]. The nanocellulose suspension selected in this study has a concentration of 0.82 wt% and still exhibits primarily liquid-like behaviour. At this initial state, the nanocellulose fibres are not sufficiently entangled to form the stable 3D-network of a gel. Introducing cross-links is therefore necessary to produce a uniform gel slab which remains stable under electrophoretic conditions.

TOCNs contain COO^- groups which can be cross-linked to improve dimensional stability and form a stable gel. Cross-linking can be achieved either by physical or chemical means [39]. Physical cross-linking of TEMPO-nanocellulose can be accomplished with divalent (Ca^{2+} , Zn^{2+} , Cu^{2+}) or trivalent (Al^{3+} , Fe^{3+}) cations which coordinate with the COO^- groups to induce chain-chain association similar to pectins and alginates. This results in very stiff gels [40]. These cations, however, are prone to movement and can leave the gel upon the introduction of electrical current.

This can lead to gel instability and collapse. Moreover, as the individual fibres are not completely neutralised in this type of cross-linking, their negative charges induce nanocellulose fibre migration during electrophoresis. Temperature and pressure have recently been reported as a trigger for nanocellulose gelation. Nonetheless, the increased gel strength and stability achieved may not be sufficient for electrophoresis operations [41,42].

Chemical cross-linking, on the other hand, provides a more stable network as the fibres are permanently bridged with a cross-linker. Carboxylic acid groups in different substances can be bridged by amine-based cross-linkers to induce amide bond formation. Amide formation is not spontaneous under ambient conditions as the carboxylic acid is deprotonated to form an ammonium carboxylate salt. Conversion to amide requires heat to overcome the activation energy with water as a by-product to be driven off for the reaction to progress [43]. Hence, when either EDA or HMDA is added to TOCNs at ambient conditions, no cross-linking occurs.

Different catalysts and co-reactants are required to produce amides at ambient conditions. For instance, coupling agents such as 1-ethyl-3-(3-dimethylaminopropyl) carbodiimide (EDC) combined with *N*-hydroxysuccinimide (NHS) is a common reaction system [44]. Boric acid, a component in DNA electrophoresis buffers, can also act as a catalyst to trigger carboxylate group – amine cross-linking to produce amide bonds [45,46]. Amide formation in TOCNs with boric acid is triggered at room temperature as shown in Fig. 1. The change in the representative spectra of COO^- groups indicates the formation of amide bonds at room temperature. Full conversion is not achieved as a stronger FTIR signal is shown after the gel is cured at 80 °C for 1 h. This increased amide formation is also demonstrated by the higher stability and ease of handling of the cured gel.

4.2. Effect of cross-linker type

The effect of two types of diamine cross-linkers on the gel slab formation and tracking dye migration behaviour is investigated. Ethylenediamine (EDA) and hexamethylenediamine (HMDA) are both diamine compounds which only differ in the length of the hydrocarbon backbone. EDA and HMDA consist of 2 and 6 carbon chain, respectively. The cross-linker chain length determines the cross-linking likelihood, bond rigidity, and average pore mesh of the resulting three-dimensional network formed by the

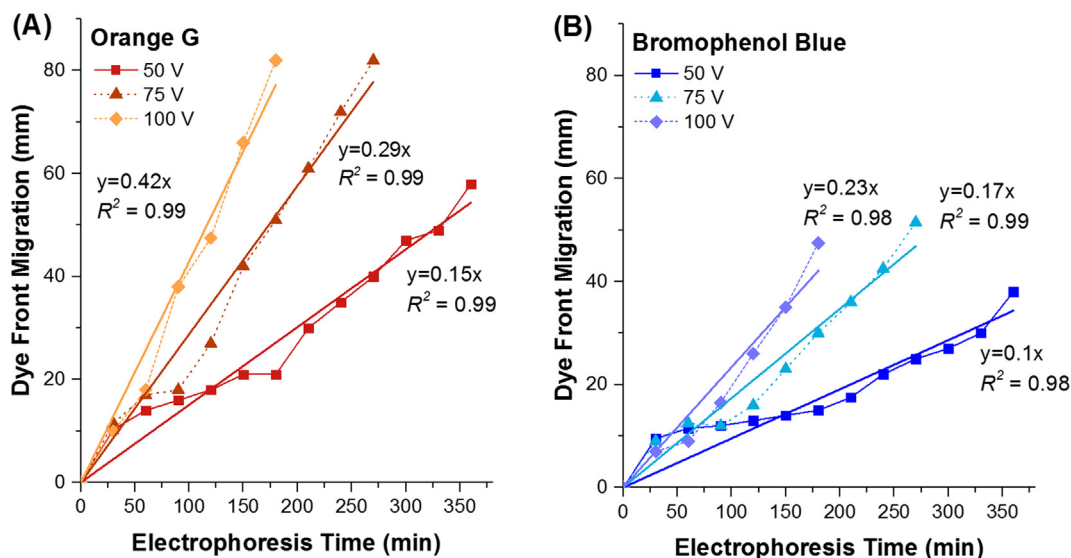


Fig. 6. Migration of (A) Orange G (OG) and (B) Bromophenol Blue (BB) in an 8:1 HMDA cross-linked nanocellulose gel at different electrophoresis voltages. The linear trendlines were added with a y-intercept set at zero. The slope represents the average migration rate under various voltages.

nanocellulose fibres. A longer cross-linker is able to bridge more effectively individual nanocellulose fibres separated by repelling electrostatic forces. It is therefore expected that a longer chain cross-linker will produce a more stable gel. HMDA-NC gels are stronger than EDA-NC gels, similarly reported in [47]. In this investigation, we extend the idea of stability from just producing a self-standing gel to maintaining its structural integrity whilst immersed in an electrophoretic environment. At constant NH_2 : COO^- ratio of 8:1, EDA-NC gels extended and contracted at different time periods throughout the electrophoresis experiment. This is in contrast with HMDA-NC which remains unchanged. The change in gel shape (extension and contraction) can be attributed to the lack of stiffness of EDA-NC gels as fibre mobility is less restricted than for HMDA-NC gels. Another reason might be that the diamine terminated cross-linkers have not fully formed amide bonds at both ends, resulting in a net positive charge on the fibre surface leading to the increased electrophoretic movement observed.

The migration rate and behaviour of orange G and bromophenol blue are also affected by HMDA and EDA. Both tracking dyes display lower migration rates in EDA-NC gels. The small chain length in EDA resulted in smaller network pores upon cross-linking in contrast to HMDA. The change in the cross-linker length impacts the migration rate as it decreases by 25.6% and 39.1% in orange G and bromophenol blue, respectively. Moreover, non-linearity in the dyes migration rates are observed for EDA-NC gels. A plateau region in the electrophoresis run is observed wherein there is very little movement (Fig. 3). This can be attributed to the movement of the tracking dyes relative to the gel dimensional instability (extension) resulting in net zero movement.

4.3. Effect of cross-linker concentration

Modifying the cross-linker concentration (NH_2 : COO^- ratio) influences the stability of the gels. The higher cross-linker concentration for HMDA-gels forms gel slabs which are more stable; they are easier to handle (i.e. stronger) and do not deform (no dimensional extension) during the electrophoresis testing. This is due to the formation of more crosslinking junctions. However, for EDA-gels, increasing the cross-linker concentration does not improve the gel stability during electrophoresis. Gel extension is still observed even at higher cross-linker concentrations (12:1). Furthermore, the amount of cross-linker concentration does not affect the migration rate of the tracking dyes (Fig. 5). For all HMDA gels (4:1 to 8:1), the tracking dyes travel at similar rates. Similarly, the migration behaviour in EDC gels does not change significantly. This indicates that the network pore sizes have not changed significantly with the increase in cross-linker concentration.

4.4. Effect of electrophoresis voltage

The electrophoresis voltage dictates the migration rate and the degree of separation between molecules and dyes. A higher electrophoresis voltage indicates a faster migration rate which may affect the quality of separation as it can cause smearing or distortion of bands. In cross-linked nanocellulose gels, the tracking dyes travels the slowest at 50 V and fastest at 100 V (Fig. 6). Doubling the voltage from 50 V to 100 V results in tripling of the migration rate of orange G and doubling for bromophenol blue. Moreover, at increasing voltage the gap between orange G and bromophenol blue increases.

4.5. Development perspectives

There are four main development issues to resolve for consistent and effective separation with nanocellulose gel electrophoresis:

- *Bubble formation during casting.* The presence of bubbles can inhibit the effective separation of tracking dyes or proteins due to the absence of current within the bubbles in contrast to the gel which carries the current. Distortion of the separation bands was observed as the dyes are dragged around the bubbles. Hence, there is a need to engineer casting methods to suit nanocellulose gels which may include mixing under vacuum prior to gelation. A well stamp can also be integrated with the caster upon curing such that wells are always well-formed.
- *Nanocellulose gels for substitution of SDS-PAGE.* Trials on casting ultra-thin (0.75 mm) nanocellulose gels to mimic SDS-PAGE (sodium dodecyl sulphate-polyacrylamide gel) for RNA separation were attempted. Concentrated solutions of Al^{3+} and Ca^{2+} cations, which are known to physically cross-link nanocellulose gels, were each applied to the casting plate via plasma-coating and spin-coating techniques. However, uneven precipitation of cations and SDS-nanocellulose interactions prevented even gelation.
- *Investigation of kinetics.* The kinetics and extent of the amide cross-linking reaction can be investigated to optimise casting methods.
- *Optimisation of nanocellulose type.* Nanocellulose properties such as aspect ratio and surface charge can be modified for optimisation of the pore size network to enable enhanced separation. This is best achieved by testing gels from cellulose nanocrystals and bacterial cellulose.

5. Conclusion

Nanocellulose gels have been increasingly studied for applications spanning agriculture [20,21], personal care and hygiene [48], biomedicine [10,31,34] and drug delivery media [35]. In this study, we report a proof-of-concept for utilising nanocellulose gels as novel electrophoresis media. Nanocellulose gels were investigated as an electrophoretic material by understanding the fundamentals which govern electrophoretic separation. Gels from TEMPO-oxidised cellulose nanofibres were chemically cross-linked by diamines to form slabs for horizontal gel electrophoresis. We demonstrated the feasibility of boric acid catalysed amide formation between the carboxylate pendant groups of the nanocellulose fibres with diamine terminated cross-linkers. Curing (80 °C) enhanced the cross-linking for increased gel stability (handleability and minimal deformation during electrophoresis). The pore size of the gel network was varied with the carbon chain length of the diamine cross-linker molecule. This affected the migration rates for both the bromophenol blue and orange G dyes. Gel stability was also influenced as shorter cross-linkers (i.e. EDA) produced unstable gels which extend and retract at both ends of the cell during electrophoresis; this is due to incomplete junctions of the short diamine and the lack of gel stiffness. Increasing the cross-linker concentration increased gel stability and handleability whilst migration rate and behaviour remained constant. Increasing the electrophoresis voltage increased the migration rate and separation gap between bromophenol blue and orange G. Further optimisation is required for developing nanocellulose gels as robust and consistent electrophoretic materials. This especially involves process improvement for producing bubble-free and homogeneous gels. Nanocellulose gels have the potential to become the next generation of efficient and safe electrophoretic media for biomolecule separation.

Acknowledgments

This work was funded by the ARC Bioprocessing Advance Manufacturing Industry Research Transformation (BAMI) Hub IH13100016, Visy, Norske Skog, Orora, CHH/Oji Fibre Solutions,

Australian Paper and Circa. Special thanks to Maheshi Udugama (Monash University) for advice and discussions regarding electrophoresis.

Appendix A. Supplementary material

Supplementary data to this article can be found online at <https://doi.org/10.1016/j.jcis.2019.01.017>.

References

- [1] J.A. Armstrong, J.R. Schulz, Agarose gel electrophoresis, in: *Current Protocols Essential Laboratory Techniques*, 2008.
- [2] A. Tiselius, A new apparatus for electrophoretic analysis of colloidal mixtures, *Trans. Faraday Soc.* 33 (1937) 524–531.
- [3] M.J. Gordon et al., Capillary electrophoresis, *Science* 242 (4876) (1988) 224–228.
- [4] D. Voytas, Agarose gel electrophoresis, *Curr. Protoc. Mol. Biol.* 51 (1) (2000) 2.5A.1–2.5A.9.
- [5] V.L. Royse, D.M. Jensen, Development of an agarose gel electrophoresis technique for determining alpha-amylase isoenzymes, *Clin. Chem.* 30 (3) (1984) 387–390.
- [6] J. Chory, J.D. Pollard, Separation of small DNA fragments by conventional gel electrophoresis, *Curr. Protoc. Mol. Biol.* 47 (1) (1999) 2.7.1–2.7.8.
- [7] R. Bravo, CHAPTER 1 – two-dimensional gel electrophoresis: a guide for the beginner, in: J.E. Celis, R. Bravo (Eds.), *Two-Dimensional Gel Electrophoresis of Proteins*, Academic Press, 1984, pp. 3–36.
- [8] M. Friedman, Chemistry, biochemistry, and safety of acrylamide. A review, *J. Agric. Food. Chem.* 51 (16) (2003) 4504–4526.
- [9] R. Westermeier, Electrophoresis, in: *Electrophoresis in Practice: A Guide to Methods and Applications of DNA and Protein Separations*, 2005, p. 16.
- [10] T. Abitbol et al., Nanocellulose, a tiny fiber with huge applications, *Curr. Opin. Biotechnol.* 39 (2016) 76–88.
- [11] D. Klemm et al., Cellulose: fascinating biopolymer and sustainable raw material, *Angew. Chem. Int. Ed.* 44 (22) (2005) 3358–3393.
- [12] A. Isogai, T. Saito, H. Fukuzumi, TEMPO-oxidized cellulose nanofibers, *Nanoscale* 3 (1) (2011) 71–85.
- [13] L. Mendoza et al., Gelation mechanism of cellulose nanofiber gels: a colloids and interfacial perspective, *J. Colloid Interf. Sci.* 509 (2018) 39–46.
- [14] L. Jowkarderis, T.G.M. van de Ven, Intrinsic viscosity of aqueous suspensions of cellulose nanofibrils, *Cellulose* 21 (4) (2014) 2511–2517.
- [15] L. Jowkarderis, T.G.M. van de Ven, Rheology of semi-dilute suspensions of carboxylated cellulose nanofibrils, *Carbohydr. Polym.* 123 (2015) 416–423.
- [16] E. Lasseguette, D. Roux, Y. Nishiyama, Rheological properties of microfibrillar suspension of TEMPO-oxidized pulp, *Cellulose* 15 (3) (2008) 425–433.
- [17] O. Nechyporchuk, M.N. Belgacem, F. Pignon, Rheological properties of micro-/nanofibrillated cellulose suspensions: wall-slip and shear banding phenomena, *Carbohydr. Polym.* 112 (Supplement C) (2014) 432–439.
- [18] O. Nechyporchuk, M.N. Belgacem, F. Pignon, Concentration effect of TEMPO-oxidized nanofibrillated cellulose aqueous suspensions on the flow instabilities and small-angle X-ray scattering structural characterization, *Cellulose* 22 (4) (2015) 2197–2210.
- [19] M. Hakalahti et al., Effect of interfibrillar PVA bridging on water stability and mechanical properties of TEMPO/NaClO₂ oxidized cellulosic nanofibril films, *Carbohydr. Polym.* 126 (2015) 78–82.
- [20] H. Zhang et al., Cellulose anionic hydrogels based on cellulose nanofibers as natural stimulants for seed germination and seedling growth, *J. Agric. Food Chem.* 65 (19) (2017) 3785–3791.
- [21] S.M.F. Kabir et al., Cellulose-based hydrogel materials: chemistry, properties and their prospective applications, *Prog. Biomater.* 7 (3) (2018) 153–174.
- [22] S. Boufi et al., Nanofibrillated cellulose as an additive in papermaking process: a review, *Carbohydr. Polym.* 154 (2016) 151–166.
- [23] P. Gatenholm, D. Klemm, Bacterial nanocellulose as a renewable material for biomedical applications, *MRS Bull.* 35 (3) (2011) 208–213.
- [24] P.R. Sharma et al., Nanocellulose from spinifex as an effective adsorbent to remove cadmium(II) from water, *ACS Sustain. Chem. Eng.* 6 (3) (2018) 3279–3290.
- [25] S. Gustafsson, L. Manukyan, A. Mihranyan, Protein-nanocellulose interactions in paper filters for advanced separation applications, *Langmuir* 33 (19) (2017) 4729–4736.
- [26] M. Vuoriluoto et al., Control of protein affinity of bioactive nanocellulose and passivation using engineered block and random copolymers, *ACS Appl. Mater. Interf.* 8 (8) (2016) 5668–5678.
- [27] J.-M. Malho et al., Enhanced plastic deformations of nanofibrillated cellulose film by adsorbed moisture and protein-mediated interactions, *Biomacromolecules* 16 (1) (2015) 311–318.
- [28] C. Xu, D.O. Carlsson, A. Mihranyan, Feasibility of using DNA-immobilized nanocellulose-based immunoadsorbent for systemic lupus erythematosus plasmapheresis, *Colloids Surf. Biointerf.* 143 (2016) 1–6.
- [29] C. Uth et al., A chemoenzymatic approach to protein immobilization onto crystalline cellulose nanoscaffolds, *Angew. Chem. Int. Ed.* 53 (46) (2014).
- [30] V. Kuzmenko et al., Universal method for protein bioconjugation with nanocellulose scaffolds for increased cell adhesion, *Mater. Sci. Eng., C* 33 (8) (2013) 4599–4607.
- [31] N.E. Zander et al., Metal cation cross-linked nanocellulose hydrogels as tissue engineering substrates, *ACS Appl. Mater. Interf.* 6 (21) (2014) 18502–18510.
- [32] J. Leppiniemi et al., 3D-printable bioactivated nanocellulose-alginate hydrogels, *ACS Appl. Mater. Interf.* 9 (26) (2017) 21959–21970.
- [33] G. Mondragon et al., Bionanocomposites based on gelatin matrix and nanocellulose, *Eur. Polym. J.* 62 (2015) 1–9.
- [34] J. Liu et al., Development of nanocellulose scaffolds with tunable structures to support 3D cell culture, *Carbohydr. Polym.* 148 (2016) 259–271.
- [35] A. Müller et al., The biopolymer bacterial nanocellulose as drug delivery system: investigation of drug loading and release using the model protein albumin, *J. Pharm. Sci.* 102 (2) (2013) 579–592.
- [36] A. Müller et al., Loading of bacterial nanocellulose hydrogels with proteins using a high-speed technique, *Carbohydr. Polym.* 106 (2014) 410–413.
- [37] A. Razaq et al., High-capacity conductive nanocellulose paper sheets for electrochemically controlled extraction of DNA oligomers (Conductive Nanocellulose for Extraction of DNA), *PLoS One* 6 (12) (2011) e29243.
- [38] L. Mendoza et al., Effects of fibre dimension and charge density on nanocellulose gels, *J. Colloid Interf. Sci.* 525 (2018) 119–125.
- [39] K. Hunger et al., Investigation of cross-linked and additive containing polymer materials for membranes with improved performance in pervaporation and gas separation, *Membranes* 2 (4) (2012) 727–763.
- [40] I. Braccini, S. Pérez, Molecular basis of Ca²⁺-induced gelation in alginates and pectins: the egg-box model revisited, *Biomacromolecules* 2 (4) (2001) 1089–1096.
- [41] J. Schmitt et al., TEMPO-oxidised cellulose nanofibrils; probing the mechanisms of gelation via small angle X-ray scattering, *PCCP* 20 (23) (2018) 16012–16020.
- [42] S. Suenaga, M. Osada, Self-sustaining cellulose nanofiber hydrogel produced by hydrothermal gelation without additives, *ACS Biomater. Sci. Eng.* 4 (5) (2018) 1536–1545.
- [43] E. Valeur, M. Bradley, Amide bond formation: beyond the myth of coupling reagents, *Chem. Soc. Rev.* 38 (2) (2009) 606–631.
- [44] H. Orelma et al., CMC-modified cellulose biointerface for antibody conjugation, *Biomacromolecules* 13 (4) (2012) 1051–1058.
- [45] R.K. Mylavarapu et al., Boric acid catalyzed amidation in the synthesis of active pharmaceutical ingredients, *Org. Process Res. Dev.* 11 (6) (2007) 1065–1068.
- [46] M.T. Sabatini, L.T. Boulton, T.D. Sheppard, Borate esters: simple catalysts for the sustainable synthesis of complex amides, *Sci. Adv.* 3 (9) (2017).
- [47] K. Syverud et al., Controlling the elastic modulus of cellulose nanofibril hydrogels—scaffolds with potential in tissue engineering, *Cellulose* 22 (1) (2015) 473–481.
- [48] L. Mendoza et al., Carboxylated nanocellulose foams as superabsorbents, *J. Colloid Interf. Sci.* 538 (2019) 433–439.

Nanocellulose for Gel Electrophoresis

Llyza Mendoza¹, Thilina Gunawardhana¹, Warren Batchelor¹, Gil Garnier^{1,}*

¹Bioresource Processing Research Institute of Australia (BioPRIA), Department of Chemical Engineering, Monash University, VIC 3800, Australia

*E-mail : gil.garnier@monash.edu

Images of Nanocellulose Gels in Electrophoresis

The following are the images (Figs. S1 and S2) of HMDA-NC gels taken at different time intervals during an electrophoresis run.

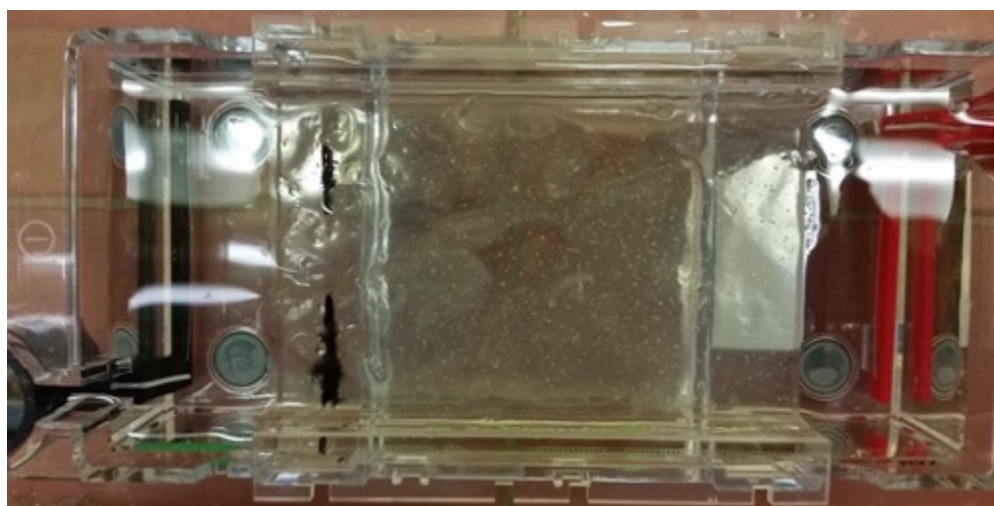
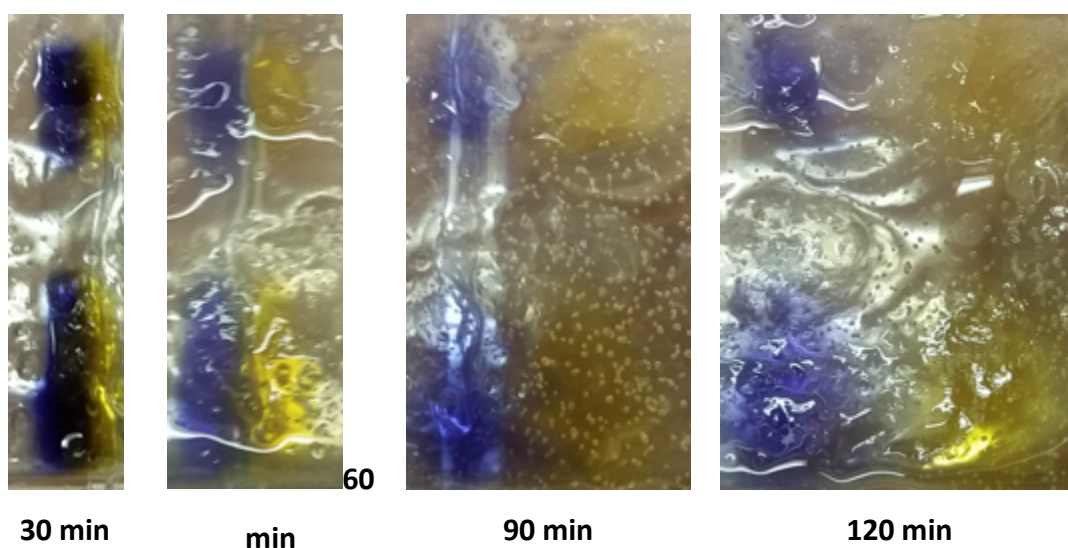


Figure S2. HMDA-NC gel loaded with tracking dye mixture prior to electrophoresis





150 min



180 min

Figure S3. Migration of Tracking Dyes at 30 min intervals in HMDA-NC gel (100V)

APPENDIX II

**CO-AUTHORED PUBLICATIONS NOT
INCLUDED IN THESIS**

THIS PAGE HAS BEEN INTENTIONALLY LEFT BLANK



Pickering Emulsions Electrostatically Stabilized by Cellulose Nanocrystals

Swambabu Varanasi^{1,2}, Leeav Henzel¹, Llyza Mendoza¹, Ragesh Prathapan³, Warren Batchelor¹, Rico Tabor³ and Gil Garnier^{1*}

¹ Department of Chemical Engineering, Bioresource Processing Research Institute of Australia, Monash University, Clayton, VIC, Australia, ² Department of Chemical Engineering, Indian Institute of Petroleum and Energy, Visakhapatnam, India, ³ School of Chemistry, Monash University, Melbourne, VIC, Australia

Cellulose Nanocrystals (CNC) are explored to stabilize oil/water emulsions for their ability to adsorb at the oil/water interface. In this work, the role of electrostatic forces in the CNC ability to stabilize oil/water emulsions is explored using canola oil/water and hexadecane/water as model systems. Canola oil/water and Hexadecane/water (20/80, v/v) emulsions were stabilized with the addition of CNCs using ultrasonication. Emulsion droplet sizes range from 1 to 4 μm as measured by optical microscopy. It is found that CNC can stabilize oil/water emulsions regardless of their charge density. However, reducing the surface charge density, by adding salts and varying pH, can reduce the amount of CNC's required to form a stable emulsion. Just by adding 3 mM Na^+ or 1 mM or less Ca^{+2} to a CNC suspension, the amount of CNC reduced by 30% to stabilized 2 mL of Canola oil. On the other hand, adding salt increases the emulsion volume. The addition of 100 mM Na^+ or the reduction of pH below 2 leads to the aggregation of CNC; emulsions formed under these conditions showed gel-like behavior. This work shows the potential of nanocellulose crystal in stabilizing food and industrial emulsions. This is of interest for applications where biodegradability, biocompatibility, and food grade requirements are needed.

OPEN ACCESS

Edited by:

Erica Wanless,
University of Newcastle, Australia

Reviewed by:

Catherine Whitby,
Massey University, New Zealand
Patrick Spicer,
University of New South Wales,
Australia

*Correspondence:

Gil Garnier
gil.garnier@monash.edu

Specialty section:

This article was submitted to
Chemical Engineering,
a section of the journal
Frontiers in Chemistry

Received: 15 May 2018

Accepted: 20 August 2018

Published: 19 September 2018

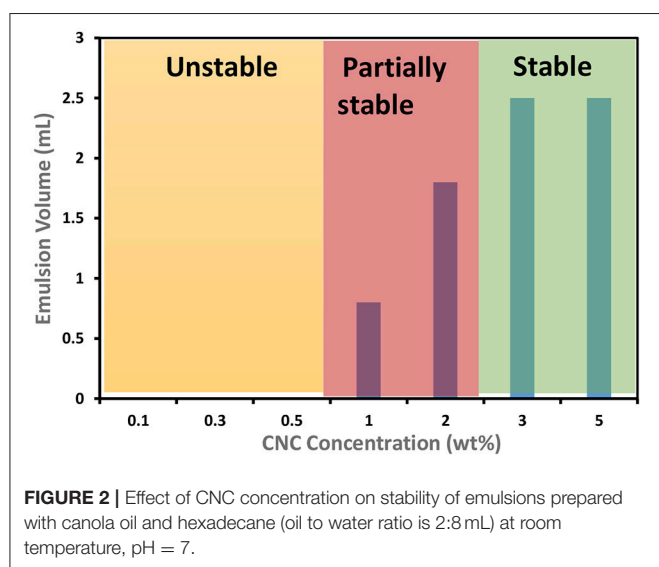
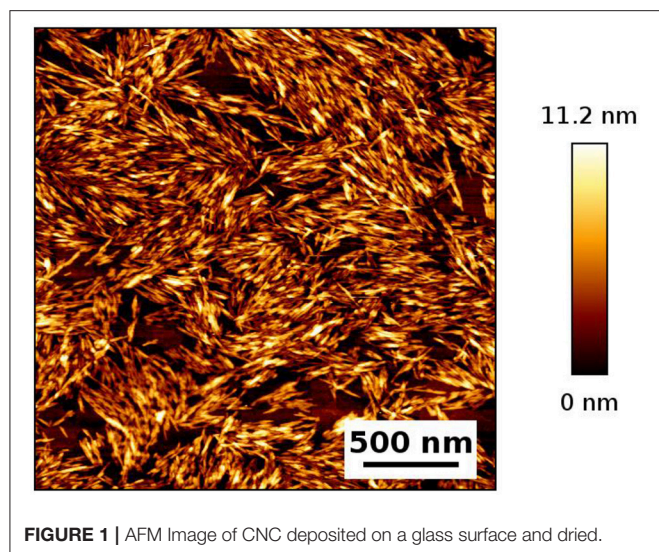
Citation:

Varanasi S, Henzel L, Mendoza L,
Prathapan R, Batchelor W, Tabor R
and Garnier G (2018) Pickering
Emulsions Electrostatically Stabilized
by Cellulose Nanocrystals.
Front. Chem. 6:409.
doi: 10.3389/fchem.2018.00409

Keywords: cellulose nanocrystals (CNC), Pickering emulsions, oil in water, gels, electrostatic stabilization

INTRODUCTION

Cellulose is the most abundant natural polymer. It consists of anhydroglucose units linearly linked through β -1,4-glycosidic bonds. Cellulose nanocrystals (CNC) and cellulose nanofibers (CNF) are two types of exciting green nanomaterials prepared from cellulosic sources (Safari et al., 2014). Nanocellulose has recently been investigated for a multitude of applications because of their renewable nature and unique properties such as wettability, large surface area, high aspect ratio, biocompatibility, being optically transparent, and amphiphilic nature, their strength and ease of chemical modification (Hosseinidoust et al., 2015; Trache et al., 2017). CNC particles are processed from native cellulose sources by controlled acid hydrolysis (Moon et al., 2011). Sulfuric acid hydrolysis dissolves the amorphous fraction, releasing the cellulose nanocrystals (CNC) with sulfate ester groups surface, resulting in electrostatically stabilized aqueous suspensions of CNC (Dong and Gray, 1997). In a dilute aqueous system, CNC particles are well dispersed and orient randomly due to electrostatic repulsion among negatively charged sulfate ester groups (Dong and Gray, 1997). The surface charge of CNC is primarily controlled by the hydrolysis conditions. Higher acid concentration, reaction time and temperature produces CNC of higher surface charge as promoted



by sulphuric acid diffusion into fibers (Nishio et al., 2016). Zeta-potential of CNC produced by sulphuric acid hydrolysis varies from -20 to -80 mV. In contrast, if hydrochloric acid is used to produce CNC, the resulting CNC has almost no charge (Nishio et al., 2016).

Many types of nano or microscale particles are used to stabilize the oil/water interface of emulsions, commonly known as Pickering emulsions (Wu and Ma, 2016). Pickering emulsions possess many unique features over classical surfactant stabilized emulsions, such as low toxicity and superior stability (Yang et al., 2017). Particle size, shape, wettability, surface properties, and particle concentration all influence the stability and drop size of emulsions (Wu and Ma, 2016). A key factor to form Pickering emulsions is wettability, which can be indicated by the contact angle at the interface. Binks et al. reported that particles of very low hydrophilicity or very high hydrophobicity are not suitable to form stable emulsions (Binks and Lumsdon, 2000). Particles having an intermediate contact angle (close to 90°) can easily

accumulate at the oil/water interface and form stable emulsions (Binks and Lumsdon, 2000). The optimum contact angle to prepare stable oil/water emulsion is around 70° and water/oil emulsion is 110° (Kaptay, 2006). Particles having smaller size will have faster adsorption kinetics and more efficient packing at the oil/water interface than bigger particles (Wu and Ma, 2016). Particle size should be at least one order of magnitude smaller than droplet size to prepare stable emulsion (Wang, 2013). Cylindrical or elliptical shaped particles showed superior stability than spherical shape particles since cylindrical particles pack like network structure and also their ability to shape capillary force between adsorbed particles at the interface is superior (Dugyala et al., 2013; Wang, 2013). In order to keep large surface area particles stable in suspension, there must be a steric hindrance or electrostatic repulsion between the particles. However, this force between particles acts as an activation barrier for particle adsorption. At present, there is very little information in the literature to describe the governing laws between surface charge and particle adsorption of CNC (Wu and Ma, 2016).

In this study, CNCs were investigated to prepare very strong and stable Pickering emulsions because of their high aspect ratio. Cellulose Nanofibers (CNF) are also being used in Pickering emulsions (Kalashnikova et al., 2011; Capron and Cathala, 2013; Carrillo et al., 2015; Wang et al., 2016; Capron et al., 2017). Although both CNCs and CNFs are not surface active, they position efficiently at the oil/water or water/oil interface because of their amphiphilic nature (Capron et al., 2017). A presence of hydrophobic edge plane is attributed to its amphiphilic nature. Kalashnikova et al. first reported preparing Pickering emulsions with bacterial CNC (Kalashnikova et al., 2011). Later they described that when sulphated cotton cellulose nanocrystals (CNC) were used, no emulsion was observed (Kalashnikova et al., 2012). To prepare Pickering emulsions with sulphated CNC, the surface charge density has to be modulated to 0.033 e/nm² or lower. The charge density of CNC can be modulated by treating sulphated CNC with mild HCl or adding salts. However, thermodynamically amphiphilic particles can form stable emulsions regardless of their charge density. Many reports concluded that the surface charge of CNCs and CNFs play a key role in the stability of emulsions (Marinova et al., 1996; Kalashnikova et al., 2011, 2012; Fujisawa et al., 2017; Miao et al., 2017). However, there is no systematic study on the role of electrostatics in CNC based emulsions.

CNCs are also being used for preparing high internal phase emulsions (HIPE) (Marinova et al., 1996; Fujisawa et al., 2017; Miao et al., 2017). Capron and Cathala reported a two-step procedure to prepare HIPEs with CNCs (Fujisawa et al., 2017). First, a low internal phase emulsion having 10% oil content was prepared using an ultrasonicator. In the second step, extra oil was added into the already formed emulsion, followed by shearing with a double cylinder-type homogenizer. The resulting final emulsions had a gel-like appearance. Miao et al. also reported another type of two-step procedure to prepare HIPEs with CNC (Marinova et al., 1996). In their study, homogenization at low shear (approximately 2,000 rpm for 1 min) was followed by high shear (10,000 rpm for 1 min). However, the viscoelastic properties of these gel-like emulsions were not reported.

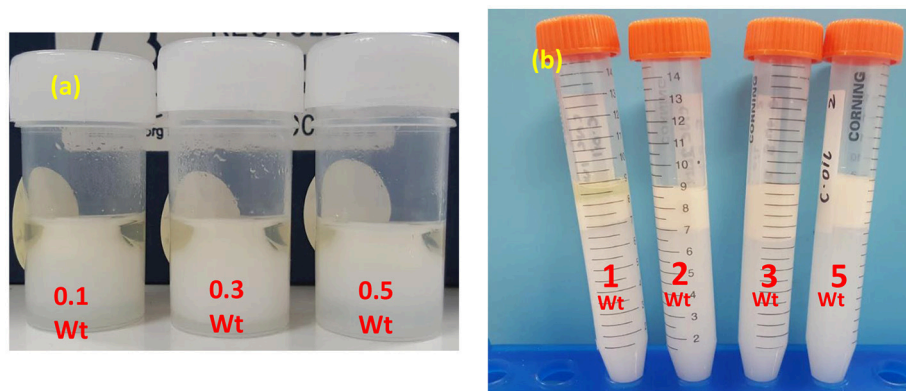


FIGURE 3 | Photographs of CNC stabilized C. Oil/water emulsion after centrifugation. **(a)** Low CNC concentrations and **(b)** high CNC concentrations.

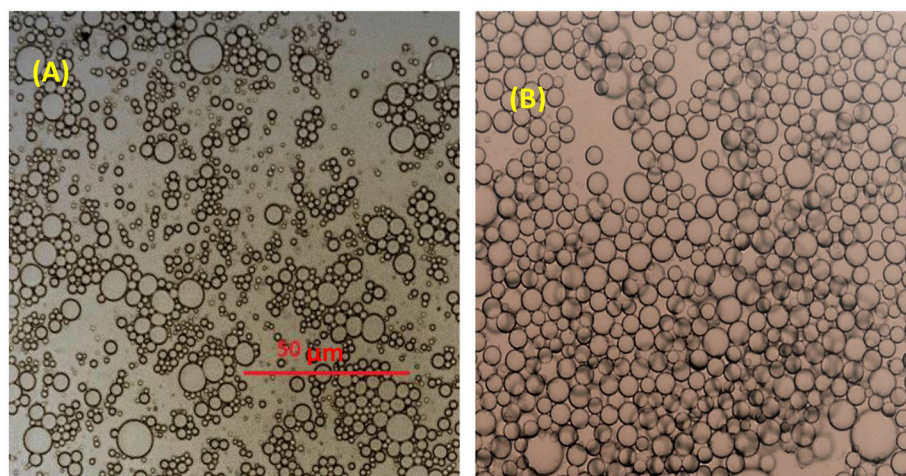


FIGURE 4 | Microscopic image of emulsions stabilized with 3 wt% CNC **(A)** C. Oil/water **(B)** hexadecane/water emulsions.

This study aims at exploring whether stable emulsions can be prepared from CNCs having surface charge density higher than 0.033 e/nm^2 and if modulating their charge density, by adding salts and varying pH, can reduce the amount of CNCs required to form a stable emulsion. This paper investigates the role played by electrostatic forces in CNC based emulsions and whether these are completely charge driven systems. This study also describes a method to prepare CNC based emulsified gels on a single shearing method.

EXPERIMENTAL SECTION

Materials

Cellulose nanocrystals (CNC, 12.6 wt %) were purchased from the University of Maine Process Development Center as a dispersion in water (sulfur content of 1–2%), with an average width of 8 nm and length 138 nm. Canola oil was purchased from the local supermarket. Hexadecane, Sodium Chloride (NaCl) and Calcium Chloride (CaCl_2) were purchased from Sigma

Aldrich, Australia. Oils were used as supplied- without further purification.

Methods

- Emulsion preparation:** All the emulsions were prepared using an oil/water ratio of 20/80 (v/v). Typically, 2 mL of canola oil was added to 8 mL of the CNC aqueous suspension in a 50 mL vial and was sonicated with a titanium probe (Sonics Vibra-cell High Intensity Ultrasonic Processor, VCX 500–VCX 750) immersed in the solution under the following conditions: 3 s on and 3 s off for an interval of 3 min, with 44 Watts power input. The sonicated emulsions were then poured into 15 mL centrifuge tubes (without any separation) and centrifuged at 4,000G for 10 min to estimate the stability of CNC-palm oil emulsion. Cream volume after centrifugation is noted as emulsion volume.
- Conductometric Titration:** Conductometric titration was performed to determine the surface charge density as reported in Kalashnikova et. al. (Kalashnikova et al., 2012). In brief, a

total of 50 mL of a CNC suspension at 1 g/L in water was titrated with freshly prepared 2 mM NaOH with a TIM900 titration manager and a CDM230 conductimeter equipped with a CDC749 titration cell (Kalashnikova et al., 2012; Zhong et al., 2012). CNC samples showed low conductance values because of their small amounts of charge so HCl and NaCl were added prior to titration.

- Z-potential measurement:** The electrophoretic mobility of aliquots of aqueous CNC suspensions at 0.1 g/L was measured in triplicate with a NanoBrook Omni (Brookhaven's Instruments).
- The optical micrographs of the prepared emulsions on transparent glass slides were taken using a microscope (Nikon upright motorized microscope Eclipse Ni-E) immediately after each preparation. Drop sizes and distribution were measured using ImageJ software.
- Rheology:** All rheological testing of the gel like emulsions were performed with an Anton Paar MCR302 rheometer. A cone (0.997°) and plate (49.975 mm) geometry were selected. Testing was done at ambient temperature (25°C). To ensure stable temperature during the testing, a solvent trap was used. Viscosity was measured at shear rate ranging from 0.5 to 100 s⁻¹. Oscillatory strain sweep was performed from 0.01 to 100% at a constant 1 Hz frequency. Frequency sweep was measured from 0.1 to 100 rad/s and at 0.1% strain. All measurements were in triplicates.
- Atomic Force Microscopy imaging:** Atomic force microscopy (AFM, JPK Nanowizard 3) was used in alternating contact, AC mode to obtain images of CNC morphology and particle size. CNC suspension drop was casted and air dried on glass slide.

RESULTS

An AFM image of the CNC studied is shown in **Figure 1**. Cellulose nanocrystals (CNC) having an average diameter 8 nm, a length 138 nm, a surface charge density of 0.11 e/nm² and a zeta potential of -70 mV were used to prepare a series of canola oil (C. Oil)/water and hexadecane/water emulsions. The CNC rods exhibit a strongly negatively charged surface because of the presence of hydroxyl and sulfate groups. CNC concentration was varied to study this effect on the stability of oil/water emulsions prepared with two types of oils. Results are shown in **Figure 2**. Hexadecane behaves similarly to C. Oil. CNCs could not stabilize the emulsions at concentrations ranging from 0.1 to 0.5 wt%. This supports the work of Kalashnikova et al. also reporting that CNC could not stabilize hexadecane/water emulsion at a concentration of 0.1 wt% (Kalashnikova et al., 2012). Interestingly, CNC stabilizes emulsions at a concentration higher than 1 wt% CNC for both types of oils, even though the CNC surface charge density is higher than 0.033 e/nm². Canola oil/water and hexadecane/water samples were centrifuged at 4,000G for 10 min to test their stability.

Figure 3 shows the appearance of C. Oil/water emulsions after centrifugation in vials and centrifuge tubes. Emulsions were prepared with CNC concentration ranging from 0.1 to 0.5 wt%

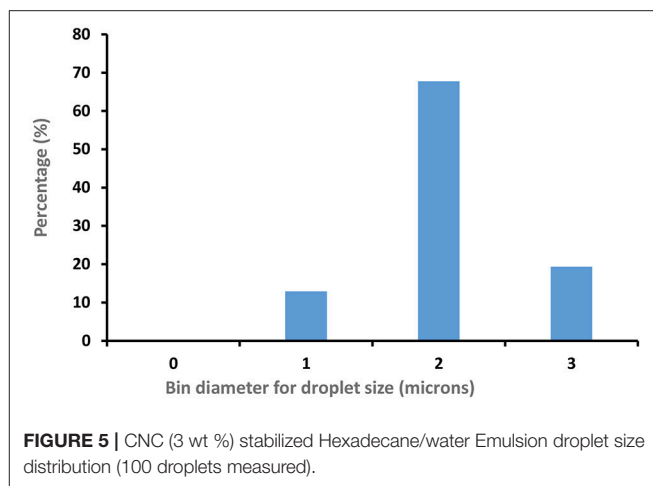


FIGURE 5 | CNC (3 wt %) stabilized Hexadecane/water Emulsion droplet size distribution (100 droplets measured).

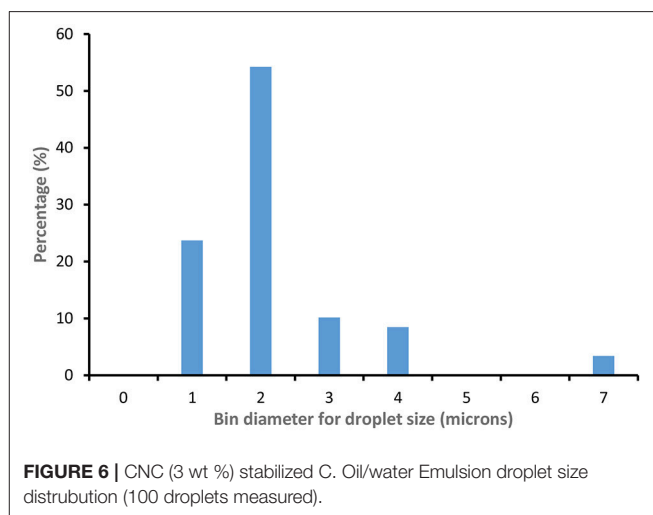


FIGURE 6 | CNC (3 wt %) stabilized C. Oil/water Emulsion droplet size distribution (100 droplets measured).

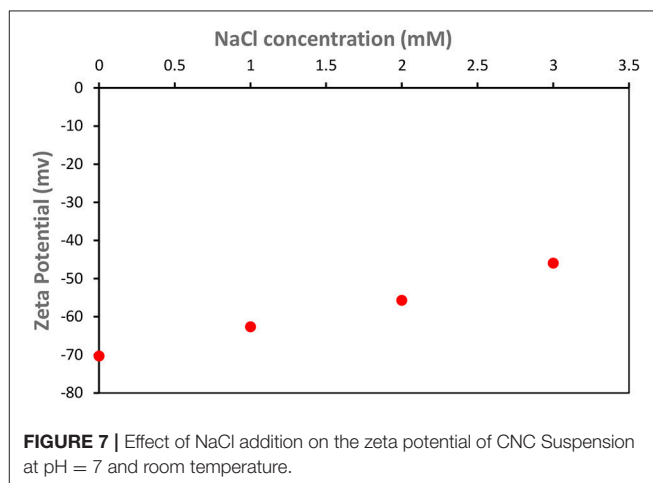


FIGURE 7 | Effect of NaCl addition on the zeta potential of CNC Suspension at pH = 7 and room temperature.

(**Figure 3a**) and from 1 to 5 wt% (**Figure 3b**). The oil and aqueous layers separated clearly. At CNC concentrations of 1 and 2 wt%, a stable emulsion is formed between the oil and the aqueous layers where the emulsion volume is lower than the initial oil volume. In

contrast, at CNC concentrations of 3 and 5 wt%, stable emulsions and aqueous layers were observed, with the emulsion volume higher than the initial oil volume. Completely stable emulsions are formed at 3 wt% CNC and higher concentrations.

Figure 4 displays optical microscopy images of CNC stabilized C. Oil and hexadecane in water emulsions. Droplets of hexadecane/water emulsion are uniformly dispersed, with an average diameter of $2.5\ \mu\text{m}$ (std. dev = $0.3\ \mu\text{m}$) microns (**Figure 5**). However, C. Oil/water emulsions with an average diameter of $2.7\ \mu\text{m}$ and a high standard deviation of $1.2\ \mu\text{m}$ (**Figure 6**) are more polydispersed and have random aggregates.

Effect of Salts on Emulsions Stability

Salt greatly affects the stability of C. Oil/water emulsions. Salts are well known for screening the electrostatic repulsion on CNC surfaces (Kalashnikova et al., 2012). The zeta potential of CNC decreased linearly from $(-70\ \text{mV})$ to $(-50\ \text{mV})$ with the addition of 0 to 3 mM NaCl (**Figure 7**). The limiting conditions of CNC based Pickering emulsions in the presence of NaCl were studied (**Figure 8**). Experiments were initially conducted with the addition of 100 mM NaCl solution to varying CNC concentrations ranging from 3 to 0.1 wt%. After identifying that 0.1 wt% CNC can stabilize C. Oil/water emulsions with 100 mM NaCl, the NaCl concentration was varied, keeping the CNC concentration constant at 0.1 wt%. It was found that CNC could stabilize C. Oil/water emulsions at 0.1 wt% concentration with as little as 3 mM NaCl concentration. Emulsion volume remained constant for NaCl concentration ranging from 3 to 20 mM. As the NaCl concentration increased from 20 to 50 mM, the emulsion volume increased by 15%. At 1 wt% CNC concentration, the emulsion volume is 2.5 mL which is 3 times higher than in absence of salt. Interestingly, the emulsion volume at 3 wt% CNC and 100 mM NaCl concentration correspond to the total volume of the aqueous suspension and oil used. Even with the centrifuge tube placed upside down, the emulsion after stability test did not flow, forming a gel-like network (**Figure 9**). Rheological properties of this gel are discussed in the last part of the discussion section.

Similarly, the effect of CaCl_2 addition on the stability of C. Oil/water emulsion was tested (**Figure 10**). It was found that CNC could stabilize C. Oil/water emulsions at 0.1 wt% concentration with CaCl_2 concentration as low as 1 mM or even lower.

Effect of pH on C. Oil/Water EMULSIONS Stability

Varying pH from 7 to 3 had no effect on the stability of C. Oil/water emulsions (**Table 1**). 0.1 wt% CNC could not form stable C. Oil/water emulsions for pH ranging between 7 and 3. In contrast, at pH 2 or below, 0.1 wt% CNC formed stable emulsions. On the other hand, 3 wt% CNC could form stable C. Oil/water emulsion at pH 7 or below. At pH below 2, the emulsion volume represented the combined volume of the aqueous suspension and oil used. The emulsion prepared with 3 wt% CNC at pH 3.9 flowed when the centrifuge tube was turned upside down; the emulsion formed with 3 wt% CNC at pH 1 did not. At lower pH, the emulsion formed a gel network (**Figure 11**).

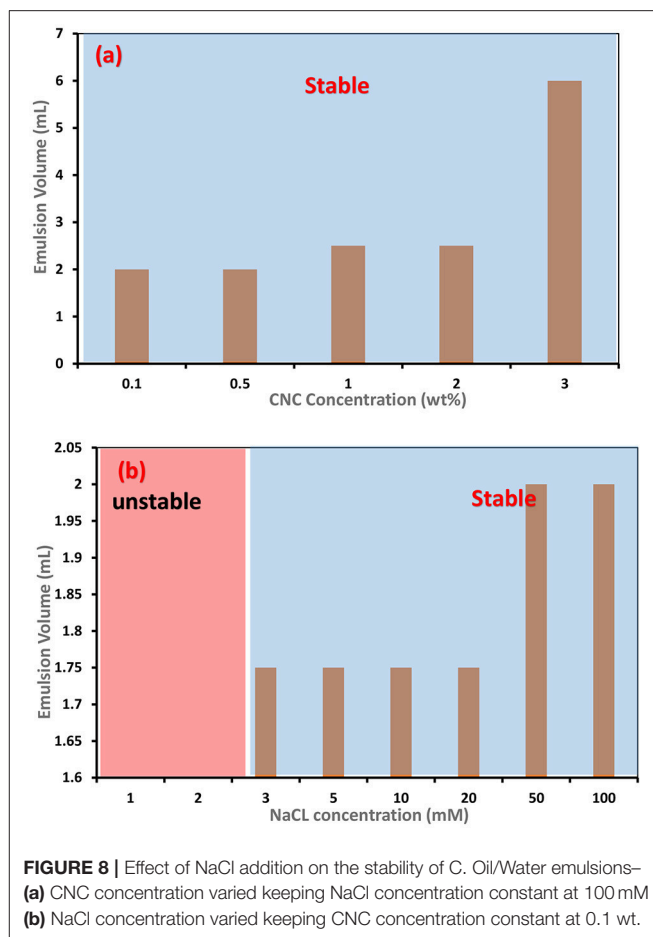


FIGURE 8 | Effect of NaCl addition on the stability of C. Oil/Water emulsions—
(a) CNC concentration varied keeping NaCl concentration constant at 100 mM
(b) NaCl concentration varied keeping CNC concentration constant at 0.1 wt.

The rheological properties of the C. Oil in water gel are shown in **Figures 12, 13**. Gel-like emulsions are subjected to strain (**Figure 12**) and frequency (**Figure 13**) sweeps. In a strain sweep, the range of viscoelastic behavior can be quantified for gels. The elastic modulus G' describes the solid-like behavior of gel whereas the loss or viscous modulus G'' defines the liquid-like behavior of the material.

DISCUSSION

Particle concentration is an important factor in the formation of particle stabilized emulsions, commonly known as Pickering emulsions. It has a remarkable influence on the emulsion stability. Stable Pickering emulsion formation is a two-step process. Firstly, particles migrate from the aqueous dispersion onto the oil–water interface. Then, particles adsorb at the oil/water interface replacing and decreasing the oil–water contact area. The adsorbed particles act as emulsifiers, by lowering the interfacial free energy primarily by reducing the interfacial area between the two phases and makes the system stable (Wang, 2013).

The amphiphilic nature of negatively charged CNC's is the driving force for their migration from solution toward the

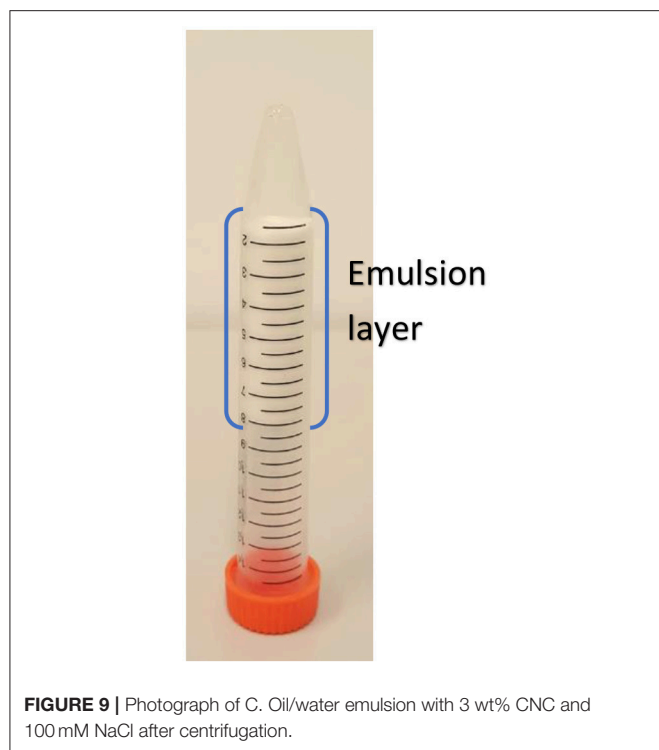


FIGURE 9 | Photograph of C. Oil/water emulsion with 3 wt% CNC and 100 mM NaCl after centrifugation.

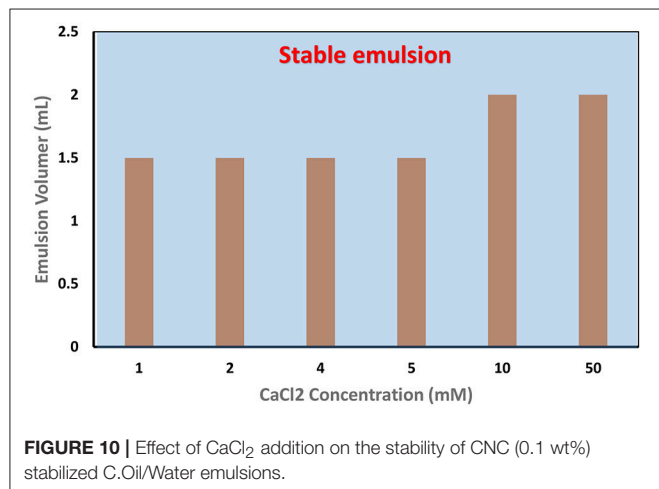


FIGURE 10 | Effect of CaCl₂ addition on the stability of CNC (0.1 wt%) stabilized C.Oil/Water emulsions.

oil/water interface during emulsification. However, significant electrostatic repulsion occurs when a negatively charged CNC (because of sulfate ester groups on the surface) approaches the oil-water interface that is also negatively charged due to the preferential adsorption of hydroxide ions (Capron and Cathala, 2013). Such repulsion can create an energy barrier preventing particle adsorption to the interface, and hinder the formation of emulsions (Danov et al., 2005; Golemanov et al., 2006). Hence, stable emulsions could not form at low concentrations of CNCs ranging from 0.1 to 0.5 wt% (Figures 2, 3).

At higher concentrations, starting from 1 wt%, CNC tend to aggregate in aqueous solution (Xu et al., 2017) because of chemical interaction (for example hydrogen bond) and

TABLE 1 | Effect of pH on the stability of C. Oil/water emulsions.

CNC concentration (wt%)	pH	Emulsion condition	Emulsion Volume (mL)
0.1	7	No Emulsion	0
	6	No Emulsion	0
	5	No Emulsion	0
	4	No Emulsion	0
	2	Stable	2
3	1.1	Stable	2
	3.9	Stable	2
3	1.1	Stable	9

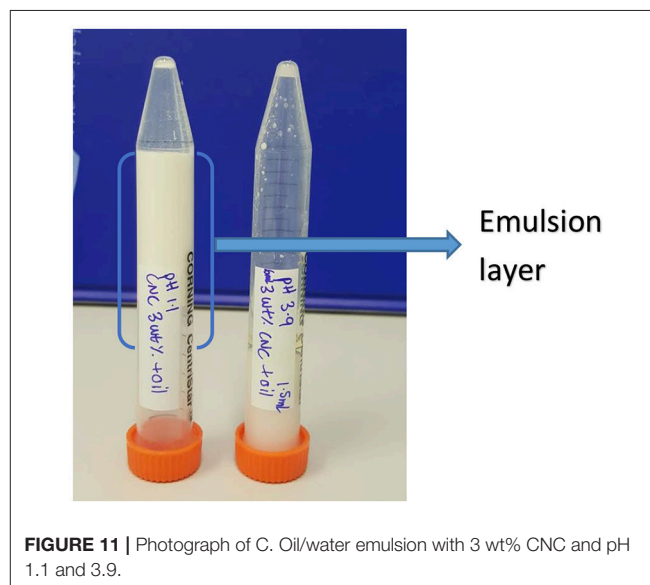


FIGURE 11 | Photograph of C. Oil/water emulsion with 3 wt% CNC and pH 1.1 and 3.9.

strong affinity toward material containing hydroxyl groups (hydrogen bonding between CNC and water molecules) (Li et al., 2015). CNC aggregates have higher adsorption energy (force of attraction) that dominates the repulsion force between CNCs and oil/water interface (Paunov et al., 2002). Adsorbed CNC aggregates minimize the interfacial free energy primarily by reducing the interfacial area between the oil/water interfaces. Hence, CNC's can stabilize the emulsions at higher concentrations than 1 wt%.

Effect of Salts Addition on Emulsion Stability

The amount of CNC required to stabilize the emulsion reduced greatly with the addition of either NaCl or CaCl₂. Figure 7 shows that the zeta potential of CNC suspension reduced gradually with increasing NaCl concentration. Zhong et al. (2012) and Prathapan et al. (2016) reported similar observations. This is because of the electrostatic screening effect from the cation counter ion Na⁺ and the Debye-Huckel screening strength augments upon increasing salt concentration; therefore, the Debye length decreases. For example, the Debye length and ionic strength of NaCl at

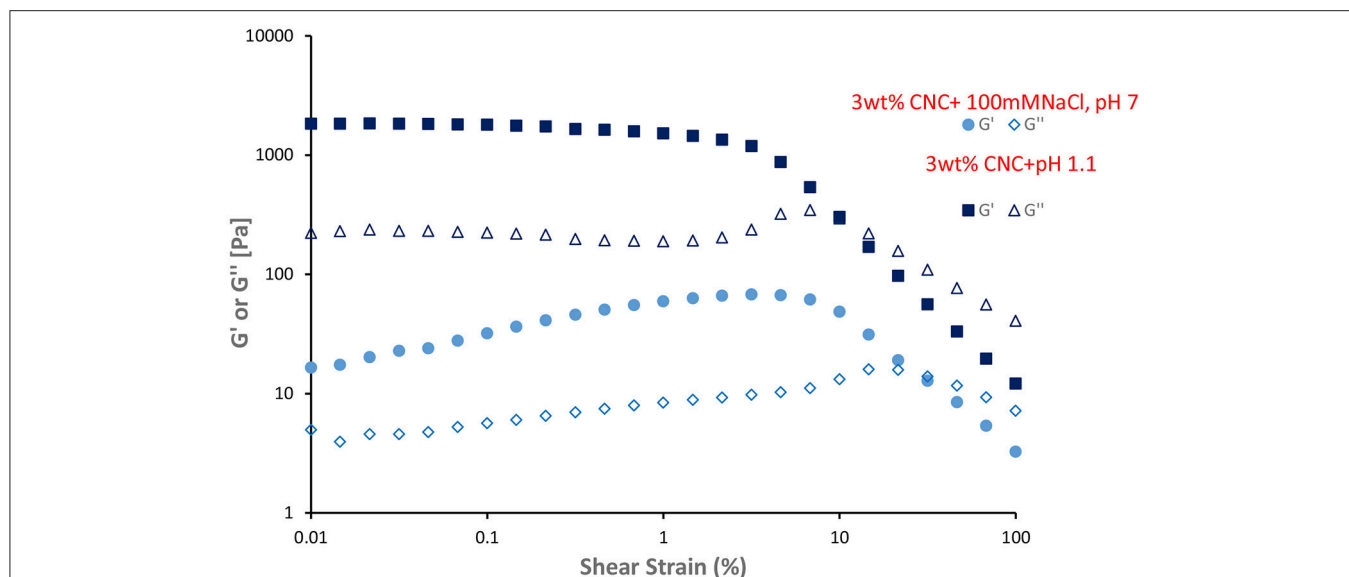


FIGURE 12 | Dynamic strain sweep of gel like emulsions (3 wt% CNC and 100 mM NaCl, 3 wt% CNC and pH 1.1) at 25°C and frequency of 1 Hz. Filled symbol indicate elastic moduli (G') and unfilled symbol indicate loss moduli (G'').

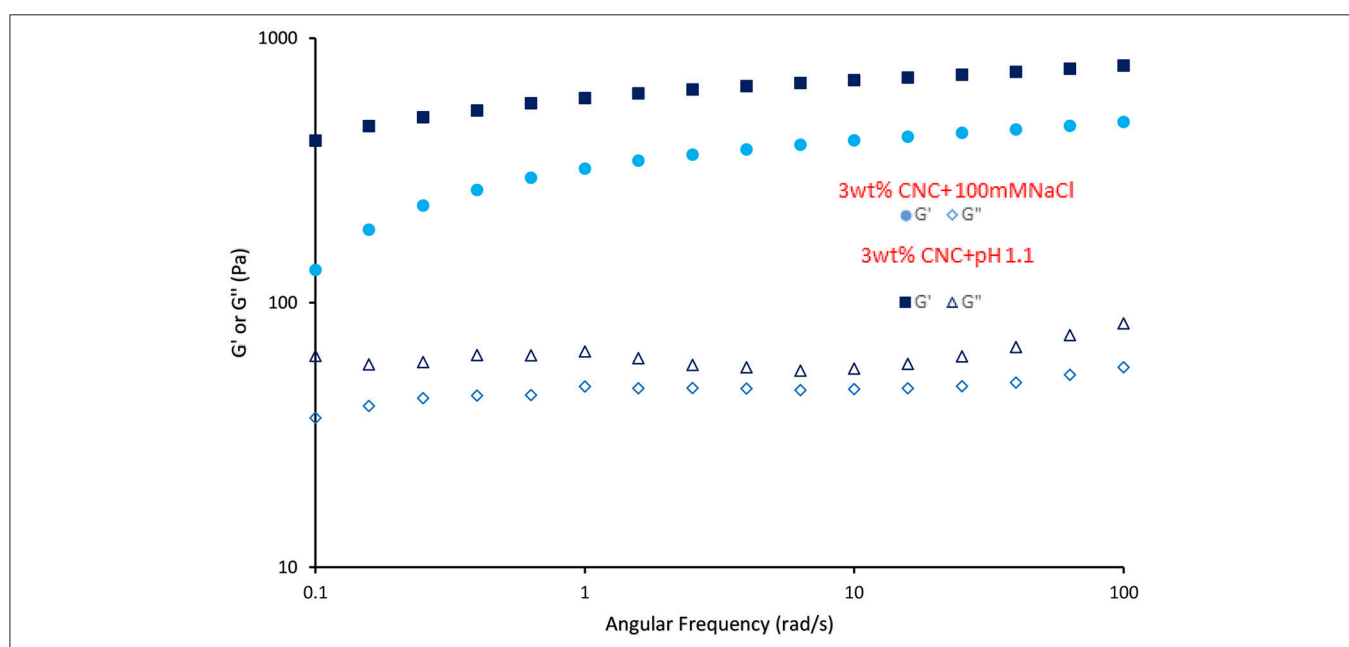


FIGURE 13 | Dynamic frequency sweep of gel like CNC emulsion (3 wt% CNC and 100 mM NaCl, 3 wt% CNC and pH 1.1) at 25°C and 0.1% strain. Filled symbol indicate elastic moduli (G') and unfilled symbol indicate loss moduli (G'').

1 mM concentration are 9.6 nm and 1 mol/m³, respectively; at 3 mM concentration, these are 5.54 nm and 3 mol/m³. Prathapan et al. (2016) further reported that Ca²⁺ ions screen stronger than Na⁺ ions. Hence, there was a greater reduction in CNC zeta potential with the addition of Ca²⁺ ions. The Debye length of CaCl₂ at 1 mM concentration is 4.52 nm, which is lower than that of NaCl at 3 mM concentration (5.54 nm).

Double layer principles imply that the adsorption of ions and ion pairs to the CNC surface shield the surface charge of CNC and reduces the electrostatic repulsion, which facilitates the CNC to migrate and adsorb onto the oil/water interface in the presence of Na⁺ and Ca²⁺ ions, even at 0.1 wt% CNC concentration. Hence, a stable C. Oil/water emulsion could form at 0.1 wt% CNC in the presence of Na⁺ and Ca²⁺ ions. The amount of CNC required to stabilize 2 mL of C. Oil is 30 times less in the presence

of salts. Interestingly, to stabilize C. Oil/water emulsion with a 0.1 wt% CNC suspension, <1 mM CaCl_2 addition to the CNC suspension is required, which is 3 times lower than for NaCl. This directly corroborates the Debye length of CaCl_2 and NaCl. These results indicate that stabilization of oil/water emulsion with CNC is governed by the surface charge in the presence of electrolytes.

Zhong et al. reported that a 0.15 wt% CNC suspension is clear and transparent, indicating a stable suspension because of charge repulsion among CNCs (Zhong et al., 2012). When ionic strength increased to 50 mM Na^+ , CNC particles tend to aggregate to a size of 980 nm, which is 10 times higher than their initial size. This is because of van der Waals forces dominating the electrostatic repulsion. Xu et al. reported that CNC tends to aggregate even in the absence of electrolytes at concentrations higher than 1 wt% (Xu et al., 2017). When the suspension concentration is higher than 3 wt%, aggregation of CNC became denser through long-range electrostatic interactions (Xu et al., 2017). When 100 mM NaCl is added to a 3 wt% CNC suspension, CNC aggregates grew in size and connected into a percolating network. Macroscopically, gel-like behavior is observed. Peddireddy et al. also reported similar observations with CNC concentrations higher than 12 g/L and 70 mM NaCl (Peddireddy et al., 2016). Emulsions prepared with a 3 wt% CNC suspension and ionic strength of 100 mM Na^+ behave like gels. The emulsion volume is 9 mL, corresponding to the total volume of oil and aqueous suspension.

Effect of pH on Emulsion Stability

Prathapan et al. (2016) and Zhong et al. (2012) reported that when the pH is varied from 11 to 2, the change in CNC suspension zeta potential is very low. This is because pH did not significantly alter the disassociation state of the sulfate ester groups present on the CNC surface since the pK_a of covalently bound sulfate ester group ($\text{pK}_a = 1.9$) is very low. However, for pH below 2, a considerable reduction in zeta potential—i.e., net charge on CNC surface, and agglomeration of CNC results because of the protonation of the sulfonic acids starting to occur. Again, reduction in the net charge of CNC at pH below 2 helps their migration and adsorption at the oil/water interface to form stable emulsions with 0.1 wt% CNC. When emulsions are prepared with 3 wt% CNC at pH 1.1, aggregates of CNC grew in size and connect into a percolating network gel.

Emulsions prepared with 3 wt% CNC, 100 mM NaCl, and pH 1.1 show gel behavior. Viscoelastic properties of these gels were presented in Figures 12, 13. G' and G'' of gel-like emulsions obtained at pH 1.1 are higher than those with 100 mM NaCl. At low shear stresses, both gel emulsions possess a linear viscoelastic region (LVR) wherein the elastic modulus G' and viscous modulus G'' are independent of shear stress. Within this region, G' is dominant over G'' , indicating that the material is acting as a solid; elastic behavior dominates over viscous compartment. At a critical shear stress, the gel yields as shown by the decrease in G' , and then reaches a “cross-over point” where

G'' becomes dominant and the gel begins to flow. Past this critical stress, the viscous regime dominates ($G'' > G'$) indicating that the network structure has yielded and begins to behave as a non-Newtonian shear thinning fluid. Figure 13 gives the frequency sweep i.e., the time-dependent behavior of the gel emulsion. For both gel emulsions, the G' and G'' values are non-intersecting with G' increasing gradually with angular frequency. This slight increase in moduli shows these gels to be weakly cross-linked (Mendoza et al., 2018).

CONCLUSION

Cellulose nanocrystals (CNC) can form stable oil/water emulsions regardless of their charge density. This contradicts the limiting condition of charge density below 0.033 e/nm^2 reported in the literature for the formation of stable emulsions with CNC. However, higher charge density CNC requires higher amounts of CNC and higher concentrations. At high CNC concentrations, the adsorption forces of CNC aggregates dominate the electrostatic repulsion between CNC and the oil/water interface. As the charge density reduces through the addition of salts, lower concentrations of CNC are required because of the salt induced reduction in electrostatic repulsion. The amount of CNC required to stabilize 2 mL of oil is 30 times less in the presence of salts. The ratio of minimum ionic strength required to prepare a stable emulsion with CaCl_2 and NaCl directly corroborates with the Debye length ratio of CaCl_2 and NaCl. This indicates that stabilization of oil/water emulsion with CNC is governed by surface charge in the presence of electrolytes. Emulsions prepared with 3 wt% CNC suspensions have an ionic strength of 100 mM Na^+ and behaved like a gel. Varying pH from 7 to 3 had no effect on the stability of emulsions. However, the emulsion prepared with 3 wt% CNC and at pH below 2 behaved like a gel. These gels are weakly cross-linked. Cellulose nanocrystal offers a new way to stabilize oil in water by forming Pickering emulsions. The systems are completely biodegradable and biocompatible and can form robust gels or not, opening new innovation avenues in food and biomedical applications.

AUTHOR CONTRIBUTIONS

SV, WB, and GG prepared manuscript. SV, LH, and LM performed experiments. RP and RT performed AFM measurements.

ACKNOWLEDGMENTS

Financial support was from Australian Research Council, Australian Paper, Carter Holt Harvey, Circa, Norske Skog and Visy through the Industry Transformation Research Hub grant IH130100016. Thanks to Monash Centre for Electron Microscopy for training and facilities, Dr. C. Henderson for assisting with an optical microscope and Dr. V. Raghuwanshi for discussion and manuscript preparation.

REFERENCES

- Binks, B. P., and Lumsdon, S. O. (2000). Influence of particle wettability on the type and stability of surfactant-free emulsions. *Langmuir* 16, 8622–8631. doi: 10.1021/la000189s
- Capron, I., and Cathala, B. (2013). Surfactant-free high internal phase emulsions stabilized by cellulose nanocrystals. *Biomacromolecules* 14, 291–296. doi: 10.1021/bm301871k
- Capron, I., Rojas, O. J., and Bordes, R. (2017). Behavior of nanocelluloses at interfaces. *Curr. Opin. Colloid Interf. Sci.* 29(Suppl. C), 83–95. doi: 10.1016/j.cocis.2017.04.001
- Carrillo, C. A., Nypelö, T. E., and Rojas, O. J. (2015). Cellulose nanofibrils for one-step stabilization of multiple emulsions (W/O/W) based on soybean oil. *J. Colloid Interf. Sci.* 445(Suppl. C), 166–173. doi: 10.1016/j.jcis.2014.12.028
- Danov, K. D., Kralchevsky, P. A., Naydenov, B. N., and Brenn, G. (2005). Interactions between particles with an undulated contact line at a fluid interface: Capillary multipoles of arbitrary order. *J. Colloid Interf. Sci.* 287, 121–134. doi: 10.1016/j.jcis.2005.01.079
- Dong, X. M., and Gray, D. G. (1997). Effect of counterions on ordered phase formation in suspensions of charged rodlike cellulose crystallites. *Langmuir* 13, 2404–2409. doi: 10.1021/la960724h
- Dugyala, V. R., Daware, S. V., and Basavaraj, M. G. (2013). Shape anisotropic colloids: synthesis, packing behavior, evaporation driven assembly, and their application in emulsion stabilization. *Soft Matter* 9, 6711–6725. doi: 10.1039/c3sm50404b
- Fujisawa, S., Togawa, E., and Kuroda, K. (2017). Nanocellulose-stabilized pickering emulsions and their applications. *Sci. Technol. Adv. Mater.* 18, 959–971. doi: 10.1080/14686996.2017.1401423
- Golemanov, K., Tcholakova, S., Kralchevsky, P. A., Ananthapadmanabhan, K. P., and Lips, A. (2006). Latex-particle-stabilized emulsions of anti-bancroft type. *Langmuir* 22, 4968–4977. doi: 10.1021/la0603875
- Hosseindoust, Z., Alam, M. N., Sim, G., Tufenkji, N., and van de Ven, T. G. (2015). Cellulose nanocrystals with tunable surface charge for nanomedicine. *Nanoscale* 7, 16647–16657. doi: 10.1039/C5NR02506K
- Kalashnikova, I., Bizot, H., Cathala, B., and Capron, I. (2011). New pickering emulsions stabilized by bacterial cellulose nanocrystals. *Langmuir* 27, 7471–7479. doi: 10.1021/la200971f
- Kalashnikova, I., Bizot, H., Cathala, B., and Capron, I. (2012). Modulation of cellulose nanocrystals amphiphilic properties to stabilize oil/water interface. *Biomacromolecules* 13, 267–275. doi: 10.1021/bm201599j
- Kaptay, G. (2006). On the equation of the maximum capillary pressure induced by solid particles to stabilize emulsions and foams and on the emulsion stability diagrams. *Colloids Surf. A* 282–283(Suppl. C), 387–401. doi: 10.1016/j.colsurfa.2005.12.021
- Li, M. C., Wu, Q., Song, K., Lee, S., Qing, Y., and Wu, Y. (2015). Cellulose nanoparticles: structure–morphology–rheology relationships. *ACS Sustain. Chem. Eng.* 3, 821–832. doi: 10.1021/acssuschemeng.5b00144
- Marinova, K. G., Alargova, R. G., Denkov, N. D., Velev, O. D., Petsev, D. N., Ivanov, I. B., et al. (1996). Charging of oil–water interfaces due to spontaneous adsorption of hydroxyl ions. *Langmuir* 12, 2045–2051. doi: 10.1021/la950928i
- Mendoza, L., Batchelor, W., Tabor, R. F., and Garnier, G. (2018). Gelation mechanism of cellulose nanofibre gels: A colloids and interfacial perspective. *J. Coll. Interface Sci.* 509(Suppl. C), 39–46. doi: 10.1016/j.jcis.2017.08.101
- Miao, C., Tayebi, M., and Hamad, W. Y. (2017). Investigation of the formation mechanisms in high internal phase Pickering emulsions stabilized by cellulose nanocrystals. *Philos. Trans. R. Soc. A* 376:20170039. doi: 10.1098/rsta.2017.0039
- Moon, R. J., Martini, A., Nairn, J., Simonsen, J., Youngblood, J., (2011). Cellulose nanomaterials review: structure, properties and nanocomposites. *Chem. Soc. Rev.* 40, 3941–3994. doi: 10.1039/c0cs00108b
- Nishio, Y., Sato, J., and Sugimura, K. (2016). “Liquid crystals of cellulose: fascinating ordered structures for the design of functional material systems,” in *Cellulose Chemistry and Properties: Fibers, Nanocelluloses and Advanced Materials*, ed O. J. Rojas (Cham: Springer International Publishing), 241–286.
- Paunov, V. N., Binks, B. P., and Ashby, N. P. (2002). Adsorption of charged colloid particles to charged liquid surfaces. *Langmuir* 18, 6946–6955. doi: 10.1021/la0203584
- Peddireddy, K. R., Capron, I., Nicolai, T., and Benyahia, L. (2016). Gelation kinetics and network structure of cellulose nanocrystals in aqueous solution. *Biomacromolecules* 17, 3298–3304. doi: 10.1021/acs.biomac.6b01061
- Prathapan, R., Thapaa, R., Garnier, G., and Tabora, R. F. (2016). Modulating the zeta potential of cellulose nanocrystals using salts and surfactants. *Coll. Surf. A Physicochem. Eng. Aspec.* 509(Suppl. C), 11–18. doi: 10.1016/j.colsurfa.2016.08.075
- Safari, S., Sheikhi, A., and van de Ven, T. G. (2014). Electroacoustic characterization of conventional and electrosterically stabilized nanocrystalline celluloses. *J. Colloid Interface Sci.* 432(Suppl. C), 151–157. doi: 10.1016/j.jcis.2014.06.061
- Trache, D., Hussin, M. H., Haafiz, M. K. M., and Thakur, V. K. (2017). Recent progress in cellulose nanocrystals: sources and production. *Nanoscale* 9, 1763–1786. doi: 10.1039/C6NR09494E
- Wang, H. (2013). *Understanding of Charge Effects in Pickering Emulsions and Design of Double Pickering Emulsion Templated Composite Microcapsules*. Chemical and Biomolecular Engineering. Georgia Institute of Technology.
- Wang, W., Du, G., Li, C., Zhang, H., Long, Y., and Ni, Y. (2016). Preparation of cellulose nanocrystals from asparagus (*Asparagus officinalis* L.) and their applications to palm oil/water Pickering emulsion. *Carbohydrate Polymers* 151(Suppl. C), 1–8. doi: 10.1016/j.carbpol.2016.05.052
- Wu, J., and Ma, G.-H. (2016). Recent studies of pickering emulsions: particles make the difference. *Small* 12, 4633–4648. doi: 10.1002/smll.201600877
- Xu, H. N., Tang, Y. Y., and Ouyang, X. K. (2017). Shear-induced breakup of cellulose nanocrystal aggregates. *Langmuir* 33, 235–242. doi: 10.1021/acs.langmuir.6b03807
- Yang, Y., Fang, Z., Chen, X., Zhang, W., Xie, Y., Chen, Y., et al., (2017). An overview of pickering emulsions: solid-particle materials, classification, morphology, and applications. *Front. Pharmacol.* 8:287. doi: 10.3389/fphar.2017.00287
- Zhong, L., Fu, S., Peng, X., Zhan, H., and Sun, R. (2012). Colloidal stability of negatively charged cellulose nanocrystalline in aqueous systems. *Carbohydrate Polymers* 90, 644–649. doi: 10.1016/j.carbpol.2012.05.091

Conflict of Interest Statement: The authors declare that the research was conducted in the absence of any commercial or financial relationships that could be construed as a potential conflict of interest.

Copyright © 2018 Varanasi, Henzel, Mendoza, Prathapan, Batchelor, Tabor and Garnier. This is an open-access article distributed under the terms of the Creative Commons Attribution License (CC BY). The use, distribution or reproduction in other forums is permitted, provided the original author(s) and the copyright owner(s) are credited and that the original publication in this journal is cited, in accordance with accepted academic practice. No use, distribution or reproduction is permitted which does not comply with these terms.